THÈSE

présentée à

L'UNIVERSITÉ SCIENTIFIQUE ET MÉDICALE ET L'INSTITUT NATIONAL POLYTECHNIQUE DE GRENOBLE

pour obtenir le grade

DOCTEUR ES-SCIENCES PHYSIQUES

par

Alain RAVEX

SUJET

Propriétés thermiques à très basses températures d'alliages supraconducteurs amorphes à base de Zirconium et effets de recuit

---

Soutenue le 7 mars 1986 devant la commission d'Examen

Président	J. DURAND
Examinateurs	N.E. PHILLIPS
	R. MAYNARD
	J.L. LASJAUNIAS
	P. HICTER
	O. BETHOUX

INTRODUCTION

Il y a une dizaine d'années des mesures de chaleur spécifique et de conduction thermique (Zeller and Pohl, 1971 ; Stephens et al., 1973 ; Lasjaunias et al., 1972 et 1974 ; Zaitlin and Anderson, 1974) ont montré qu'à basses températures les propriétés thermiques à l'état amorphe (désordonné) de solides isolants diffèrent notablement de leurs propriétés à l'état cristallin (ordonné). Nous avons en particulier mis en évidence expérimentalement dans le cas de la silice amorphe a-SiO_2 (Lasjaunias et al., 1975 ; Ravex, thèse 1976) sur près de deux décades de température (20 mK à 1 K) un excès de chaleur spécifique voisin de la linéarité en température et une variation quadratique avec la température de la conduction thermique.

Ces comportements très différents de ceux de l'état ordonné (chaleur spécifique et conduction thermique des phonons variant avec le cube de la température pour un cristal isolant) surprennent car l'on s'attendait à ce qu'au fur et à mesure que la température ou plus généralement l'énergie diminue , une description en continuum de la matière qui efface les différences structurales entre l'amorphe et le cristal soit de mieux en mieux appropriée.

L'expérience montre au contraire qu'il existe dans le solide désordonné des excitations de basse énergie qui n'ont pas d'équivalent systématique dans l'état cristallin ordonné. Quasi simultanément des comportements inhabituels ont été également observés dans les propriétés acoustiques (Hunklinger et al., 1972 ; Piché et al., 1974 ; Golding et al., 1973) et diélectriques à basse température d'isolants amorphes : variation logarithmique avec la température de la vitesse du son et de la constante diélectrique, saturation de l'atténuation ultrasonore résonante. Ces comportements nouveaux tant pour les propriétés thermiques qu'acoustiques ou diélectriques peuvent être justifiés en supposant que les excitations de basse énergie observées en chaleur spécifique sont assimilables à des systèmes à deux niveaux SDN (ou "two level systems" : TLS) qui peuvent interagir avec les phonons. Un tel modèle a été développé simultanément par Anderson et al., 1972 et Phillips, 1972.

L'exposé de ce modèle ainsi que la revue des résultats expérimentaux obtenus pour les isolants ont récemment fait l'objet d'une monographie (Amorphous Solids - Low Temperature Properties - W.A. Phillips).

Actuellement la nature microscopique de ces excitations de basse énergie n'est pas éclaircie, en particulier à cause de son universalité liée à l'état amorphe, bien que les structures locales des systèmes étudiés puissent être très différentes. Quelques modèles structuraux ont été proposés - par exemple dans la silice avec hydroxyle (W.A. Phillips, 1981) - toujours reliés à l'aspect covalent des liaisons atomiques (J.C. Phillips, 1981). Il apparut donc intéressant dans une phase ultérieure d'étudier des solides amorphes métalliques afin de savoir si la présence de liaisons covalentes était une condition nécessaire à l'existence de SDN. En outre se posait la question de l'interaction éventuelle de ces SDN avec les électrons de conduction.

C'est dans cette perspective que faisant suite aux mesures des propriétés thermiques de la silice amorphe, nous avons entrepris l'étude des propriétés thermiques d'alliages métalliques amorphes rapportée dans ce mémoire.

Une première série de mesures sur un alliage PdCuSi, facilement amorphisable par trempe du liquide à température ambiante et déjà étudié par d'autres auteurs au-dessus de 2 K (Chen and Haemmerle, 1972; Golding et al., 1972) ne nous a pas permis de conclure quant à la présence de SDN qui n'auraient représenté que quelques pour-cents de la contribution des électrons normaux à la chaleur spécifique. Néanmoins ces mesures rapportées en Annexe A ont permis de mettre en évidence par la contribution quadrupolaire nucléaire à la chaleur spécifique une grande similitude de l'ordre local dans les états amorphes et recristallisés. D'autre part est apparue la nécessité de travailler sur des alliages supraconducteurs pour s'affranchir de la contribution dominante des électrons de conduction aux propriétés thermiques.

Une seconde tentative sur un alliage supraconducteur amorphe a-LaZn rapportée en Annexe B s'est avérée également infructueuse quant à la mise en évidence des SDN à cause de la contribution des impuretés magnétiques contenues dans la terre rare. Cette étude a toutefois permis

d'observer pour la première fois un phénomène de relaxation d'énergie lié à la transformation ortho-para de l'hydrogène moléculaire piégé dans un échantillon. De plus ces mesures ont permis d'analyser et de comparer les propriétés supraconductrices dans les états amorphes et recristallisés.

Suite à ces deux essais préliminaires, l'étude d'une série d'alliages supraconducteurs à base de Zirconium obtenus par pulvérisation cathodique sur substrat froid a permis de mettre en évidence des SDN par les propriétés thermiques caractéristiques qui leur sont associées (excès de chaleur spécifique, conduction thermique). Le couplage de ces SDN aux noyaux de Zirconium a également été observé. Les mesures de chaleur spécifique permettent en outre l'étude des propriétés électroniques tant à l'état normal (densité d'état au niveau de Fermi) qu'à l'état supraconducteur (couplage électronon-phonon, champ critique thermodynamique, etc.). La comparaison des résultats obtenus pour nos échantillons bruts de pulvérisation aux résultats d'autres auteurs pour des échantillons de composition similaire généralement obtenus par trempe rapide du liquide suggère un plus grand désordre (en termes de densité d'état de SDN) dans nos échantillons.Des études structurales indiquent d'autre part le caractère plus désordonné des alliages pulvérisés. De plus le traitement thermique à l'état amorphe (recuits au-dessous de la température de cristallisation) de ces échantillons pulvérisés engendre des effets importants sur les SDN (en opposition avec le comportement des isolants amorphes) et les propriétés électroniques (en opposition avec le comportement des échantillons trempés du liquide). L'effet de ces traitements thermiques a également été étudié sur les mêmes échantillons au moyen d'autres techniques complémentaires de mesure des propriétés électroniques (résistivité électrique, champ critique H_{c_2}) ou structurales (diffusion des rayons X aux petits angles, EXAFS). L'ensemble de ces résultats et leur analyse sont développés dans ce mémoire suivant le plan ci-après :

1. Elaboration et caractérisation des échantillons, définition des traitements thermiques

2. Technique expérimentale et résultats expérimentaux

3. Analyse des résultats : propriétés électroniques et supraconductrices - excitations de basse énergie (SDN)

4. Effets des recuits sur les propriétés électroniques et supraconductrices et sur les excitations de basse énergie (SDN)

5. Etude des propriétés structurales

6. Conclusion.

- ANDERSON P.W., HALPERIN B.I. and VARMA C.H., Phil. Mag. 25, 1 (1972).
- CHEN H.S. and HAEMMERLE W.H., J. Non-Cryst. Solids 11, 161 (1972).
- GOLDING B., BAGLEY B.G. and HSU F.S.L., Phys. Rev. Lett. 29, 68 (1972).
- GOLDING B., GRAEBNER J.E., HALPERIN B.I. and SCHUTZ R.J., Phys. Rev. Lett. 30, 223 (1973).
- HUNKLINGER S., ARNOLD W., STEIN S., NAVA R. and DRANSFELD K., Phys. Lett. 42A, 253 (1972).
- LASJAUNIAS J.C., MAYNARD R., THOULOUZE D., Solid State Comm. 10, 215 (1972).
  LASJAUNIAS J.C., THOULOUZE D., F. PERNOT, Solid State Comm. 14, 957 (1974).
- LASJAUNIAS J.C., RAVEX A., VANDORPE M. and HUNKLINGER S., Solid State Commun. 17, 1189 (1975).
- PHILLIPS J.C., Phys. Rev. B24, 1744 (1981).
- PHILLIPS W.A., Amorphous Solids, Low Temperature Properties, Springer Verlag.
- PHILLIPS W.A., Philosophical Mag. B 43, 747 (1981).
- PHILLIPS W.A., J. Low Temp. Phys. 7, 351 (1972).
- PICHE L., MAYNARD R., HUNKLINGER S., JACKLE J., Phys. Rev. Letters 32, 1426 (1974).
- RAVEX A., Thèse Ingênieur Docteur, Grenoble (1976).
- STEPHENS R.B., CIELOSZYK G.S., SALINGER G.L., Phys. Letters 38A, 215 (1972).
- STEPHENS R.B., Phys. Rev. B8, 2896(1973).
- ZAITLIN M.P., ANDERSON A.C., Phys. Rev. Lett. 33, 1158 (1974).
- ZELLER R.C., POHL R.O., Phys. Rev. B 4, 2029 (1971).

C H A P I T R E I

ELABORATION ET CARACTERISATION DES ECHANTILLONS, DEFINITION DES TRAITEMENTS THERMIQUES

I - PREPARATION

Les échantillons sont élaborés par le Service Métallurgie du laboratoire par pulvérisation cathodique à grande vitesse à l'aide d'un système diode magnétron sous atmosphère réduite d'argon.

Pression d'argon	=	$\sim 5 \times 10^{-3}$ torr
Courant ionique	=	de 100 à 400 mA
Tension	=	600 V
Vitesse de pulvérisation	=	$\sim$ 10 µm/hr
Temps moyen de pulvérisation	=	$\sim$ 5 à 10 heures

L'alliage cible est obtenu par fusion en semi-lévitation et coulée par centrifugation dans un moule de cuivre refroidi. Deux familles d'alliages ont été élaborés dans le cadre de cette étude :

a) $La_{.78}Zn_{.22}$ à partir de Lanthane 3N ou 4N et de Zinc 6N.

b) une série $Zr_{(1-n)}M_x$ à partir de Zirconium (4N) et d'éléments d'addition M de pureté 5N :

M	x (at %)
Ni	24 (analysé)
Cu	24 (analysé)
Ag	35 (nominal)
Pt	25 (nominal)
Fe	24 (nominal)
Mo	30 (nominal)

II - CARACTERISATION

La caractérisation des échantillons porte essentiellement sur des contrôles d'amorphicité et d'homogénéité.

1. Contrôle d'amorphicité : diagrammes de rayons X

Les échantillons bruts de pulvérisation sont systématiquement étudiés par diffraction des rayons X en utilisant la radiation K_α du cuivre. Un enregistrement typique de diffractomètre est représenté en figure 1.

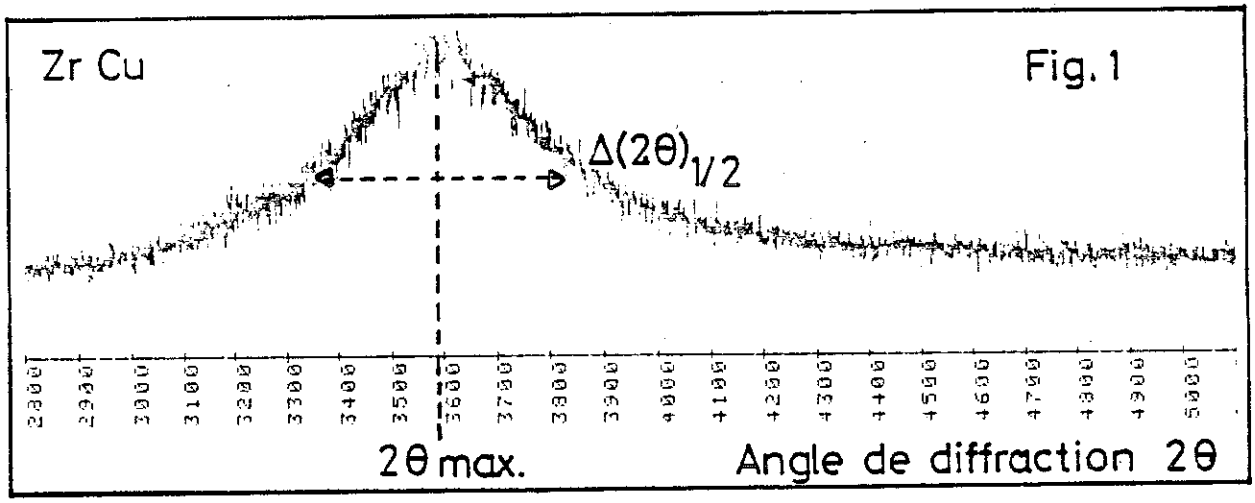

La forme générale du diagramme est caractéristique de la structure amorphe avec un large premier anneau de diffraction. La position $2\theta_{max}$ et la largeur à mi-hauteur $\Delta(2\theta)_{1/2}$ de ce premier pic pour les divers échantillons étudiés sont rapportées dans le tableau 1.

Les cibles obtenues ont un diamètre de 60 mm (en 3 secteurs de 120°) et une épaisseur de 1,5 mm. Lors de la pulvérisation le dépôt s'effectue directement (sans graisse à vide) sur un substrat de cuivre sablé refroidi par circulation d'eau (dépôt à 300 K) ou circulation d'azote liquide (dépôt à 77 K). Ce substrat composé de facettes rectangulaires constituant approximativement une calotte sphérique permet d'obtenir l'échantillon sous forme de 6 plaquettes :

dimensions = 23 x 46 mm
épaisseur = ≃ 80÷100 µm
poids = quelques grammes.

Cette méthode de préparation a été choisie de préférence à la trempe rapide du liquide (enclume ou rouleau) car elle permet d'obtenir des échantillons relativement massifs facilitant les mesures de chaleur spécifique à très basse température et parce qu'il est d'autre part possible d'obtenir par pulvérisation des compositions d'alliages amorphes non obtenues actuellement par trempe du liquide. Les résultats exposés dans la suite de ce mémoire montrent par ailleurs que l'état de désordre obtenu par les deux méthodes n'est pas forcément identique (voir les résultats de résistivité, EXAFS et diffusion de rayons X aux petits angles discutés lors de l'étude des Propriétés Structurales), les échantillons pulvérisés présentant une densité de SDN et une contribution électronique plus élevées, ainsi qu'une plus grande sensibilité aux traitements thermiques.

2. Etude de la cristallisation : analyse thermique différentielle

Une analyse thermique différentielle est systématiquement effectuée sur un témoin de quelques dizaines de milligrammes prélevé sur chaque échantillon afin de déterminer sa température de cristallisation. La figure 2 montre l'enregistrement obtenu à une vitesse de chauffe de 40 K mn^{-1} pour un échantillon $Zr_{76}Cu_{24}$.

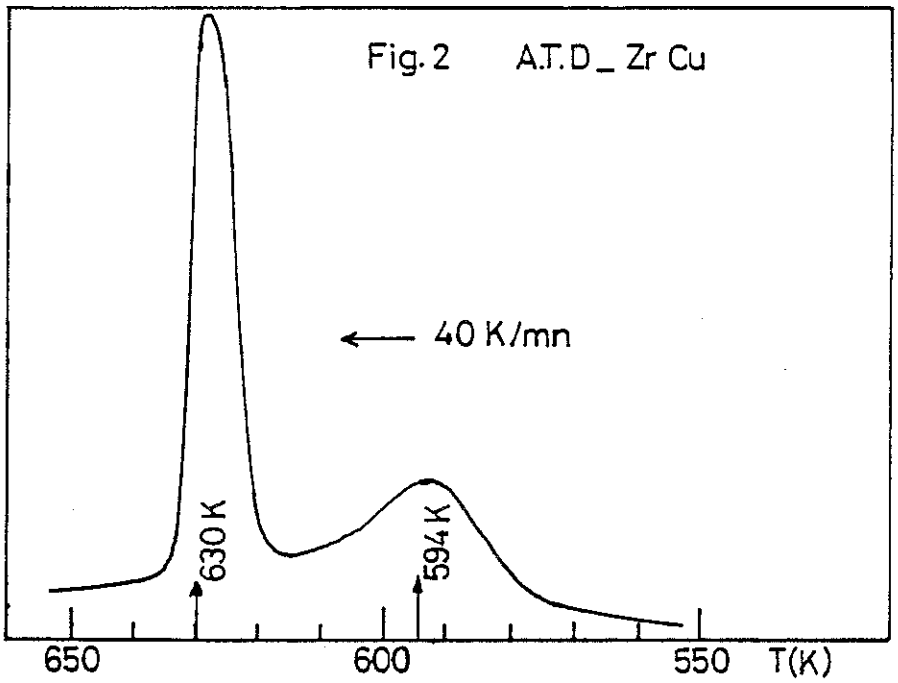

On observe deux pics de cristallisation successifs caractérisés par des maxima à environ 321°C et 357°C. La déviation par rapport à la ligne de base indique un début de cristallisation à environ 300°C. La détermination de cette température de début de cristallisation est indispensable pour déterminer les niveaux de température auxquels nous pourrons recuire les échantillons en préservant l'état désordonné. Le résultat présenté en figure 2 est en bon accord avec ceux obtenus par Samwer et von Löhneysen (1982) ; Calvayrac et al. (1983) sur une série d'échantillons $Zr_x Cu_{1-x}$ trempés du liquide. La présence de deux pics successifs de cristallisation semble être générale pour les alliages amorphes à forte concentration de Zirconium que nous avons étudiés : les températures des pics d'ATD sont reportées dans le tableau 1. Pour certains échantillons (ZrNi notamment) les deux pics ne sont observés qu'en diminuant la vitesse de chauffe (de 20 K mn^{-1} à 5 K mn^{-1} puis 2,5 K mn^{-1} on sépare nettement les deux pics (fig. 3)).

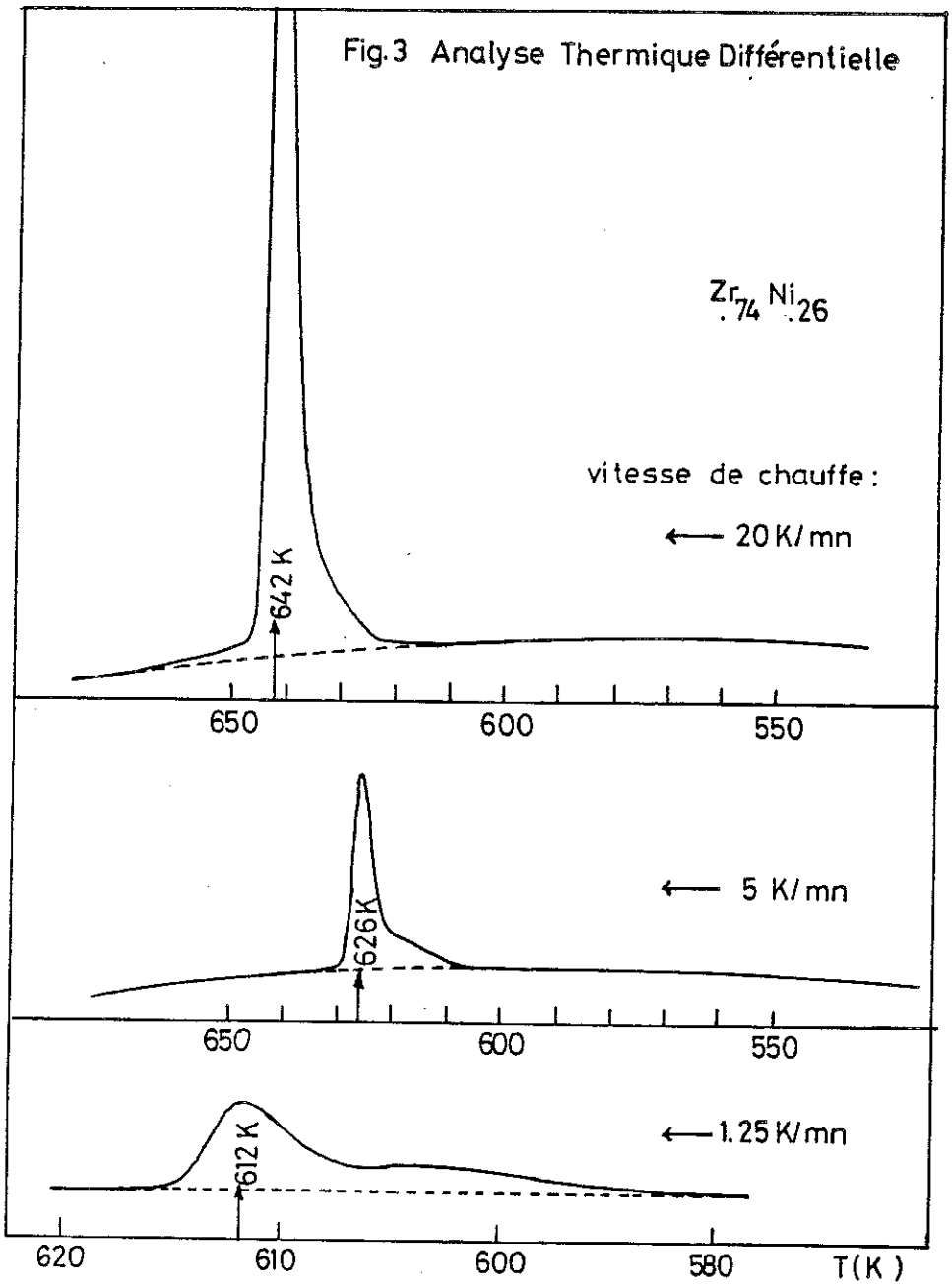

L'apparition successive de deux phases de cristallisation a été analysée plus en détail pour l'échantillon $Zr_{76}Cu_{24}$ dont la courbe d'ATD est reportée en fig. 1. La formation des deux phases cristallines possédant des cinétiques de croissance différentes a également été suivie par mesure de résistivité (Ravex et al., 1984). L'analyse par diffraction de rayons X de ces deux phases a permis de mettre en

évidence dans un premier temps l'apparition superposée au fond amorphe de raies caractéristiques de la structure métastable ω du Zirconium. Cette phase apparaît généralement dans les alliages trempés cubiques à face centrée riches en Zirconium ou sous pression supérieure à 40 kbars dans le Zirconium pur. La seconde étape correspond à un mélange des phases d'équilibre Zr_2Cu et α-Zirconium hexagonal compact avec subsistance d'un peu de phase ω . Ces résultats suggèrent que le traitement thermique entraîne une décomposition de l'alliage amorphe en de petits domaines (clusters) d'une phase amorphe de Zirconium presque pur qui cristallise dans la structure ω et d'une seconde phase amorphe plus riche en cuivre qui par la suite cristallise dans les phases d'équilibre (Zr_2Cu et Zr-α). L'apparition de la phase ω en début de cristallisation a été également observée récemment par Buschow et al. (1983) sur des alliages à base de Zirconium aux mêmes concentrations obtenus par trempe du liquide.

3. Analyse chimique - homogénéité des échantillons - densité

Des mesures de composition chimique et de densité sont effectuées pour évaluer l'homogénéité des échantillons.

La densité est mesurée par la méthode d'Archimède dans le toluène. La précision de cette méthode est de l'ordre de 0,01 gcm^{-3} pour des morceaux d'échantillon de 0,5 g. Des mesures effectuées sur les six plaquettes de $Zr_{76}Cu_{24}$ obtenues lors d'une même pulvérisation font apparaître une fluctuation de l'ordre de $\pm$ 0,015 g cm^{-3} entre plaquettes (fig. 4). Si l'on attribue ces fluctuations à des différences de composition, elles correspondent à des variations de concentration atomique de l'ordre de $\pm$ 1 at % - en effet dans le cas d'alliages $Zr_{1-x}Cu_x$ la variation de la densité en fonction de la composition vaut $d\rho/dx$ = 0,017 g cm^{-3} (at %)$^{-1}$. Une telle dispersion de composition est en bon accord avec par exemple la largeur de la transition supraconductrice observée en chaleur spécifique. En effet, à partir des mesures de Garoche et al. (1982), Samwer et al. (1982), Altounian et al. (1983) pour une série d'alliages $Zr_{1-x}Cu_x$ on peut évaluer dT_c/dx = 0,11 K(at %)$^{-1}$. Les mesures de densité mettent donc en évidence une inhomogénéité de

Fig. 4 Variations de densité entre plaquettes

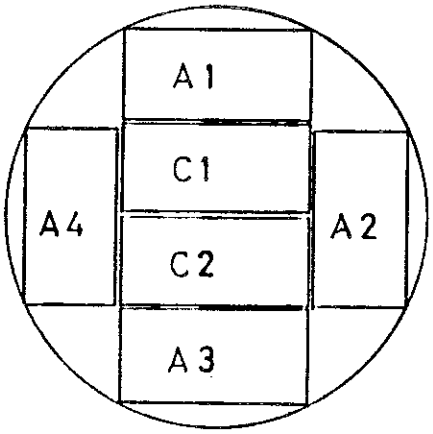

échantillon :

$Zr_{.76}Cu_{.24}$ brut de pulvérisation

plaquette	densité	écart moyenne
C 1	6,81	- 0,01
C 2	6,81	- 0,01
A 1	6,81	- 0,01
A 2	6,81	- 0,01
A 3	6,83	+ 0,01
A 4	6,84	+ 0,02
moyenne	6,82	

Fig. 5 Analyse chimique d'une plaquette

échantillon : $Zr_{.76}Ni_{.24}$ brut

1	2	3
4	5	6
7	8	9

plaquette A3

morceau	composition x (%at. Ni)
1	25,4
2	27,4
3	26,8
4	23,3
5	25,0
6	24,7
7	20,6
8	21,9
9	21,6
moyenne	24,0 ± 3,4

plaquette à plaquette. Une étude de composition par analyse chimique a par ailleurs été entreprise sur plusieurs morceaux (9) d'une même plaquette de $Zr_{76}Ni_{24}$(fig. 5). Les fluctuations de concentration atomique observées sont de l'ordre de ± 3 at % pour une composition nominale de 24 at %.

4. Les "gaz résiduels"

Un sujet de préoccupation concernant les échantillons amorphes est la présence de gaz résiduels inclus lors de la préparation et qui pourraient contribuer aux propriétés physiques mesurées. On développera lors de l'analyse des résultats expérimentaux une argumentation basée sur la mise en évidence d'un couplage SDN-noyaux qui permet d'écarter une telle origine pour les résultats de chaleur spécifique et sur l'interaction SDN-phonons en ce qui concerne les mesures de conduction thermique. Nous insistons ici sur les analyses ou contrôles effectués sur les échantillons afin d'évaluer la quantité de gaz inclus.

Lors de séries de mesures de densité, de faibles pertes de poids d'échantillon ont été observées en fonction du temps de stockage et des traitements thermiques. Par exemple la perte de poids d'une plaquette traitée 1 h à 200°C a été de 0,07 %. Après fusion de cette même feuille sous vide, la perte de poids est de 0,12 %. Si l'on attribue ces pertes à de l'Argon piégé dans l'échantillon au cours de la pulvérisation, le contenu initial serait donc de l'ordre de 0,4 at % d'Argon. L'hypothèse Argon est très probable car les autres gaz usuels (O_2, N_2, H_2) peuvent donner des composés stables avec le Zirconium lors du traitement thermique et ainsi ne s'échappent pas de l'alliage.

D'autre part des mesures de la teneur en hydrogène ont été effectuées au Service de Microanalyse du CNRS de Gif-sur-Yvette. Pour la plupart des échantillons (voir tableau 1), la quantité d'hydrogène présente était inférieure à la limite de détection de la méthode, soit 100 ppm en poids, soit moins de 1 at %. Pour deux échantillons seulement (ZrNi déposé à 300 K et ZrMo) la teneur en hydrogène atteint 4 at %.

Echantillon	Rayons X 2θ(degré)	Rayons X $\Delta\theta_{1/2}$(degré)	Densité (g/cm^3)	A.T.D. pied du 1er pic (°Celcius) à 20 K/mn	Teneur en hydrogène % at.
$Zr_{76}Ni_{24}$ 77 K	36,5± 0,2	5,0± 0,2	*6,85± 0,01	362	< 1 %
recuit	36,4	4,8	6,95	365	< 1 %
$Zr_{76}Ni_{24}$ 300K	36,0	4,5	6,85	349	4 %
$Zr_{76}Cu_{24}$ 77 K	36,0	4,0	6,78	297	< 1 %
2 mois 300K	36,0	3,8			< 1 %
$Zr_{76}Cu_{24}$ 77 K 1h à 200°C			**6,805	282	< 1 %
			6,82	290	< 1 %
$Zr_{76}Pt_{25}$ 77 K	36,0	4,7	9,27		
$Zr_{65}Ag_{35}$ 300K	36,3	3,6	7,49	354	
$Zr_{76}Fe_{24}$ 77 K	36,7	5,6	6,87	380	
$Zr_{70}Mo_{30}$ 77 K			7,40		4 %

* Mesures effectuées sur des morceaux d'échantillons différents.

** Mesures effectuées sur le même morceau d'échantillon.

Tableau 1 - Récapitulatif des mesures de caractérisation effectuées pour les échantillons étudiés.

Ces valeurs sont loin d'atteindre certains chiffres avancés parfois pour certains échantillons préparés par pulvérisation cathodique (Boucher et Chieux, 1983) et sont du même ordre de grandeur que celles observées dans des échantillons trempés du liquide (Calvayrac et al., 1983) quand les mesures ont été effectuées.

III - TRAITEMENTS THERMIQUES

Afin d'étudier l'effet de la relaxation structurale sur les propriétés thermiques liées au désordre (SDN) et les propriétés électroniques (supraconductivité) des métaux amorphes, des traitements thermiques ont été effectués au-dessous de la température de cristallisation déterminée en ATD afin de faire évoluer la structure de l'échantillon tout en restant à l'état amorphe (température de recruit de l'ordre de 0,7 fois la température de cristallisation). Le tableau ci-après caractérise les recuits effectués sur deux échantillons pour lesquels les effets sur les propriétés thermiques (chaleur spécifique et conduction thermique) sont analysés dans la suite de ce mémoire.

Echantillon	Traitement
$Zr_{76}Ni_{24}$	24 heures à 250°C sous vide (température de cristallisation ∿ 350°C)
$Zr_{76}Cu_{24}$ (A)	1 heure à 200°C sous atmosphère d'argon (température de cristallisation ∿ 300°C)
$Zr_{76}Cu_{24}$ (B)	vieilli 70 jours à température ambiante puis 1 heure à 200°C sous argon

L'amorphicité des échantillons après recuit a été sytématiquement contrôlée par diffraction des rayons X. Aucune évolution n'a été observée dans la limite de résolution.

Des mesures de densité effectuées avant et après traitement thermique sur une même plaquette d'échantillon (ZrCu recuit 1 h à 200°C) montrent une augmentation de 6,805 g cm^{-3} à 6,822 g cm^{-3}. Cette variation de densité est du même ordre de grandeur que celle observée par d'autres auteurs (Garoche et al., 1982 ; Chen et al., 1983 ; Johnson et al. 1983) sur des échantillons trempés du liquide.

Des mesures de résistivité, de diffraction de rayons X, de diffusion de rayonx X aux petits angles, d'EXAFS ont été effectuées en collaboration avec d'autres laboratoires sur nos échantillons avant et après recuit afin de chercher à mettre en évidence des évolutions de structure. Ces résultats seront évoqués lors de la discussion des résultats expérimentaux.

- ALTOUNIAN Z. and STROM-OLSEN J.O., Phys. Rev. B27, 4149 (1983).
- BOUCHER B., CHIEUX P., CONVERT P., TOURNARIE M., J. Phys. F : Met. Phys. 13, 1339 (1983).
- BUSCHOW K.H.J., VINEZE I., van der WONDE F., J. Non Cryst. Solids 54, 101 (1983).
- CALVAYRAC Y., CHEVALIER J.P., HARMELIN M., QUIVY A., BIGOT J., Phil. Mag. B 48, 323 (1983).
- CHEN H.S., AUST K.T., WASEDA Y., J. of Mat. Science Letters 2, 153 (1983).
- GAROCHE P., CALVAYRAC Y., CHENG W. and VEYSSIE J.J., J. Phys. F : Met. Phys. 12, 2783 (1982).
- JOHNSON W.L., ANDERSON A.C.,Phys. Rev. B27, 1586 (1983).
- RAVEX A., LASJAUNIAS J.C., BETHOUX O., J. Phys. F : Met. Phys. 14, 329 (1984).
- SAMWER K. and LÖHNEYSEN H.v., Phys. Rev. B26, 107 (1982).

C H A P I T R E II

TECHNIQUE EXPERIMENTALE ET RESULTATS EXPERIMENTAUX

Les matériaux supraconducteurs amorphes sont caractérisés par leur faible chaleur spécifique (typiquement $C_p \simeq 10^{-7}$ J g^{-1} K^{-1} à 50 mK) et leur mauvaise conductibilité thermique (de l'ordre de $k \simeq 10^{-6}$ W cm^{-1} K^{-1} à 100 mK). D'autre part les techniques d'élaboration ne permettent pas d'obtenir des masses importantes d'échantillon (plaquettes d'environ 500 mg) ni de fortes épaisseurs ($\sim$ 100 µm). Nous allons donc exposer dans ce chapitre les techniques adoptées pour mesurer de très faibles capacités calorifiques ainsi que de fortes résistances thermiques à très basse température.

I - CHALEUR SPECIFIQUE

1. Technique de mesure

La mesure de faibles capacités calorifiques nécessite l'emploi de méthodes transitoires. En effet les puissances parasites (rayonnement, vibrations, conduction par les supports d'échantillon, gaz résiduels, etc.) des divers montages cryogéniques que nous avons utilisés (réfrigérateur à désaimantation adiabatique - Keystone et al., 1968 ; réfrigérateur à dilution - Gandit, Thèse, 1983), de l'ordre du nanowatt (10^{-9} W) à 50 mK, interdisent toute mesure en adiabatique. Nous avons donc adopté une technique par impulsion de chaleur, l'échantillon étant relié à la source froide par une fuite thermique. Cette méthode déjà utilisée pour les mesures de chaleur spécifique d'isolants amorphes (Ravex, 1976 ; Lasjaunias et al., 1977) a été adaptée à la nouvelle géométrie et aux capacités calorifiques plus faibles des échantillons supraconducteurs amorphes.

La figure 1a montre un schéma du montage expérimental adopté ainsi qu'un circuit thermique équivalent (fig. 1b). Les plaquettes d'échantillon (généralement 4, soit environ 2g) sont serrées entre deux plaquettes de Silicium monocristallin très pur (très bonne diffusivité thermique et faible capacité calorifique). Le contact thermique entre plaquettes est assuré par de la graisse à vide Apiezon N (environ

Fig.1 CHALEUR SPECIFIQUE _ Technique experimentale

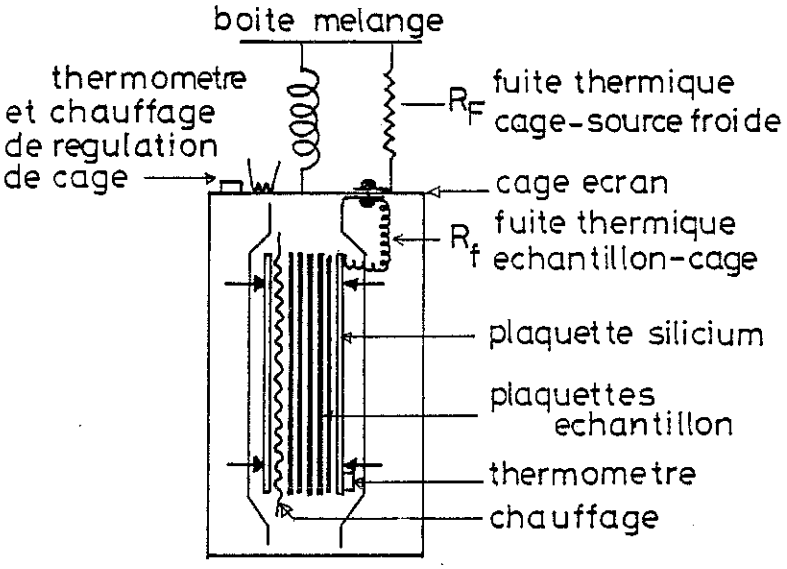

1.a montage experimental

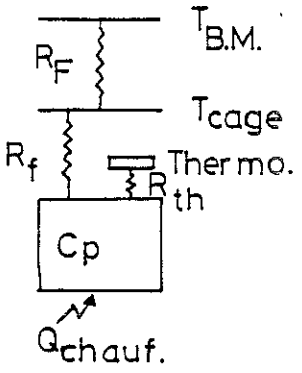

1.b schema thermique equivalent

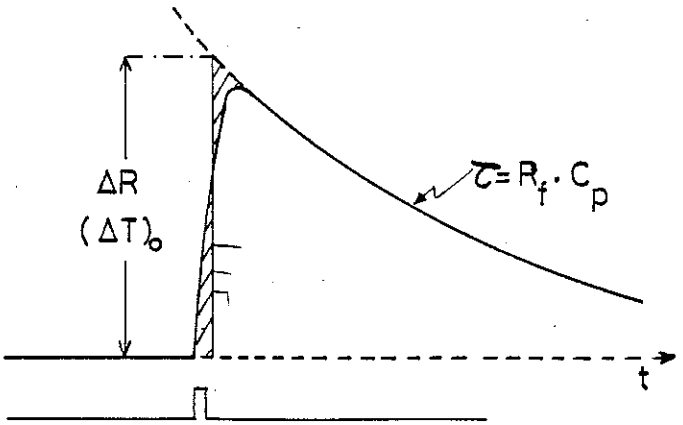

1.c reponse du thermometre á une impulsion de chaleur

10 mg) déposée par immersion des plaquettes d'échantillon dans une solution graisse-trichloréthylène puis évaporation. L'ensemble est comprimé par quatre vis nylon dans un cadre de cuivre.

Le chauffage constitué d'un fil de Platine-Tungstène (PtW, 8 %) de 12 µm de diamètre est placé entre une des plaquettes de silicium et une plaquette d'échantillon. Le choix du Platine Tungstène se justifie par la grande stabilité en température de sa résistance électrique (variation de quelques pour mille de la résistance entre 10 mK et 10 K) et par sa faible contribution à la capacité calorifique des addenda. Ainsi la chaleur spécifique quadrupolaire nucléaire qui apparaît à très basse température ($T < 100$ mK) est deux ordres de grandeur inférieure à celle du constantan (Ho et al., 1965).

Le thermomètre, une pastille de Silicium dopé au Phosphore (Frossati et al., 1975), est collé (graisse Apiezon N) sur la seconde plaquette de Silicium dorée sur laquelle est en outre soudée la fuite thermique R_f reliant l'échantillon à une cage-écran régulée en température. Ce montage dans lequel l'énergie de chauffage doit nécessairement traverser l'échantillon avant de s'évacuer à la source froide évite les problèmes rencontrés pour l'étude de matériaux de faible diffusivité thermique avec des montages où chauffage, thermomètre et fuite thermique sont regroupés sur un même côté du support.

La fuite thermique doit être choisie de façon à ce que la constante de temps $\tau = R_f \times C_p$ de retour à l'équilibre du système après une impulsion de chaleur soit nettement supérieure à la constante de temps de mise en équilibre interne de l'échantillon. Cette dernière commandée soit par la diffusivité de l'échantillon, soit par les résistances thermiques de contact échantillon-chauffage ou échantillon-thermomètre a pu être estimée expérimentalement récemment lors de la mise au point d'un système d'acquisition automatique de données : elle est de l'ordre de quelques centièmes de seconde dans la zone la plus critique (400-500 mK) où la constante de retour à l'équilibre atteint sa valeur minimale ($\simeq$ 0,8 sec). Dans la pratique, l'enregistrement graphique du temps de montée en température après le pulse de chaleur est limité vers les constantes de temps rapides par les caractéristiques

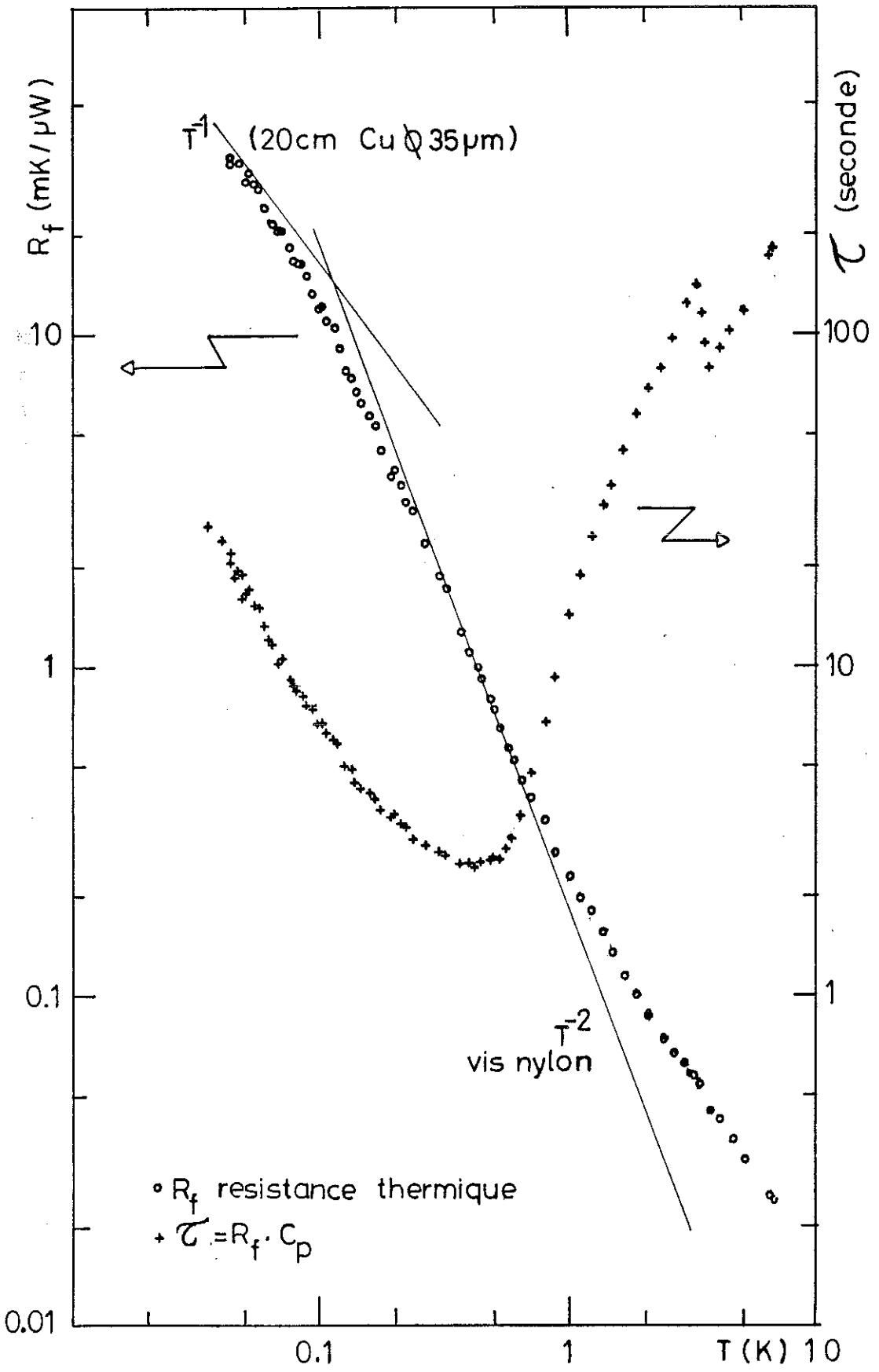

Fig. 2 Fuite thermique et Constante de temps

de la chaîne de mesure : pont de mesure* (constante de temps 0,3 sec) et enregistreur.

La fuite thermique est pratiquement assurée par les vis Nylon pour la plus grande partie de la gamme de température explorée ($T \geqslant 150$ mK) ; un fil de cuivre (diamètre $\emptyset$ = 35 µm, longueur 20 cm) limite la résistance de fuite R_f à très basse température et permet ainsi d'obtenir des mesures jusqu'à 40 mK. Les valeurs de constantes de temps observées dans le cas le plus critique rencontré au cours des mesures sont reportées en figure 2. Sur la même figure est tracée la variation avec la température de la résistance de fuite déterminée expérimentalement ($R_f = \frac{\tau}{C_p}$). Le régime en T^{-2} suivi d'un plateau caractéristique de l'état amorphe correspond au régime de fuite par les vis nylon alors qu'à très basse température la conduction métallique du cuivre impose un régime en T^{-1}.

La fuite thermique R_f ne relie pas directement l'échantillon à la source froide mais à une cage-écran de cuivre elle-même reliée à travers une fuite R_F à la source froide, en l'occurrence la boîte à mélange du réfrigérateur à dilution. La cage écran est suspendue à la boîte à mélange par un ressort jouant le rôle de filtre pase-bas afin de diminuer les apports de puissance parasite par vibrations. La cage écran est régulée en température ce qui assure une référence de température très stable à nos mesures. D'autre part la fuite R_F est calibrée de façon à imposer à très basse température un gradient très faible (quelques milliKelvins) avec la boîte à mélange et par contre pouvoir réguler jusqu'à 7 K sans désamorcer ou rendre instable le réfrigérateur à dilution.

Dans ces conditions la réponse du thermomètre à une impulsion de chaleur W telle qu'on l'enregistre est représentée en figure 1c. Pour toutes les mesures effectuées dans le cadre de l'étude des alliages amorphes à base de Zirconium, une seule constante de temps bien définie de retour à l'équilibre a été observée, conduisant à une détermination sans ambiguïté de la capacité calorifique C_p. La capacité calorifique C_p

---

* détecteur multifonction développé au CRTBT.

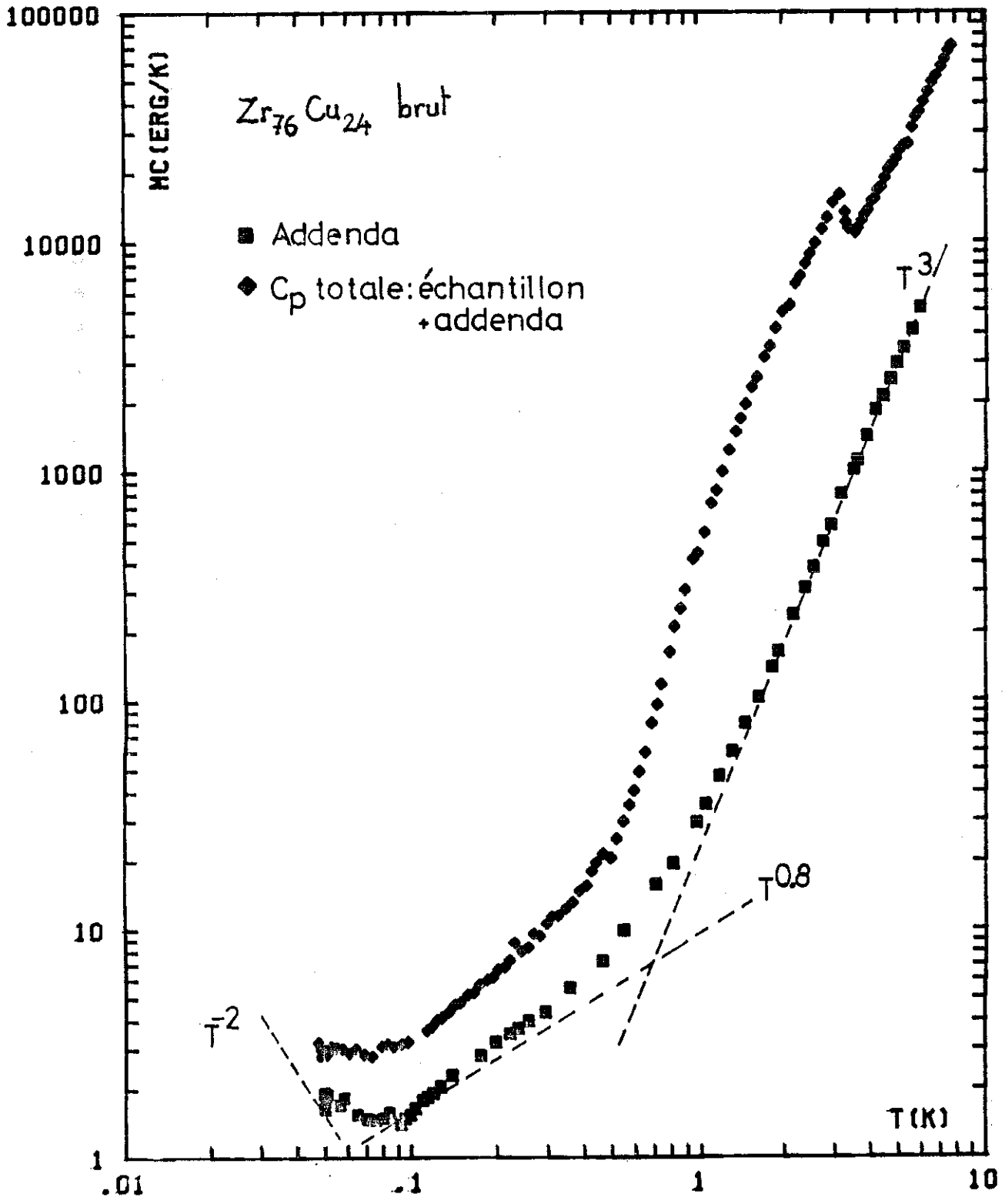

Fig.3 CHALEUR MASSIQUE (TOTALE et ADDENDA)

est déterminée par la relation $C_p = \frac{W}{\Delta T}$ où ΔT est le saut de température déterminé par la loi des aires (pointillés et hachures sur fig. 1c) qui correspondrait à un temps de chauffe infiniment court, une diffusivité thermique infinie et des résistances thermiques de contact nulles entre échantillon, chauffage et thermomètre. L'énergie de l'impulsion de chaleur W est calculée ($W = R_{ch} i^2 t$) à partir de la mesure de la résistance de chauffage R_{ch} (pont 4 fils), des courants (i) et temps de chauffe (t)(source de courant programmable construite au laboratoire).

2. Addenda - résultats expérimentaux

La capacité calorifique obtenue expérimentalement est celle de l'ensemble échantillon-addenda (porte-échantillon : plaques de Silicium, graisse à vide, thermomètre, chauffage, ...). Une mesure indépendante du groupe de mesure seul a donc été effectuée afin de pouvoir le soustraire aux mesures avec échantillon. Les résultats expérimentaux présentés figure 3 montrent que la contribution des addenda peut s'analyser grossièrement sous la forme

$$C_{addenda} = aT^3 + bT^{.8} + cT^{-2} \qquad \begin{array}{l} a = 24 \ \ erg.K^{-4} \\ b = 10 \ \ erg.K^{1,8} \\ c = 2.10^{-3} \ erg.K \end{array}$$

Ces valeurs correspondent raisonnablement à ce que l'on peut calculer. On peut en effet a priori chercher à déterminer les contributions des principaux éléments constitutifs des addenda : plaquettes de Silicium, couche d'or évaporé, graisse à vide, fil de chauffage, masses thermiques,... Toutefois une telle évaluation ne peut être qu'approximative étant donné l'incertitude sur la chaleur spécifique de certains de ces éléments (papier à cigarettes, isolant des fils, etc.). Afin de prendre en compte dans l'analyse des mesures de chaleur spécifique une bosse observée vers 100 mK sur la courbe expérimentale ainsi que la remontée basse température certainement due à des impuretés magnétiques, nous avons pour tous les résultats présentés dans la suite de ce mémoire retranché la contribution des addenda sous la forme d'un polynôme du sixième degré ($\sum_{i=1}^{6} a_i T^i$) ajusté par moindres carrés sur les données expérimentales du groupe de mesure. Les valeurs des coefficients et les écarts valeurs calculées - valeurs expérimentales sont données en Annexe C.

Fig.4 CHALEUR SPECIFIQUE

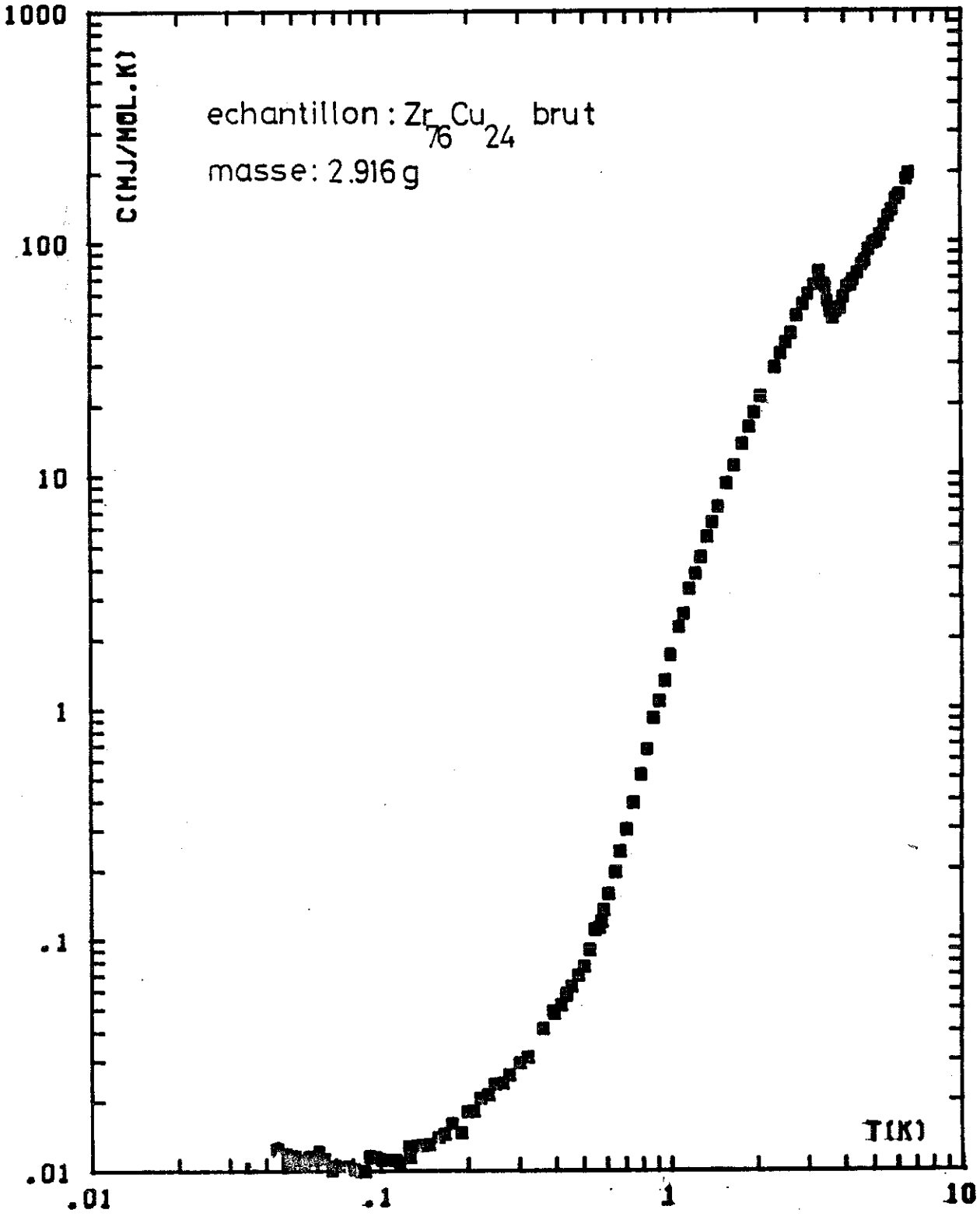

En figure 3 est également reportée la mesure de capacité calorifique totale (échantillon + addenda) la plus défavorable (contribution d'échantillon la plus faible rencontrée). Ceci permet de situer la contribution relative des addenda.

3. Méthodes d'analyse des mesures

La figure 4 donne un exemple de courbe de chaleur spécifique obtenue après soustraction de la contribution des addenda. Toutes les courbes de la série d'alliages ZrM étudiée présentent un aspect similaire. Dans l'annexe C sont fournies sous forme de tableau les valeurs numériques de la chaleur spécifique pour tous les échantillons étudiés. La procédure d'analyse des résultats expérimentaux pour extraire les différents paramètres physiques qui seront discutés dans la suite du mémoire est développée sur l'exemple de la figure 4. La courbe de chaleur spécifique est découpée en trois zones : la partie haute température ($T > T_c$), au-dessus du saut de chaleur spécifique caractéristique de la transition supraconductrice (T_c), correspondant à l'état normal, la région de la transition supraconductrice et enfin la zone très basse température ($T < 500$ mK).

a. Etat normal $T > T_c$

A l'état normal, dans la gamme de température explorée ($T < 7$ K), la chaleur spécifique comporte deux contributions. L'analyse habituelle $C/T = f(T^2)$ présentée en figure 5 permet de mettre en évidence la contribution linéaire en température (γT) due aux électrons normaux et la contribution cubique en température (βT^3) caractéristique des phonons. En particulier il n'est pas nécessaire d'introduire de terme en T^5 pour rendre compte des résultats expérimentaux du côté haute température.

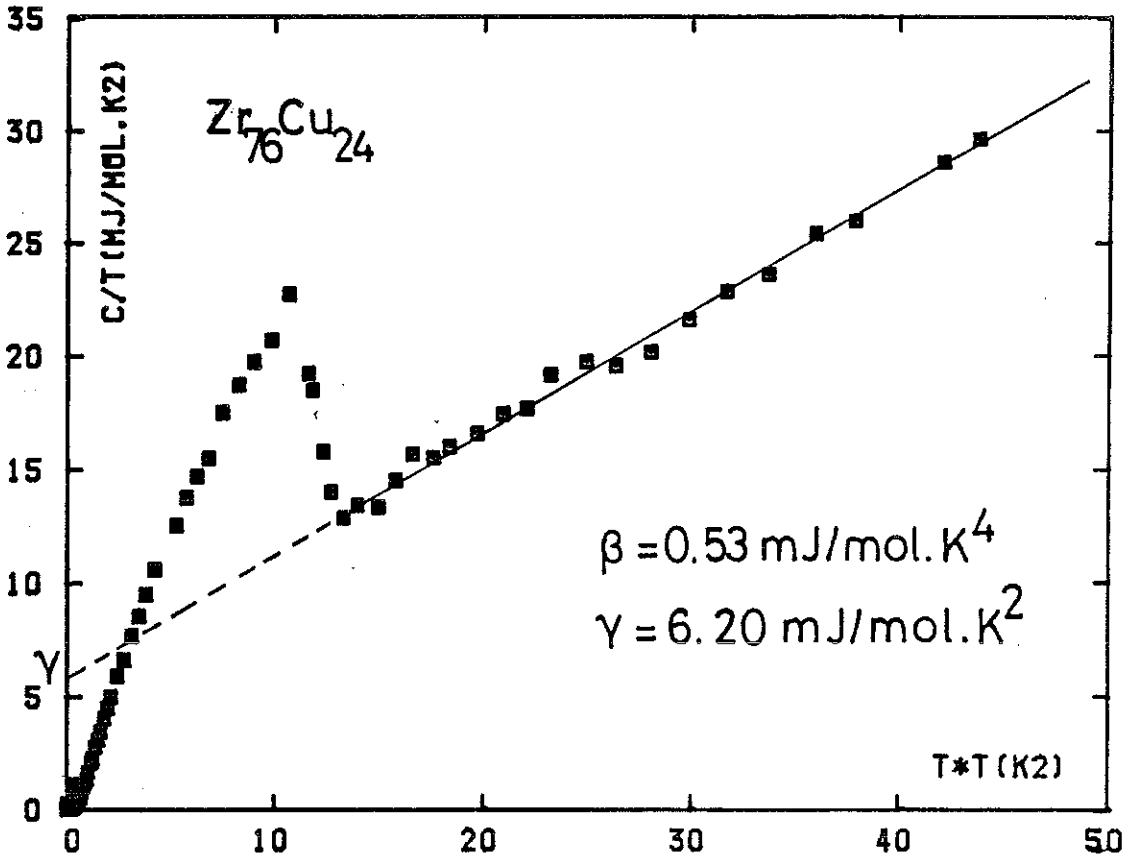

Fig.5 Etat normal. Détermination β , γ

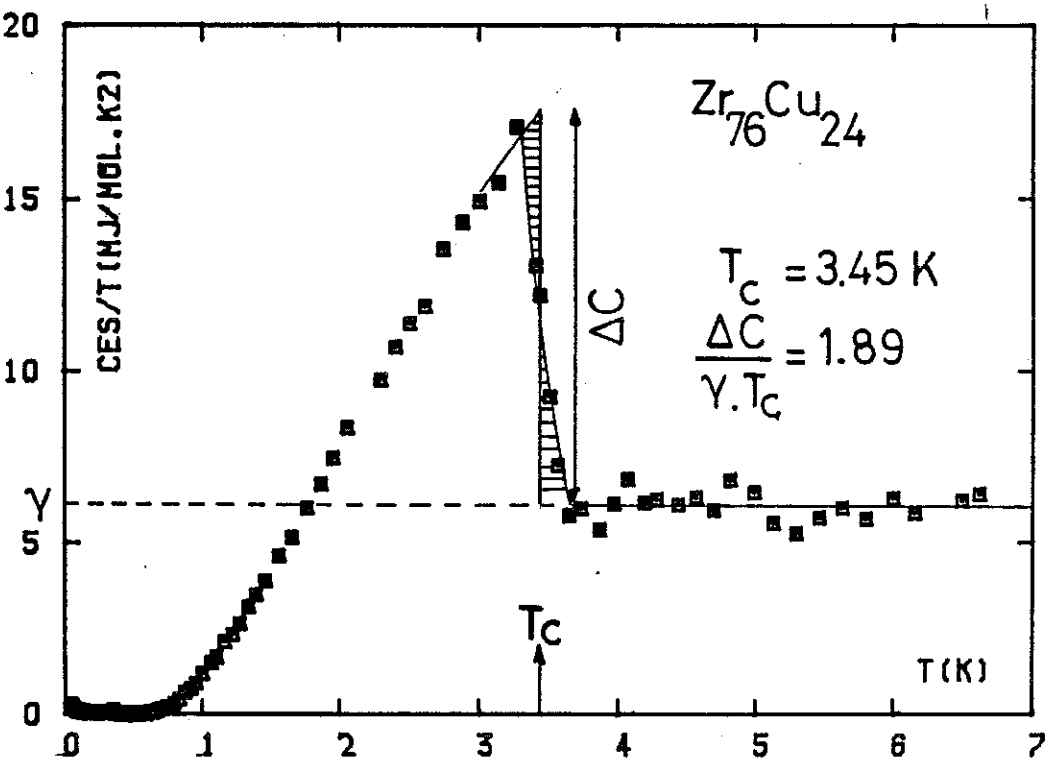

Fig.6 Transition supraconductrice

b. Transition supraconductrice ($T \simeq T_c$)

A l'état supraconducteur, la condensation en paires de Cooper des électrons doit théoriquement entraîner une décroissance exponentielle de leur contribution à la chaleur spécifique. Si l'on admet que dans l'état supraconducteur la contribution du "réseau" demeure identique à celle déterminée dans l'état normal (ce problème sera discuté pour certains échantillons par la suite), il est possible de calculer la chaleur spécifique électronique $C_e = C_{totale} - \beta T^3$ aussi bien à l'état normal C_{en} qu'à l'état supraconducteur C_{es}.

En portant $C_e/T = f(T)$, figure 6, on peut étudier la transition supraconductrice. On observe une largeur de transition de quelques dixièmes de Kelvin due à l'inhomogénéité des échantillons (en particulier gradients de concentration), la température de transition T_c est alors déterminée par une loi des aires correspondant dans ce diagramme à un bilan entropique.

Le saut de chaleur spécifique à la transition $(\Delta C/\gamma T_c)$ est également déterminé au moyen de cette loi des aires.

A ce niveau de l'analyse, le critère de l'égalité de l'entropie à T_c des états normal et supraconducteur constitue un test de la validité de l'extrapolation en dessous de T_c des contributions électroniques et phononiques sous la forme γT et βT^3, telles qu'elles sont déterminées à l'état normal au-dessus de T_c. En supposant que le terme βT^3 est entièrement phononique, et donc qu'il n'est pas modifié entre l'état normal et l'état supraconducteur, l'égalité des entropies se réduit à celle des contributions électroniques

$$S_n(T_c) = S_s(T_c) \Rightarrow \int_0^{T_c} \frac{C_{en}}{T}\, dT = \int_0^{T_c} \frac{C_{es}}{T}\, dT$$

où C_{es} est déterminé expérimentalement au-dessous de T_c : $C_{es} = C_{totale} - \beta T^3$ et $C_{en} = \gamma_s T$ déterminé expérimentalement au-dessus de T_c est extrapolé au-dessous. Les deux déterminations sont en assez bon accord avec toutefois une valeur systématiquement plus forte pour $S_s(T_c)$. Cet accord conforte la validité des résultats expérimentaux ainsi que l'analyse de ces résultats à l'état normal. Nous reviendrons

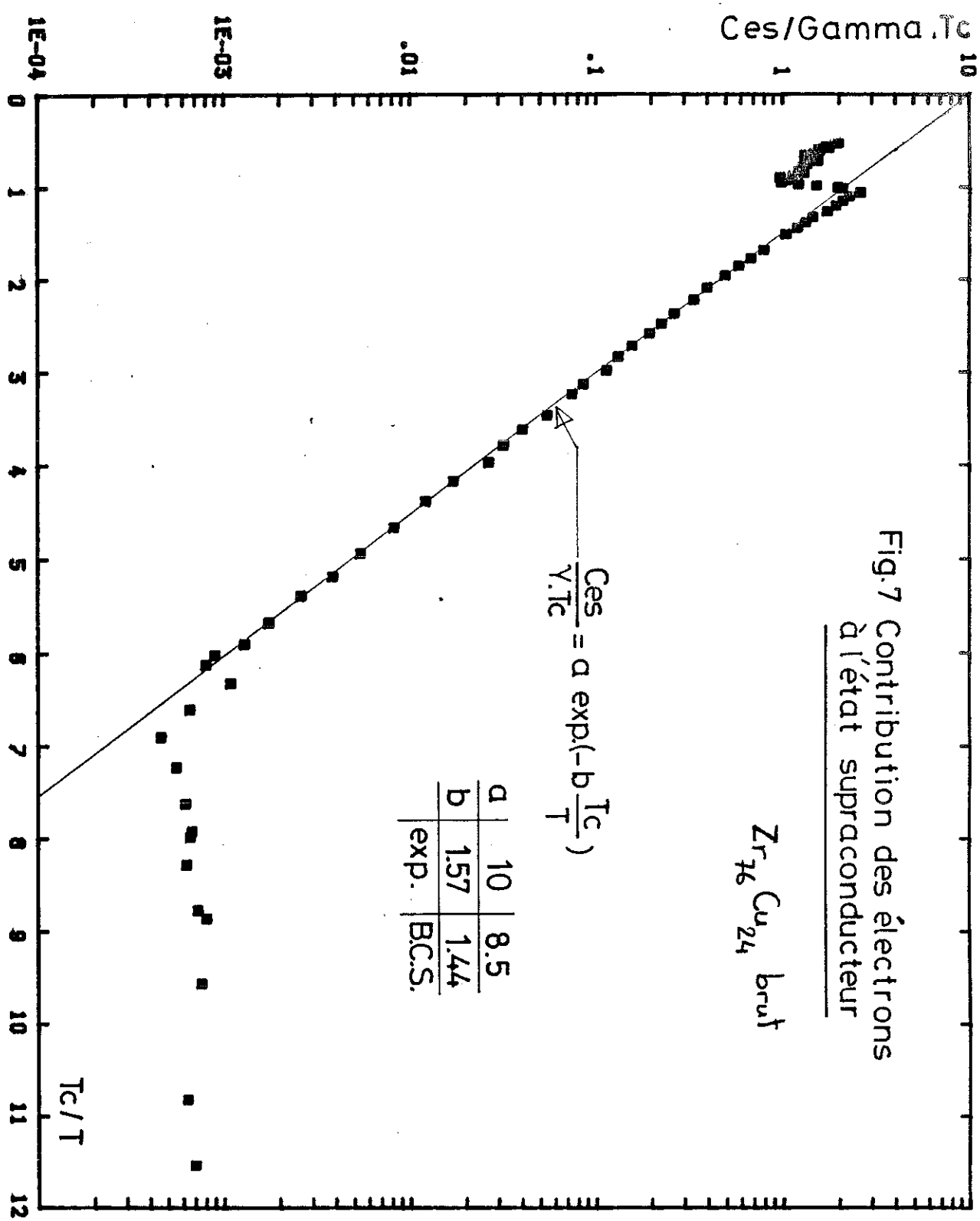

Fig.7 Contribution des électrons à l'état supraconducteur

dans le chapitre suivant et en annexe E sur cette analyse en discutant le problème d'un terme T^3 additionel éventuel.

Aux températures inférieures à T_c, la décroissance de la chaleur spécifique électronique supraconductrice s'écrit dans un modèle type BCS sous la forme

$$C_{es} \sim \gamma T_c \exp\left(-\frac{\Delta_o}{kT_c}\ \frac{T_c}{T}\right)$$

où $2\Delta_o$ est la largeur de bande interdite à T = 0 K. La figure 7 représente dans un diagramme semi-logarithmique Log $\frac{C_{es}}{\gamma T_c} = f(\frac{T_c}{T})$ les résultats expérimentaux. On constate pour $1 < \frac{T_c}{T} < 6$ un bon accord avec la loi théorique, la valeur de la pente semi-logarithmique variant d'un échantillon à l'autre autour de la valeur théorique du modèle BCS (1,44 dans cette gamme de température). Pour $\frac{T_c}{T} > 6$ la courbure observée met en évidence l'apparition de contributions supplémentaires à la chaleur spécifique totale.

Notons enfin qu'à partir des mesures de la chaleur spécifique électronique on peut déterminer le champ critique thermodynamique

$$H_c(T) = \left[\frac{8\pi}{V_M} \int_T^{T'} dT' \int_{T'}^{T_c} \frac{C_{es}(T'') - C_{en}(T'')}{T''} dT''\right]^{1/2} .$$

Ce champ critique $H_c(T)$ est une mesure quantitative de la différence d'énergie entre les états normaux et supraconducteurs, $H_c^2(0)/8\pi$ étant l'énergie de condensation. La comparaison de la variation thermique de ce champ critique avec la température à une variation quadratique en $(1 - (\frac{T}{T_c})^2)$ est un critère très sensible de l'intensité du couplage électron-phonon. Le calcul et l'analyse du champ critique sont développés pour certains échantillons dans les publications reproduites au chapitre suivant.

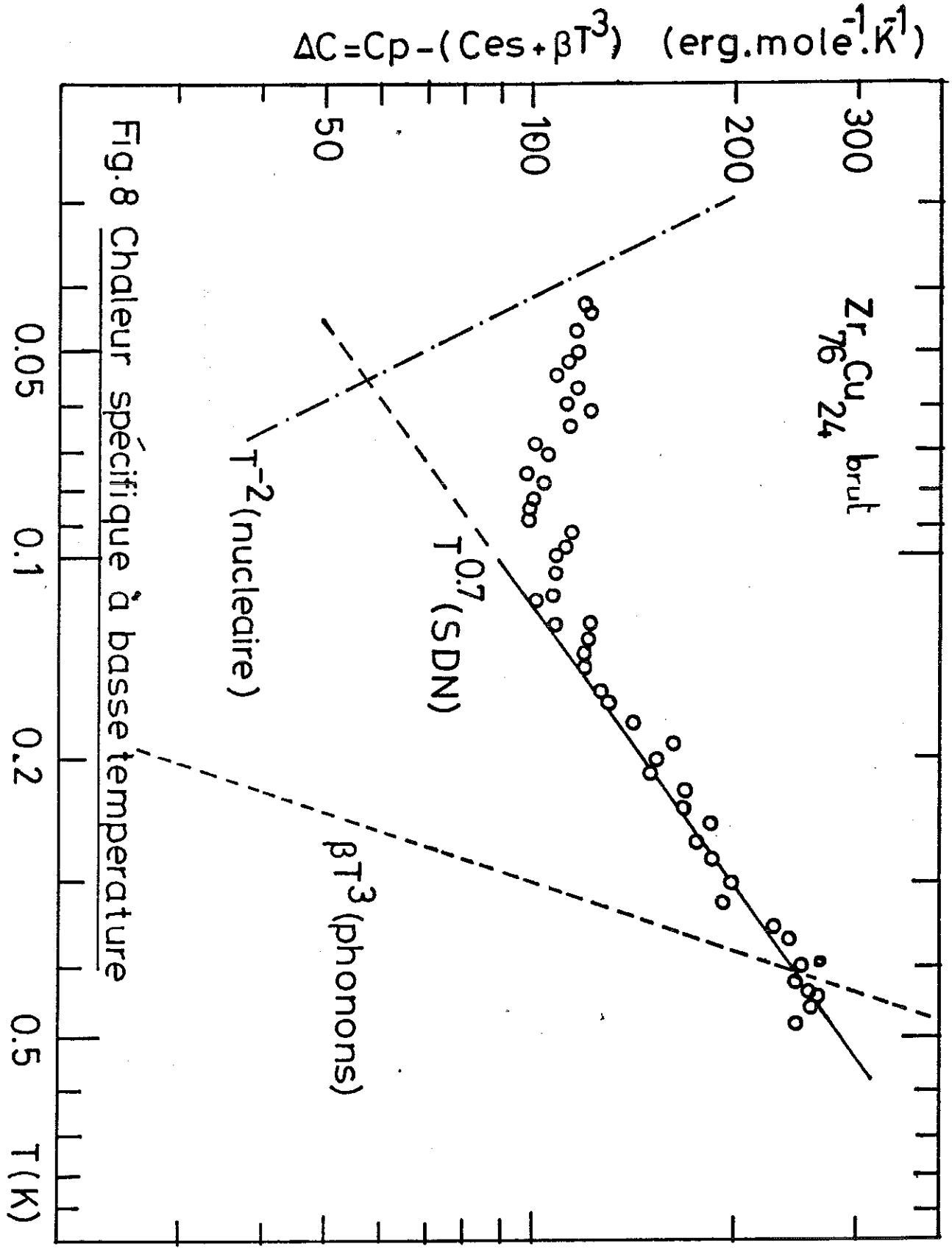

Fig.8 Chaleur spécifique à basse température

c. Chaleur spécifique à très basse température

Au-dessous d'environ 500 mK,si l'on retranche à la chaleur spécifique totale les contributions du réseau (βT^3) et des électrons supraconducteurs (C_{es} obtenu par extrapolation de la loi de décroissance exponentielle), il reste une contribution rapportée en figure 8. Comme expliqué dans le chapitre suivant, cet excès de chaleur spécifique est attribué aux excitations de basse énergie (SDN) caractéristiques de l'état amorphe et à la contribution quadrupolaire hyperfine des noyaux de Zirconium. Le choix du mode d'analyse pour déterminer les variations thermiques de ces deux contributions n'est pas unique. Nous aurions pu a priori fixer une variation linéaire en température de la chaleur spécifique des SDN comme suggéré par les modèles théoriques les plus simples. Cela conduit alors à une contribution résiduelle à très basse température difficilement exploitable physiquement. De plus des mesures antérieures (Lasjaunias et al., 1972 et 1975) ont montré que la variation thermique de la chaleur spécifique des TLS est rarement rigoureusement linéaire. Nous avons donc choisi d'extrapoler la loi de puissance T^{α} observée expérimentalement au-dessus de 100 mK et de l'affecter aux SDN. Une telle analyse conduit systématiquement à une contribution très basse température en T^{-2}, physiquement attribuée à des interactions nucléaires dues aux noyaux de Zirconium (^{91}Zr). La mise en évidence d'une corrélation entre les deux contributions ainsi analysées pour toute la série d'échantillons étudiés (Lasjaunias and Ravex, 1983) contribue a posteriori à justifier ce choix.

II - CONDUCTION THERMIQUE

1. Technique de mesure

La figure 9 représente le montage adopté pour les mesures de conduction thermique. Une demi-plaquette d'échantillon (4cm x 5 mm x 80 µm) est attachée à une extrémité sur un bloc de cuivre solidaire de la cage-écran (identique à celle utilisée en chaleur spécifique). Le thermomètre Th 1 pilote la régulation de cette cage et maintient donc une température constante au niveau du contact 1 . Un second contact 2 équipé d'un thermomètre Th2 permet la mesure du gradient thermique ΔT entre contacts. Deux mesures successives sont effectuées pour une même température de régulation T_1 en l'absence de chauffage puis en présence d'une puissance $\dot{Q}$ dissipée par une jauge de contrainte collée à l'extrémité libre de l'échantillon. Le gradient à vide est imposé par les apports de chaleur parasite $\dot{Q}_o$ du montage expérimental. Malgré d'excellentes performances cryogéniques ($\dot{Q}_o \simeq 10^{-10}$ à 10^{-9} Watt), la très grande résistance thermique des échantillons nous impose une température minimale de l'ordre de 100 mK. Il s'agit d'une méthode classique à deux chauffages, deux thermomètres ; un seul thermomètre sert à la détermination du gradient de température ce qui élimine les erreurs d'étalonnage liées à l'utilisation de deux thermomètres distincts. Une courbe expérimentale de conduction thermique ($K = R^{-1} = \frac{\dot{Q}}{\Delta T}$) est montrée en figure 10. Cette conduction étant très faible, il est indispensable de vérifier que la conduction par les fils d'amenée de courant au chauffage et de prise de tension aux thermomètres est négligeable. La conduction thermique de ces fils est essentiellement due à leur gaine de cupronickel (Cu-Ni) (Fairbank and Lee, 1960), l'âme supraconductrice (Nb-Ti) ayant une très faible conductivité. Les longueurs de fil utilisées nous permettent de calculer que seulement quelques pourcents de la puissance de chauffe est ainsi court-circuitée.

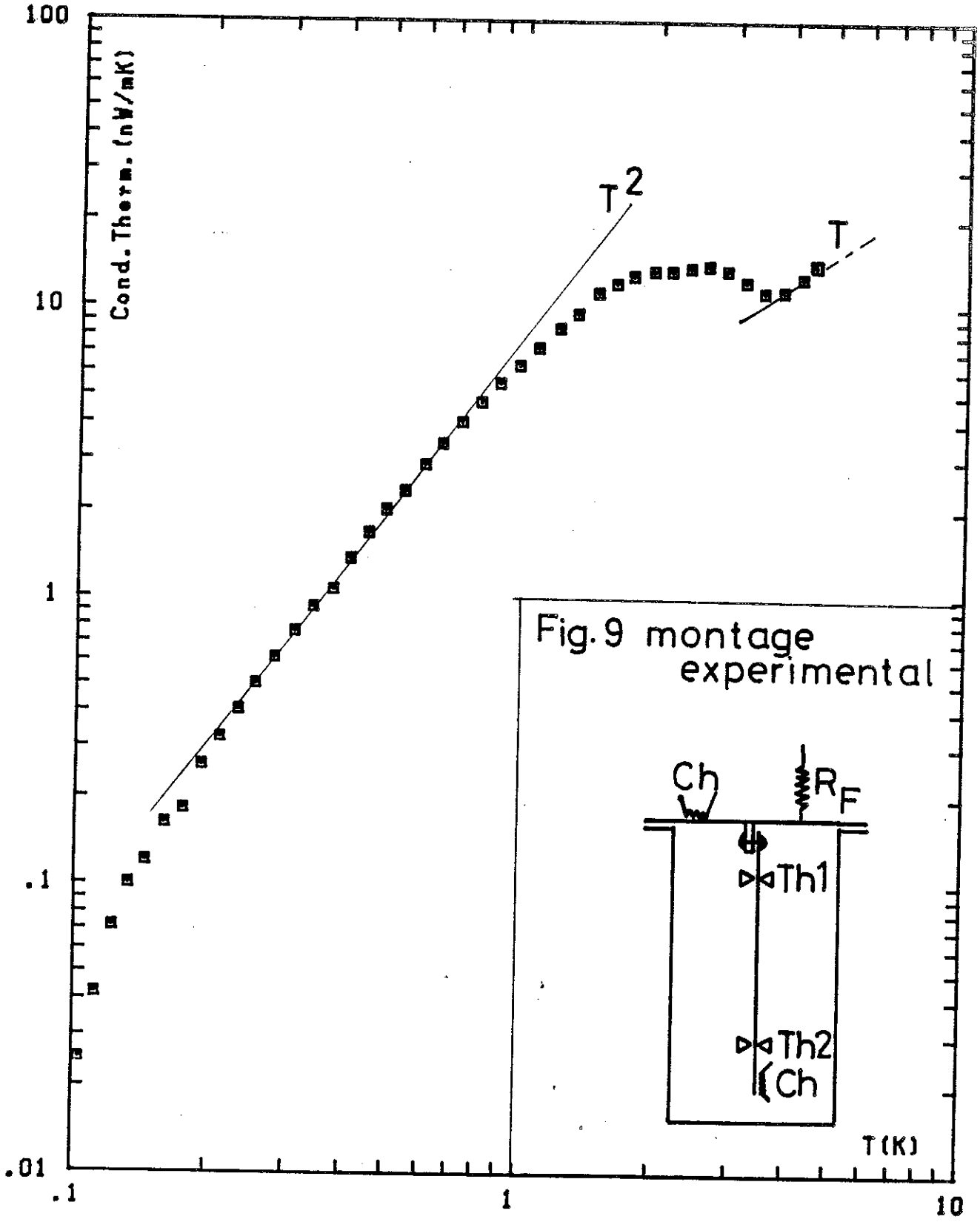

Fig.10 Conduction thermique

2. Analyse des résultats

Le principal problème pour le calcul de la conductibilité thermique k est la détermination du facteur géométrique de l'échantillon $\frac{s}{\ell}$ ($k = K \cdot \frac{\ell}{s}$). La distance ℓ entre contacts (de l'ordre de 20 mm) est déterminée à l'épaisseur près de ceux-ci ($\sim$ 0,5 mm). D'autre part la section s n'est pas constante au long de l'échantillon du fait même des variations d'épaisseur liées à la technique de pulvérisation. Nous avons déterminé pour chaque échantillon une section moyenne obtenue à partir de la mesure de sa masse et de sa densité en l'assimilant à un parallépipède. Il est donc clair que les valeurs absolues des conductibilités thermiques ne sont déterminées qu'à 10 % ou 15 % près. Etant principalement intéressés par les variations de cette grandeur sous l'effet de traitements thermiques, nous avons le plus souvent effectué les mesures sur le même échantillon afin d'éliminer l'incertitude liée au facteur géométrique. Ce point sera d'ailleurs précisé dans chaque cas lors de la discussion des résultats.

III - THERMOMETRIE

L'élément crucial de toute mesure thermique est évidemment la thermométrie. On demande en général à un thermomètre secondaire un certain nombre de qualités : sensibilité, reproductibilité et faible capacité calorifique (pour diminuer les temps de réponse et la contribution aux addenda). Les thermomètres au Silicium dopé au phosphore ou au bore par implantation ionique développés au laboratoire en collaboration avec le LETI remplissent ces conditions.

1. Sensibilité

La sensibilité de ces thermomètres (variation Résistance-Température) varie fortement avec les conditions d'implantation et de recuit (Bourgoin et al., 1979). A titre d'exemple est présentée en figure 11 la caractéristique R(T) du thermomètre utilisé pour les mesures de chaleur spécifique. La sensibilité de ces thermomètres est largement suffisante pour couvrir la gamme de température explorée (10 mK - 10 K), en particulier avec l'utilisation des ponts de mesure alternatifs à détection synchrone de grande sensibilité développés et utilisés au laboratoire.

2. Reproductibilité

Les thermomètres au silicium dopé sont utilisés depuis environ 7 ans. Ils ont été étalonnés au moins trois fois sur toute leur gamme d'utilisation suivant un processus décrit dans un paragraphe ci-après. En outre,après chaque mesure de chaleur spécifique,nous faisons quelques points d'étalonnage en fonction de la pression de vapeur saturante de l'hélium 4 (entre 1,3 K et le point lambda 2,19 K). Dans le cadre de ces contrôles systématiques les variations de la caractéristique R(T) n'ont jamais dépassé 2 à 3 °/₀₀, ce qui est excellent en comparaison des résistances au carbone.

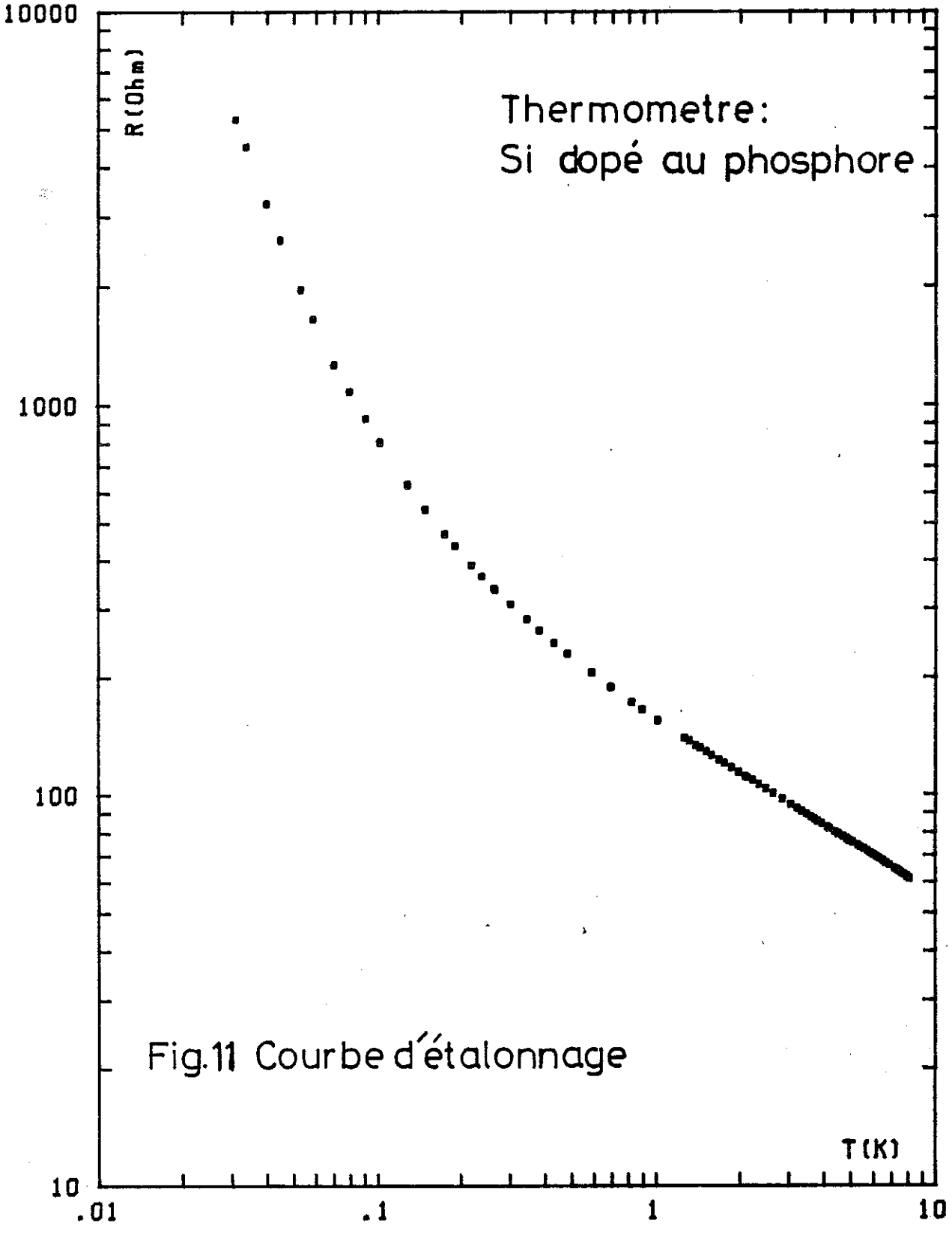

Fig.11 Courbe d'étalonnage

3. Capacité calorifique

Aucune mesure spécifique de la capacité calorifique des thermomètres au Silicium n'a été effectuée. Toutefois des recoupements de mesures d'addenda permettent de supposer que cette capacité calorifique est principalement gouvernée par la matrice de Silicium ($C \sim T^3$).

4. Etalonnages

Les thermomètres sont étalonnés périodiquement par rapport à un thermomètre primaire (monocristal de CMN). On établit dans un premier temps entre 10 mK et 2 K la relation R(M) entre la résistance du thermomètre et la susceptibilité du CMN mesurée par un pont de mutuelle inductance. Ensuite en introduisant du gaz d'échange dans le calorimètre et en mesurant la tension de vapeur du bain d'hélium on détermine la relation R(T) (tables NBS T-76 ^{4}He) entre 1,2 et 4,2 K. La loi M(T) n'est pas directement établie pour éliminer l'effet éventuel d'un léger paramagnétisme dû au calorimètre. A partir des mesures R(M) et R(T) on calcule la loi de Curie du thermomètre primaire ($M = A/T + B$) par moindres carrés entre 1,2 et 2 K. Par extrapolation de cette loi jusqu'à 10 mK on établit la loi d'étalonnage R(T).

Entre 4,2 K et 8 K les thermomètres sont étalonnés par rapport à un thermomètre de Germanium lui-même étalonné par ailleurs au laboratoire. Lors de cet étalonnage la loi du thermomètre Germanium est contrôlée entre 1,2 et 2 K par rapport à la tension de vapeur de l'hélium, puis un point fixe (transition supraconductrice du Plomb : $T_c = 7,20$ K) sert de contrôle à haute température.

Pour le dépouillement des mesures, les courbes d'étalonnage R(T) sont approximées par moindres carrés au moyen de lois paraboliques de la forme $\log R = a(\log T)^2 + b\log T + c$. La précision de cette loi, sur des tranches de température correspondant à 7 points d'étalonnage, atteint la dispersion expérimentale de nos étalonnages soit environ quelques 10^{-3} au-dessous de 50 mK et mieux que 10^{-4} jusqu'à 8 K. Les valeurs des coefficients a,b,c, pour la gamme de température couverte et le thermomètre utilisé pour les mesures de ce mémoire sont rapportées en Annexe C.

- BOURGOIN J.C., FROSSATI G. , RAVEX A., THOULOUZE D., VANDORPE M., WAKSMANN B., Phys. Stat. Sol. (b) 92, 1068 (1979).
- FAIRBANK H.A. and LEE D.M., Rev. Sci. Instr. 31, 660 (1960).
- FROSSATI G., IMBERT D., PECCOUD D., THOULOUZE D., WAKSMANN B., Int. Conf. on "Low Temp. Physics LT 14", Helsinki (1975).
- GANDIT Ph., Thèse Docteur-Ingénieur, Grenoble (1983).
- HO J.C., PHILLIPS N.E., Rev. Sci. Instr. 36, 1382 (1965).
- KEYSTONE J.R.G., LACAZE A., THOULOUZE D., Cryogenics 8, 265 (1968).
- LASJAUNIAS J.C. and RAVEX A., J. Phys. F : Met. Phys. 13, L101 (1983).
- LASJAUNIAS J.C., PICOT B., RAVEX A., THOULOUZE D., VANDORPE M., Cryogenics (Feb. 1977), 111.
- LASJAUNIAS J.C., RAVEX A., VANDORPE M., HUNKLINGER S., Solid State Comm. 17, 1045 (1975).
- LASJAUNIAS J.C., MAYNARD R., THOULOUZE D., Solid State Comm. 10, 215 (1972).
- RAVEX A., Thèse Docteur Ingénieur, Grenoble (1976).

C H A P I T R E III

ANALYSE DES RESULTATS : PROPRIETES ELECTRONIQUES ET SUPRACONDUCTRICES - EXCITATIONS DE BASSE ENERGIE (TLS)

Dans ce chapitre, nous présentons et analysons les résultats de chaleur spécifique et de conduction thermique des alliages bruts de pulvérisation.

Les effets de recuit ou de vieillissement à température ambiante seront analysés dans le chapitre suivant.

L'étude des propriétés physiques développées ici reprend le plan utilisé lors de la présentation des méthodes expérimentales au chapitre précédent :

- propriétés à l'état normal ($T > T_c$) : densité d'état électronique, température de Debye ;

- propriétés supraconductrices ($T \leqslant T_c$) : intensité du couplage électron-phonon ;

- propriétés à très basse température ($T \ll T_c$) : excitations de basse énergie - densité d'état, couplage aux noyaux, couplage aux phonons.

I - ETAT NORMAL - DENSITE D'ETAT ELECTRONIQUE - TEMPERATURE DE DEBYE

L'analyse des résultats expérimentaux exposée au chapitre précédent ($C/T = f(T^2)$) a montré qu'au-dessus de T_c et jusqu'à environ 8 K (température limite supérieure de nos mesures),on peut définir deux contributions à la chaleur spécifique. L'une cubique en température peut être attribuée aux phonons (C_{ph}), l'autre linéaire aux électrons de conduction (C_{en}) ainsi :

$$C_{totale} = C_{ph} + C_{en} = \beta T^3 + \gamma T$$

Température de Debye :

L'observation de la contribution cubique βT^3 invite à utiliser le modèle de Debye qui permet d'exprimer le coefficient β en fonction de la température de Debye θ_D ou de la vitesse du son :

$$\beta = \frac{12}{5} R \pi^4 \frac{1}{\theta_D^3} \quad (J\ mole^{-1}\ K^{-4})$$

avec

$$\frac{1}{\theta_D^3} \alpha \frac{1}{\rho} \left(\frac{1}{V_\ell^3} + \frac{2}{V_t^3}\right) \quad , \quad \rho = \text{densité}$$

L'observation de la loi et l'utilisation du modèle de Debye pour décrire une contribution de "réseau" peuvent paraître surprenantes dans le cas d'un matériau amorphe. Ceci d'autant plus qu'il n'a jamais été observé une pure loi en T^3 dans le cas des isolants amorphes pour lesquels un excès systématique de chaleur spécifique apparaît par rapport aux valeurs calculées à partir des mesures de vitesse du son. Les coefficients β et les températures de Debye θ_D correspondantes sont rassemblées dans le tableau 1 ci-joint.

Pour certains de nos échantillons l'analyse des résultats à basse température (notamment entre 300 et 500 mK) nécessite d'utiliser comme contribution des "phonons" des valeurs inférieures à celles obtenues en extrapolant la loi βT^3 déterminée au-dessus de T_c qui contient probablement des excitations non propagatives. Nous verrons lors de la discussion des propriétés supraconductrices qu'une partie du terme en T^3 pourrait être d'origine électronique et disparaître à l'état supraconducteur (voir également Annexe E).

Il n'existe actuellement qu'un seul échantillon ($Zr_{40}Cu_{60}$ trempé du liquide) pour lequel existent à la fois des mesures acoustiques (Arnold et al., 1982) et calorimétriques (Garoche et al., 1980) permettant une double détermination de la température de Debye θ_D. Les mesures de vitesse du son ($V_\ell = 4{,}3 \cdot 10^5$ cm/sec et $V_T = 2{,}1 \cdot 10^5$ cm/sec) conduisent à une valeur ($\theta_D = 272$ K) nettement plus forte que celle tirée du coefficient de chaleur spécifique ($\theta_D = 230$ K). En l'absence d'autres

résultats de vitesse du son qui permettraient de systématiser cette comparaison, nous analysons nos résultats, en utilisant des valeurs de températures de Debye calculées à partir de nos mesures de chaleur spécifique comme cela a d'ailleurs été fait de façon systématique par d'autres auteurs pour les alliages correspondants obtenus par trempe du liquide.

Les températures de Debye observées sont systématiquement plus faibles que celles déterminées pour le Zirconium cristallin ou pour des alliages cristallisés (Garoche et al., 1983). L'effet de l'amorphisation sur les propriétés élastiques semble d'ailleurs plus important sur nos échantillons pulvérisés que sur les alliages trempés du liquide (Garoche et al., Samwer et al., 1982, Kroeger et al., 1983). Par exemple pour un alliage $Zr_{\sim 75}Cu_{\sim 25}$ on obtient les températures de Debye suivantes : pulvérisé : 155 K , trempé du liquide : 189 K , cristallisé : 315 K. Un modèle théorique de liaisons fortes (Cyrot-Lackmann, 1980) explique semi-quantitativement pour les métaux de transition les variations de propriétés élastiques ainsi observées. La diminution de θ_D s'explique principalement par la réduction de la vitesse transverse des ondes acoustiques V_t simplement reliée au module de cisaillement μ ($V_t = \sqrt{\mu/\rho}$). Comme les variations de densité ρ ne sont que de l'ordre du pourcent, les variations de vitesse transverse dépendent directement de celles du module de cisaillement. En l'absence d'information sur les arrangements atomiques, une estimation moyenne des fréquences de vibrations supposant que tous les sites atomiques sont plus ou moins équivalents conduit à une diminution de l'ordre de 10 % de la température de Debye à l'état amorphe. L'écart avec les réductions observées expérimentalement (dê l'ordre de 35 % pour les alliages trempés du liquide et 50 % pour nos alliages pulvérisés) peut s'expliquer par le fait que dans la réalité les fluctuations de densité et les régions "molles" rencontrées dans le matériau peuvent localement diminuer fortement le module de cisaillement.

ZrAg	ZrNi (300K)	ZrNi (77K)	ZrNi recuit	ZrCu	ZrCu recuit	ZrCu vieilli	ZrCu vielli + recuit	ZrPt	ZrFe	ZrMo	Zr cristal-lisé	échantillon
0,55	0,474	0,492	0,350	0,531	0,395	0,471	0,357	0,668	0,351	0,58		β (mJ/mole K^4)
152	160	158	177	154	170	161	176	144	177	150	291*	θ_D(K)
4,7	6,95	7,80	5,80	6,20	5,00	5,54	5,53	5,57	8,67	7,20	3,0	γ_N (mJ/mole K^2)
1,99	2,95	3,30	2,46	2,63	2,12	2,35	2,34	2,36	3,68	3,05	1,27	$N_\gamma(E_F)$ états $eV^{-1}atom^{-1}$
5,7	7,17	8,26	6,24	6,60	5,44	5,90	5,60	6,28	supra	7,36	analyse	γ_s (mJ/mole K^2)
17,5	3	5,5	7	6	8	6	1,5	11	non obser-vée	2	non effec-tuée	$\Delta\gamma/\gamma$ (%) $= \frac{\gamma_S - \gamma_N}{\gamma_N}$

Tableau 1 - Propriétés à l'état normal - température de Debye - densité d'état électronique.

* Valeur mesurée par Gschneider (1964) et Collings and Ho (1971)

Densité d'état électronique :

A partir du coefficient γ de la contribution linéaire à la chaleur spécifique au-dessus de T_c attribuée aux électrons de conduction, on peut calculer la densité d'états électroniques au niveau de Fermi $N_\gamma(E_F)$. Dans un modèle d'électrons indépendants on a la relation

$$N_\gamma(E_F) = 3\pi^{-2}\, k_B^{-2}\gamma \qquad \gamma(\text{mJ/mole K}^2)$$

La densité d'états $N_\gamma(E_F)$ ainsi calculée et exprimée en états eV^{-1} $atom^{-1}$ est amplifiée par rapport à la densité d'état "nue" N_o calculée dans le modèle de l'électron libre par les interactions électron-phonon. En négligeant d'autres interactions éventuelles (telles que fluctuations de spin par exemple), on peut écrire

$$N_\gamma(E_F) = N_o(1 + \lambda)$$

La constante de couplage électron-phonon λ sera déterminée ultérieurement à partir des températures critiques de transition supraconductrice (T_c) et de Debye (θ_D) dans le cadre de la formulation de McMillan. Nous avons reporté dans le tableau 1 les valeurs de γ_N (déterminées pour $T \geqslant T_c$ par l'analyse $C_{totale} = \beta T^3 + \gamma_N T$) ainsi que les valeurs de densité d'état électronique "habillée" $N_\gamma(E_F)$ que l'on en déduit.

Comme nous l'avons vu au chapitre précédent, la détermination de l'entropie à T_c dans les deux états normal et supraconducteur est en fait un test de l'analyse effectuée au-dessus de T_c ($\gamma T + \beta T^3$). Nous avons donc également reporté dans le tableau 1 la valeur de γ déterminée à partir de l'entropie dans l'état supraconducteur

$$\gamma_s = \frac{S_s(T_c)}{T_c} = \frac{1}{T_c}\int_0^{T_c} \frac{C_{totale} - \beta T^3}{T}\, dT$$

ainsi que l'écart relatif entre les deux déterminations $\frac{\Delta\gamma}{\gamma} = \frac{\gamma_s - \gamma_N}{\gamma_N}$.
Dans la majorité des cas l'accord est bon ($5\ \% < \frac{\Delta\gamma}{\gamma} \leq 10\ \%$) sinon excellent (ZrMo (2 %) ; ZrCu vieilli et recuit (1,5 %)) à l'exception de l'échantillon ZrAg.

Toutefois on constate que la valeur déterminée à l'état supraconducteur γ_S est systématiquement plus élevée de celle obtenue à l'état normal γ_N. Notons que la contribution résiduelle due aux systèmes à deux niveaux est totalement négligeable dans ce calcul et ne peut donc pas justifier cet écart systématique. Par contre, ainsi que cela sera discuté au chapitre suivant (Ravex et al., 1983), il apparaît que le terme βT^3 attribué aux phonons présente une valeur trop forte pour l'analyse à plus basse température ($T \simeq 0,5$ K). Il n'est donc pas exclu qu'une partie de cette contribution soit d'origine électronique et disparaisse progressivement dans l'état supraconducteur en même temps que la contribution électronique correspondant au terme γ_N. En l'absence d'expériences sous champ magnétique nous ne pouvons confirmer l'existence d'un tel terme en dessous de T_c à l'état normal, ni donc prévoir dans quelles proportions sera modifié l'écart des entropies. Ainsi que nous le discutons dans la suite, la présence d'un terme électronique en T^3 permet une analyse des propriétés supraconductrices en meilleur accord avec la théorie BCS (voir Annexe E).

II - PROPRIETES SUPRACONDUCTRICES - COUPLAGE ELECTRON-PHONON

L'analyse des résultats expérimentaux à la transition supraconductrice permet de déterminer le saut relatif de chaleur spécifique électronique $\frac{C_{es}(T_c) - C_{en}(T_c)}{C_{en}(T_c)}$ (C_{es} chaleur spécifique électronique à l'état supraconducteur, C_{en} à l'état normal). Les valeurs obtenues pour cette discontinuité de chaleur spécifique (souvent notée $\frac{\Delta C}{\gamma T_c}$) sont données dans le tableau 2.

Tableau 2 - Propriétés supraconductrices

Echantillon	ZrAg	ZrNi 300K	ZrNi 77K	ZrCu	ZrPt	ZrMo	BCS
T_c(K)	1,76	3,22	3,17	3,45	2,91	4,28	
$\Delta C/\gamma T_c$ (± 0,05)	1,75	1,70	1,75	1,90	1,85	2,10	1,43
a (± 0,5)	11	9,5	8,5	10	11	8,5	8,5
b (± 0,02)	1,44	1,51	1,43	1,57	1,51	1,51	1,44

Ces valeurs expérimentales sont proches de la valeur théorique du modèle B.C.S. (1,43) pour des supraconducteurs à couplage faible. Ce même modèle prévoit une décroissance exponentielle de la chaleur spécifique électronique au-dessous de T_c exprimée sous la forme

$$\frac{C_{es}}{\gamma T_c} = \frac{3}{2\pi^2} \left(\frac{\Delta}{k_B T_c}\right)^3 \left(\frac{T_c}{T}\right)^2 \left[3K_1 \left(\frac{\Delta}{k_B T}\right) + K_2 \left(\frac{\Delta}{k_B T}\right)\right]$$

où Δ représente la bande interdite et K_1, K_3 les fonctions de Bessel modifiées de deuxième espèce. Dans la limite $\frac{\Delta}{kT} \gg 1$, plus précisément pour $2{,}5 < \frac{T_c}{T} < 6$, cette expression est bien approximée par une loi du type

$$\frac{C_{es}}{\gamma T_c} = a \exp(-b \frac{T_c}{T}) \qquad \text{avec} \quad a = 8{,}5 \quad \text{et} \quad b = 1{,}44$$

L'analyse des résultats expérimentaux dans un diagramme semi-logarithmique $\text{Log} \frac{C_{es}}{\gamma T_c} = f(T_c/T)$ (comme exposé au chapitre précédent) a permis de déterminer les coefficients a et b rapportés dans le tableau 2. Les valeurs obtenues par cette analyse confirment la tendance indiquée par la discontinuité de chaleur spécifique : les alliages étudiés ont un comportement compatible avec les hypothèses du modèle BCS. Ils peuvent être qualifiés de supraconducteurs à couplage faible ou intermédiaire (cas de ZrMo).

Dans le cas des alliages $Zr_{76}Cu_{24}$ et $Zr_{76}Ni_{24}$, l'analyse du champ critique thermodynamique $H_c(T)$ et de sa fonction déviation par rapport à une loi parabolique, qui est un critère très sensible pour la détermination du couplage, confirment un très bon accord avec la théorie BCS (Laborde et al., 1984). Les résultats sont présentés en même temps que les effets de recuit dans le chapitre suivant. La même analyse pour ZrMo (Lasjaunias et al., 1985) conduit à un couplage intermédiaire.

Cet accord avec le modèle BCS nous a conduit à une analyse nouvelle des résultats expérimentaux(développée en Annexe E) qui permet de déterminer la contribution des phonons au-dessous de T_c. Cette contribution apparaît plus faible que celle obtenue au-dessus de T_c. Cette nouvelle analyse confirme l'éventualité d'une contribution cubique supplémentaire à la chaleur spécifique électronique.

Couplage électron-phonon :

Dans le cadre de la théorie de BCS, la température de transition T_c peut être calculée en fonction de la densité d'état au niveau de Fermi N_o, d'une fréquence moyenne des phonons $< \omega >$(par exemple la fréquence de Debye ω_D) et du potentiel d'interaction électron-phonon V

$$T_c = 1{,}14 < \omega > \exp(-1/N_o V)$$

L'introduction par Eliashberg (1960) de l'interaction coulombienne électron-électron et d'un traitement plus précis de l'interaction électron-phonon valable même pour les couplages forts a conduit à une expression analogue à la précédente

$$T_c = \omega_o \exp\left(\frac{-(1 + \lambda)}{\lambda - \mu^*(<\omega> / \omega_o)\lambda\mu^*}\right)$$

Dans la limite des couplages faibles $\lambda \ll 1$ cette expression se réduit à celle de BCS, $\lambda - \mu^*$ jouant le rôle de $N_o V$; ω_o est la fréquence maximum du spectre de phonon. La constante de couplage électron-phonon est définie par

$$\lambda = 2 \int_0^{\omega_o} \alpha^2(\omega) F(\omega) \frac{d\omega}{\omega} \quad ,$$

$F(\omega)$ étant la densité d'état des phonons et $\alpha^2(\omega)$ une moyenne de l'interaction électron-phonon.

En l'absence de mesures de tunneling, la quantité $\alpha^2(\omega).F(\omega)$ n'étant pas connue, l'expression numérique obtenue par McMillan (1968) à partir de données expérimentales relatives au Niobium et à des alliages de métaux de transition constitue le seul moyen de relier T_c et λ :

$$T_c = \frac{\theta_D}{1.45} \exp\left(- \frac{1{,}04(1 + \lambda)}{\lambda - \mu^*(1 + 0{,}62\ \lambda)}\right)$$

En prenant pour la constante de couplage coulombien $\mu^* = 0{,}13$, valeur préconisée par McMillan pour les métaux de transition, on tire pour la série d'alliages étudiés les valeurs de la constante du couplage électron-phonon λ (tableau 3).

Tableau 3 - Couplage électron-phonon ; densité d'état"nue"

Echantillon	ZrAg	ZrNi 300K	ZrNi 77K	ZrCu	ZrPt	ZrMo	Zr cristal-lisé
$\lambda_{McMillan}$	0,58	0,69	0,68	0,70	0,68	0,77	0,41
N_o (états eV^{-1} at^{-1})	1,26	1,75	1,97	1,55	1,40	1,72	0,84

Les valeurs de λ obtenues correspondent bien à des couplages faibles ou intermédiaires comme prévu précédemment.

La densité d'état électronique nue N_o (densité d'état de structure de bande) peut donc être obtenue à partir de γ et λ (tableau 3) :

$$N_o(E_f) = 3\gamma/\pi^2 k_B^2(1 + \lambda)$$

Varma et Dynes (1976) ont montré à partir de relations empiriques entre les paramètres déterminant la supraconductivité que pour une même série d'alliages de métaux de transition la constante de couplage électron-phonon ne dépendait que de la densité d'état électronique au niveau de Fermi N_o. Ils ont établi empiriquement que dans l'expression de cette constante de couplage,

$$\lambda = \frac{N_o < I^2 >}{M < \omega^2 >}$$

- N_o densité d'état électronique au niveau de Fermi.
- $< I^2 >$ moyenne du carré de l'élément de matrice d'interaction électron-phonon.
- $< \omega^2 >$ moyenne du carré des fréquences de phonon.

le terme $\frac{< I^2 >}{M < \omega^2 >}$ est quasiment constant si bien qu'il existe une relation linéaire entre λ et N_o : $\lambda = \delta N_o$.

Tenhover et Johnson (1982) ont étendu cette corrélation à des alliages amorphes de Zirconium et de métaux de transition 3d ou 4d ($Zr_{70}X_{30}$) de composition proche de nos échantillons. En figure 1 nous portons les points représentatifs de nos alliages de Zirconium sur le diagramme établi par Varma et Dynes pour les métaux et alliages cristallins 4d et utilisé également par Tenhover et Johnson.

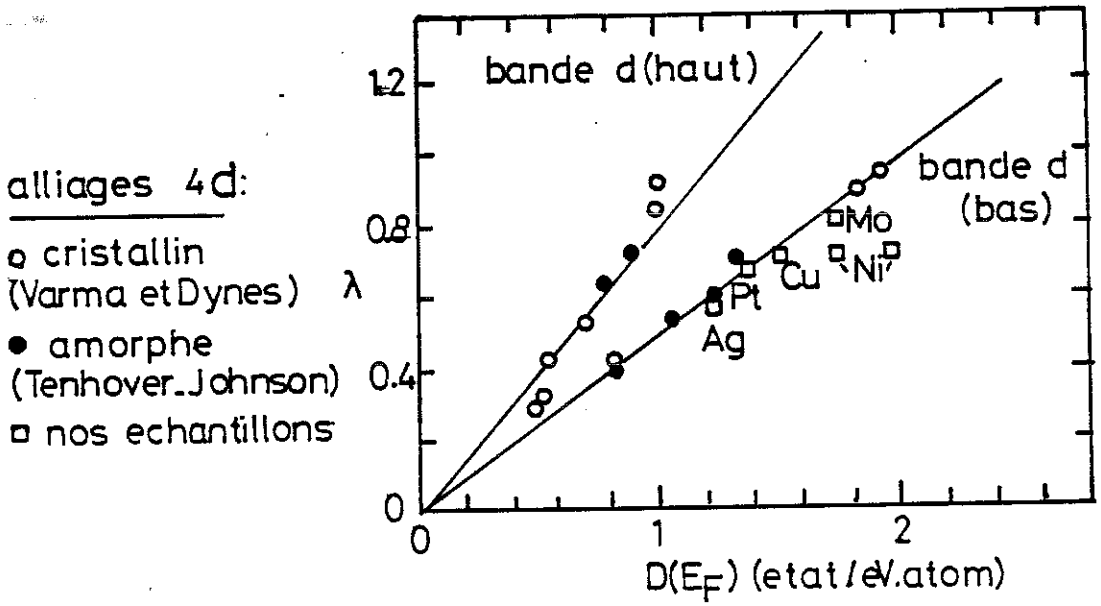

Fig 1. couplage electron_phonon (λ) fonction de la densite d'états au niveau de Fermi

Le bon accord de nos résultats expérimentaux avec la ligne de corrélation établie pour les métaux de transition 4d dont le niveau de Fermi se situe dans la partie inférieure de la bande d montre que l'intensité du couplage des alliages étudiés est déterminée principalement par les propriétés électroniques elles-mêmes largement influencées par le Zirconium. La structure électronique de l'élément d'addition (3d : Ni et Cu, 4d : Mo et Ag, 5d : Pt) ne semble pas déterminant. Ce résultat est en bon accord avec les mesures existantes de spectres de photoémission sur des alliages amorphes de Zirconium de compositions proches des nôtres (Amamou et al., 1978 ; Oelhafen et al., 1979 et 1980),

qui montrent que la structure électronique au voisinage du niveau de Fermi est principalement déterminée par la bande d du Zirconium pour les alliages ZrCu, ZrNi et ZrPt. Aucune donnée expérimentale n'existe pour les alliages ZrAg et ZrMo. D'après les mesures d'Oelhafen et al. (1980) qui ont étudié l'effet du nombre d'électrons de conduction et de la série de l'élément d'addition on peut prévoir que la situation sera identique pour ZrAg. Par contre dans le cas de ZrMo les deux pics 4d de chaque élément se confondent probablement en un seul pic unique (Tenhover-Johnson, 1983) et dans ce cas la densité électronique de Mo doit être aussi déterminante.

D'autres auteurs ont étudié les effets de composition sur des séries a-Zr_xCu_{1-x} (von Minnigerode and Samwer, 1981 ; Samwer and v. Löhneysen, 1982) ou a-Zr_xNi_{1-x} (Onn et al., 1983) avec $0,5 < x < 0,75$. Globalement les propriétés supraconductrices observées entraient parfaitement dans la corrélation λ - N_o établie ci-dessus : la supraconductivité est déterminée essentiellement par le Zirconium. Une analyse plus fine montre quelques différences de comportements dans la dépendance en composition des propriétés supraconductrices entre les deux systèmes qui peuvent être expliquées par des différences de structure de bande observées en photoémission.

Dans tous les cas où la comparaison est possible ($Zr_{76}Cu_{24}$, $Zr_{76}Ni_{24}$, $Zr_{76}Fe_{24}$), les densités d'états N_o de nos alliages pulvérisés sont supérieures de 20 % environ à celle de l'alliage correspondant obtenu par trempe du liquide. D'autre part, l'effet d'un traitement thermique est de réduire N_o, rapprochant sa valeur de celle de l'alliage trempé (voir chapitre suivant).

Ci-après nous rapportons un travail sur $Zr_{70}Mo_{30}$. Cet alliage présente un couplage supraconducteur plus fort que les alliages ZrNi et ZrCu qui seront analysés au chapitre suivant.

Solid State Communications, Vol. 54, No. 9, pp. 835–838, 1985
Printed in Great Britain.

0038–1098/85 $3.00 + .00
Pergamon Press Ltd.

SUPERCONDUCTING PROPERTIES OF AMORPHOUS SPUTTERED $Zr_{70}Mo_{30}$

J.C. Lasjaunias, O. Laborde*, A. Ravex and F. Zougmore

Centre de Recherches sur les Très Basses Températures, C.N.R.S., B.P. 166X,
38042 Grenoble-Cédex, France

(*Received* 26 *January* 1985 *by E.F. Bertaut*)

Specific heat, resistivity and critical superconducting fields (H_c and H_{c_2}) measurements show that amorphous $Zr_{70}Mo_{30}$ is an intermediate superconductor ($T_c = 4.3$ K; $\lambda = 0.77$). The coupling strength is mainly governed by the electronic properties. Like in the Zr–3*d* alloys previously investigated, a discrepancy between the measured and calculated upper critical field slope is reported. The effect of two-level systems (TLS) needs to be clarified.

INTRODUCTION

WE REPORT SYSTEMATIC low-temperature calorimetric, resistive and superconductive measurements on an amorphous $Zr_{70}Mo_{30}$ alloy prepared by sputtering. A similar study was previously done on several Zr–3*d* alloys (mainly on Zr–Cu and Zr–Ni) and appeared to be very fruitful [1, 2]. To our knowledge, it is the first time that such a work is achieved on the amorphous Zr–Mo system; T_c data were reported for amorphous films evaporated at 4.2 K [3], but samples of this system prepared by fast quenching from the melt were reported to be crystalline [4]. This system is *a priori* more simple than the Zr–3*d* alloys since it is composed of two neighbouring 4*d* metallic elements, what leads to a different electronic structure [5]. The superconducting transition temperature T_c is 4.28 ± 0.05 K from calorimetric measurements, and 4.35 ± 0.007 K from resistive ones: it follows the Collver–Hammond law where T_c is only a function of the number of electrons per atom [3]; on the contrary, T_c data for ZrCu or ZrNi are at variance with the Collver–Hammond curve [6].

EXPERIMENTAL

Full details concerning the preparation and characterization of samples and the experimental techniques will be found elsewhere [7]. The alloy was prepared by a high-rate (12 μm h^{-1}) sputtering technique [8]. Amorphicity was checked by X-ray analysis; the first diffraction halo is located at $q_p = 2.58$ Å^{-1}. Density is 7.40 ± 0.07 g cm^{-3}. Differential thermal analysis shows no indication for recrystallization up to 900 K. The transition widths ΔT_c defined as usually are respectively 100 mK and 14 mK from calorimetric and resistive determinations. Both are narrow (much more than for sputtered Zr–Cu and Zr–Ni), what is often referred as a criterion of good homogeneity. Specific heat (C_p) and resistive (ρ) measurements were performed on the same sample.

THERMODYNAMIC PROPERTIES

The specific heat data analysis is similar to that previously described for other Zr-based alloys [7, 9]. Below 0.6 K, C_p is dominated by low-energy excitations that we ascribe to two-level systems (TLS), like for the other Zr-based alloys of this series (Fig. 1). Similarly to the other "as-sputtered" samples [9] C_{TLS} varies as $T^{0.5}$; but the absolute value is about two times larger than in $Zr_{76}Ni_{24}$ (see figure) which already exhibits the largest TLS signal among this class of alloys prepared either by sputtering or melt-spinning [2].

Between T_c and 7 K, the highest temperature of measurements, C_p obeys the usual $\gamma T + \beta T^3$ law. The

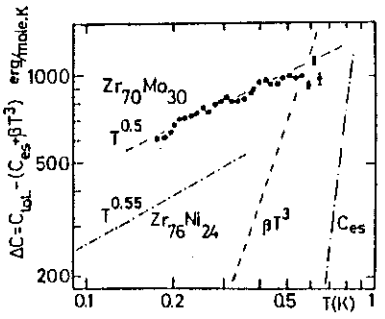

Fig. 1. Residual specific heat anomaly due to TLS excitations in sputtered $Zr_{70}Mo_{30}$ and $Zr_{76}Ni_{24}$. βT^3 and C_{es} refer to phonon and electronic contributions for $Zr_{70}Mo_{30}$.

*Also: Service National des Champs Intenses, same address.

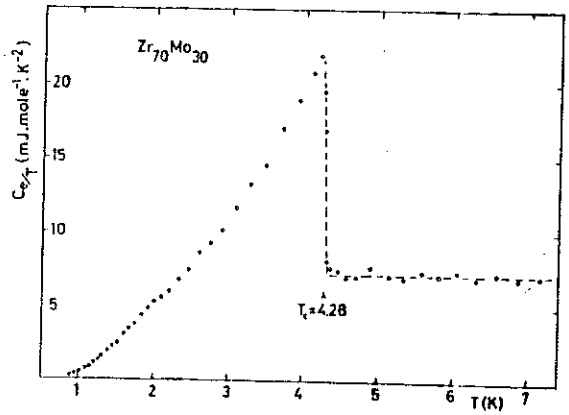

Fig. 2. Electronic specific heat plotted as C_e/T against T.

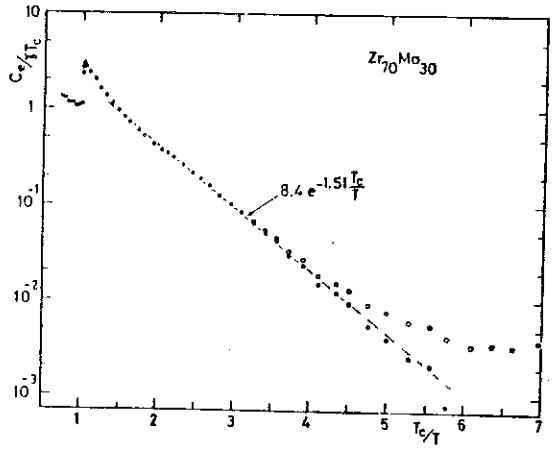

Fig. 3. $C_e/\gamma T_c$ versus T_c/T. Specific heat including the TLS excitations (○); and after subtracting this contribution (●).

electronic contribution obtained after subtracting the phonon term βT^3, is shown in the whole temperature range in Fig. 2. Using the criterion of equalization of entropy $S_n(T_c) = S_s(T_c)$ for both normal and superconducting states below T_c, we determine a value of C_{en}/T below T_c which agrees to 2% with γ determined above T_c. The different thermodynamic parameters such as the electronic density of states at the Fermi level, the Debye temperature, are collected in Table 1.

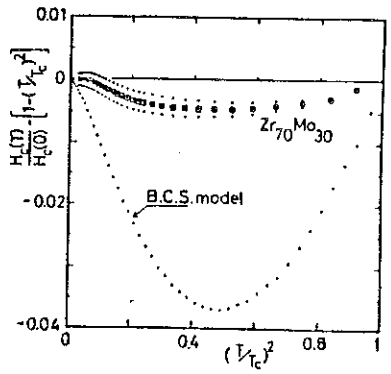

Fig. 4. Deviation function for the thermodynamic critical field H_c. Error bars result from the indetermination on the limit of integration related to the width of T_c.

The reduced specific heat jump at T_c, $(\Delta C/\gamma T_c) = 2.12$, a value larger than the B.C.S. one (1.43) expected for a weak-coupling superconductor. In Fig. 3, the electronic specific heat plotted as $\log C_e/\gamma T_c$ versus T_c/T shows an exponential decay with a slope of 1.51, somewhat larger than the B.C.S. value of 1.44. The thermodynamic critical field $H_c(T)$ is obtained from the specific heat below T_c [1]. The ratio $\gamma T_c^2/H_c^2(0)$ is 0.149, smaller than the B.C.S. value of 0.168. The thermal variation $H_c(T)$ is analysed as the deviation from the parabolic law, which is a sensitive test to evaluate the coupling strength. It is plotted in Fig. 3 versus $(T/T_c)^2$.

All these results indicate a significant deviation from a weak-coupling behaviour described by the B.C.S. model like that, for instance, of crystalline niobium characteristic of an intermediate-coupling superconductor [10]. This is confirmed by the electron–phonon coupling parameter $\lambda = 0.77$ calculated from the McMillan formula [11] (with $\mu^* = 0.13$ and $\theta_D = 150$ K). The coupling character is therefore stronger than that of Zr–Cu and Zr–Ni which were found to be weak-coupling superconductors.

Varma and Dynes [12] pointed out that in a plot of λ versus $N_0(E_F)$ (the bare density of states $= N_\gamma(E_F)/(1+\lambda)$, the experimental data for a given series of

Table 1. Thermodynamic parameters and transport properties of amorphous $Zr_{70}Mo_{30}$

γ	$N_\gamma(E_F) = \frac{3\gamma}{\pi^2 k_B^2}$	$N_0 = \frac{N_\gamma}{1+\lambda}$	β	θ_D	$H_c(0)$	$\rho_{273\,K}$	$\left(\frac{dH_{c_2}}{dT}\right)_{T_c}$
(mJ mole^{-1} K^{-2})	(states eV^{-1} atom^{-1})		(mJ mole^{-1} K^{-4})	(K)	(Oe)	($\mu\Omega$ cm)	(kOe K^{-1})
7.20 ± 0.1	3.05	1.72	0.580 ± 0.002	150	840	152	25 ± 1

crystalline transition metals and alloys lie on two well defined lines according to whether E_F is located in the upper or lower half of the d-band. Data for $4d$-based amorphous alloys also lie on the same lines [13]. For $Zr_{70}Mo_{30}$ the result is in good agreement with the lower $4d$-band line corresponding to the bonding half-band, as expected for alloys from two early transition metals. This result is close to that of crystalline niobium, due to close values of botn λ and $N_0(E_F)$ [11]; this implies that the strength of coupling is mainly governed by the electronic properties in these metallic systems, independently of the Debye temperature.

RESISTIVITY AND UPPER CRITICAL FIELD

The resistivity $\rho(T)$ is plotted against T from T_c to room temperature in Fig. 5. It depicts the typical variation observed for amorphous metals with a negative temperature coefficient above about 10 K; with $\rho(273\,\mathrm{K}) = 152\,\mu\Omega\,\mathrm{cm}$, and $[\rho(10\,\mathrm{K}) - \rho(273\,\mathrm{K})]/\rho(273\,\mathrm{K}) = 4.8 \times 10^{-2}$. Superconductive fluctuations are apparent from T_c to about $3T_c$. They are responsible for the decrease of ρ with decreasing T in this range of temperature.

The upper critical field is measured resistively with H perpendicular to the sheet. Two examples of transitions measured at different constant temperatures by varying the field are shown in the insert of Fig. 5, together with the transition versus T at $H = 0$. The slope of the critical field near T_c is: $H'_{c_2} = -(\mathrm{d}H_{c_2}/\mathrm{d}T)_{T_c} = 25 \pm 1\,\mathrm{kOe\,K^{-1}}$.

The parameter $\kappa_1(T) = H_{c_2}(T)/\sqrt{2}H_c(T)$ is plotted against T/T_c in Fig. 6. Its thermal variation is in good

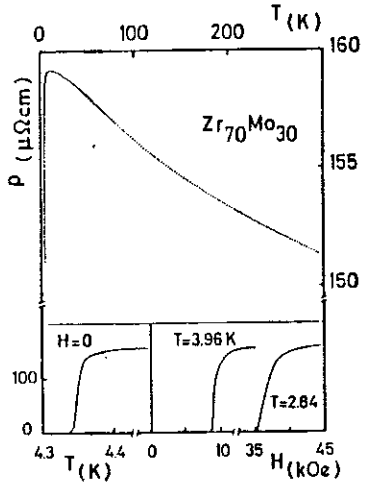

Fig. 5. Resistivity and superconducting transitions of amorphous $Zr_{70}Mo_{30}$.

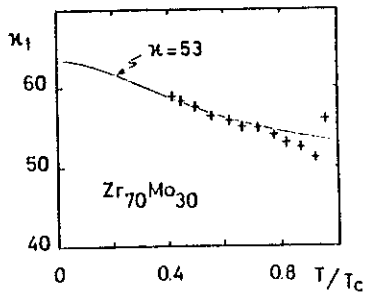

Fig. 6. Thermal variation of the κ_1 parameter.

agreement with that predicted by the G.L.A.G. model [14], also drawn in Fig. 6 with $\kappa = 53$. Deviations between experimental and calculated variations were larger in the case of Zr–Cu and Zr–Ni, but κ was of the same order of magnitude.

The formula

$$H'_{c_2} = 4.48 \times 10^{-5}\,\gamma \times \rho \qquad (1)$$

using the measured values $\rho(10\,\mathrm{K}) = 159\,\mu\Omega\,\mathrm{cm}$ and $\gamma = 5.74 \times 10^3\,\mathrm{erg\,cm^{-3}\,K^{-2}}$, gives a calculated slope of $40.9\,\mathrm{kOe\,K^{-1}}$. As previously pointed out, especially for Zr–Ni [1], we note a large discrepancy between the measured and the calculated values. In all amorphous systems we have investigated up to now [2] we remark that large deviations between the experimental and calculated slopes are correlated to large T.L.S terms in the specific heat and also to large γ.

Indeed formula (1) has only been verified in case of amorphous alloys like Mo–Ru–B [15] or Zr–Cu [16], which exhibit γ values about two times smaller than for $Zr_{70}Mo_{30}$. Large densities of states could involve corrections to relation (1), not accounted for by the model. However, we still have not obvious explanations for these high γ values. Moreover, in order to conclude about the origin of these discrepancies, we need theoretical calculations for the effect of the T.L.S. on $H_{c_2}(T)$ which are as yet not available.

CONCLUSION

From this extensive calorimetric and resistive study of amorphous $Zr_{70}Mo_{30}$ which obeys the Collver–Hammond law, we conclude that it is an intermediate-coupling superconductor. The coupling strength and the electronic density of states are close to those of crystalline Nb. The corresponding data lie, in a Varma–Dynes plot, on the right lower $4d$-band line, showing that the strength of the coupling is driven by the electronic properties.

This alloy exhibits a very high density of two-level systems. The discrepancy between the measured and

calculated upper critical field slope previously reported in weak-coupling Zr–3*d* alloys is still observed: hence, the lack of correlation between this deviation and the coupling strength is confirmed. The effect of the TLS on the upper critical field needs to be clarified.

Acknowledgements – We wish to thank O. Béthoux for supplying the samples.

REFERENCES

1. O. Laborde, A. Ravex, J.C. Lasjaunias & O. Béthoux, *J. Low Temp. Phys.* 56, 5/6, 461 (1984).
2. J.C. Lasjaunias, A. Ravex, O. Laborde & Béthoux, *Physica* B-126, III, 126 (1984).
3. M.M. Collver & R.H. Hammond, *Phys. Rev. Lett.*, 30, 92 (1973).
4. S.J. Poon, *Solid State Commun.* 47, 431 (1983).
5. M. Tenhover, D. Lukco & W.L. Johnson, *J. Non-Cryst. Solids* 61–62, 1049 (1984).
6. E. Babić, R. Ristić, M. Miljak, M.G. Scott & G. Gregan, *Solid State Commun.* 39, 139 (1981).
7. A. Ravex, J.C. Lasjaunias & O. Béthoux, *J. Phys. F: Met. Phys.* 14, 329 (1984).
8. The purity specifications for parent materials are the following: for Mo, W: 50 ppm, Fe: 12 ppm, C: 10 ppm, other elements $\lesssim$ 20 ppm; for Zr, Fe: 190 ppm, Hf: 90 ppm, Cr: 42 ppm, other $\lesssim$ 20 ppm.
9. A. Ravex, J.C. Lasjaunias & O. Béthoux, *Physica* B-107, 395 (1981).
10. *Superconductivity* (Edited by R.D. Parks) Marcel Dekker, New York, 1969, p. 165 and 784–785.
11. W.L. McMillan, *Phys. Rev.* 167, 331 (1968).
12. C.M. Varma & R.C. Dynes, p. 507 in *Superconductivity in d- and f-band Metals* (Edited by D.H. Douglass) Plenum, New York (1976).
13. W.L. Johnson & M. Tenhover, in *The Magnetic, Chemical, and Structural Properties of Glassy Metallic Alloys* (Edited by R. Hasegawa) CRC, Boca Raton (1982).
14. D. Saint-James & G. Sarma, Chap. 5 in *Type II Superconductivity*, Pergamon Press, Oxford and New York (1969).
15. S.T. Hopkins & W.L. Johnson, *Solid State Commun.* 43, 537 (1982).
16. K. Samwer & H. v. Löhneysen, *Phys. Rev.* B-26, 107 (1982).

III - PROPRIETES THERMIQUES A TRES BASSE TEMPERATURE - EXCITATIONS DE BASSE ENERGIE

La chaleur spécifique résiduelle qui subsiste au-dessous de 500 mK lorsque l'on a retranché à la capacité calorifique totale les contributions des phonons (terme βT^3 extrapolé de l'état normal) et des électrons supraconducteurs (extrapolation de la loi de décroissance exponentielle type BCS) est affectée aux excitations de basse énergie caractéristiques de l'état désordonné. Ces excitations,décrites en terme de systèmes à deux niveaux (SDN),ont été largement étudiées dans les isolants amorphes et leur présence dans des verres métalliques a été évoquée pour analyser un certain nombre d'expériences : chaleur spécifique et conduction thermique (Graebner et al., 1977), vitesse et atténuation ultrasonore (Belessa et al., 1971 ; Weiss et al., 1980 ; Doussineau, 1981).

L'analyse des résultats expérimentaux, effectuée comme décrit au chapitre précédent conduit à représenter la contribution des SDN sous la forme

$$C_{SDN} = aT^n$$

Les valeurs de l'exposant n de la loi de puissance pour divers échantillons ainsi que l'amplitude de la contribution C_{SDN} à 100 mK sont données dans le tableau 4 ainsi que dans la publication ci-après.

Physica 107B (1981) 395-396
North-Holland Publishing Company

GC 5

LOW TEMPERATURE SPECIFIC HEAT OF AMORPHOUS SUPERCONDUCTING ZIRCONIUM ALLOYS

A. Ravex, J.C. Lasjaunias and O. Béthoux

Centre de Recherches sur les Très Basses Températures, C.N.R.S., B.P. 166 X, 38042 Grenoble Cédex, France

We have measured from 40 mK up to 6 K the specific heat of a series of amorphous superconducting Zr alloys to study the low temperature contribution assigned to two level systems. We also deduce normal electronic and phonon contributions to the specific heat and thermodynamical superconducting properties.

1. SAMPLES PREPARATION AND CHARACTERISATION

Samples are obtained in the form of thick films (about 100 µm) by high rate sputtering. Condensation occurs on a substrate held either at 300 K($Ag_{.35}Zr_{.65}$, $Ni_{.24}Zr_{.76}$) or at 77 K ($M_{.24}Zr_{.76}$, M = Ni, Cu, Pt). Samples are checked to be amorphous by X-rays analysis. The specific heat is measured by a transient heat pulse technique (1) on samples of about 3 grams weight.

2. SPECIFIC HEAT ABOVE T_c

Above the superconducting transition temperature T_c, the specific heat of each sample is well fitted by a $\gamma T + \beta T^3$ law. The values obtained for γ and β with this analysis are verified below T_c by checking both normal and superconducting state entropies to be equal. Calculated values of the normal electronic contribution γ, phonon contribution β' and corresponding Debye temperature θ_D are reported in table 1.

M	Ag	Ni 300 K	Ni 77 K	Cu	Pt	pure Zr
γ(mJ/mole K^2)	5,4 ± 0,4	7,15 ± 0,15	8,15 ± 0,2	6,5 ± 0,15	5,85 ± 0,25	3,05*
β(mJ/mole K^4)	0,525	0,45	0,465	0,505	0,65	
θ_D (K)	155	163	161	157	144	291**

Table 1 : γ, β and θ_D for Zr M alloys
* measured value of the parent crystalline Zr
** from literature for crystalline Zr

3. SUPERCONDUCTING PROPERTIES

Transition temperature T_c, specific heat jump $\Delta C/\gamma T_c$ deduced from the specific heat curves are reported in table 2. From the slope of the logarithmical variation of the superconducting electronic specific heat C_{es} versus T_c/T we obtain the value of Δ_o/k_BT_c where Δ_o is the superconducting gap at 0 K. Superconductivity in these alloys will be discussed elsewhere.

M	Ag	Ni 300 K	Ni 77 K	Pt	Cu
T_c	1,8	3,30	3,15	2,92	3,43
$\Delta C/\gamma T_c$	1,75	1,70	1,85	1,80	1,85
Δ_o/k_BT_c	1,35	1,50	1,40	1,50	1,50

Table 2 : Superconducting properties of Zr alloys

4. SPECIFIC HEAT EXCESS AT LOW TEMPERATURE

After subtracting the phonon and superconducting electronic contributions from the total specific heat, it remains below about 500 mK a residual contribution as shown in fig. 2. If we assume the presence of two level systems (TLS) as it has been suggested in similar alloys (2,3,4),the theory predicts a linear temperature dependence of the specific heat excess. However experimental data are well fitted by a power law T^n down to about 100 mK. Values of n and of the TLS contribution at 100 mK are reported in table 3. If this power law is still valid at lower temperatures, it is necessary to introduce a suplementary contribution to take into account the whole specific heat excess. It could be the onset of a quadrupolar nuclear effect (C_NT^{-2}) due to Zirconium ; from specific heat measurements we know the value of C_N for the crystalline parent Zr in normal state, but the difference in electrical field gradients between crystalline Zr and amorphous Zr alloys enables us to check precisely this assumption.

M	Ag	Ni 300 K	Ni 77 K	Cu	Pt
n from $C_{TLS} = aT^n$	0,85	0,5	0,55	0,5	0,5
C_{TLS} (erg/mole K) at 0.1 K	70	195	260	95	180
C_N (erg K/mole)	7.10^{-2}	33.10^{-2}		11.10^{-2}	34.10^{-2}

Table 3 : TLS and nuclear contributions

The TLS specific heat varies from an alloy to the other but the order of magnitude at 0.1 K is similar to that of insulating glasses or to that of other glassy metals quenched from the melt (2,3). We note that the highest TLS contribution is obtained for a ZrNi sample which has been sputtered at a lower speed than ours other samples (a factor 3 in deposition speed). Our feeling is that low pulverisation speed induces a higher degree of disorder which enhances the

0378-4363/81/0000–0000/$02.50

TLS contribution. Indeed, we have observed the reverse effect in an annealed ZrNi sample (5). Furthermore, for two different samples (ZrCu and ZrPt) with the same composition and sputtered in the same manner, we observe a large variation in the TLS contribution.

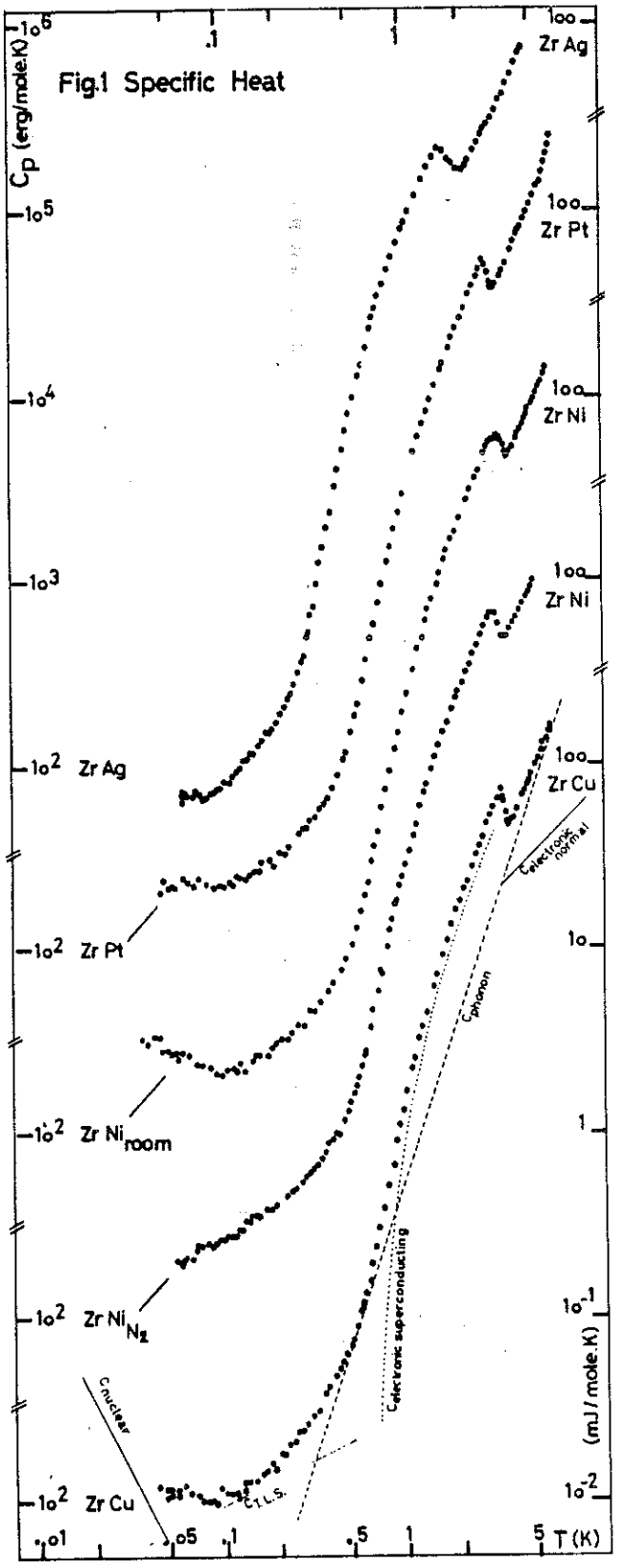

(1)J.C. Lasjaunias, B. Picot, A. Ravex, D. Thoulouze, M. Vandorpe, Cryogenics 17, 111 (1977).
(2) J.E. Graebner, B. Golding, R.J. Schutz, F.S.L. Hsu, H.S. Chen, Phys. Rev. Lett. 39, 1480 (1977).
(3) H.V. Löhneysen, M. Platte, W. Sander, H.J. Schink, G.v. Minnigerode and K. Samwer, J. Phys. (Paris), C8-745 (1980).
(4) G. Weiss, W. Arnold, K. Dransfeld, H.J. Güntherodt, Sol. State Comm. 33, 111 (1980).
(5) A. Ravex, J.C. Lasjaunias, O. Béthoux, to be published in this issue.

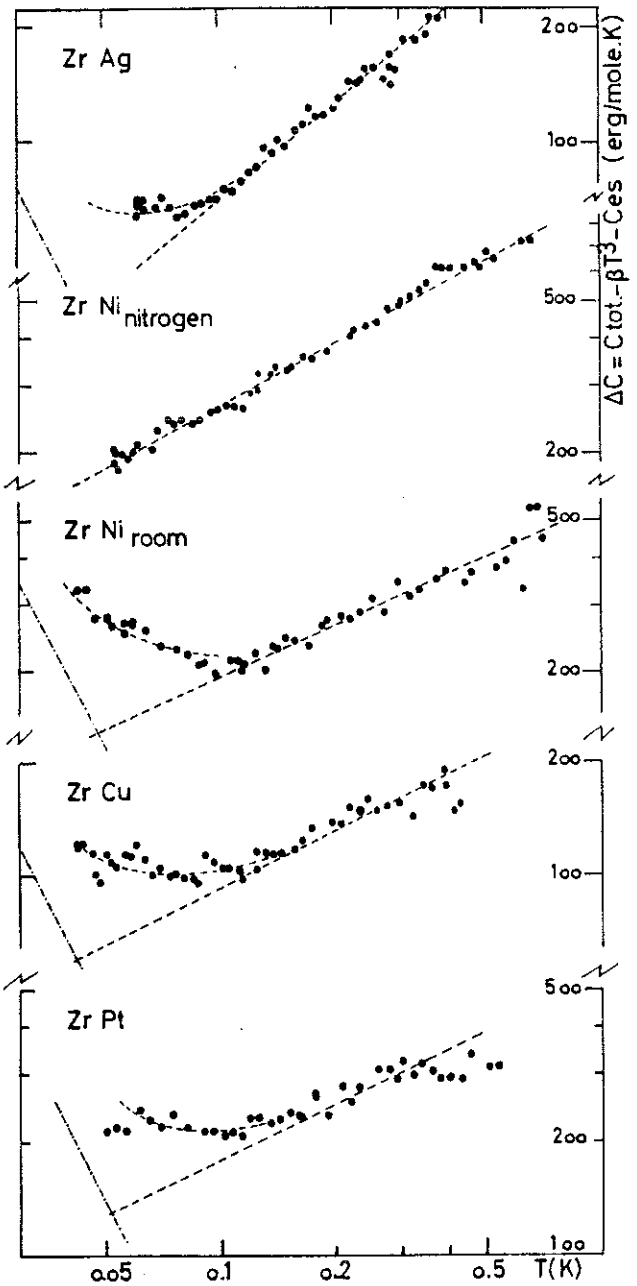

Fig. 2 : Residual specific heat at low temperature.

Tableau 4 - Excitations de basse énergie pour les échantillons bruts de préparation

Echantillon	$Zr_{85}Ag_{35}$	$Zr_{76}Ni_{24}$ 300 K	$Zr_{76}Ni_{24}$ 77 K	$Zr_{76}Cu_{24}$	$Zr_{80}Cu_{20}$	$Zr_{75}Pt_{25}$	$Zr_{70}Mo_{30}$	SiO_2
n	1	0,4	0,55	0,7	0,65	0,5	0,5	1,3
C_{SDN} à 0,1 K erg/moleK^2	60±5	190±5	260	90±5	140	165±5	∿500	50

* La comparaison de ces valeurs avec celles obtenues pour la silice amorphe (Lasjaunias et al., 1975) - valeurs standards représentatives des propriétés des isolants amorphes - et avec celles publiées pour des verres métalliques obtenus par trempe du liquide (Graebner et al., 1977 ; Samwer et al., 1982) appelle quelques commentaires :

i) les valeurs absolues du signal affecté aux SDN sont systématiquement plus élevées dans nos échantillons pulvérisés que dans les échantillons métalliques trempés du liquide ou dans les isolants. Ceci est à rapprocher des résultats précédents sur les densités d'états électroniques $N_0(E_F)$.

ii) la loi de variation thermique (coefficient n généralement < 1) est différente de la variation linéaire observée par Graebner (1977) et Samwer (1982) sur des échantillons trempés du liquide. Cette dernière semble conforme aux prédictions du modèle théorique de Phillips (1972) et Anderson (1972). Toutefois il est à noter que ces auteurs se contentent d'analyser les résultats bruts sans chercher à retrancher les contributions phononiques et électroniques. Dans une telle analyse nos résultats bruts se rapprocheraient également d'une variation linéaire ! D'autre part nos mesures sur la silice amorphe (Ravex, 1976) ont montré que même pour les isolants amorphes la variation linéaire n'était qu'une première approximation. Cependant dans ce cas l'exposant n était plutôt supérieur à 1.

iii) l'amplitude et la loi de variation thermique de la contribution des SDN peuvent être modifiées sous l'effet de traitements thermiques. Ce point qui fait l'objet du chapitre suivant constitue une différence essentielle par rapport aux autres systèmes étudiés (isolants amorphes, verres métalliques trempés du liquide) qui semblent peu sinon pas sensibles aux recuits.

Ces constatations amènent bien sûr à s'interroger dans un premier temps sur la validité de l'analyse, plus précisément sur l'éventualité d'une autre origine pour l'excès de chaleur spécifique observé. L'hypothèse la plus souvent avancée est la présence de gaz inclus qui pourraient être à l'origine d'une partie de l'excès de chaleur spécifique. Dans du cuivre hydrogéné, par exemple, une anomalie de chaleur spécifique de type Schottky a été observée entre 1 et 2 K (Waterhouse, 1969). Aucun signal de ce type n'a été détecté dans nos mesures.Plus récemment une anomalie de chaleur spécifique approximativement linéaire en température au-dessous de 1 K a été observée dans du Niobium Titane cristallin dopé à l'hydrogène ou au deuterium (de 0,3 à 3 at %) (Neumaier et al., 1982). Une explication avancée pour expliquer ce résultat est la possibilité pour les atomes d'hydrogène (ou de deutérium) de tunneler entre deux sites tétraédriques voisins. Il est à noter que les atomes d'hydrogène (deuterium) ne sont piégés qu'en présence d'impuretés interstitielles (O, N ou C). Un tel phénomène pourrait être envisagé pour nos échantillons étant donné la grande affinité du Zirconium pour l'Hydrogène et la présence probable (voir chapitre "Caractérisation des échantillons") d'Azote et d'Hydrogène. Toutefois aucune mesure d'effets de recuits ou de conduction thermique n'a été effectuée sur les échantillons de Niobium Titane dopés permettant de pousser plus avant les comparaisons des résultats avec ceux bien connus de l'état amorphe et plus particulièrement ceux de notre série d'échantillons. Enfin lors des mesures effectuées sur l'alliage amorphe LaZn (Annexe B), la présence d'Hydrogène s'est traduite par un important dégagement d'énergie jamais observé dans la série d'alliages à base de Zirconium.

Par contre, deux faits expérimentaux permettent de confirmer l'origine de l'anomalie dans des défauts de structure intrinsèques décrits par le modèle tunnel classique :

i) une corrélation établie entre l'amplitude de l'anomalie affectée aux SDN (aT^n) et celle du terme quadripolaire ($C_N T^2$) observée à très basses températures s'interprète par une interaction (TLS)-SDN noyaux de Zirconium.

ii) la relation systématique lors des recuits entre les variations du signal de chaleur spécifique et celles du terme quadratique de la conduction thermique généralement assigné à l'interaction SDN-phonons.

Avant d'expliciter ces deux points dans les deux publications reproduites ci-après, nous rappelons rapidement les hypothèses et résultats essentiels du modèle théorique des SDN (ou TLS) (Phillips, 1972 ; Anderson et al., 1972).

1. Modèle des systèmes à deux niveaux ou "défauts tunnels" :

Notre propos n'est pas de détailler les calculs du modèle original exposés dans de nombreux ouvrages ou publications (voir par exemple Anderson, 1979 ; Güntherodt and Beck, 1981) mais simplement d'en rappeler l'esprit et les principaux résultats appliquables à nos mesures.

L'idée de base est qu'un verre se trouve figé pour des raisons cinétiques dans un état qui n'est pas l'état d'équilibre (qui est le cristal). Il existe certainement un grand nombre d'autres configurations énergétiques équivalentes énergétiquement dans lesquelles le système aurait pu être figé. Alors les excitations de basse énergie (TLS pour two level systems) correspondent à des transitions par effet tunnel à très basse température que le système peut effectuer entre deux de ces configurations dans l'échelle de temps de la mesure physique. Il apparaît donc que les TLS sont très probablement associés à des réarrangements locaux de petits groupes d'atomes. Cette situation peut être représentée en mécanique quantique par le problème d'une particule se mouvant dans un double puits de potentiel asymétrique.

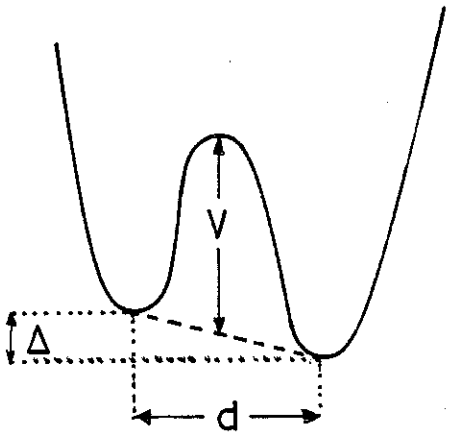

V: hauteur de barriere
Δ : energie d'asymetrie
d : distance entre minima

En prenant comme base les états fondamentaux de chacun des deux puits pris indépendamment, et le zéro de l'énergie à la moyenne des énergies de ces deux états fondamentaux, la matrice représentant l'Hamiltonien du système s'écrit

$$H_o = \frac{1}{2} \begin{pmatrix} \Delta & -\Delta_o \\ -\Delta_o & -\Delta \end{pmatrix}$$

avec $\Delta_o = \hbar\omega_o \exp(-\lambda)$, $\lambda = \frac{d}{\hbar}\sqrt{2mV}$

m étant la masse de la "particule" et $\hbar\omega_o$ étant de l'ordre de l'énergie de point zéro de chacun des puits (de l'ordre de 10^{-2} eV).

La diagonalisation de cet Hamiltonien conduit aux valeurs propres vraies du système qui possèdent les énergies $\pm \frac{E}{2}$. Dans cette base l'Hamiltonien devient

$$H'_o = \frac{1}{2} \begin{pmatrix} E & 0 \\ 0 & -E \end{pmatrix} \quad \text{avec } E^2 = \Delta^2 + \Delta_o^2$$

L'interaction des TLS avec les phonons est prise en compte par un Hamiltonien de déformation

$$H_1 = \begin{pmatrix} \gamma & 0 \\ 0 & -\gamma \end{pmatrix} \varepsilon \quad \text{où } \varepsilon \text{ représente le champ de contrainte au}$$

niveau d'un TLS et $\gamma = \frac{\partial \Delta}{\partial \varepsilon}$ le potentiel de déformation. Dans la base

propre du système cet Hamiltonien s'écrit :

$$H'_1 = \varepsilon\gamma \begin{pmatrix} \Delta/E & 2\Delta_o/E \\ 2\Delta_o/E & -\Delta/E \end{pmatrix}$$

En utilisant la notation de Pauli $S_x = \frac{1}{2}\begin{pmatrix} 0 & 1 \\ 1 & 0 \end{pmatrix}$ et $S_z = \frac{1}{2}\begin{pmatrix} 1 & 0 \\ 0 & -1 \end{pmatrix}$ l'Hamiltonien $H' = H'_o + H'_1$ devient

$$H' = ES_z + (2MS_x + DS_z)\varepsilon \quad \text{avec} \quad \begin{cases} E^2 = \Delta^2 + \Delta_o^2 \\ M = \frac{\Delta_o}{E}\gamma \\ D = \frac{2\Delta}{E}\gamma \end{cases}$$

Le splitting en énergie E des TLS ne peut pas être inférieur à Δ_o (en effet $E = \Delta_o$ pour un double puits symétrique $\Delta = 0$). Ceci implique, du fait que les TLS ne sont observés expérimentalement qu'à basse température (typiquement $E < 1$ K), qu'il existe une hauteur de barrière minimale V_{min} (correspondant à $\lambda_{min} = \ell n(\hbar\omega_o/E)$).

L'observation expérimentale des TLS implique la possibilité d'induire la transition de l'état fondamental à l'état excité par l'intermédiaire de l'élément de couplage hors-diagonale de la matrice soit $MS_x\varepsilon$. Pour une valeur donnée de E la valeur de la constante de couplage M varie de sa valeur maximale $M = \gamma$ dans le cas symétrique ($\Delta = 0$, λ_{min}) à une valeur minimale liée à l'échelle de temps de la mesure physique (λ_{max}) : tous les TLS de même énergie ne seront donc pas tous couplés identiquement aux phonons.

Afin de compléter le cadre du modèle, il est nécessaire de se donner une distribution des paramètres descriptifs du système Δ et Δ_o. Les hypothèses habituelles du modèle sont que la fonction de distribution est indépendante de Δ et ne dépend de Δ_o qu'à travers le paramètre λ qui est supposé uniformément distribué. On a donc une probabilité constante $P(\Delta,\lambda) = \overline{P}$ de trouver par unité de volume un double puits de caractéristiques (Δ,λ). En passant aux variables E et Δ_o et en écrivant $P(\Delta,\lambda)d\Delta d\lambda = P(E, \Delta_o)dE\, d\Delta_o$, il vient :

$$P(E,r) = \frac{1}{2}\overline{P}\, r^{-1}(1 - r)^{-1/2} \quad \text{avec } r = \frac{\Delta_o^{2-}}{E^2} \quad \text{(Jäckle, 1972)}$$

La densité de TLS s'écrit alors :

$$n(E) = \int_{\Delta_0 min}^{\Delta_0 max} P(E,\Delta_0)d\Delta_0 = \int_{r_{min}}^{1} \frac{\overline{P}}{2} \frac{dr}{r(1-r)^{1/2}}$$

Chaque TLS donnera lieu en chaleur spécifique à un terme du type Schottky

$$C_{TLS} = k \frac{x^2 e^x}{(e^x+1)^2} \quad \text{avec } x = \frac{E}{kT}$$

La contribution totale sera la somme de chacune de ces contributions soit :

$$C = \int_0^{\infty} k \frac{x^2 e^x}{(e^x+1)^2} n(E)dE = \frac{\pi^2}{6} k^2 T \overline{P} \int_{r_{min}}^{1} \frac{dr}{r}(1-r)^{-1/2} \quad (1)$$

On obtient ainsi avec les hypothèses faites une contribution linéaire à la chaleur spécifique dont la mesure expérimentale permet d'accéder à la densité de TLS

$$\frac{\overline{P}}{2} \int_{r_{min}}^{1} \frac{dr}{r(1-r)^{1/2}}$$

D'autre part, r_{min} est directement relié au temps de relaxation maximum (λ_{max}) des TLS accessibles pendant le temps de mesure

$$r_{min} = \frac{\tau^*}{\tau_{max}}$$

où τ^* est le temps de relaxation minimum (cas des puits symétriques) et $\tau_{max} \simeq$ temps de mesure ce qui conduit à la formule du modèle tunnel prévoyant la dépendance en temps de la chaleur spécifique.

$$C_p(,tT) = \frac{\pi^2}{12} k_B^2 T \overline{P} \text{ Log } \frac{4t}{\tau^*(T)}$$

avec $\tau^*(T) \sim AT^{-3}$ (J.L. Black, Phys. Rev. B17, 2740 (1978)).

En conduction thermique, si l'on suppose que toute la chaleur est transportée par des phonons acoustiques et que leur libre parcours moyen est déterminé par les interactions résonantes avec les TLS ($\ell(\omega) = v.\tau(\omega)$), on peut en utilisant le spectre de Debye et en sommant sur tous les modes de phonons acoustiques écrire

$$K = \int_0^\infty C(\omega)\ v\ \ell(\omega)\ d\omega$$

où $C(\omega)$ est la chaleur spécifique d'un phonon de fréquence ω,
v la vitesse moyenne du son.

Le libre parcours $\ell(\omega)$ est défini par

$$\ell^{-1}(\omega) = \frac{\pi\omega}{\rho v^3}\ \overline{P_\gamma}^2\ \tanh\left(\frac{\hbar\omega}{2kT}\right)$$

où γ correspond à une valeur moyenne sur tous les TLS de la constante de couplage phonons-TLS relative aux puits symétriques :

$$M_{max} = \frac{\Delta_o}{E}\ \gamma$$

qui déterminent la diffusion des phonons la plus efficace (le plus faible temps de vie).

Ceci conduit à l'expression de la conduction thermique

$$K = \frac{\rho k^2 v}{6\pi\hbar^2}\ \frac{1}{\overline{P_\gamma}^2}\ T^2 \qquad (2)$$

dans laquelle la dépendance quadratique en température est en excellent accord avec l'expérience. Les données expérimentales permettent la détermination du produit $\overline{P_\gamma}^2$.

2. Excitations de basse énergie : densité d'états et couplage aux noyaux

L'analyse des résultats expérimentaux ne permet pas la détermination de la loi $C_{TLS} = aT^n$ sur une gamme de température suffisamment étendue avec une précision assez grande pour une analyse numérique à l'aide de la formule (1). Par contre si en première approximation on fait l'hypothèse d'une variation purement linéaire de la chaleur spécifique au voisinage de 100 mK ($C_{TLS} \simeq \frac{\pi^2}{6} k^2 n_o T$) on peut tirer une valeur de densité d'état constante n_o. Celle-ci varie de $n_o = 1,4.10^{40} J^{-1}cm^{-3}$ pour ZrAg à $n_o = 1,110^{41} J^{-1}cm^{-3}$ pour ZrMo ; elle est systématiquement plus élevée que pour la silice amorphe ($n_o = 8 . 10^{39} J^{-1}cm^{-3}$). En outre si l'on compare la valeur obtenue pour notre échantillon brut de pulvérisation ZrCu ($n_o = 2,3 . 10^{40} J^{-1}cm^{-3}$) à celle publiée pour un échantillon de composition voisine obtenu par trempe du liquide ($n_o = 1,6 . 10^{40} J^{-1}cm^3$, Löhneysen, 1980), on observe que la densité de TLS est plus forte pour l'échantillon pulvérisé. Cette tendance est confirmée par les mesures de conduction thermique (voir paragraphe suivant) et par les effets de recuit (voir chapitre suivant).

La publication rapportée ci-après met en évidence une corrélation entre l'amplitude du signal TLS et celle de la chaleur spécifique résiduelle $C_N T^{-2}$ observée à très basse température. Cette dernière contribution attribuée à un effet quadrupolaire nucléaire ne peut être observée que s'il existe dans l'état amorphe supraconducteur un couplage supplémentaire des noyaux de Zirconium (^{91}Zr) qui diminue le temps de relaxation nucléaire. En effet nous avions vérifié (annexe D) sur un échantillon de Zirconium cristallin que le couplage des noyaux de Zirconium via les électrons de conduction est effectif ($\tau_1 < 10$ sec) à l'état normal. Par contre à l'état supraconducteur le temps de relaxation τ_1 devient supérieur à la minute: nous n'avons donc pu observer aucune remontée de chaleur spécifique en T^{-2}. L'hypothèse avancée dans cette publication d'un couplage via les TLS permet d'expliquer à la fois la restauration du signal quadrupolaire et sa corrélation avec l'amplitude du signal TLS. Ceci fournit en outre un argument solide en faveur de l'existence de TLS dans nos échantillons à l'origine des excitations de basse énergie observées en chaleur spécifique.

J. Phys. F: Met. Phys. 13 (1983) L101–L106. Printed in Great Britain

LETTER TO THE EDITOR

Two-level systems in zirconium-based amorphous alloys: evidence of a coupling with Zr nuclei

J C Lasjaunias and A Ravex

Centre de Recherches sur les Très Basses Températures, CNRS, BP 166 X, 38042 Grenoble Cedex, France

Received 18 March 1983

Abstract. We report very low-temperature specific heat measurements on a series of amorphous superconducting zirconium-based alloys. After subtracting the electron and phonon contributions, we determine from the analysis of the data in a large temperature interval the specific heat excess due to the low-energy excitations (TLS) characteristic of the amorphous state. Furthermore, at the lowest temperature ($T \leqslant 0.1$ K) the onset of a nuclear contribution is observed, numerically correlated to that of the TLS, which suggests a coupling between the ^{91}Zr nuclear spins and these excitations.

Over the past ten years a lot of work devoted to the investigation of insulating glasses has indicated the existence of low-energy excitations typical of the amorphous state. A phenomenological model developed simultaneously by Phillips (1972) and Anderson *et al* (1972) ascribes these excitations (TLS) to atomic tunnelling motions between the two states of a double-well potential. Their characteristic behaviour is now also well established in the case of metallic glasses: specific heat excess, quadratic T^2 variation of thermal conductivity due to a strong scattering of phonons by TLS (Graebner *et al* 1977), saturable nature of the ultrasonic power absorption and logarithmic dependence of sound velocity with temperature (see, for example, Belessa and Béthoux 1977, Weiss *et al* 1980, Doussineau 1981). In this study we have undertaken a systematic determination of the specific heat contribution of TLS for a series of amorphous superconducting zirconium-based alloys.

The samples are obtained by high-rate sputtering with a DC magnetron under an argon atmosphere (5×10^{-3} Torr). Condensation occurs on a copper substrate held either at room or liquid nitrogen temperature. Samples (4×2 cm^2 foils, 100 μm thick) are studied either as-sputtered (AS) or after thermal annealing below the crystallisation temperature. They are characterised by different techniques (x-ray diffraction, DTA, density) widely described in the cases of ZrNi and ZrCu alloys (Ravex *et al* 1981a, b, 1983).

The specific heat is measured from 50 mK up to 6 K by a transient heat-pulse technique. Experimental details of this method together with typical total specific heat curves and a complete analysis of the data are published elsewhere (Ravex *et al* 1981a, b, 1983). Concerning the transient response of the thermometer following the heat pulse, we indicate that in the very low-temperature range ($T \leqslant 100$ mK) these regimes remain well defined by a unique exponential decay with a time constant τ varying from about 10 s at 100 mK to 20–40 s at 50 mK. With this technique τ is defined as the product of the heat capacity and the thermal link resistance. Let us just recall the usual process of analysis:

from the data above the superconducting transition temperature T_c we use a plot of C/T against T^2 to determine the values of the normal electronic specific heat γT and of the phonon contribution βT^3 from which we estimate a Debye-like temperature θ_D. Below T_c (for $2 < T_c/T < 6$) we verify that the superconducting electronic specific heat ($C_{es} = C - \beta T^3$) obeys an exponential decay ($C_{es} \propto \gamma T_c \exp|-(\Delta_0/k_B T_c)(T_c/T)|$) from which we get an estimate of $\Delta_0/k_B T_c$, where Δ_0 is the superconducting gap at 0 K. A summary of these experimental data is given in table 1.

Subtracting the phonon and electron contributions determined previously from the measured total specific heat, there remains a residual contribution below about 500 mK as shown in figure 1 for some typical samples of the series. We assign this specific heat excess to the low-energy excitations (i.e. TLS). All the experimental data are well fitted by power laws ($C_{TLS} = aT^n$) down to about 100 mK. Values of n and of the amplitude of the TLS signal at 100 mK for each sample are reported in table 1. Generally for the samples in the AS state the temperature dependence of C_{TLS} is lower than the linearity usually expected for an energy-independent distribution of these TLS: this indicates a weak decreasing energy dependence of $n(E)$ in the corresponding energy interval. However, we observe that by structural relaxation induced by thermal annealing (Ravex *et al* 1981a, b, 1983), one approaches a more linear variation for the specific heat excess, corresponding to a constant TLS distribution with energy. Moreover, in the case of ZrCu, after thermal annealing the specific heat tends towards the value of a sample of very close composition prepared by rapid quenching from the melt. Beyond the differences in the power laws the amplitude of the specific heat excess, i.e. the density of TLS, is, for all the samples investigated in this study, of the same order of magnitude as that previously reported for a great variety of insulating glasses. For the samples subjected to a thermal annealing, we have verified that the decrease in excess specific heat is correlated to an increase in the quadratic term of the thermal conductivity associated with the TLS scattering of phonons. In particular this correlation rules out the hypothesis of a spurious origin for this excess attributed to the presence of gases: indeed such gaseous impurities would not be so strongly coupled with phonons. Moreover, it would be very surprising to have such a reproducible content of gases in different samples from different laboratories obtained by different techniques (sputtering or quenching from the melt).

Hence our measurements confirm the intrinsic nature of these low-energy excitations present in metallic glasses as well as in insulators. However, more interesting is the fact that we can induce large modifications of their density of states by thermal treatment. Such a behaviour, which has never been observed in insulators nor so clearly in metallic glasses quenched from the melt (Grondey *et al* 1983, Esquinazi *et al* 1982), seems to be a particular property of sputtered samples. It will be of great interest for an understanding of the physical nature of TLS to correlate these results to structural or local-order investigations such as EXAFS, RMN or small-angle x-ray diffraction which are in progress.

If the TLS specific-heat temperature dependence is still valid at lower temperatures, it is necessary to introduce a supplementary contribution to take into account the measured specific heat below 100 mK. The best fit of the data between 50 mK and 0.5 K is obtained with a T^{-2} term in addition to C_{TLS}: it could be the onset of a quadrupolar nuclear contribution $C_N T^{-2}$ due to ^{91}Zr nuclei, with $C_N \propto (e^2 qQ/k_B)^2 f(I)$, where eq is the main contribution of the electric field gradient at a ^{91}Zr nucleus, Q is the quadrupolar moment and $I = \frac{5}{2}$ is the nuclear spin of this nucleus. No other nuclear origin seems possible, either hyperfine magnetic or quadrupolar, from the secondary element since the amplitude C_N is not correlated to its nuclear spin ($I = \frac{1}{2}$ for example in the case of Ag or Pt forbids any quadrupolar contribution). Moreover, specific heat measurements performed on the parent

Table 1. Specific heat parameters (see text). T_c is the superconducting transition temperature. For the parent crystalline Zr in the normal state $C_N = (170 \pm 40) \times 10^{-2}$ erg mol^{-1} K. (AS = as sputtered.)

Alloy	Deposition temperature (K)	Conditions of measurement	T_c (K)	γ (mJ mol^{-1} K^{-2})	β (mJ mol^{-1} K^{-4})	θ_D (K)
A: $Zr_{0.65}Ag_{0.35}$	300	AS	1.76	5.4	0.525	155
B: $Zr_{0.76}Cu_{0.24}$	77	AS	3.45	6.25	0.53	154
C: $Zr_{0.76}Cu_{0.24}$	77	Sample B annealed 1 h at 200 °C	3.29	5.0	0.395	170
D: $Zr_{0.76}Cu_{0.24}$	77	Aged at room temperature	3.28	5.55	0.47	160
E: $Zr_{0.76}Ni_{0.24}$	300	AS	3.32	7.15	0.45	163
F: $Zr_{0.76}Ni_{0.24}$	77	Annealed 24 h at 250 °C	3.0	6.3	0.315	184
G: $Zr_{0.76}Pt_{0.24}$	77	AS	2.92	5.85	0.65	144

Alloy	Δ_0/k_BT_c (BCS value = 1.44)	C_{TLS} at 0.1 K (erg mol^{-1} K^{-1})	$n(C_{TLS} \sim T^n)$	$C_N \times 10^2$ (erg mol^{-1} K)	Nuclear spin of second element (and natural abundance)
A: $Zr_{0.65}Ag_{0.35}$	1.44	60 ± 5	1.0	13 ± 3	$\frac{1}{2}$
B: $Zr_{0.76}Cu_{0.24}$	1.44	90 ± 5	0.7	18 ± 5	$\frac{3}{2}$(100%)
C: $Zr_{0.76}Cu_{0.24}$	1.57	50 ± 5	0.9	6.5 ± 2.5	$\frac{3}{2}$(100%)
D: $Zr_{0.76}Cu_{0.24}$	1.64	120 ± 5	0.5	23 ± 3	$\frac{3}{2}$(100%)
E: $Zr_{0.76}Ni_{0.24}$	1.51	190 ± 5	0.4	35 ± 5	$\frac{3}{2}$(1%)
F: $Zr_{0.76}Ni_{0.24}$	1.40	115 ± 10	0.85	20 ± 5	$\frac{3}{2}$(1%)
G: $Zr_{0.76}Pt_{0.24}$	1.51	165 ± 5	0.5	40 ± 10	$\frac{1}{2}$

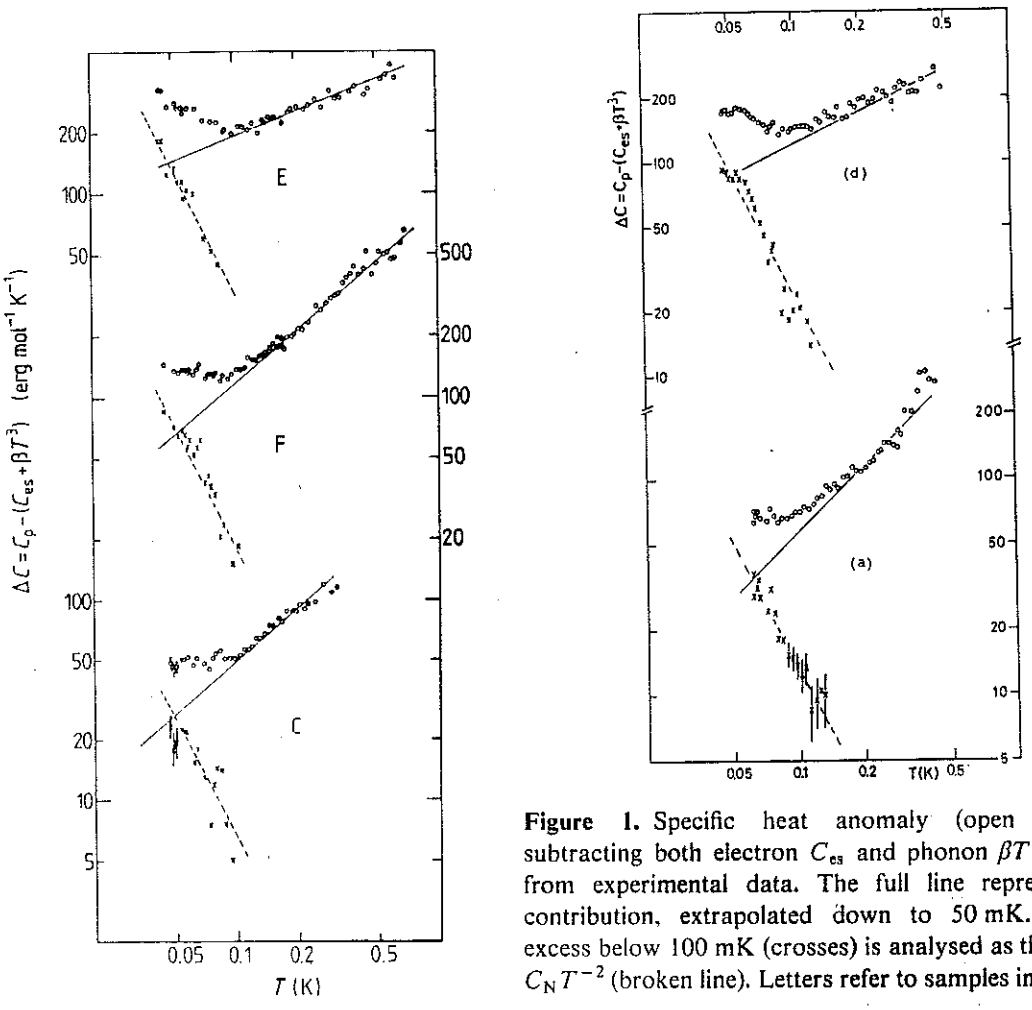

Figure 1. Specific heat anomaly (open circles) after subtracting both electron C_{es} and phonon βT^3 contributions from experimental data. The full line represents the TLS contribution, extrapolated down to 50 mK. The residual excess below 100 mK (crosses) is analysed as the nuclear term $C_N T^{-2}$ (broken line). Letters refer to samples in table 1.

crystalline zirconium (Lasjaunias and Ravex 1982) have shown a similar onset of a nuclear contribution in the normal state. In a metal the nuclear moments have a strong magnetic interaction with the moments of the conduction electrons leading to a short relaxation rate T_1 for the nuclei. Due to the condensation of conduction electrons in the superconducting state one expects a drastic exponential enhancement of this relaxational process: in fact for the parent crystalline zirconium we no longer observe a nuclear contribution in the superconducting state within the timescale of our measurements (about 40 s at 50 mK). Likewise a process consisting of the modulation of the electric field gradient by phonons is not efficient at low temperatures ($T \ll \theta_D$). Under these conditions it seems quite surprising to observe a nuclear signal in these amorphous alloys. However, the analysis of the experimental results (table 1 and figure 2) indicates a systematic correlation between the amplitude of the TLS specific heat anomaly and the amplitude of the nuclear contribution. These features lead us to suggest a relaxational process of the nuclear spins via the TLS. Such a restoration, or at least a dramatic decrease of T_1, in the amorphous state compared with the corresponding crystalline solid has already been indicated by NMR or NQR measurements in amorphous insulators (Szeftel and Alloul 1978, Jellison *et al* 1980).

It is supposed that the relaxation is achieved through the modulation of the electric field gradient at the nuclear site by the elastic field of its nearest-neighbour TLS. In view of the rapid decrease (like r^{-3}) of this coupling it is assumed by analogy with the paramagnetic impurity-induced relaxation (Khutsishvili 1966, De Gennes 1958) that a nucleus is primarily relaxed by the TLS which is closest to it. The relaxation is thereafter achieved between Zr nuclei by nuclear spin diffusion. The coefficient of diffusion for nuclear spin is

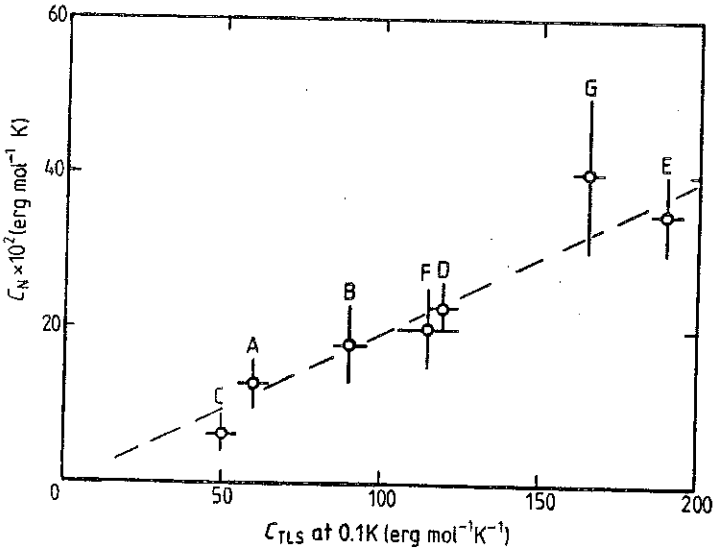

Figure 2. Coefficient of the nuclear term as a function of the amplitude of TLS specific heat at 0.1 K. Letters refer to samples in table 1.

given by $D = Wd^2$ where W is the probability per unit time of a flip-flop transition of a pair of nearest nuclei and d is the distance between them. This distance, estimated from the molar weight and the density of samples (around 7 g cm^{-3}), taking into account the natural abundance of ^{91}Zr (11%), is of the order of 6.5 Å. The probability of a flip-flop transition can be expressed (Khutsishvili 1966, Abragam 1961) as $W \simeq \frac{1}{30}[\frac{3}{5}I(I+1)g]^{1/2}(\hbar\gamma_N^2/d^3)$ where γ_N is the NMR frequency ($\gamma_N/2\pi = 400$ Hz G^{-1}), I is the nuclear spin and g is a coefficient of the order of 10 which is a function of the structure. This leads to a value for the diffusivity $D \sim 2 \times 10^{-14}$ cm^2 s^{-1} which is a common value for solids. Consequently during a time interval t all relaxed nuclei are located inside spheres centred at each TLS and with radii $r = (Dt)^{1/2}$. For an experimental time of about 10 s at 100 mK, $r \sim 45$ Å. From the TLS specific heat contribution we can estimate their density of states n_0, assuming in a first approximation a linear variation for this specific heat with temperature: $C_{TLS} = \frac{1}{6}\pi^2 k_B^2 n_0 T$. For our series of samples these contributions (50 erg mol^{-1} K^{-2} $\leqslant C_{TLS}/T \leqslant$ 150 erg mol^{-1} K^{-2}) correspond to densities of states: 1.3×10^{33} erg^{-1}cm^{-3} $\leqslant n_0 \leqslant 4 \times 10^{33}$ erg^{-1} cm^{-3}. With the approximation that at the temperature T the TLS involved in the specific heat are mainly those with an energy splitting $E \leqslant 3k_B T$ we get an estimate of their mean distances: 180 Å $\leqslant d_{TLS} \leqslant$ 260 Å. These distances are larger than the extension of the relaxation by spin diffusion around each TLS. This is in good agreement with the fact that the observed nuclear contributions in the amorphous alloys are smaller than those observed in the parent zirconium in the normal state. The unique well defined time constant which characterises the transient response indicates that we measure the actual contribution of nuclei which thermally equilibrate via the TLS during this timescale, and it allows comparison with the data of parent Zr measured under similar experimental conditions.

Moreover, the observed numerical correlation between the TLS and nuclear contributions is well taken into account by the proposed mechanism, if one assumes that for all samples investigated, in either AS or 'relaxed' states, the local electric field gradient eq at each ^{91}Zr site is the same and is not affected by the nature of the additional element. We also suppose that the TLS by themselves do not modify the local environment of the Zr nuclei: this seems reasonable since the concentration of such configurational defect is only a few PPM in the energy interval of the present investigation, and can be estimated up to

10^{-2} or 10^{-3} of Zr atoms with the hypothesis of a constant density of states extrapolated up to about 0.1 eV.

In conclusion, we have analysed the very low-temperature specific heat in this series of amorphous alloys by the contribution of TLS excitations and a nuclear quadrupolar term assigned to ^{91}Zr nuclei. The correlation between the amplitude of both terms enables us to ascribe the relaxation of the nuclei within our experimental timescale to a process of spin diffusion among the nuclei, initiated in the close vicinity of the TLS defects. These results strongly support the existence of TLS at the origin of the low-temperature specific heat excess.

The authors are grateful to Dr O Béthoux for preparation of the samples and Dr P Averbuch for stimulating discussions.

References

Abragam A 1961 *The Principles of Nuclear Magnetism* (Oxford: Clarendon) ch. 4–5
Anderson P W, Halperin B J and Varma C M 1972 *Phil. Mag.* **25** 1
Belessa G and Béthoux O 1977 *Phys. Lett.* **62A** 125
De Gennes P G 1958 *J. Phys. Chem. Solids* **7** 345
Doussineau P 1981 *J. Physique Lett.* **42** L83
Esquinazi P, de la Cruz M E, Ridner A and de la Cruz F 1982 *Solid State Commun.* **44** 941
Graebner J E, Golding B, Schutz R J, Hsu F S L and Chen H S 1977 *Phys. Rev. Lett.* **39** 1480
Grondey S, Löhneysen H V, Schink H J and Samwer K 1983 *Z. Phys.* to be published
Jellison G E, Petersen G L and Taylor P C 1980 *Phys. Rev.* B **22** 3903
Khutsishvili G R 1966 *Sov. Phys.–Usp.* **8** 743
Lasjaunias J C and Ravex A 1982 *Phys. Lett.* **88A** 157
Phillips W A 1972 *J. Low Temp. Phys.* **7** 351
Ravex A, Lasjaunias J C and Béthoux O 1981a *Solid State Commun.* **40** 853
—— 1981b *Physica* B **107** 395
—— 1983 *J. Phys. F: Met. Phys.* submitted for publication
Samwer K and Löhneysen H V 1982 *Phys. Rev.* B **26** 107
Szeftel J and Alloul H 1978 *J. Non-Cryst. Solids* **29** 253
Weiss G, Arnold W and Dransfeld K 1980 *Solid State Commun.* **33** 111

3. Excitations de basse énergie - interaction avec les phonons :

Pour un certain nombre d'échantillons de la série étudiée, qu'il s'agisse d'échantillons bruts de préparation ou recuits, la mesure simultanée de la chaleur spécifique et de la conduction thermique a permis de confirmer la présence de TLS à l'origine à la fois de l'excès de chaleur spécifique et de la variation quadratique de la conduction thermique. Il est même possible, comme rapporté dans la publication ci-après, d'établir une corrélation entre l'amplitude du signal de chaleur spécifique (proportionnelle à $\overline{P}$ d'après la relation (1)) et celle de la conduction thermique (proportionnelle à $\frac{1}{\overline{P\gamma}^2}$ d'après (2)). Cette constatation exclut quasiment l'hypothèse d'un artefact pour l'anomalie de chaleur spécifique, plus précisément d'un effet dû à des gaz inclus pour lesquels on ne pourrait pas justifier d'une interaction avec les phonons entraînant la limitation observée de leur libre parcours. En effet, la forte valeur de la constante de couplage déterminée expérimentalement ($M \simeq 1$ eV) est incompatible avec l'image d'atomes de gaz inclus faiblement corrélés à la structure (Rosenstock, 1972). Dans cette publication, les résultats sont présentés en chaleur spécifique, et paramètre de couplage ($\overline{P}\gamma^2$) réduits. L'état de référence est celui de l'échantillon ZrCu brut de pulvérisation (fig. 3).

(Phonon Scattering in Condensed Matter - Stuttgart, 1983)

Low-Energy Excitations in Zr-Based Amorphous Alloys Studied by Thermal Conductivity and Specific Heat

J.C. Lasjaunias, A. Ravex, and O. Béthoux

Centre de Recherches sur les Très Basses Tempêratures, CNRS, BP 166 X
F-38042 Grenoble Cedex, France

For temperatures well below their superconducting transition T_c, the thermal properties of amorphous superconducting alloys become very similar to amorphous insulators, that means governed by the low-energy excitations (Two-Level Systems) successfully proposed by the tunneling model [1] : $T^{1.9}$-T^2 regime for thermal conductivity below about 1 K and a residual specific heat anomaly roughly linear with T and almost universal in magnitude, of the order of a few erg/g.K at 100 mK.

We present specific heat (C) and thermal conductivity (K) data related to T.L.S. for a few Zr-Cu sputtered amorphous alloys, with Zr concentration of 76-80 at %, of different thermal history : $Zr_{76}Cu_{24}$-I in its "as-prepared" state and after annealing 1 hr at 200°C, below the crystallization temperature of $\simeq$ 320°C ; $Zr_{76}Cu_{24}$-II aged at room-temperature ; $Zr_{80}Cu_{20}$ "as-prepared". Also data for a $Zr_{76}Ni_{24}$ "as-prepared" [2] are reported for comparison. All alloys have T_c included between 3 and 3.5 K [2]. Details about the preparation and characterization of these samples are given elsewhere [2,3].

In Fig.(1) are reported specific heat data below 0.8 K only. In order to obtain a precise analysis, measurements were performed to about 7 K, which includes the normal state range where C follows the usual $\gamma T + \beta T^3$ relation. Below 0.5 K the electronic term C_{es} varnishes exponentially and the remaining contributions are phonons (indicated by solid lines) and T.L.S. : $C = \beta T^3 + C_{TLS}$. Below 0.1 K the specific heat ceases to decrease, which indicates the progressive influence of a nuclear hyperfine contribution ($\sim T^{-2}$) assigned to ^{91}Zr nuclei (for a discussion of this term and its relation to T.L.S., see ref. [3]).

The first striking feature is the large spreading of the amplitude of the anomaly mainly due to T.L.S. between 0.1 and 0.3 K, for this series of ZrCu samples of close chemical composition. Including ZrNi, this spread reaches a factor of five at 0.1 K. This is at variance with the insulating glasses (e.g. oxide glasses, fluoride glasses) where continuous variations of chemical composition (or annealing near T_G) has much less effect on the TLS density of states ; however universality of the magnitude of the anomaly (about 1 erg/g.K at 0.1 K) remains. This effect is corroborated by the thermal conductivity data (Fig.(2)). Well below T_c (in the present case below 1 K), due to condensation of normal electrons the dominant phonon scattering process is the resonant scattering by TLS, characterized by a $T^{1.9}$-T^2 regime obeyed in this series of alloys. There appears a good correlation between the C and K raw data for the TLS regimes : a larger value for K corresponding to a lower for C. This will be confirmed in the precise analysis.

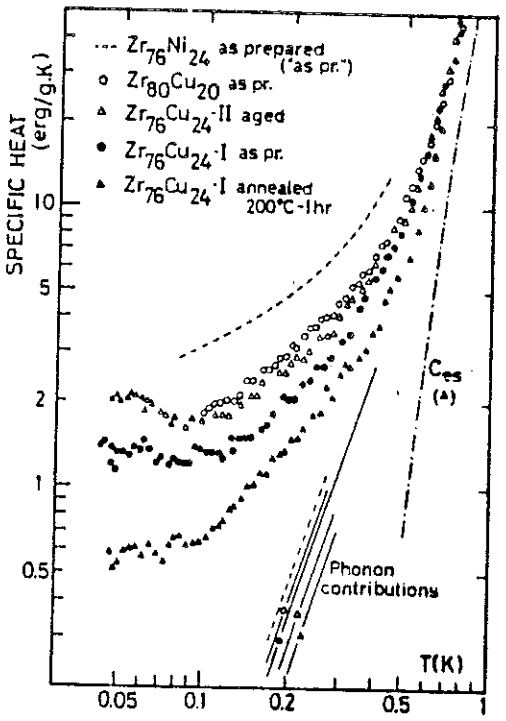

Fig. 1 : Specific heat data

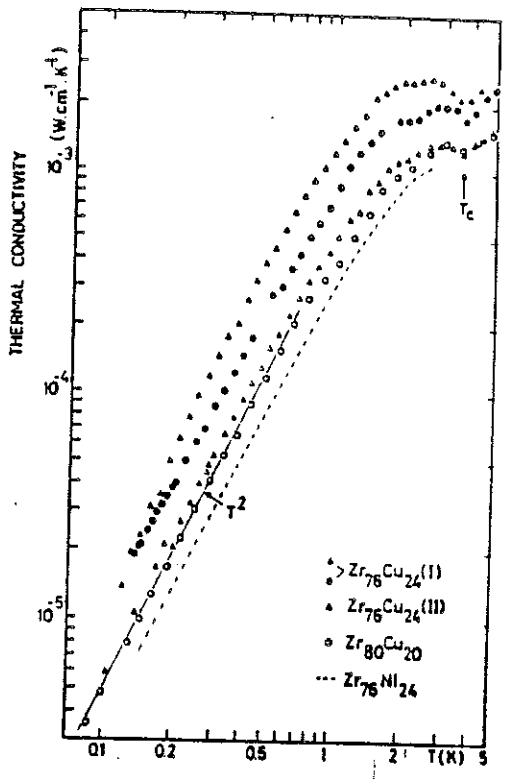

Fig. 2 : Thermal conductivity data

Secondly, a large effect of decrease of the TLS density of states occurs upon annealing (sample $Zr_{76}Cu_{24}$-I). Similar increase of K was detected in different melt-spun Zr_xCu_{1-x} alloys (x = 0.6, 0.7, 0.74 [4]) but *not* correlated to the specific heat, which remained unchanged.

In order to give precise numerical TLS parameters, we have to separate the phonon contribution βT^3 in the specific heat data. In the series of ZrCu, contrary to ZrNi or ZrPt [2], the $C_{TLS}(T)$ variation is very sensitive to this phonon term above 0.3 K : if one uses for β the value B defined in the normal state above T_c, it results in an abnormal behaviour for C_{TLS} which *decreases* with T above 0.3 K [5]; it means that the actual phonon term to be used in this T range is probably smaller than B. Indeed a complete analysis of the thermodynamics of superconductivity based on the B.C.S. model (jump at T_c, parameters of C_{es}) leads to a β value smaller than B, which restores a monotonous increasing variation for C_{TLS} up to $\sim$ 0.5 K, in agreement with all other results of amorphous materials. Since a significant variation of the sound velocity has never been detected in the T_c range for other Zr-based alloys, this suggests the presence in βT^3 of an extra-phononic contribution which rapidly vanishes in the superconducting state, probably of electron-phonon interaction origin .

Generally, the $C_{TLS}(T)$ variation for the "as-prepared" samples is slower than aT (i.e. $\sim T^{0.5}$ to $T^{0.7}$ [2]) but a linear dependence is almost verified after annealing which indicates, in the frame of the tunneling model, the tendency for the TLS density of states n(E) to a more energy-independent distribution, simultaneously to its decrease for $\frac{E}{k_B} \lesssim 1$ K.

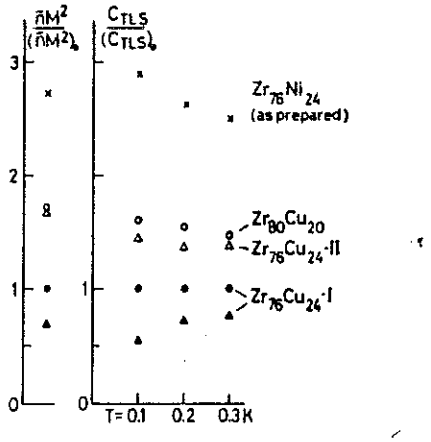

Fig. 3 : Correspondence between the reduced TLS specific heat (at three temperatures) and thermal conductivity coupling parameter $\bar{n}M^2$ for the ZrCu samples and ZrNi [ref. 2]. The reference values $(C_{TLS})_0$ and $(\bar{n}M^2)_0 = 4.1 \times 10^7$ erg.cm^{-3} are those of "as-prepared" $Zr_{76}Cu_{24}$-I

From the quasi T^2 regime of K(T) we calculate the coupling parameter $\bar{n}M^2$ which mainly determines the variations of K in this series of samples ($K \propto \frac{k_B^3}{\hbar^2} \cdot \frac{\rho v_D}{\bar{n}M^2} T^2$, with ρ = density, v_D = mean sound velocity calculated from $\beta = (2\pi^2 k_B^4)/(5\hbar^3 \rho v_D^3)$), where $\bar{n}$ represents a constant density of states of TLS, the most strongly coupled to phonons, which is only a fraction of n(E) active in specific heat, and M a mean phonon-TLS coupling constant. Fig.(3) demonstrates the excellent numerical correlation between both thermal properties of this series of alloys, which strongly supports their common origin in the tunneling states.

In conclusion, we have pointed out the sensitivity of the TLS density of states to the conditions of preparation and thermal history, contrary to insulating glasses : this is probably a direct consequence of metallic bonding. Moreover this property is perhaps related to the high concentration of Zr atoms which could determine the TLS characteristics [5].

REFERENCES

[1] : "Amorphous Solids : Low Temperature Properties", ed. W.A. Phillips (Springer - Verlag, Berlin, 1981).
[2] : A. Ravex, J.C. Lasjaunias, O. Béthoux, Physica 107 B, 395-397 (1981) and Solid State Comm., 40, 853 (1981).
[3] : J.C. Lasjaunias and A. Ravex, J. Phys. F : Met. Phys. 13, L 101(1983).
[4] : S. Grondey, H.v. Löhneysen, H.J. Schink and K. Samwer, Z. Physik (in press).
[5] : A. Ravex, J.C. Lasjaunias, O. Béthoux, to be published in J. Phys. F.

- AMAMOU A., KRILL G., Solid State Commun. 28, 957 (1978).
- ANDERSON P.W., HALPERIN B.I., VARMA C.H., Phil. Mag. 25, 1 (1972).
- ANDERSON P.W.,"Lectures on Amorphous Systems", in Physics of Ill-Condensed Matter, North-Holland (1979).
- ARNOLD W., BILLMANN A., DOUSSINEAU P., LEVELUT A., 5th Int. Conf. Physics of Non Crystalline Solids, Montpellier, july 1982.
- BARDEEN J., COOPER L.N., SCHRIEFFER J.R., Phys. Rev. 108, 1175 (1957).
- BELESSA G. and BETHOUX O., Phys. Lett. 62A, 125 (1977).
- COLLINGS E.W. and HO J.C., Phys. Rev. B4, 349 (1971).
- CYROT-LACKMANN F., Phys. Rev. B22, 2744 (1980).
- DOUSSINEAU P., J. Physique Lett. 42, L83 (1981).
- ELIASHBERG G.M., Soviet Phys. JETP 11, 696 (1960) ; 12, 1000 (1961).
- GAROCHE P., CALVAYRAC Y., VEYSSIE J.J., Journal de Physique 41, C8-766 (1980).
- GAROCHE P., BIGOT J., Phys. Rev. B 28, 6286 (1983).
- GRAEBNER J.E., GOLDING B., SCHUTZE R.J., HSU F.S.L., CHEN H.S., Phys. Rev. Lett. 39, 1480 (1977).
- GSCHNEIDER K.A., Solid State Phys. 16, 351 (1964).
- GÜNTHERODT H.J. and H. BECK, "Glassy Metals I in Topics in Applied Physics, vol. 46, Springer Verlag (1982).
- JÄCKLE J., Z. Physik, 257, 212 (1972).
- KROEGER D.M., KOCH C.C., SCARBROUGH J.O., Mc KAMEY C.G., Phys. Rev. B29, 1199 (1983).
- LABORDE O., RAVEX A., LASJAUNIAS J.C., BETHOUX O., J. Low Temp. Phys. 56, 516 (1984).
- LASJAUNIAS J.C., LABORDE O., RAVEX A., ZOUGMORE F., Solid State Comm. 54,
- LASJAUNIAS J.C., RAVEX A., VANDORPE M., HUNKLINGER S., Solid State Comm. 17, 1189 (1975).
- LÖHNEYSEN H.v., PLATTE M., SANDER W., SCHINK H.J., MINNIGERODE G.v., SAMWER K., J. Physique 41, C8-745 (1980).
- Mc MILLAN W.L., Phys. Rev. 167, 331 (1968).
- Von MINNIGERODE, K. SAMWER, Physica, 107B+C, 1217 (1981).
- NEUMAIER K., WIPF H., CANNELLI C., CANTELLI R., Phys. Rev. Lett. 49, 1423 (1982).
- PHILLIPS W.A., J. Low Temp. Phys. 7, 351 (1972).
- OELHAFEN P., HAUSER E., GÜNTHERODT H.J., BENNEMANN K.K., Phys. Rev. Lett. 43, 1134 (1979).

- OELHAFEN P., HAUSER E., GÜNTHERODT H.J., Solid State Commun. 35, 1017 (1980).
- ONN D.G., WANG L.Q., OBI Y., FUKAMICHI K., Solid State Commun. 46, 37 (1983).
- RAVEX A., Thèse Ingénieur Docteur, Grenoble (1976).
- RAVEX A., LASJAUNIAS J.C., BETHOUX O., J. Phys. F : Met. Phys. 14, 329 (1984).
- ROSENSTOCK H.B., J. Non Cryst. Solids 7, 123 (1972).
- SAMWER K. and LÖHNEYSEN H., Phys. Rev. B26, 107 (1982).
- TENHOVER M. and JOHNSON W.L., Phys. Rev. B27, 1610 (1983).
- VARMA C.M. and DYNES R.C., Superconductivity in d- and f- band Metals, edited by D.H. Douglass (Plenum, New York, 1976), p. 507.
- WATERHOUSE N., Canadian Journal of Physics 47, 1485 (1969).
- WEISS G., ARNOLD W., DRANSFELD K., Solid State Commun. 33, 111 (1980).

C H A P I T R E IV

EFFETS DES RECUITS SUR LES PROPRIETES ELECTRONIQUES ET SUPRACONDUCTRICES ET SUR LES EXCITATIONS DE BASSE ENERGIE (TLS)

Les effets de traitements thermiques au-dessous de la température de cristallisation ont été étudiés pour deux alliages d'élément additif distinct ($Zr_{76}Ni_{24}$ et $Zr_{76}Cu_{24}$). Dans un premier temps, l'influence sur les propriétés thermiques a été mesurée (chaleur spécifique et conduction thermique). Les résultats obtenus, présentés ci-après, permettent un certain nombre de constatations :

i) le comportement observé en chaleur spécifique (fortes diminutions de la contribution des TLS, de celle des phonons et des électrons normaux) est très différent de celui des isolants amorphes (pas d'effet de recuit sur le terme TLS (Lasjaunias et al., 1980) et des alliages supraconducteurs amorphes obtenus par trempe du liquide (pas d'effet sur la contribution des TLS,pas ou peu d'effet sur la contribution électronique normale (Grondey et al., 1983 ; Garoche et al., 1982).

ii) l'augmentation systématique de la conduction thermique sous l'effet de recuits est par contre en accord avec les résultats obtenus sur des supraconducteurs amorphes trempés du liquide (Esquinazi et al., 1982).

iii) malgré les fortes variations de la densité d'état électronique et de la température de Debye induites par le recuit, les effets sur la température critique supraconductrice et sur le couplage électron-phonon sont faibles. Nous observons au recuit une diminution de T_c de quelques dizièmes de Kelvins : cette diminution est un point commun aux deux catégories d'alliages et permet en particulier de mettre sérieusement en doute l'hypothèse que l'évolution de T_c est essentiellement gouvernée par la densité d'état électronique (Karkut et Hake, 1983 ; Civale et al., 1983).

Ce dernier point nous a incité à effectuer une analyse particulière de l'évolution des propriétés électroniques et supraconductrices en incluant dans la discussion des mesures de résistivité et de champ critique H_{c_2} effectuées au laboratoire.

Solid State Communications, Vol.40, pp.853-857.
Pergamon Press Ltd. 1981. Printed in Great Britain.

0038-1098/81/450853-05$02.00/0

EFFECT OF STRUCTURAL RELAXATION ON THE LOW TEMPERATURE THERMAL PROPERTIES OF THE SUPERCONDUCTING AMORPHOUS ALLOY $Zr_{.76}Ni_{0.24}$

A. Ravex, J.C. Lasjaunias and O. Béthoux

Centre de Recherches sur les Très Basses Températures, CNRS,

B.P. 166 X, 38042 Grenoble Cedex, FRANCE

Received 2 September 1981 by E.F. BERTAUT

We have measured the low temperature (from 50 mK up to 5 K) specific heat and thermal conductivity of an amorphous ZrNi superconducting alloy as sputtered and after annealing in the amorphous state. We observe after annealing a decrease of the specific heat anomaly below 0.5 K together with an increase of the thermal conductivity. These variations are in agreement with a decrease of the density of two-level systems (T.L.S.) due to the structural relaxation.

Introduction

The existence of low-energy excitations in metallic glasses is now well established by measurements of specific heat and thermal conductivity on superconducting amorphous alloys (ZrPd,[1] ZrCu,[2] ZrBe[3]). Recently a structural mechanism particular to metallic glasses was proposed by Banville and Harris[4] for the two-level tunneling states : they assumed that a TLS corresponds to the motion of a single atom between two or more alternate equilibrium positions within a void. Using computer simulation of the structure they pointed out a relation between the concentration of TLS associated with the presence of voids and the stage of structural relaxation of the material. In order to test this model we have measured the effect of a structural relaxation obtained by thermal annealing on the thermal properties of a similar alloy (ZrNi). For the first time we have evidenced a correlation between the low temperature specific heat and thermal conductivity variations related to a modification of the density of TLS during the annealing.

Sample preparation and characterization

Up to now the thermal properties measurements have been performed on Zirconium alloys[1-3] obtained by rapid quenching from the melt. In our case the alloy is sputtered and deposited in the form of a thick film (thickness about 100 µm) on a substrate held at nitrogen temperature. The deposition rate is about 3 µm/hr. The sample unstuck from the substrate is available in foils (4 cm x 2 cm) of about 0.6 gram weight. The over-all variations of the thickness of the foils are about ± 20 %. A chemical analysis performed on different parts of the sample shows fluctuations of ± 3 at. % around the nominal composition $Zr_{.76}Ni_{.24}$. The amorphicity is checked by X-rays diffraction and D.T.A.

After the measurements of the thermal properties the sample is annealed under vacuum for 24 hrs. at 250°C, temperature lower than the crystallization temperature determined by D.T.A. (350°C). The amorphicity is checked again by X-rays. The two X-rays patterns before and after annealing are essentially identical : within the precision of our measurements the width and the position of the first peak of diffraction are unchanged (table I). Density measurements show a slight increase for the annealed sample (table I) indicating a tendency to a more packed structure. The variations of the room temperature and low temperature (∿ 10 K) resistivity are respectively - 0,8 % and - 2 %.

Table I : X-rays diffraction data and density. $(2\theta)_{max}$ is the diffraction angle (in degrees) of the first peak and $\Delta(2\theta)_{1/2}$ its half height width.

$Zr_{0.76}Ni_{0.24}$	$(2\theta)_{max}$	$\Delta(2\theta)_{1/2}$	density (g/cm^3)
as sputtered	36.3 ± 0.2	5.0 ± 0.2	6.85 ± 0.01
annealed	36.4 ± 0.2	4.8 ± 0.2	6.95 ± 0.01

Specific heat measurements and results

The specific heat C of both samples was measured from 0.04 up to 5 K by a transient heat pulse technique[5]. Four or five foils were pressed between two silicon plates of the same surface. On one plate the thermal link is soft soldered on a gold film evaporated on it and the thermometer - a doped silicon slice[6] - is glued with grease. The heater is pressed between the opposite silicon plate and a sample foil. The thermometer is calibrated below 1.5 K against the magnetic susceptibility of CMN and from 4.2 K up to 7 K by comparison with a calibrated germanium thermometer. Characteristic time

constants for the equilibrium with the heat sink after heat pulses are between a few seconds and a few tenth of seconds. The addenda heat capacity has been measured in a separate experiment : their contribution to the total heat capacity in the worst case varies from 30 % at the lowest temperature to 13 % at 5 K.

In figure 1 we report the specific heat data for both samples. Arrows indicate the superconducting transition temperatures T_c (table 2). The relatively broad transition widths ΔT_c are probably related to the fluctuations of the concentration observed by chemical analysis. Below the transition temperature the electronic specific heat C_{es} decreases exponentially due to electron condensation. But below 0.5 K a residual contribution in addition to those of C_{es} and phonons is clearly apparent.

Above T_c the specific heat obeys a $\gamma T+\beta T^3$ law as can be verified in fig. 2 where C/T is plotted versus T^2. From this analysis we obtain values for γ and β (table 2) which are checked below T_c by verifying that both normal and superconducting state entropies are equal. The presence of the βT^3 term significant of acoustic phonons, which is not observed in amorphous insulators, allows the determination of a Debye temperature θ_D (table 2). However no sound velocity measurements are available in order to get an acoustical determination of θ_D. We observe an important increase of θ_D for the annealed sample : this corresponds to an increase of the structural stiffness. Such an effect has already been observed on PdSi alloys[7]. We also note a decrease of 22 % of γ. However T_c is little modified by the thermal annealing (the effect of structural relaxation on superconducting and electronic properties will be published elsewhere).

Below T_c the superconducting electronic term C_{es} decreases as $A\ \gamma T_c \exp - \Delta_o/kT$. Below 0.5 K after subtracting the phonon term βT^3 and C_{es} we obtain a residual specific heat reported in fig. 3 that we can assign mainly to the low-energy excitations. For both samples the thermal variation is not linear, which rules out the presence of normal inclusions. At the lowest temperature we observe for the annealed sample an increasing contribution which can be attributed to the onset of the nuclear quadrupolar specific heat of Zirconium : this term has also been observed in three other Zr alloys and will be discussed elsewhere. It becomes negligible above 0.1 K. Therefore we analyze the residual specific heat of this sample as the sum of a nuclear contribution $C_N T^{-2}$ (C_N = 15 x 10^{-2} erg.K/mole) and a low-energy excitations contribution with a temperature dependence slightly smoother than linearity

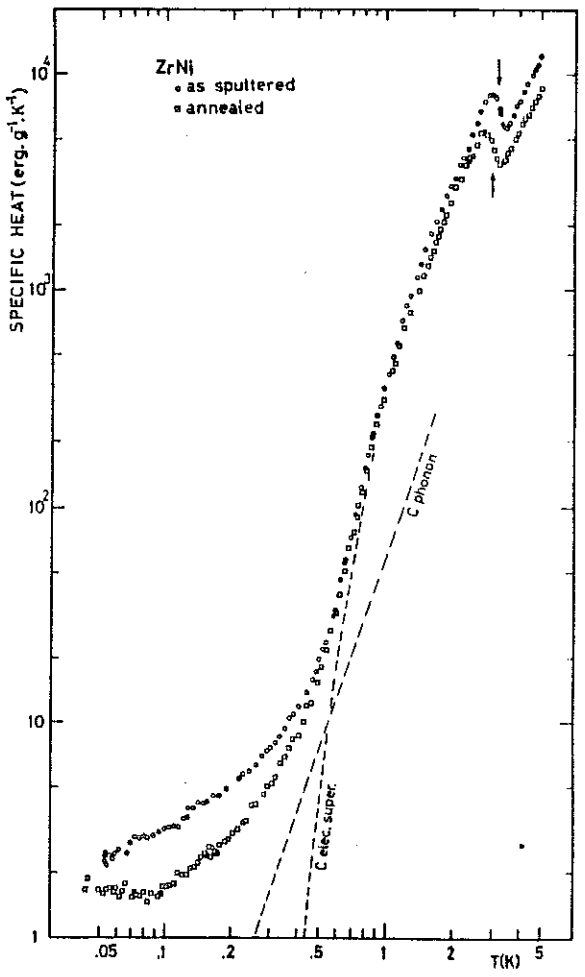

Fig. 1 : Specific heat of the $Zr_{0.76}Ni_{.24}$ amorphous alloy before and after annealing. Arrows indicate the superconducting transition temperatures for each sample. Dashed lines indicate the calculated phonon and superconducting electronic contributions in the case of the "as sputtered" sample.

(see the fit in fig. 3).

For the "as-sputtered" sample such a nuclear term is not apparent and therefore we cannot determine in the same way the temperature dependence of the low-energy excitations below 0.1 K. Anyway we observe that the effect of the annealing is to reduce the excess specific heat. If we suppose that this excess is

Table 2 : Specific heat parameters. v_D is the Debye sound velocity obtained from θ_D

$Zr_{0.76}Ni_{0.24}$	T_c(K)	ΔT_c(K)	γ(mJ/mole.K^2)	β(mJ/mole.K^4)	θ_D(K)	v_D(cm/s)
as sputtered	3.15	0.55	8.15 ± 0.2	0.465	161	1.47 x 10^5
annealed	3.0	0.55	6.30 ± 0.1	0.315	184	1.67 x 10^5

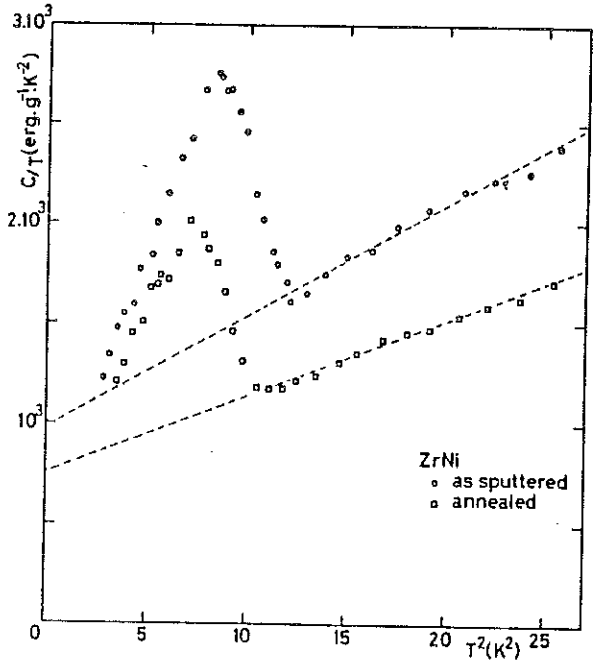

Fig. 2 : Specific heat of the ZrNi alloy above 2 K in a C/T versus T^2 diagramm. Dashed lines indicate the fit of the data in the normal state by a $\gamma T + \beta T^3$ law.

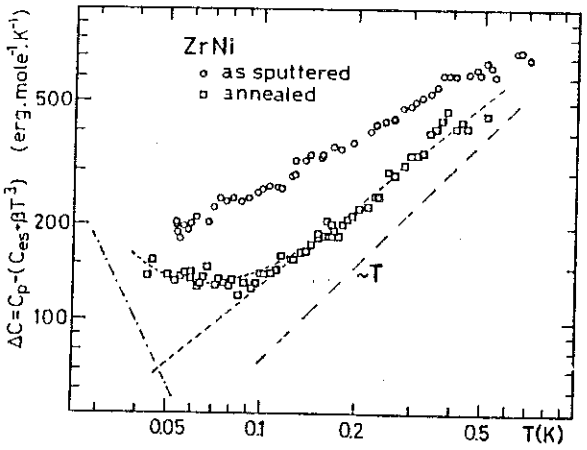

Fig. 3 : Residual specific heat after subtracting from the experimental values the phonon and superconducting electronic contributions. Dashed lines indicate the analysis of the data for the annealed sample by the sum of a nuclear T^{-2} term plus a low-energy excitations contribution. The linear temperature dependence is shown for comparison.

mainly due to the low-energy excitations, the net effect of annealing is to reduce their density of states. In order to verify this hypothesis we have measured the thermal conductivity.

Thermal conductivity measurements and results

The thermal conductivity K of both samples was measured between 0.1 K and 5 K by the permanent heat flow method with two thermometers and one heater. In each sample we cut two bands 4 cm long and 1 cm large. The heater and the heat sink were clamped between the two foils. The thermometers (doped silicon slabs) were glued on copper clamps ; between the two thermometers separated by 1.50 ± 0.05 cm, we have measured precisely the thickness of both foils of each sample. The geometrical factor S/ℓ was respectively 1.30×10^{-2} cm for the "as sputtered" sample and 1.08×10^{-2} cm for the annealed one, with a precision of about 10 %. Because of the low thermal conductance of the samples, we verified that at the lowest temperature the heat loss through electrical leads (Nb-Ti wires in a Cu-Ni matrix) was less than a few percent of the total heat input.

Results of the measurements are shown in fig. 4. The superconducting transition temperatures T_c determined in the specific heat measurements are indicated by arrows : they correspond very well to the change of regime in the phonon-electron scattering due to the rapid decrease of the number of normal-state electrons below T_c.

Well below T_c, both electron heat transport and phonon-electron scattering become negligible. Then the phonon conductivity K_{ph} is mainly limited by the interactions with the low-energy excitations and sample boundary scattering. In fact, above 0.2 - 0.3 K we observe a $T^{1.9}$ - like variation, characteristic in the amorphous materials of the resonant scattering of phonons by the TLS tunneling states. Below 0.2 - 0.3 K the thermal conductivity decreases more rapidly, indicating the progressive influence of the boundary scattering[8]. In the whole temperature range, the value of K for the annealed sample are enhanced in comparison with the "as sputtered" one. In order to evaluate quantitatively the role of these two different mechanisms, we have calculated K(T) from the exact Debye formula :

$$K_{ph} = \frac{1}{3}\int_0^{\infty} \frac{3\omega^2}{2\pi^2 v_D^3} \cdot v_D^2 \cdot \frac{kx^2 e^x}{(e^x-1)^2} \cdot \frac{d\omega}{\tau^{-1}} ,$$

with $x = \frac{\hbar\omega}{kT}$, and the inverse relaxation time

$\tau^{-1} = \frac{\pi}{\rho v_D^2} n\bar{M}^2 \omega \tanh \frac{\hbar\omega}{2kT} + \frac{v_D}{L}$ is determined by the resonant scattering with the TLS[9] and the Casimir limitation (L being the thickness of the sample) ; $\bar{M}$ is an average coupling constant of the TLS with phonons, n the density of states of TLS strongly coupled to the phonons and ρ the density. In absence of any acoustical measurements on such samples we used an average Debye sound velocity v_D obtained from the θ_D value of the specific heat measurements (table 2). Introducing in the above formula the mean thickness of each sample (95µm ± 5µm for the "as sputtered", 82µm ± 5µm for the annealed) from the fit of the data we obtain the value of the unique adjustable parameter $n\bar{M}^2$. The fits are drawn in fig. 4 : they correspond to values of $n\bar{M}^2$ of 9.1×10^7 erg.cm^{-3} and 6.7×10^7 erg.cm^{-3} respectively for the

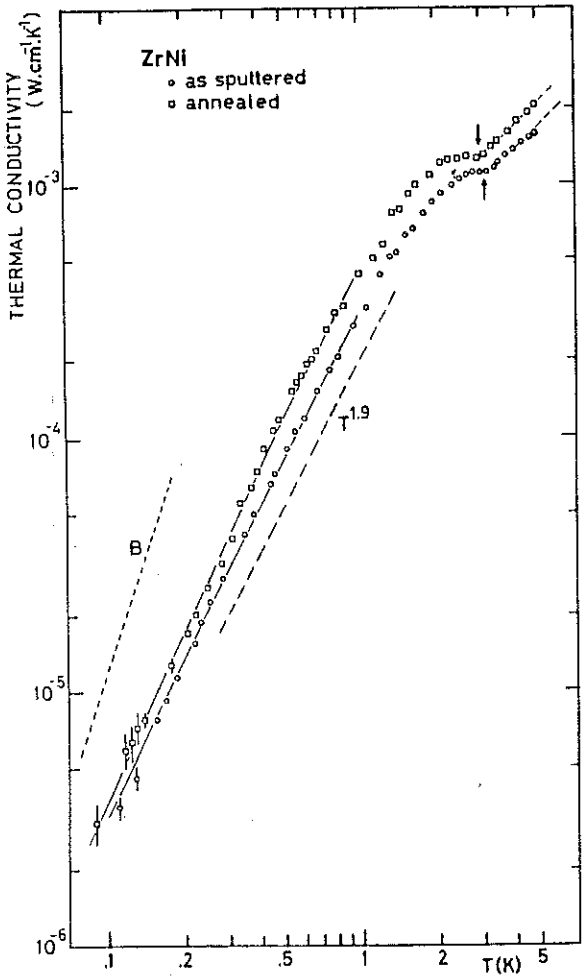

Fig. 4 : Thermal conductivity before and after annealing. Arrows indicate the superconducting transition temperatures determined by specific heat measurements. Solid lines represent the fit of the data by the phonon thermal conductivity limited by both scattering due to TLS and boundary scattering, as described in the text. The $T^{1.9}$ variation is drawn for comparison. Dashed line B represents the boundary scattering term for the annealed sample.

"as sputtered" and the annealed samples, which are close to those obtained in amorphous insulators (SiO_2 : $\sim 1.2 \times 10^8$ erg.cm^{-3}). In the temperature range where the Casimir limitation is negligible, the phonon conduction can be described as :

$$K_{ph\text{-}TLS} = A \frac{k^3 \rho}{\pi^3 \hbar^2} T^2 \frac{v_D}{n\bar{M}^2}$$

Experimentaly one gets :

$K_{ph\text{-}TLS} = 3.0 \times 10^{-4} T^{1.85 \pm 0.05}$ (as sputtered)

$= 4.5 \times 10^{-4} T^{1.90 \pm 0.05}$ (annealed)

expressed in W.cm^{-1}.K^{-1} units.

It shows an increase of the thermal conductivity of 50 % by annealing. Taking into account the variation of the density (+1,5 %, table 1) and of the sound velocity v_D (+14 %, table 2), a significant decrease of $n\bar{M}^2$ by a factor 1.35 remains. This variation is well correlated to the diminution of the residual specific heat if it is ascribed mainly to the TLS low-energy excitations. Moreover, in comparison with the other amorphous superconducting alloys studied up to now[1-3], we obtain a relatively low absolute thermal conductivity which confirms the higher amplitude of the specific heat residual anomaly.

Above T_c, the experimental thermal conductivity follows a linear temperature variation :

$K_{T \geq T_c} = 3.3 \times 10^{-4} T$ W.cm^{-1}K^{-1} (as sputtered)

$= 4.1 \times 10^{-4} T$ W.cm^{-1}K^{-1} (annealed)

K(T) is the sum of two contributions : the electronic heat conduction K_{el} plus the phonon heat conduction K_{ph}. K_{el} can be calculated from the Wiedemann-Franz law

$K_{el} = \frac{2.45 \times 10^{-8}}{\rho_o} T$: we get for both samples the same value $K_{el} \simeq 1.2 \times 10^{-4} T$ W.cm^{-1}.K^{-1} because of the very slight variation of the resistivity ($\rho_o \simeq 200$ μΩ x cm) by about 2 % during annealing. Withdrawing this value from experimental data there remains the phonon contribution K_{ph} which is limited by scattering by both electrons and structural disorder : $K_{ph}^{-1} = K_{ph\text{-}el}^{-1} + K_{ph\text{-}disorder}^{-1}$. The phonon conductivity of the annealed sample is 40 % higher than the "as sputtered" one. Unfortunately we cannot distinguish clearly the contribution of each scattering process. For instance the scattering due to disorder is difficult to estimate in this range of temperature intermediate between the T^2 regime and the "plateau" regime ; anyway we expect a diminution of the scattering by TLS with annealing.

Conclusion

Our thermal conductivity measurements confirm the hypothesis of a reduction by thermal annealing of the intrinsic low-energy excitations density of states suggested by the specific heat results. In fact the analysis of the specific heat data alone is not significant enough : indeed we can evoke other origins for the variation of the anomaly, for example a magnetic component due to Ni clusters or a contribution of gaz inclusions. But such explanations cannot take in account the significant variation of the thermal conductivity which can only be interpreted, in the framework of the tunneling model, by a reduction of excitations strongly coupled to phonons, which rule out the previous hypothesis.

However it is difficult to correlate quantitatively the variation of the TLS contribution observed in the specific heat to the variation of thermal conductivity due to the resonant scattering of phonons by the TLS. From thermal conductivity we have an access to $n\bar{M}^2$ variation, but we cannot distinguish variations of n or $\bar{M}$. Moreover there are not necessarly the same TLS, i.e. the same n, which act in specific heat and thermal conductivity[10]. But qualitatively these results are coherent and agree with the theoretical model of structural relaxation developed by Banville and Harris[4], which predicts a

decrease of TLS density associated with the disappearance of voids during annealing : this is what we observe, the disappearance of voids being confirmed by the 1.5 % increase of the density. Moreover our specific heat results are in reasonable agreement with the calculation of Banville and Harris who obtain a reduction by a factor of 10 of the TLS concentration together with an increase of 4.2 % in the density of their model structure.

Finally we think that our samples prepared by sputtering are more "disordered" than similar alloys prepared by rapid quenching from the melt : the specific heat anomaly is larger and the thermal conductivity lower, both indicating a larger density of TLS. This fact has been recently confirmed by Hillairet et al.[11] who compared by electrical resistivity measurements the thermal structural relaxation of our samples to samples obtained by a melt spinning technique.

References

1. J.E. Graebner, B. Golding, R.J. Schutz, F.S.L. Hsu and H.S. Chen, Phys. Rev. Letters, 39, 1480 (1977).
2. H.v. Löhneysen, M. Platte, W. Sander, H.J. Schink, G.V. Minnigerode and K. Samwer, J. Phys. (Paris) 41, C8-745 (1980).
3. A.K. Raychaudhuri and R. Hasegawa, Phys.Rev. B 21, 479 (1980).
4. M. Banville and R. Harris, Phys.Rev.Lett.44, 1136 (1980).
5. J.C. Lasjaunias, B. Picot, A. Ravex, D. Thoulouze and M. Vandorpe, Cryogenics 17, 111 (1977).
6. G. Frossati, D. Imbert, L. Peccoud, D. Thoulouze and B. Waksmann, Proc. of LT 14 Conf., M. Krusius ed., 4, 206 (1975).
7. U. Mizutani and T.B. Massalski, J. Phys. F 10, 1093 (1980).
8. This effect was not observed in the case of PdZr [1] obtained by melt-spinning technique.
9. J. Jäckle, Z. Physik 257, 212 (1972).
10. B. Golding and J.E. Graebner, Phys. Rev. Letters 37, 852 (1976).
11. J. Hillairet, Private communication.

J. Phys. F: Met. Phys. 14 (1984) 329–346. Printed in Great Britain

Heat treatment effect on thermal, superconducting and structural properties of amorphous sputtered $Zr_{76}Cu_{24}$ alloy

A Ravex, J C Lasjaunias and O Béthoux

Centre de Recherches sur les Très Basses Températures, CNRS, BP 166 X, 38402 Grenoble Cédex, France

Received 23 March 1983, in final form 19 July 1983

Abstract. We report and discuss measurements of low-temperature specific heat and thermal conductivity, upper critical field near T_c, electrical resistivity, mass density and x-ray diffraction, performed on an amorphous superconducting $Zr_{76}Cu_{24}$ alloy obtained by high-rate sputtering deposition at 77 K. A thermal annealing of the samples in the amorphous state before crystallisation induces a large decrease of the very low-temperature specific heat related to the two-level system excitations, whereas thermal conductivity increases in a correlative way. Both electron and phonon contributions to the specific heat in the normal state decrease and tend towards the values of liquid-quenched (LQ) alloys of corresponding composition. At the same time, the other properties studied are less affected, likewise in LQ alloys. The occurrence upon annealing of a chemical phase separation in the amorphous state is proposed to explain the results.

1. Introduction

In recent years a large amount of experimental data has been obtained in the field of amorphous metals. By thermal annealing in the amorphous state, these materials undergo a structural relaxation. Its effect on different physical properties is of great importance in order to elucidate their relations to the structural disorder.

To date mainly metallic alloys prepared by fast quenching ($\sim 10^6$ K s^{-1}) from the melt have been investigated. Apart from systematic studies of the superconductive transition temperature T_c, electrical resistivity, or elastic constants (Young's modulus), very few experiments have been performed on the effect of thermal relaxation in the amorphous state on structural or thermal properties (for a review, see Chen 1980), and almost all referred to liquid-quenched (LQ) alloys. In the continuation of our previous work on a sputtered $Zr_{76}Ni_{24}$ alloy (Ravex *et al* 1981b), we have now investigated the effect of thermal annealing on different physical properties (heat capacity, thermal conductivity, electrical resistivity, superconductivity and 'averaged' structure) of $Zr_{76}Cu_{24}$ obtained by the same sputtering deposition technique. Moreover, this alloy enables a comparison to be made with the corresponding liquid-quenched alloys of the series ZrCu which has been widely studied. We present here the analysis of the specific heat results in a more detailed way than in previous papers; from data in a large temperature interval (from 7 K down to 0.05 K), one can get successive information about the Debye temperature θ_D, the normal electronic density of states, the electronic contribution in the superconducting state, the low-energy excitations (two-level system—TLS) related to the structural disorder and,

0305-4608/84/020329 + 18 $02.25

finally, nuclear quadrupolar interactions. For almost all these contributions, the effect of thermal annealing is large, especially in comparison with the small effect, if any, for LQ alloys. One observes a general trend toward a state of lower entropy, approaching that of the corresponding melt-spun ZrCu. Simultaneously, the phonon thermal conductivity which, well below T_c, is determined by resonant scattering by the TLS shows a variation well correlated to its specific heat counterpart.

The other properties investigated, 'averaged' structure from density and x-ray diffraction, electrical resistivity and superconductive properties (T_c, upper critical field slope at T_c) are close to those of LQ materials and exhibit much smaller variations under annealing than the thermal properties.

2. Sample preparation

The amorphous samples are prepared in the form of thick films by high-rate (10 μm h^{-1}) DC magnetron sputtering of a bulk pre-alloyed target. The alloy is prepared by levitation melting of pure Zr and Cu under a high-purity argon atmosphere. The alloy is then cast in a rotating cold copper mould to obtain a target without any chemical contamination.

For the parent Zr, the results of chemical analysis are as follows: Cr, Mn, Co, Ni, each <10 PPM; Fe, 35 PPM; Hf, 100 PPM. We have measured its low-temperature specific heat previously between 0.03 and 1 K (Lasjaunias and Ravex 1982). The parent Cu is of 5N purity, ASARCO. Sputtering is performed under a pressure of 5×10^{-3} Torr of high-purity argon and the film is deposited on a copper substrate held at liquid-nitrogen temperature. For each deposition run (and target) six foils are removed from the substrate; each has dimensions about 2×4 cm^2, 80–100 μm in thickness and about 0.6 g weight. The samples are usually stored in liquid nitrogen before experiments. In the present study, we used mainly two different samples (A and B) corresponding to two distinct deposition runs and targets. Other samples have been used in characterisation experiments (density, x-ray).

The amorphism is checked by routine x-ray measurements (Cu K_α radiation). The first broad maximum is always located at $2\theta = 36.0° \pm 0.2°$ for the different samples, in either the 'as prepared' state or after annealing at 200 °C.

3. Thermal treatments

3.1. Crystallisation

DTA measurements with a heating rate of 40 K min^{-1} show two successive crystallisation peaks with maxima located at 321 and 357 °C. From the deviation from the base line, the crystallisation appears to start at $T_{cr} \simeq 300$ °C. These results agree with those obtained by Samwer and von Löhneysen (1982) at a rate of 70 K min^{-1} on a series of LQ Zr_xCu_{1-x} alloys. The appearance of two successive crystallisation stages has also been observed by isothermal measurements of electrical resistance at 240 °C as shown in figure 1. The measurement was performed with a sensitive four-wire AC method, using a heating copper sample holder under high vacuum. The resistance begins to decrease significantly after 1.5 h of annealing at 240 °C, indicating the onset of crystallisation. For durations longer than 8 h, ΔR shows two different behaviours as a function of lg t with different slopes corresponding to the formation of successive crystalline phases (denoted as stages I and II) with different growth kinetics. For stage I, an x-ray diffraction diagram obtained on a

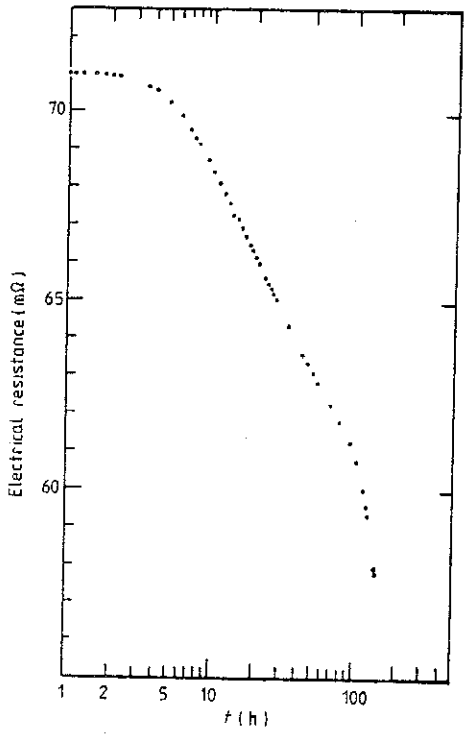

Figure 1. Electrical resistance evolution under thermal annealing: evolution with time at an annealing temperature $T_a = 240$ °C, indicating the crystallisation process.

sample annealed for 24 h at 240 °C under vacuum shows 14 lines superimposed on the amorphous background. By indexing these lines, the crystalline structure is determined to be hexagonal with $c/a = 0.622$, $a = 5.03$ Å and $c = 3.13$ Å. This phase is the metastable ω form of Zr which appears in quenched BCC Zr-rich alloys (Sass 1972) or in pure Zr under pressures greater than 40 kbar (Olinger and Jamieson 1973). Stage II has been investigated by x-ray diffraction on a sample annealed at 370 °C until its resistance does not change further with time: the 20 lines analysed correspond to a mixture of the equilibrium phases (Zr_2Cu and HCP α-Zr) and some remaining ω-Zr phase.

These results suggest that annealing causes the amorphous alloy to decompose into a nearly pure Zr amorphous phase which thereafter crystallises into ω-Zr type, and a second phase more rich in Cu which further crystallises into the equilibrium phases. The first step of crystallisation (ω-Zr) is in agreement with the recent findings of Buschow *et al* (1983) on series of LQ Zr-based alloys.

3.2. Relaxation in the amorphous state

In order to study the structural relaxation, we have measured the dependence of electrical resistance on annealing temperature T_a, which is less than the crystallisation temperature. The room-temperature resistivity ($\rho_{293\,K} = 153 \pm 3\ \mu\Omega$ cm) decreases monotonically with increasing T_a; for $T_a = 200$ °C, $(\Delta\rho/\rho)_{293\,K} = -0.9\%$. The absolute value of the thermal coefficient ($\alpha_{293\,K} = (1/\rho)(d\rho/dT)_{293\,K} = -1.24 \times 10^{-4}\ K^{-1}$) also decreases monotonically with increasing T_a; for $T_a = 200$ °C, $(\Delta\alpha/\alpha)_{293\,K} = -14\%$. The irreversible change of ρ at T_a is achieved within about ten minutes for $T_a > 50$ °C, any further change being of about 10^{-4} in one hour. In the following, the samples termed 'annealed' have been subjected to

this unique thermal treatment for 1 h at 200 °C under a normal pressure of high-purity argon (for specific heat and thermal conductivity measurements) or helium (for other experiments: x-ray diffraction, upper critical field).

4. 'Averaged' structure studies of the amorphous samples

4.1. Density measurements

Density measurements were performed using Archimedes' method with toluene as fluid. The accuracy of the method, checked by numerous measurements, is probably better than 0.01 g cm^{-3} for one foil of mass 0.5–0.6 g. Typically, extreme fluctuations of 0.03 g cm^{-3} are observed over the values of six different foils obtained from the same sputtering experiment. From a total of about 20 measurments on 18 foils obtained from sputtering of three different targets, subjected to various heat treatments (storage at room temperature for several months, annealing at 200 °C), all data are situated between 6.78 and 6.84 g cm^{-3}. These values are in very good agreement with the recent ones for melt-spun samples from Samwer (1983) and Karkut and Hake (1982) and in particular with the results of Altounian and Strom-Olsen (1983), which agree to within 1%.

The fluctuations, ± 0.015 g cm^{-3}, observed between six foils from the same sputtering deposition can be ascribed to variations of Cu concentrations x of about ± 1 at.% from the slope $d\rho/dx = 0.017$ g cm^{-3} (at.%)$^{-1}$ determined for the series $Zr_{1-x}Cu_x$. This is in accord with the widths of superconductive transitions in specific heat experiments as discussed below (§ 5).

On the same foil, we have measured the effect of thermal annealing for 1 h at 200 °C: the density changes from an initial value of 6.805 g cm^{-3} to 6.822 g cm^{-3}, an increase of 0.25%; this variation is comparable with that usually obtained in LQ alloys. A smaller variation (~0.1%) was obtained by a similar annealing of a foil previously aged at room temperature for two months. These results are at variance with our previous observation of a surprisingly large change of density by 1.5% on ZrNi induced by annealing at 250 °C (Ravex *et al* 1981b). Actually, this variation was not significant, since data were taken on two different foils which could not have exactly the same concentration. Indeed, we have since verified by chemical analysis that the concentration fluctuations are larger in ZrNi samples (± 3 at.%) than in ZrCu samples.

We have observed small losses of weight of the samples depending on the time of storage and thermal treatments: for example, the loss of weight for a foil annealed for 1 h at 200 °C is 0.07%; after melting the same foil under vacuum, the loss of weight is 0.12%. These weight losses can be attributed to emission of gases trapped during the deposition process, probably Ar since the usual gases (O_2, N_2, H_2) give stable compounds with Zr and cannot escape from the alloy. With this hypothesis the initial Ar content for this foil should be 0.4 at.%.

4.2. X-ray diffraction measurements

Accurate diffraction spectra have been performed with Mo K_α radiation on piece of sample B, firstly in its 'as prepared' state and after subsequent annealing for 1 h and 12 h at 200 °C. The results will be presented and discussed in detail elsewhere (Samwer and Lasjaunias 1984). Briefly, the total radial distribution functions $G(r)$ obtained up to $r = 16$ Å are only weakly modified upon annealing: the average nearest-neighbour distance

r_1 increases by 0.5%, whereas the second maximum position r_2 decreases by 0.5% after annealing for 1 h at 200 °C. The basic shape of $G(r)$ is similar to that of the LQ ZrCu alloys (Chen and Waseda 1979).

We conclude from these studies on the 'averaged' structure that there is no indication for any significant difference between liquid-quenched and our sputtered samples; moreover, only minor modifications occur for the present sputtered samples upon annealing for 1 h at 200 °C.

5. Specific heat and superconducting measurements

The specific heat measurements have been performed between 0.04 and 7 K in a unique cryostat using a transient heat-pulse technique described previously (Lasjaunias *et al* 1977,

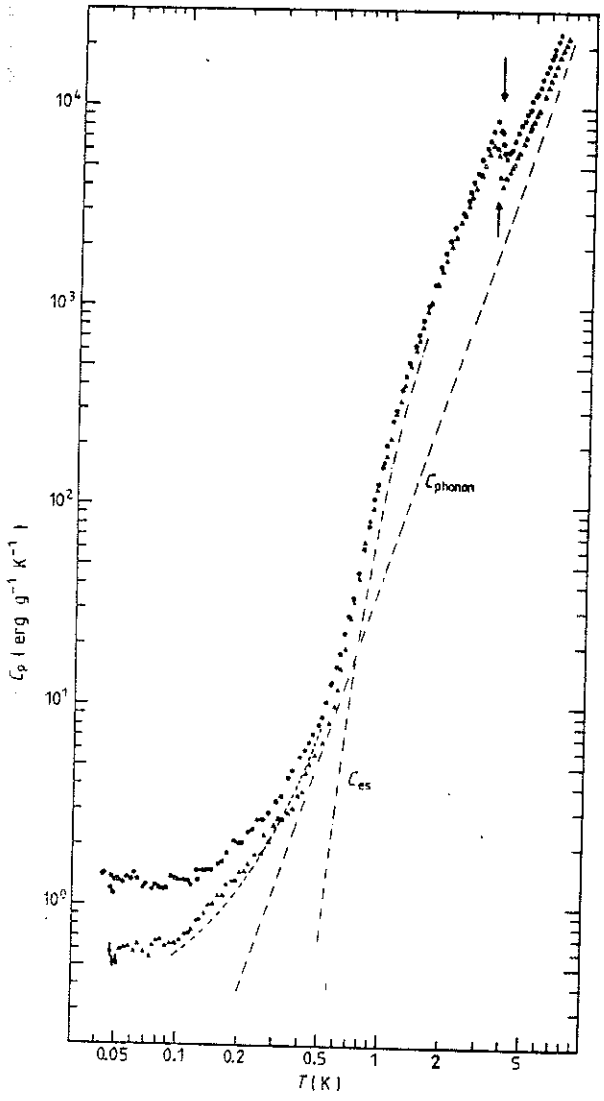

Figure 2. Specific heat of $Zr_{76}Cu_{24}$ (sample A) amorphous alloys in the 'as prepared' state (●) and after annealing for 1 h at 200 °C (▲). The calculated contributions of phonons and electrons in the superconducting state are given for the annealed sample. The broken curve between 0.1 and 0.5 K represents the specific heat of liquid-quenched $Zr_{74}Cu_{26}$ alloy (from Samwer and von Löhneysen 1982) for comparison.

Ravex *et al* 1981a, b); the sample holder consists of two silicon plates and the thermometer is a doped silicon slice. This highly sensitive thermometer is calibrated against the magnetic susceptibility of CMN (cerium magnesium nitrate) below 1.5 K, the ^{4}He vapour pressure between 1.2 and 4.2 K (EPT-76 scale (BIPM 1979), instead of T_{58} scale) and by reference to a calibrated Ge resistor above 4.2 K using the fixed point of the superconducting transition of Pb at 7.20 K (EPT-76 value) for reference. Generally, we measure four or five foils in order to minimise the sample holder contribution (about 1.5 erg K^{-1} at 0.1 K) to the total heat capacity. The uncertainty in the total heat capacity data is of the order of a few per cent; for comparison, the change of thermodynamic ^{4}He scales from T_{58} to EPT-76 induces modification by about 1% of the heat capacity over the whole T range. A larger uncertainty arises at ultra-low temperature, and can be estimated from the scatter of the data.

Results over the whole temperature range for both amorphous states ('as prepared' and annealed for 1 h at 200 °C) of sample A are given in figure 2; the general behaviour is very similar to that previously reported for $Zr_{76}Ni_{24}$ (Ravex *et al* 1981b): the large effect of annealing is observed around and above the superconductive transition temperature (indicated by arrows at the middle of the transition). Below T_c the specific heat is dominated by the electronic contribution in the superconducting state, C_{es}, which decreases exponentially; around 1 K both specific heat curves join, but at very low temperatures ($T \leqslant 0.5$ K) where the low-energy excitations (TLS) become predominant, a large difference occurs rapidly: annealing lowers the specific heat considerably so that it comes close to that of the LQ alloy of very close composition, $Zr_{74}Cu_{26}$ (Samwer and von Löhneysen 1982). In the following we discuss the analysis of these data in successive temperature ranges.

5.1. *Normal state above T_c and superconductive transition*

The data are reported for samples A (figure 3(*a*)) and B (figure 3(*b*)) in a C/T against T^2 plot: above T_c the specific heat obeys a $\gamma T + \beta T^3$ law up to 7 K as in crystalline metals and LQ Zr–Cu amorphous alloys (Garoche 1982, Samwer and von Löhneysen 1982). From the coefficient β, one can extract a Debye-like temperature θ_D and the corresponding sound velocity v_D in the usual form:

$$\beta = \tfrac{12}{5} R \pi^4 \frac{1}{\theta_D^3} = \frac{1944}{\theta_D^3} \text{ (J mol}^{-1}\text{ K}^{-4}\text{)} \qquad \text{or} \qquad \beta = \frac{2\pi^2 k_B^4}{5\hbar^3 \rho v_D^3}. \tag{1}$$

ρ is the mass density. The values of β, θ_D and v_D are given in table 1.

A problem arises concerning the validity of this analysis: it is wrong in the case of insulating glasses where the lattice specific heat over a large range of measuring times always exceeds the acoustic contribution calculated from sound velocities (Pohl 1981, Loponen *et al* 1980). The question is still open in the case of amorphous metals where sound velocity data are very scarce: recent measurements on $Cu_{60}Zr_{40}$ (Arnold *et al* 1982) lead to an acoustic value for θ_D of 275 K compared with (228 ± 6) K from specific heat data (Garoche *et al* 1980, Garoche 1982). Nevertheless, we continue our analysis with the θ_D values obtained from our calorimetric data and the corresponding mean sound velocity v_D that will be used in the analysis of thermal conductivity (§ 6). Thermal annealing results in an increase in θ_D of about 10%, a trend similar, but amplified, to that in other LQ alloys: Pd–Si (Mizutani and Massalski 1980) and FeNiPB (Onn 1981). Such an increase could be

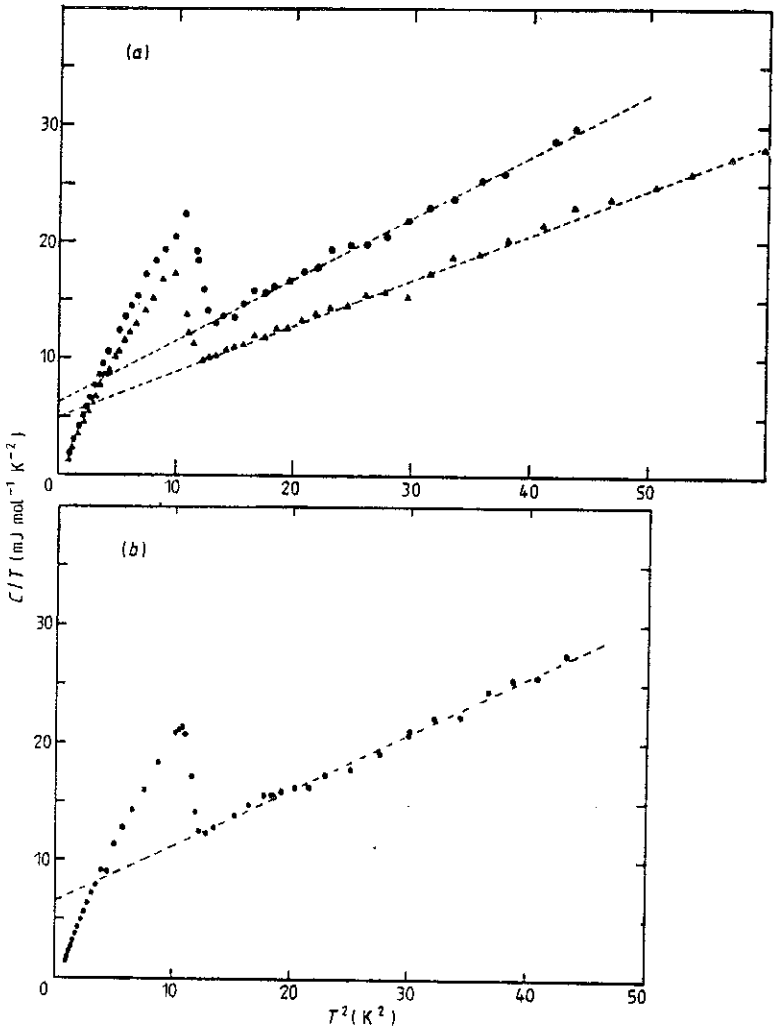

Figure 3. Specific heat of $Zr_{76}Cu_{24}$ shown on a C/T against T^2 diagram: the broken lines indicate the fit to a $\gamma T + \beta T^3$ law for data in the normal state: (*a*) sample A in both the 'as prepared' (●) and annealed (▲) states; (*b*) sample B in the 'as prepared' state.

related to the increase of stiffness as evidenced by measurements of Young's modulus in different amorphous alloys (Chen 1978, Kursumovic and Scott 1980).

In the normal state, we obtain the electronic contribution and the corresponding density of states at the Fermi level:

$$N_\gamma(E_F) = \gamma/\tfrac{1}{3}\pi^2 k_B^2 \tag{2}$$

expressed in states eV^{-1} $atom^{-1}$ (both spin directions). This experimental value is increased in comparison with the 'bare' density of states $N(0)$ by many-body mass enhancement due to electron–phonon interactions and possible spin fluctuations:

$$N_\gamma(E_F) = (m^*/m)N(0) = N(0)(1 + \lambda_{e\text{-}ph} + \lambda_{sf}). \tag{3}$$

The values of γ and $N_\gamma(E_F)$ are given in table 1 and figure 4 together with the data available

Table 1. Specific heat parameters (T above 0.5 K).

	γ (mJ mol^{-1} K^{-2})	$N_\gamma(E_F)$ (states eV^{-1} atom^{-1})	β (mJ mol^{-1} K^{-4})	θ_D (K)	v_D (10^5 cm s^{-1})	T_c (K)	ΔT_c (K)	λ	$\Delta C/\gamma T_c$	a	b
Sample A 'as prepared'	6.25	2.65	0.53	154	1.42	3.45	0.3	0.70	1.89	8.5 (BCS)	1.44 (BCS)
annealed (200 °C for 1 h)	5.0	2.12	0.395	170	1.57	3.30	0.3–0.4	0.67	1.84	10	1.57
Sample B 'as prepared'	6.5	2.75	0.475	160	1.47	3.40	0.2	0.69	1.63	not analysed (no measurement below 1 K)	

Notes. (i) Molecular weight of $Zr_{76}Cu_{24} = 84.58$ g. (ii) a and b are used in the definition of $C_{es}/\gamma T_c = a\exp(-bT_c/T)$. (iii) λ is the electron–phonon coupling constant obtained from McMillan's (1968) formula:

$$T_c = \frac{\theta_D}{1.45}\exp\left(-\frac{1.04(1+\lambda)}{\lambda-\mu^*(1+0.62\lambda)}\right)$$

with $\mu^* = 0.13$ for transition metals.

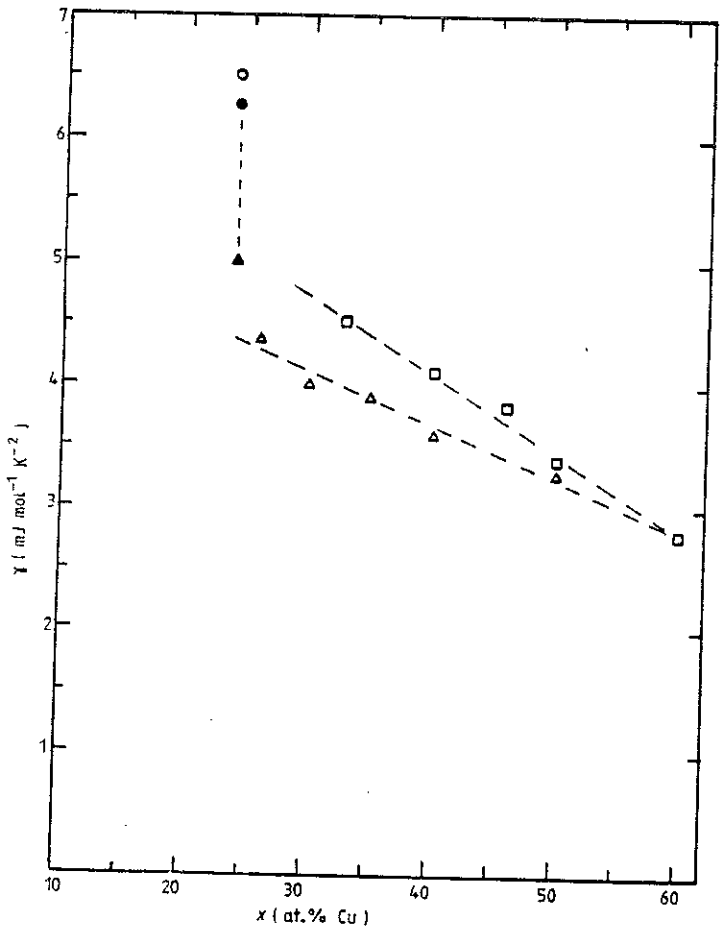

Figure 4. Electronic specific heat coefficient γ as a function of Cu concentration for liquid-quenched ZrCu alloys from two groups: □, Garoche *et al* (1980, 1982) and Garoche and Veyssié (1981) for relaxed samples; △, Samwer and von Löhneysen (1982) for 'as quenched' samples. Our data on sputtered $Zr_{76}Cu_{24}$ alloys are shown: sample A (●, as sputtered; ▲, annealed); sample B (○, as sputtered).

for LQ ZrCu alloys. Both samples A and B show similar higher γ values than the LQ alloys; the large decrease of γ induced by annealing, first observed in sputtered ZrNi, is confirmed here by a similar variation of 20%. Moreover, the value in the annealed state approaches the extrapolated value for similarly relaxed LQ alloys (Garoche *et al*). For these alloys with higher Cu concentration the variations of γ under annealing are small or insignificant ($Zr_{70}Cu_{30}$, Grondey *et al* 1983; $Zr_{54}Cu_{46}$, Garoche *et al* 1982: in this case a variation of 4% in the opposite sense occurs).

Figure 5 shows the electronic specific heat (after subtracting the βT^3 term from total specific heat) divided by T. From this diagram we can define the value of T_c, using the criterion of equalisation of entropy (broken line in the figure). One also obtains an ideal specific heat jump of amplitude ΔC at T_c. The values of T_c, the normalised specific heat jump $\Delta C/\gamma T_c$ and the width of the transition ΔT_c are given in table 1.

The T_c values are in very good agreement with the $T_c(x)$ curve defined by numerous

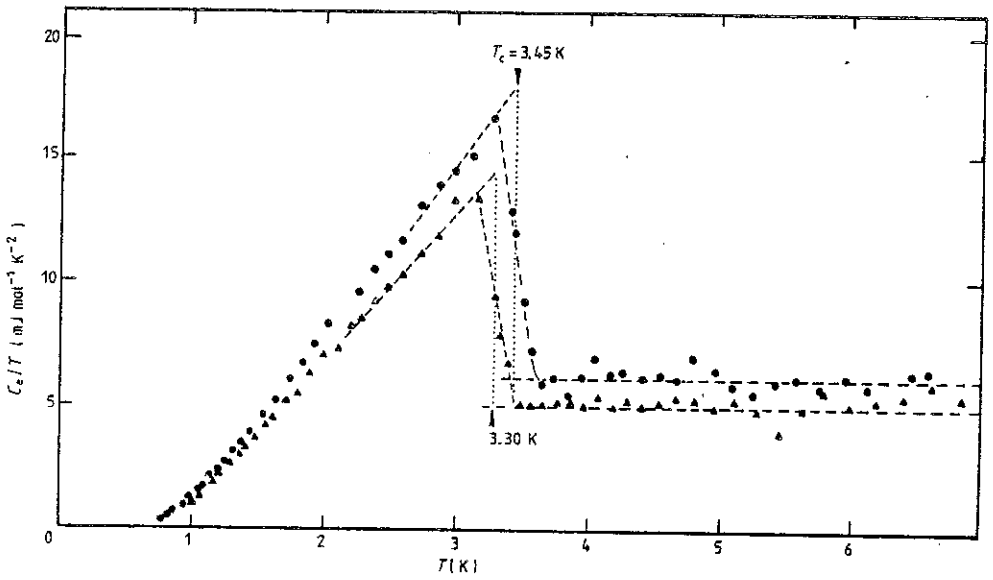

Figure 5. Electronic specific heat C_e shown as C_e/T against T between 1 and 7 K for sample A in both states (●, as sputtered; ▲, annealed). The vertical dotted lines represent the specific heat jump at T_c. The superconductive transition temperatures, indicated by arrows, are determined by equalisation of areas under the experimental C_e/T curve.

results on LQ Zr_xCu_{1-x} alloys (Garoche *et al* 1982, Samwer and von Löhneysen 1982, Altounian and Strom-Olsen 1983).

The width ΔT_c depends on the amount of material used for the experiment (2.5 g for sample A, only 0.5 g for sample B) and hence can be accounted for by concentration fluctuations. From $dT_c/dx \simeq 0.11$ K (at.%)$^{-1}$, one obtains fluctuations of ± 1.5 at.% for sample A and ± 1 at.% for sample B, in good agreement with those estimated from density measurements.

Thermal treatment decreases T_c by 0.15 K: this diminution by a few tenths of a degree is a common feature for numerous amorphous Zr-based alloys (ZrCu, Altounian *et al* 1981, Garoche *et al* 1982; ZrNi, Ravex *et al* 1981a, b, Anderson *et al* 1982; ZrRh, Drehman and Johnson 1979; ZrPd), whatever the sense of variation (if any) for θ_D or γ may be. This lack of correlation is more evident in the present case where such large variations of both γ and θ_D would imply, within the usual framework of superconductivity, much larger variations for T_c. Another example of lack of correlation between the measured value of γ and superconductivity is given by the absence of variation of the upper critical field slope at T_c, measured by a resistive method on sample B (table 2): indeed $(dH_{c_2}/dT)_{T_c}$ should be proportional to the product $\gamma\rho$ and hence should vary by 21%.

Table 2. Density, electrical resistivity and upper critical field slope at T_c.

Sample	Density (g cm^{-3})	$\rho_{300\,K}$ ($\mu\Omega$ cm)	$(dH_{c_2}/dT)_{T_c}$ (kOe K^{-1})
'as prepared'	6.805	153.0 ± 3	26.7 ± 0.5
annealed	6.822	151.7 ± 3	26.6 ± 0.5

Such discrepancies confirm the hypothesis of phase separation upon annealing into two amorphous phases previously suggested by the crystallisation studies. Indeed, if the annealed sample is now a mixture of two phases of different chemical compositions, its measured γ value will be less than that of the homogeneous 'as prepared' sample. On the other hand, depending on the scale of the inhomogeneities, its T_c will be governed by proximity effects and will not be related to the measured γ by the classical BCS relation as in the homogeneous 'as prepared' sample. The fact that the annealed sample behaves as a single superconductor with a slightly changed T_c indicates an inhomogeneity scale less than the zero-temperature superconducting coherence length (~70 Å).

5.2. The superconducting range: 0.5 K $\leqslant T \leqslant T_c$

Below T_c two contributions to the specific heat are present: the electronic term C_{es} and the 'lattice' βT^3 term. In order to determine C_{es} we have to subtract the cubic term from the measured specific heat. As we shall discuss later concerning the temperature dependence of the TLS contribution, the more convincing analysis in the case of the 'as prepared' sample is obtained with a β value lower than that determined for $T > T_c$. We have chosen to use the same value for both states: that obtained above T_c for the *annealed* sample. Note that the choice of β is not important for the determination of C_{es}, except in the very low-temperature range: $T \leqslant 0.8$ K. The thermal variation of C_{es} determined in this way is shown in figure 6 in the usual normalised plot $\lg(C_{es}/\gamma T_c)$ against T_c/T. For $1 \leqslant T_c/T \leqslant 2$, a good fit is obtained with the Mühlschlegel numerical data. For $T_c/T > 2$ variations are linear for both samples, which corresponds to the usual exponential decay $C_{es}/\gamma T_c = a \exp(-bT_c/T)$. In the range $2.5 \leqslant T_c/T \leqslant 6$, the BCS relation for weak coupling

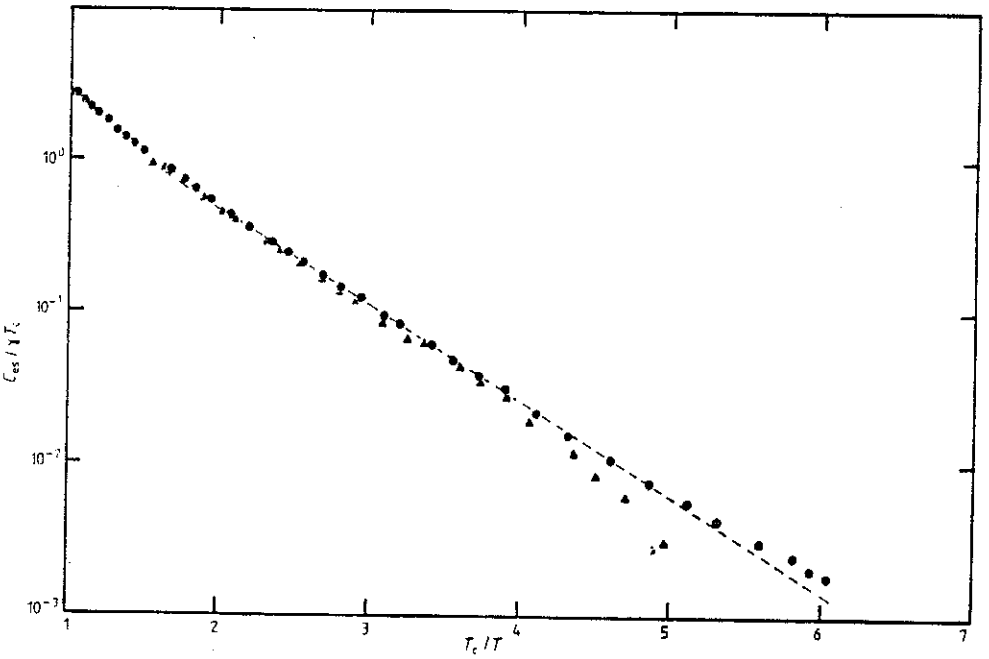

Figure 6. Electronic specific heat of sample A (●, as sputtered; ▲, annealed) in the superconducting state plotted as $C_{es}/\gamma T_c$ against T_c/T. The broken line represents the BCS variation valid in this temperature range: $C_{es}/\gamma T_c = 8.5 \exp(-1.44\, T_c/T)$.

gives $a=8.5$ and $b=1.44$, which are the values obtained for the 'as prepared' sample (table 1).

From the electronic specific heat we have calculated the superconducting entropy and, with the criterion of equality of entropy at T_c for both states, determined the γ value as

$$S(T_c)=\int_0^{T_c}\frac{C_{es}}{T}\,dT=\gamma T_c.$$

This value is higher by 6% and 9% respectively for 'as prepared' and annealed samples than that obtained from data above T_c.

5.3. Temperatures below 0.5 K

Below 0.5 K, C_{es} becomes rapidly negligible. Down to 0.1 K, two contributions are dominant: the lattice and the TLS excitations. The residual specific heat ΔC obtained after subtracting the βT^3 term and C_{es} is shown in figure 7. The thermal variation of ΔC above 0.2 K is very sensitive to the value of β. contrary to the previous case of other sputtered Zr–M alloys of the same composition (ZrNi, ZrPt, Ravex *et al* 1981a, b, Lasjaunias and Ravex 1983), where a much larger (by a factor of two or three) TLS contribution partly hid the influence of a βT^3 term roughly similar to the one here. If one subtracts the βT^3 term determined from data above T_c, this leads to a variation for ΔC which rapidly decreases with T above 0.3 K (open circles for the 'as prepared' sample in figure 7). Since this peculiar thermal variation has never been observed in the other amorphous Zr–M alloys,

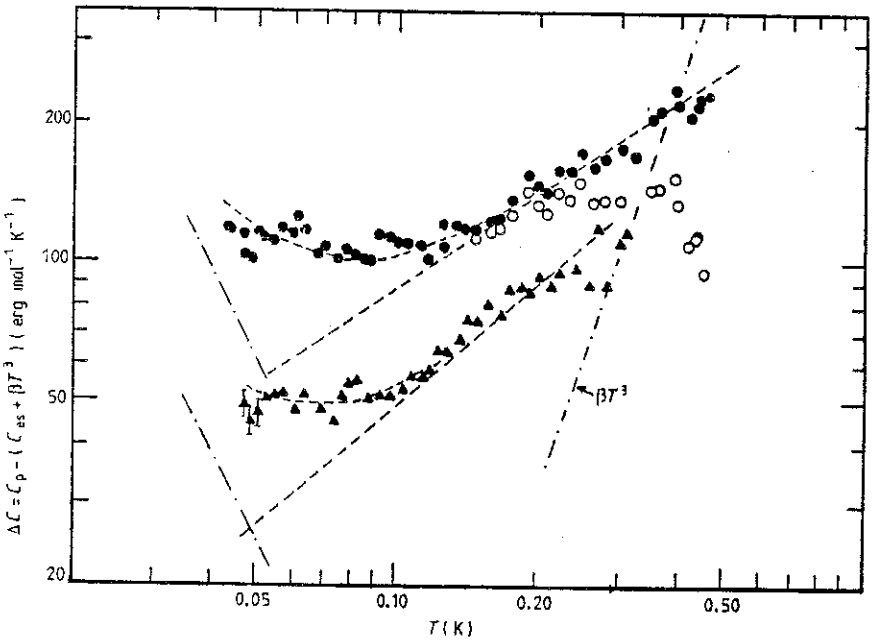

Figure 7. Residual low-temperature specific heat after subtracting the electronic C_{es} and the phonon βT^3 contributions from experimental data. For the 'as sputtered' sample, ○ corresponds to the analysis with its own βT^3 term and ● to that of the annealed (▲) sample (chain line). The broken curves indicate the fit of the data by the sum of a nuclear T^{-2} term plus a TLS term ($C_{TLS}\approx T^{\alpha}$, $\alpha\leqslant 1$).

this would rather suggest that the actual βT^3 value to be used in this low-temperature range is lower than that determined in the normal state above T_c. In the absence of experimental acoustic data, it is difficult to speculate on the possible evolution of the true Debye term well below T_c, but this could also imply the existence of a cubic term additional to the true acoustic one in the normal state, which progressively disappears in the superconducting state, suggesting a possible origin in electron–phonon interactions (Danino and Overhauser 1982). Nevertheless, if one uses the value of β determined for the annealed sample in its normal state for the 'as prepared' sample, one recovers a monotonic increase $\Delta C(T)$, in agreement with the other alloys.

For $T \leqslant 0.2$ K, the residual anomaly is then analysed as the sum of the TLS contribution plus a very low-temperature nuclear contribution $C_N T^{-2}$ ($C_N = (18 \pm 5) \times 10^{-2}$ erg mol^{-1} K^{-1} for the 'as prepared' sample) very probably due to the electric quadrupolar moment of ^{91}Zr nuclei (nuclear spin $I = \frac{5}{2}$) and observable through a coupling process between nuclei and TLS, which is discussed elsewhere (Lasjaunias and Ravex 1983). For the 'as sputtered' sample, C_{TLS} increases smoothly as $T^{0.7}$; this temperature dependence is very similar to other 'as prepared' sputtered alloys (ZrNi, ZrPt, Ravex *et al* 1981a, b) with C_{TLS} variations between $T^{0.5}$ and $T^{0.7}$, which indicates a smooth decreasing energy dependence for the density of states $n(E)$. For the annealed sample the nuclear contribution is about two times smaller than for the 'as prepared' state, and that of TLS is also reduced by a factor 1.5–2, now approaching a linear variation ($\sim T^{0.9}$–$T^{1.0}$).

Both these effects of annealing on C_{TLS}, the reduction of magnitude and simultaneously a temperature dependence closer to linearity, corresponding to a more energy-independent density of states, exactly confirm our previous results on ZrNi. Moreover, upon annealing the C_{TLS} value of our sputtered sample tends towards that measured in LQ $Zr_{74}Cu_{26}$ (figure 2), for which a similar thermal treatment has no effect (Grondey *et al* 1983). This trend is similar to that in the $T > T_c$ range.

If we approximate C_{TLS} for the annealed states of both ZrCu and ZrNi by an exact linear variation, we can estimate a density of states n_0 from $C = \frac{1}{6}\pi^2 n_0 k_B^2 T$: $n_0 \simeq 3.6 \times 10^{33}$ erg^{-1} cm^{-3} for ZrNi and $n_0 \simeq 1.3 \times 10^{33}$ erg^{-1} cm^{-3} for ZrCu.

6. Thermal conductivity measurements—discussion of the low-energy excitations (TLS)

The thermal conductivity experiments were performed on the same unique foil of sample A of width about 1 cm and length 4 cm, successively measured in the 'as prepared' and annealed states. We used the permanent heat flow method with two thermometers (Si doped) separated by a distance $l = 1.50 \pm 0.05$ cm and one heater. One thermometer is used to regulate the temperature either under forced flux or under natural parasitic heat flow. The second is used to measure the temperature difference due to the forced flux. We verified that the thermal shunt by the electrical wires (Nb–Ti in a Cu–Ni matrix) is always less than 2%. From the volume of the foil (calculated from weight and density) and its surface, we deduced a mean thickness of 80 μm and a corresponding geometrical factor $S/l = 5.25 \times 10^{-3}$ cm with a total uncertainty of about 5%.

The results are shown in figure 8. In the superconducting state, between ~0.2 K and 1 K, for both samples $K(T)$ obeys the usual $T^{1.9-2.0}$ variation characteristic of the resonant scattering of phonons by the tunnelling states: $K = 8.5 \times 10^{-4}\, T^{1.90 \pm 0.02}$ W cm^{-1} K^{-1} for the 'as prepared' sample and $K = 15 \times 10^{-4}\, T^{2.0 \pm 0.05}$ W cm^{-1} K^{-1} for the annealed sample.

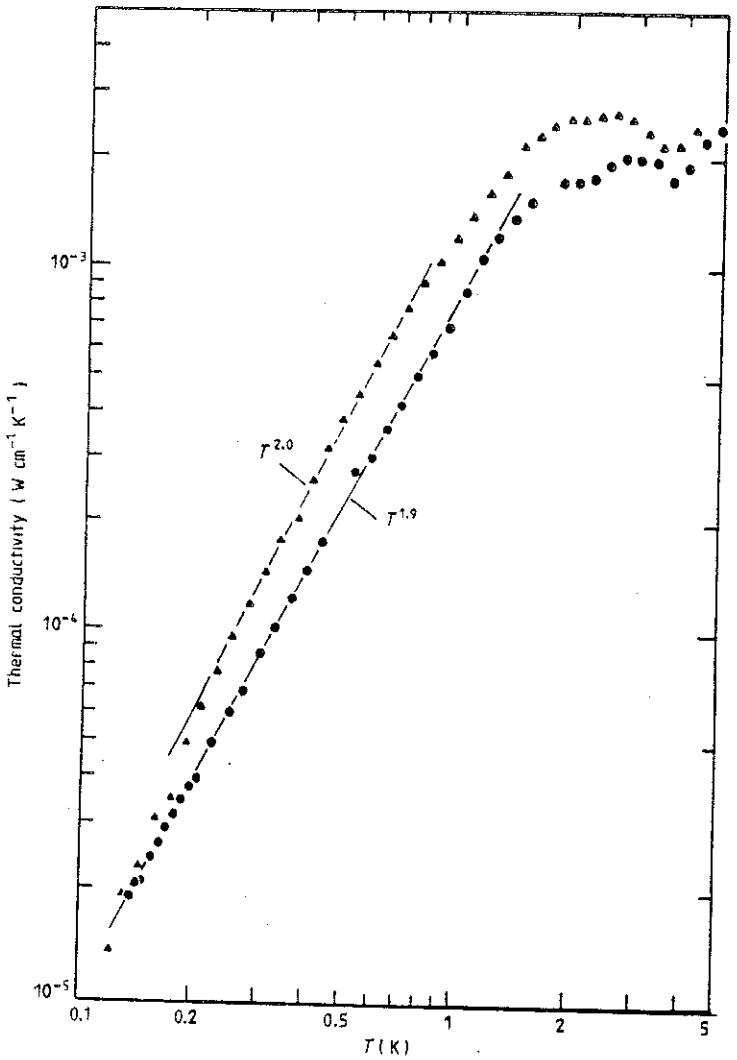

Figure 8. Thermal conductivity data on $Zr_{76}Cu_{24}$. ●, as sputtered; ▲, annealed.

In a similar way as for our previous results on sputtered ZrNi, the effect of thermal annealing is to increase K by a factor of about 1.6–1.7, which implies, in agreement with the reduction of residual specific heat anomaly, a reduction of the density of TLS.

For the annealed sample below 0.2 K, K decreases more rapidly than T^2 suggesting an additional scattering mechanism. The same effect observed in ZrNi samples was attributed to the progressive influence of boundary scattering. This interpretation cannot apply here since this effect should also occur in the 'as prepared' sample which has the same thickness as the annealed one.

The increase of K upon annealing is a general feature of amorphous ZrCu alloys (Esquinazi *et al* 1982, Grondey *et al* 1983).

From the quasi-quadratic T^2 regimes, we can obtain a first numerical estimation of the characteristic scattering parameter $\tilde{n}M^2$ where $\tilde{n}$ represents the constant density of states

for the tunnelling states most strongly coupled to the phonons (which can be only a small fraction of the usual value $n(E)$ determined from specific heat measurements on the timescale of a few seconds (Black 1978)) and M is the average phonon–TLS coupling constant. Applying the kinetic approximation and using the Debye specific heat of phonons, the numerical expression for K is (Graebner *et al* 1977)

$$K(T)=1.65\,\frac{\rho k_B^3}{\pi^3\hbar^2}\left(\frac{v_l}{\tilde{n}M_l^2}+\frac{2v_t}{\tilde{n}M_t^2}\right)T^2. \tag{4}$$

l and t stand for the longitudinal and transverse polarisations. In the absence of sound velocity data, we make the usual approximation $v_l \approx 2v_t$, obeyed in amorphous materials, with $v_t \simeq 0.9\,v_D$ obtained from the βT^3 specific heat. Usually $M_l^2 \approx 2M_t^2$, and one obtains

$$K(T)=1.26\times 10^5\rho\,\frac{3v_t}{\tilde{n}M_t^2}\,T^2 \simeq 3.4\times 10^5\,\frac{\rho v_D}{\tilde{n}M_t^2}\,T^2 \tag{5}$$

(CGS units: K expressed in erg s^{-1} cm^{-1} K^{-1}).

Within this rough analysis, we have to approximate our data to exact T^2 laws. For the 'as prepared' sample, a good approximation is $K \simeq 9\times 10^{-4}\,T^2$ W cm^{-1} K^{-1}. For the annealed sample, we use the experimental T^2 law between 0.2 and 0.7 K.

As we discussed previously in the specific heat analysis, a problem occurs concerning the actual value of the phonon contribution (here phonon velocity) in the very low-temperature range, which can differ from that obtained from the specific heat in the normal state above T_c. In the case of the 'as prepared' sample, it appears more appropriate to use the Debye term corresponding to the annealed sample. Therefore we indicate in table 3 the values of $\tilde{n}M_t^2$ calculated with both values of v_D in the case of the 'as prepared' samples. In order to compare numerically with our previous results on ZrNi (Ravex *et al* 1981b) we have also calculated the $\tilde{n}M_t^2$ coupling terms for this alloy in the same way (table 3). The effect of annealing is to decrease $\tilde{n}M_t^2$ by a factor of 1.68 in the ZrCu alloy and 1.57 in the ZrNi alloy.

These values are very similar, and it is worth noting the good numerical correlation for the four samples between the coupling parameter and the amplitude of the TLS specific heat (except the low value of C_{TLS} at 0.1 K for ZrNi annealed; table 3). Note the large variation

Table 3. Low-temperature thermal conductivity and specific heat regimes related to TLS excitations ($T \ll T_c$) for $Zr_{76}Cu_{24}$ and $Zr_{76}Ni_{24}$ alloys.

		C_{TLS} (erg mol^{-1} K^{-1})		
Sample	$\tilde{n}M_t^2$ (erg cm^{-3})†	$T=0.1$ K	0.2 K	0.4 K
$Zr_{76}Ni_{24}$	12.9×10^7	260	395	680
'as prepared'	(11.2×10^7)	(260)	(380)	(570)
annealed	8.2×10^7	120–130	210	400–450
$Zr_{76}Cu_{24}$	4.03×10^7	90	145	225
'as prepared'	(3.64×10^7)	(90)	(140)	
annealed	2.4×10^7	50–55	90	not estimated

† $\tilde{n}M_t^2$ is obtained from the approximate formula (5) valid for a T^2 regime. For the 'as prepared' states, the two values correspond either to the Debye term of the corresponding state (in parentheses) or to that of the annealed state (see text).

of the TLS parameters for these Zr-based alloys, never previously obtained with insulating glasses. This correlation supports unambiguously the common TLS origin of both low-temperature specific heat and thermal conductivity. In particular, it rules out a possible origin for the specific heat anomaly in gaseous impurities (Ar in the present case) loosely bound within cavities of the material (Rosenstock 1972), and evidenced experimentally in vitreous silica (Van Maaren *et al* 1980, Fisher 1980).

The strong reduction of the TLS density upon annealing is not related, as we previously supposed in ZrNi amorphous alloys (Ravex *et al* 1981b), to a significant increase of the mass density since it has not been observed here. But it is more probably related to the phase separation suggested by the crystallisation studies and the superconducting behaviour. A striking analogy can be made with the effect of annealing on a quenched ZrNb (20%) single crystal which exhibits glassy-like low-temperature thermal properties (Lou 1976). This analogy suggests a common structural origin for the TLS in these two kinds of Zr alloy. In ZrNb quenched crystals, Lou has identified the TLS with atomic motions associated with fluctuations between two local atomic orders: those of the BCC β-Zr and hexagonal ω-Zr phases which coexist in the material. The observed decrease of the TLS density of states in the annealed crystal is attributed to the decrease of the fluctuation frequency induced by the growth of the ω domains.

Since the first stage of crystallisation in our Zr–Cu samples is the ω phase of (nearly) pure Zr, we suppose that isolated groups of Zr atoms (about 10 atoms) with such a local ω order exist in the amorphous state and can fluctuate by tunnelling into other metastable configurations of higher energy. Then, the segregation of Zr during the early stage of the chemical phase separation induced by annealing causes these groups to grow rapidly. Consequently, the fluctuation frequency decreases just as the observed TLS density of states does. This scheme is in accordance with the hypothesis of Mon and Ashcroft (1978), who relate the presence of TLS to the occurrence of polymorphism of the material, Zr in the present case.

In corresponding liquid-quenched alloys, the chemical phase separation could be achieved during the quenching process. The consequence will be a lower TLS density and specific heat, with no further effect upon annealing; this is observed experimentally (Grondey *et al* 1983).

7. Conclusion

Contrary to the behaviour of glassy alloys prepared by fast quenching from the melt, the amorphous alloy $Zr_{76}Cu_{24}$ obtained by high-rate sputtering deposition at 77 K exhibits rather large variations of its low-temperature thermal properties upon annealing in the amorphous state. Over the whole temperature range investigated, the specific heat of the 'as prepared' state is higher than that of the annealed state. Thus, annealing induces a reduction of the low-temperature entropy, which indicates a structural evolution to a more stable state very similar to that of liquid-quenched alloys. From a thermodynamic point of view, the deposited amorphous alloys appear more 'disordered' than their liquid-quenched counterparts. It should be noted that all the contributions to the specific heat (two-level systems, electrons and phonons) are reduced upon annealing, the largest reduction being observed for the TLS contribution.

This behaviour, the crystallisation studies and the qualitative disagreement between the variation of the superconducting properties and electronic specific heat upon annealing

strongly suggest that a chemical phase separation occurs during the heat treatment. Probably due to the very short scale of the inhomogeneities induced by the phase separation (a few tens of angstroms), the annealing has very little effect on the 'averaged' amorphous structure (mean interatomic distances, density) and only small effects on electrical resistivity and superconducting properties, as observed also in liquid-quenched amorphous alloys.

As discussed before, the TLS excitations can be attributed to fluctuations of local atomic order in small groups of Zr atoms. Then, the reduction of the TLS specific heat upon annealing is associated with the growth of these groups of atoms during the phase separation.

Finally, it is still not clear whether the cubic term of the specific heat can be attributed to a pure Debye term or whether an extra contribution exists which decreases at low temperature: more direct measurements of the sound velocity or shear modulus would be necessary to clear up this point.

Acknowledgments

One of the authors (JCL) would like to thank Professor W L Johnson for his hospitality during his stay at the California Institute of Technology and for the opportunity to perform critical field and accurate x-ray diffraction experiments. He is also grateful to Dr K Samwer for his interest and active participation in the diffraction experiments.

References

Altounian Z, Guo-Hua Tu and Strom-Olsen J O 1981 *Solid State Commun.* **40** 221–4
Altounian Z and Strom-Olsen J O 1983 *Phys. Rev.* B **27** 4149–56
Anderson A C, Koch C C and Scarbrough J O 1982 *Phys. Rev.* B **26** 1156–63
Arnold W, Billmann A, Doussineau P and Levelut A 1982 *Proc. 5th Int. Conf. on the Physics of Non-Crystalline Solids, Montpellier* (*J. Physique Coll.* C9 537–9)
Black J L 1978 *Phys. Rev.* B **17** 2740–61
Bureau International des Poids et Mesures 1979 *Metrologia* **15** 65–8
Buschow K H J, Vincze I and van der Woude F 1983 *J. Non-Cryst. Solids* **54** 101–6
Chen H S 1978 *J. Appl. Phys.* **49** 3289–91
—— 1980 *Rep. Prog. Phys.* **43** 353–432
Chen H S and Waseda Y 1979 *Phys. Status Solidi* a **51** 593–9
Danino M and Overhauser A W 1982 *Phys. Rev.* B **26** 1569–73
Drehman A J and Johnson W L 1979 *Phys. Status Solidi* a **52** 499–507
Esquinazi P, de la Cruz M E, Ridner A and de la Cruz F 1982 *Solid State Commun.* **44** 941–4
Fisher R A 1980 *J. Non-Cryst. Solids* **41** 251–6
Garoche P 1982 *Thesis* University of Paris (Orsay)
Garoche P, Calvayrac Y, Cheng W and Veyssié J J 1982 *J. Phys. F: Met. Phys.* **12** 2783–96
Garoche P, Calvayrac Y and Veyssié J J 1980 *J. Physique Coll.* **41** C8 766–9
Garoche P and Veyssié J J 1981 *J. Physique* **42** L365–8
Graebner J E, Golding B, Schutz R J, Hsu F S L and Chen H S 1977 *Phys. Rev. Lett.* **39** 1480–3
Grondey S, von Löhneysen H, Schink H J and Samwer K 1983 *Z. B* **51** 287–95
Karkut M G and Hake R R 1982 *Physica* B **109–110** 2033–5
Kursumovic A and Scott M G 1980 *Appl. Phys. Lett.* **37** 620–2
Lasjaunias J C, Picot B, Ravex A, Thoulouze D and Vandorpe M 1977 *Cryogenics* **17** 111–7
Lasjaunias J C and Ravex A 1982 *Phys. Lett.* **88A** 157–8
—— 1983 *J. Phys. F: Met. Phys.* **13** L101–6
Loponen M T, Dynes R C, Narayanamurti V and Garno J P 1980 *Phys. Rev. Lett.* **45** 457–60

Lou L F 1976 *Solid State Commun.* **19** 335–8
McMillan W L 1968 *Phys. Rev.* **167** 331
Mizutani U and Massalski T B 1980 *J. Phys. F: Met. Phys.* **10** 1093–100
Mon K K and Ashcroft N W 1978 *Solid State Commun.* **27** 609–12
Olinger B and Jamieson J C 1973 *High Temp. –High Pressures* **5** 123
Onn D G 1981 *J. Appl. Phys.* **52** 1788–93
Pohl R O 1981 *Amorphous Solids (Low-Temperature Properties)* ed. W A Phillips (Berlin: Springer)
Ravex A. Lasjaunias J C and Béthoux O 1981a *Physica* B **107** 395–6, 397–8
—— 1981b *Solid State Commun.* **40** 853–7
Rosenstock H B 1972 *J. Non-Cryst. Solids* **7** 123–6
Samwer K 1983 Private communication
Samwer K and Lasjaunias J C 1984 to be published
Samwer K and von Löhneysen H 1982 *Phys. Rev.* B **26** 107–23
Sass S L 1972 *J. Less-Common Met.* **28** 157
Van Maaren M H, Olijhoek J F and Parlevliet C 1980 *Solid State Commun.* **35** 867–70

Journal of Low Temperature Physics, Vol. 56, Nos. 5/6, 1984

Effect of Structural Relaxation on Critical Fields H_c and H_{c2} and on Resistivity in Sputtered Amorphous Alloys $Zr_{76}Cu_{24}$ and $Zr_{76}Ni_{24}$

O. Laborde,* A. Ravex, J. C. Lasjaunias, and O. Béthoux

Centre de Recherches sur les Très Basses Températures, CNRS, Grenoble, France

(Received December 12, 1983; revised February 22, 1984)

We report critical field results on sputtered amorphous $Zr_{76}Cu_{24}$ and $Zr_{76}Ni_{24}$ alloys. The $H_c(T)$ obtained from calorimetric measurements is well described by assuming that both systems are weak coupling superconductors. A similar good agreement is not found for $H_{c2}(T)$ obtained by a resistive method; tentative explanations of this discrepancy are suggested. We also report resistivity measurements in the normal state on $Zr_{76}Ni_{24}$ alloys. Results are well interpreted in the framework of the Faber–Ziman diffraction model. An alternative explanation, the Kondo-like model for two-level systems, is also discussed.

1. INTRODUCTION

Amorphous zirconium alloys with transition metals have been the subject of intensive research for the last few years; indeed, these binary alloys are relatively easy to prepare and display a large variety of physical properties, from superconductivity to magnetism. Most of the results have been obtained on rapidly melt-quenched samples, and few results are available for samples prepared by sputtering. The structural relaxation that can be achieved by a moderate annealing makes it possible to vary different properties of the amorphous state[1]; this is an easy way to modify a system under investigation without changing its chemical concentration. Conversely, from these variations one can get information about the structural relaxation itself.

The two amorphous systems Zr–Cu and Zr–Ni were chosen with the same concentrations of 76 at % Zr and 24 at % $3d$ metal; their superconducting transition temperature T_c is high enough to allow the study of the superconducting state. We have systematically measured these two alloys

*Also at the Service National des Champs Intenses.

0022-2291/84/0900-0461$03.50/0

with different techniques (calorimetric, electric transport) in a wide temperature range from 100 mK to room temperature. In previous publications[2,3] we have reported the large effect of structural relaxation on the different thermodynamic parameters of these sputtered materials, such as the normal electronic coefficient γ, the "lattice" T^3 term, and especially the two-level systems density of states, which together correspond to a decrease of the low-temperature entropy. This behavior is very different from liquid-quenched alloys,[4,5] and indicates a higher degree of structural disorder for the "as-sputtered" alloys.

Here we report measurements of thermodynamic properties and upper superconducting critical fields for Zu_{76} Cu_{24} and $Zr_{76}Ni_{24}$ samples, and of resistivity in the normal state for $Zr_{76}Ni_{24}$. The role of the structural relaxation due to annealing is investigated.

2. SAMPLES

The samples (4×2 cm^2 foils, 100 μm thick) are prepared by a high-rate sputtering technique. They are deposited on a copper substrate held at 77 K in argon atmosphere ($P = 5 \times 10^{-3}$ Torr). We have also studied another Zr–Ni sample deposited at 300 K. As far as possible, measurements are done on the same sample. Details of preparation and characterization of these alloys are described elsewhere.[2,3] All characterization data, such as X-ray diffrac-

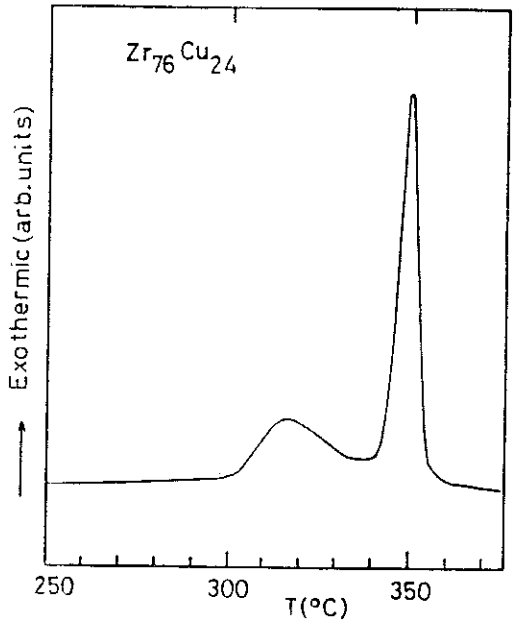

Fig. 1. Differentiating scanning calorimetry thermogram for "as-prepared" $Zr_{76}Cu_{24}$ corresponding to a heating rate of 20 K/min.

tion spectra, mass density d, crystallization temperature, superconducting transition T_c, and electrical resistivity ρ, are in excellent agreement with corresponding melt-spun alloys. For example, the density lies within 0.5% for Zr–Cu and 1% for Zr–Ni of the results of Altounian and Strom-Olsen.[6] We also report in Fig. 1 an analysis by differential scanning calorimetry (Perkin-Elmer DSC-2C) of sample $Zr_{76}Cu_{24}$ in its "as-prepared" state: the main sharp crystallization peak is located at 350°C, in excellent agreement with the literature.[7,8]

In order to study the effect of the structural relaxation, measurements are carried out first in the as-prepared state and after an annealing well below the crystallization temperature, $T_{ann} \simeq 0.8\,T_{crys}$. Thermal treatments were 1 h at 200°C for Zr–Cu and 24 h at 250°C for Zr–Ni under a normal pressure of high-purity Ar.

3. CRITICAL SUPERCONDUCTING FIELDS

3.1. Results and Analysis

The thermodynamic critical field $H_c(T)$ is shown in Fig. 2 for Zr–Cu and Zr–Ni. It is obtained from calorimetric measurements down to 0.1 K using the expression

$$H_c^2(T) = \frac{8\pi}{V} \int_T^{T_c} dT' \int_{T'}^{T_c} \frac{C_{es} - C_{en}}{T}\, dT$$

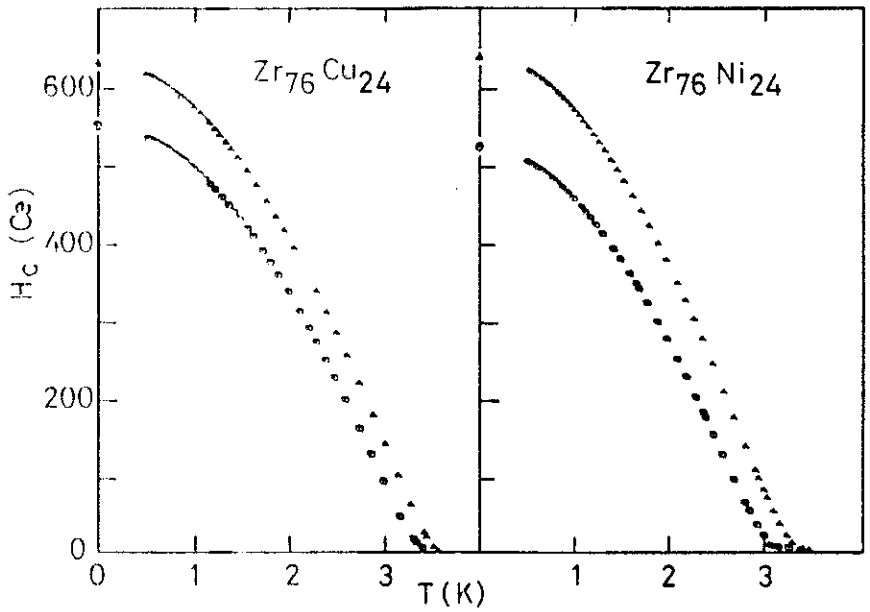

Fig. 2. Superconducting thermodynamic critical field versus temperature for (△) "as-prepared" and (⊙) annealed $Zr_{76}Cu_{24}$ and $Zr_{76}Ni_{24}$ amorphous alloys.

where V is the molar volume, $C_{es} = C - \beta T^3$ is the electronic superconducting specific heat (βT^3 is the phonon contribution and C the measured specific heat) and $C_{en} = \gamma T$ is the electronic specific heat in the normal state. Both γ and β were determined in the normal state above T_c.[2,3]

For both systems annealing induces a weak decrease of T_c by about 0.2 K. This result is generally observed in other superconducting amorphous alloys and has been extensively studied in the case of zirconium-based systems.[9,10] We also observe a decrease for $H_c(T=0)$, larger than that for T_c, which corresponds to a decrease of the initial slope dH_c/dT near T_c.

The upper critical field $H_{c2}(T)$ is shown in Fig. 3. It is obtained between 1.5 K and T_c by a conventional four-probe ac resistive method also used for the resistivity study. A strip (3×15 mm^2) is cut from the initial foil and the magnetic field is applied perpendicularly to its surface. The sample is immersed in the liquid helium bath. We define H_{c2} as the field where the resistance reaches half its normal state value, and the transition width as the range where it varies between 10 and 90% of this value. In this way, ΔT_c in zero field is found to be about 200 mK and remains almost unchanged under high magnetic field. A similar width is obtained for the inductive transition measured by an ac susceptibility method on 1×7 mm^2 strips, the applied magnetic field being parallel to the axis of the strip. The width is larger (0.3–0.5 K) for calorimetric measurements. Examples of the three kinds of transitions, before and after annealing, are shown in Figs. 4a and 4b.

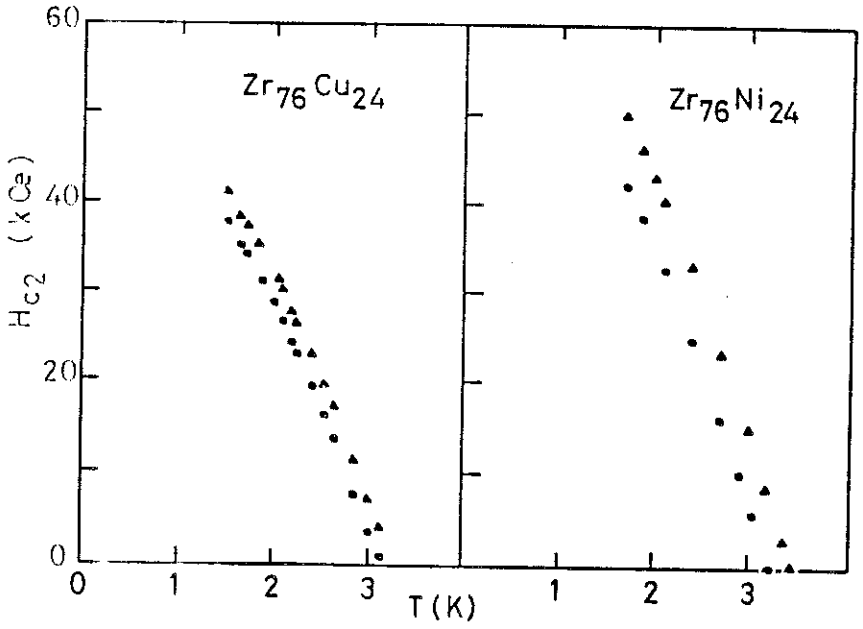

Fig. 3. Superconducting upper critical field versus temperature for (△) "as-prepared" and (⊖) annealed $Zr_{76}Cu_{24}$ and $Zr_{76}Ni_{24}$ amorphous alloys.

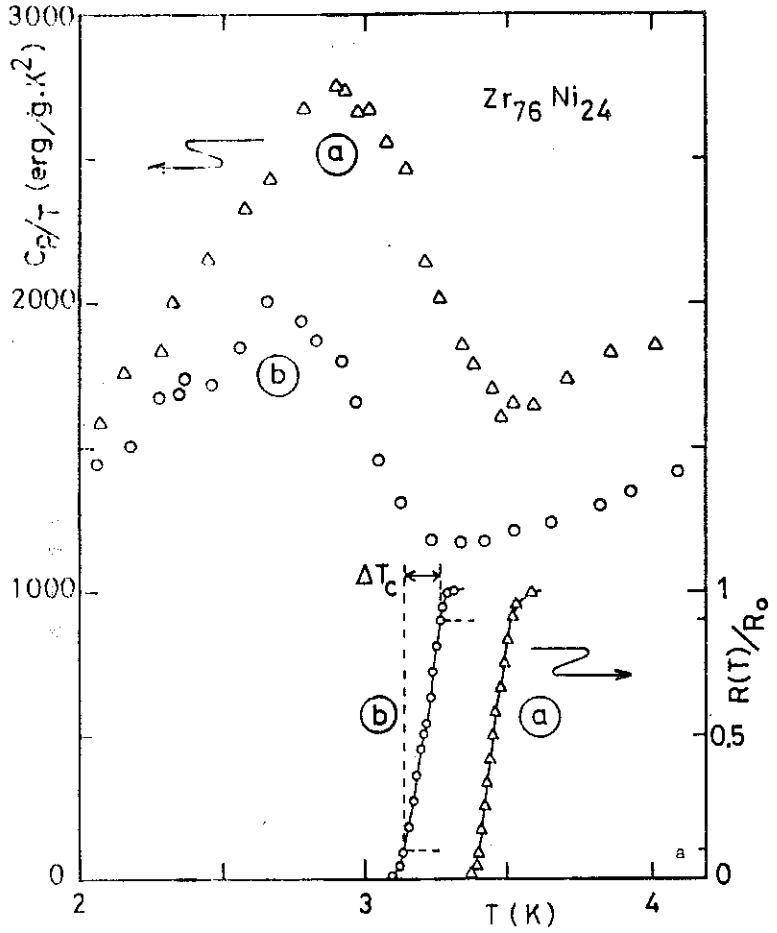

Fig. 4a. Calorimetric and resistive superconducting transitions of (a) "as-prepared' and (b) annealed $Zr_{76}Ni_{24}$.

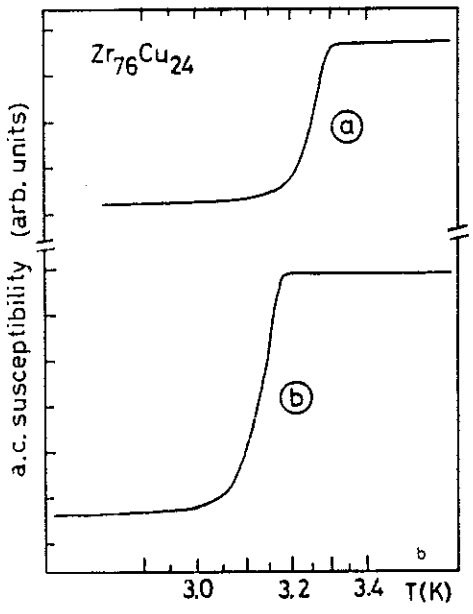

Fig. 4b. Inductive superconducting transition of (a) "as-prepared" and (b) annealed $Zr_{76}Cu_{24}$.

This large calorimetric value is likely due to a larger amount of material (four or five initial foils) used in these experiments, which also involves larger concentration fluctuations.[3] Calorimetric widths of the same order of magnitude can be observed in melt-spun samples;[11,12] moreover, a good agreement is found with the literature for the inductive width.[9,13] However, resistive widths one order of magnitude smaller have been reported[11,13] and interpreted as a homogeneity criterion. As discussed above, no anomalous behavior was detected in our samples from the usual characterization experiments and this large transition width, like the important variations on annealing of γ and Debye temperature, should be an intrinsic property of these sputtered materials. We note that the resistive width is not affected by annealing (which can be interpreted as an absence of homogenization), and gives a reliable meaning to the variation of H_{c2} and T_c defined in this way. These variations upon annealing are sometimes smaller than the transition width; nevertheless, they are significant, especially when measurements are performed on the same sample and with the same technique. Furthermore, the agreement among the values of T_c obtained from these different methods (Table I) is satisfying when one considers the arbitrariness of the definition together with the uncertainties of the measurements.

Similar to the $H_c(T)$ results, $H_{c2}(T)$ data show a lowering of T_c on annealing. However, for both alloys, in the case of the upper critical field no significant variation of the slope dH_{c2}/dT near T_c is apparent (Fig. 3).

For clarity, the results for the Zr–Ni sample prepared by deposition at 300 K have been omitted in Fig. 3. they will be discussed later.

3.1.1. H_c Results

According to the BCS theory, the thermodynamic critical field $H_c(T)$ is given by

$$H_c^{\mathrm{BCS}}(T) = T_c N(E_F)^{1/2} h_c^{\mathrm{BCS}}(T/T_c)$$

where $N(E_F)$ is the electronic density of states at E_F, which is proportional to the electronic specific heat coefficient γ; h_c^{BCS} is a unique function of the reduced variable T/T_c and has been tabulated by Mühlschlegel.[14]

We have plotted $H_c(T)/T_c$ versus T/T_c in fig. 5. As noted previously, $H_c(T)/T_c$ decreases for both systems upon annealing. The behavior is well accounted for by the observed decrease of γ. The experimental values measured at temperatures above T_c are reported in Table I. Moreover, we can see (Table I) that the ratio $\gamma T_c^2/H_c^2(0)$ remains almost constant for a same system and is also very close to the BCS value of 0.168 especially for Zr–Ni alloys. It is just slightly weaker for Zr–Cu.

TABLE I

Superconducting and Thermodynamic Parameters of the Studied Samples

	T_c,[a] K	T_c,[b] K	γ mJ mole^{-1} K^{-2}	γ erg cm^{-3} K^{-2}	$\gamma T_c^2/H_c^2(0)$	$\rho(\sim 10\ \mathrm{K})$,[c] $\mu\Omega$-cm	H'_{c2},[d] kOe K^{-1}	θ_D, K	λ[e]
$Zr_{76}Cu_{24}$									
As-prepared	3.48	3.30	6.25 ± 0.15	5.0×10^3	0.154	161	36	154	0.71
Annealed (200°C, 1 h)	3.33	3.18	5.0 ± 0.1	4.0×10^3	0.149	159.5	28.5	170	0.67
$Zr_{76}Ni_{24}$									
As-prepared	3.21	3.46	8.15 ± 0.2	6.7×10^3	0.170	178.4	53.5	161	0.68
Annealed (250°C, 24 h)	2.995	3.22	6.3 ± 0.1	5.2×10^3	0.171	176.6	41	184	0.64
$Zr_{76}Ni_{24}$									
Deposited at 300 K	3.39	3.22	7.15 ± 0.15	5.9×10^3	0.169	177.9	47	163	0.69

[a] From H_c measurement.
[b] From resistive measurement.
[c] Values of ρ used in formula (1). The uncertainty is $\pm 3\ \mu\Omega$-cm for all samples.
[d] Calculated with formula (1).
[e] Calculated with McMillan's formula[18] ($\mu^* = 0.13$), using values of T_c from H_c measurement.

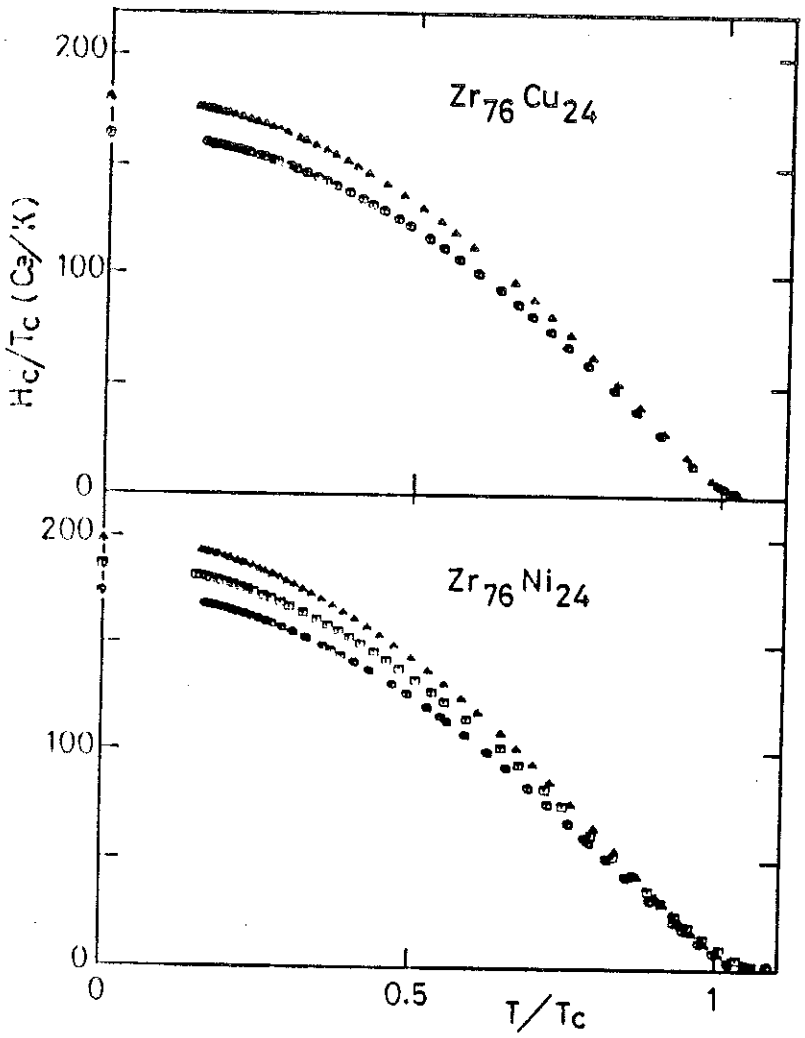

Fig. 5. Plot of H_c/T_c versus T/T_c for (△) "as-prepared" and (⊙) annealed $Zr_{76}Cu_{24}$ and $Zr_{76}Ni_{24}$, and (□) for $Zr_{76}Ni_{24}$ deposited at 300 K.

In order to compare the thermal variation of $H_c(T)$ to the BCS predictions, we have as usual[15] plotted in Fig. 6 the deviation of $H_c(T)$ from a parabolic law:

$$D\left(\frac{T}{T_c}\right)=\frac{H_c(T)}{H_c(0)}-\left[1-\left(\frac{T}{T_c}\right)^2\right]$$

versus $(T/T_c)^2$.

We obtain a very good superposition for all samples of the same system. Furthermore, the results for Zr–Ni are in excellent agreement with the BCS theory, while a small deviation appears for Zr–Cu.

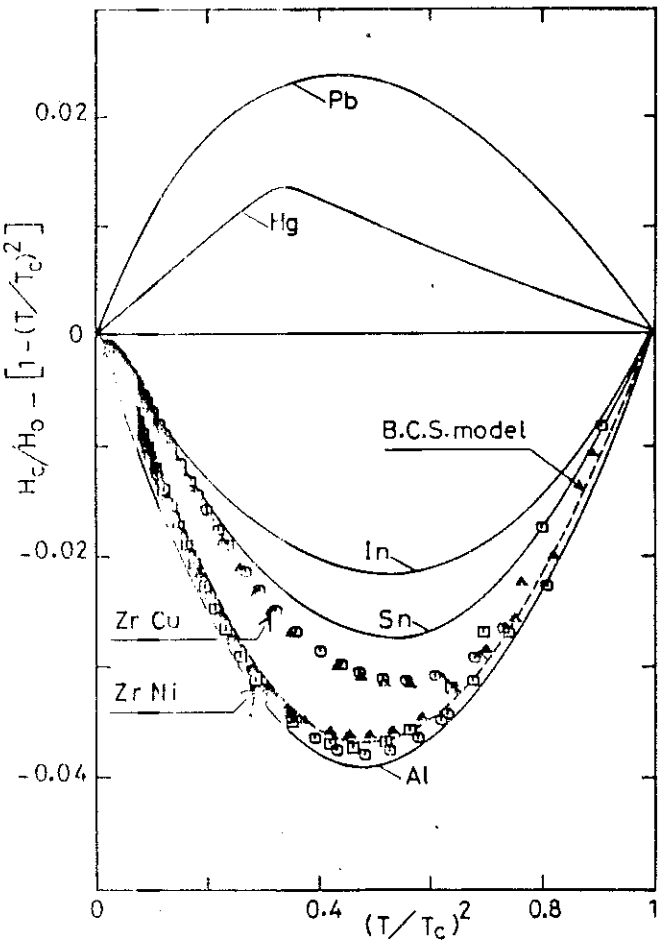

Fig. 6. Deviation function $D(T/T_c)$ versus $(T/T_c)^2$ for the different $Zr_{76}Cu_{24}$ and $Zr_{76}Ni_{24}$ amorphous alloys (same symbols as in other figures).

3.1.2. H_{c2} Results

According to the GLAG theory,[16] in the case of an isotropic dirty superconductor the slope of the upper critical field near T_c is given by

$$H'_{c2} = \left.\frac{dH_{c2}}{dT}\right|_{T_c} = -4.48 \times 10^{-5} \gamma \rho \qquad (1)$$

where γ is in erg cm^{-3} K^{-2}; ρ, the resistivity in the normal state, is in $\mu\Omega$-cm; and H'_{c2} is in kOe K^{-1}.

In Fig. 7 we have plotted $H_{c2}(T)/T_c$ versus T/T_c for both systems. The straight lines show the slopes H'_{c2} calculated from formula (1) (values in table I). Within the limit of precision of the measurements, the data are

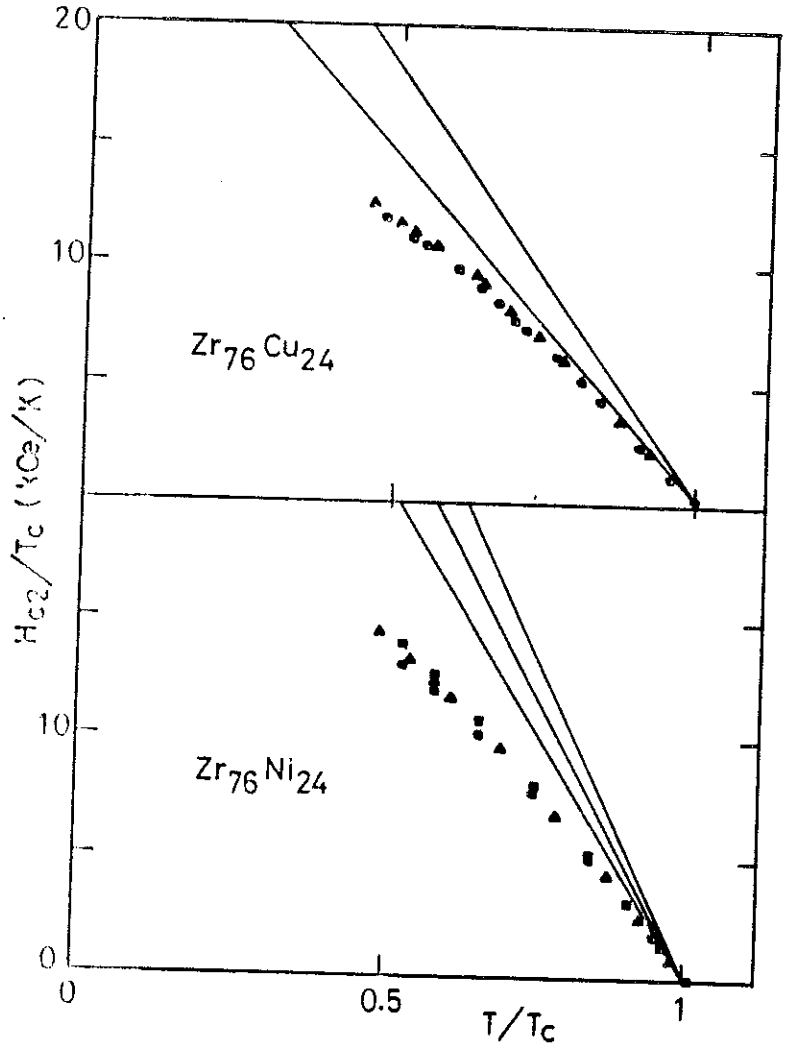

Fig. 7. Plot of H_{c2}/T_c versus T/T_c for (△) "as-prepared" and (⊙) annealed $Zr_{76}Cu_{24}$ and $Zr_{76}Ni_{24}$, and (□) for $Zr_{76}Ni_{24}$ deposited at 300 K. Straight lines show the slopes H'_{c2} calculated from formula (1) (see text).

superposed for each system. The experimental values of H'_{c2} are 26 ± 0.5 kOe K^{-1} for Zr–Cu and 32 ± 0.5 kOe K^{-1} for Zr–Ni, in reasonable agreement with the results reported for alloys of similar concentration obtained by a melt-spinning technique.[6,11,17] Taking into account the uncertainties on the different parameters, only for one sample, annealed Zr–Cu, is good agreement achieved between the calculated H'_{c2} and the experimental data. For the other four samples discrepancies occur as large as 40% for as-prepared Zr–Ni and 20% for as-prepared Zr–Cu, which are beyond the uncertainty of the measurement. We note that experimental values of H'_{c2}, which are different for both systems, do not vary significantly on annealing

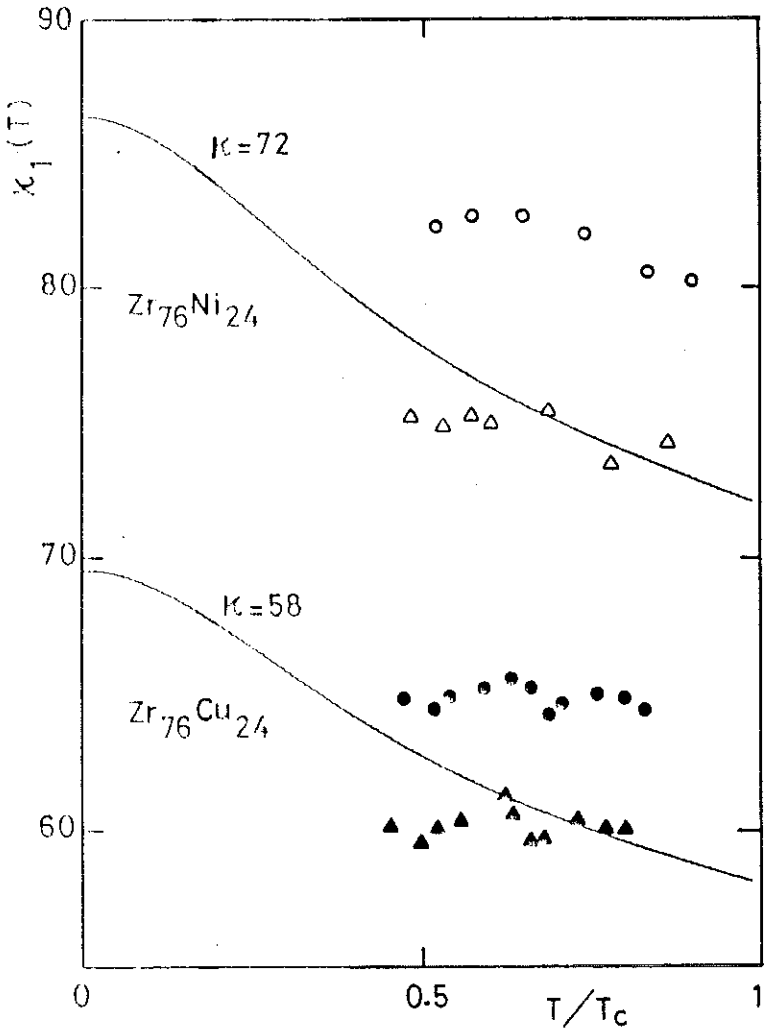

Fig. 8. Plot of $\kappa_1(T) = H_{c2}(T)/\sqrt{2}H_c(T)$ versus T/T_c for (▲) "as-prepared" and (●) annealed $Zr_{76}Cu_{24}$, and for (△) "as-prepared" and (○) annealed $Zr_{76}Ni_{24}$. Solid lines indicate $\kappa_1(T)$ calculated from the GLAG model with $\kappa = 58$ and 72.

or on conditions of preparation,* while, the calculated value decreases by more than 20% on annealing, mainly due to the variation of γ. Such a large change should be easily detected experimentally.

The thermal variation of H_{c2} relative to H_c is described by the parameter $\kappa_1(T)$ defined as

$$\kappa_1(T) = \frac{H_{c2}(T)}{\sqrt{2}H_c(T)}$$

*Recent experiments[11] on melt-spun Zr_3Rh and Zr_3Ni point out a similar lack of variation on annealing.

For T near T_c, κ_1 becomes equal to the Ginzburg–Landau value κ. Figure 8 gives $\kappa_1(T/T_c)$ calculated from the measured H_{c2} and H_c for four samples. The omitted Zr–Ni sample (deposited at 300 K) still shows an intermediate behavior. We have also indicated $\kappa_1(T)$ calculated according to the GLAG model[16] using $\kappa = 58$ and 72, which are, respectively, in accordance with the results at higher temperatures for Zr–Cu and Zr–Ni as-prepared samples.

For both systems annealing leads to an increase of κ. But this is just an alternative way to describe the variations of H_c and H_{c2} previously discussed. On the other hand, Fig. 8 shows that the temperature dependence expected from the GLAG model is not obeyed for $\kappa_1(T)$, which is almost constant for a given sample. Deviations from the GLAG model occurring in $H_{c2}(T)$ [or $\kappa_1(T)$] for high-κ superconductors are generally accounted for by a balance of the Pauli paramagnetic limitation and the spin–orbit coupling. From the experimental slope $H'_2(T_c)$, we can deduce[16,17] the Maki parameter $\alpha = 1.71$ for Zr–Ni and 1.39 for Zr–Cu and, assuming that $\kappa_1(T)$ becomes constant down to 0 K, we obtain for the spin–orbit λ_{so} parameter 2.5 for Zr–Ni and 1.5 for Zr–Cu, values that are physically reasonable. Both α and λ_{so} remain constant upon annealing. In the case of Zr–Ni, these values are in good agreement with data of Karkut and Hake[17] for the same concentration.

3.2. Discussion

3.2.1. Thermodynamic Critical Field H_c

We can see in Fig. 6 that our results lie between those of weak coupling superconducting crystalline Al and Sn, for which the electron–phonon coupling parameter λ is less than 0.7.[18] The present values of T_c and θ_D for our alloys lead to the values of λ,[18] using McMillan's formula, that are quoted in Table I. they are smaller for Zr–Ni than for Zr–Cu, in agreement with the trend of the H_c results. A large variation of λ occurs on annealing, which corresponds to a change as large as 20% for T_c/θ_D, which does not appear in the H_c behavior. Similar deviations from the BCS theory occur for the specific heat jump at T_c.[3]

Crystalline indium and tin with similar values of λ (~0.6–0.8) deviate much more from the BCS curve (Fig. 6) than our amorphous alloys, for which λ is comparable. These deviations are not surprising because in the exact relation between H_c and λ, parameters like $\alpha^2F(\omega)$ are implied that are not exactly the same for crystalline and amorphous metals. Calculations by Rainer and Bergmann[19] that try to account for these particularities of the amorphous state reproduce the trend of our results, but small discrepancies remain. For instance, a value of $T_c/\langle\omega\rangle$ larger by a factor of three is

needed to explain the observed $\gamma T_c^2/H_c^2(0)$ for Zr–Cu. Nevertheless, the agreement between existing theories and these $H_c(T)$ data is satisfying.

3.2.2. *Upper Critical Field H_{c2}*

A similar good agreement is not found for the upper critical field. Indeed, formula (1), which relates H'_{c2} to ρ and γ, is seldom verified for our results, contrary to the assertion of the literature,[20] although significant discrepancies can sometimes occur.* Unexpected behavior of $H_{c2}(T)$ is also reported,[22] which is sometimes assigned to structural inhomogeneities.[23] In addition to the different characterization tests discussed above, the quality of our samples is confirmed by the coherence between the measurements by different techniques. In this connection, we note that we do not observe the significant broadening of the resistive transition at high magnetic fields that is sometimes reported;[17] the result is perhaps due to its large value in the present case. For the first time a change of γ as large as 20% was achieved by annealing, which implies drastic conditions for verification of expression (1). Uncertainties due to reproducibility from one sample to another are thus eliminated.

Deviations from the GLAG model are usually ascribed to a strong coupling effect, or a gap anisotropy effect, or paramagnetic limiting and spin–orbit effects.[24] The only ones that can play a role here are the magnetic effects, which occur at large field (40–50 kOe) and cannot explain anomalous behavior near T_c. The more realistic point that could account for the disagreement between measurements and formula (1) is the relation between ρ and the mean free path and then the coherence length. Indeed, electronic scattering due to disorder is very large, and mean free paths are of the order of the interatomic distances. So small a value leads one to question the validity of the definition of this parameter.

Finally, we note that specific heat is a bulk property of the material, whereas resistivity vanishes as soon as superconducting paths are able to percolate in a part of the sample; this could explain the different values of T_c measured by the two methods (Fig. 4a). The disagreement encountered in application of formula (1) could result from these two different ways used to study the superconductivity. This fact is likely due not to sample inhomogeneity on a large scale, but rather to a specific property of highly disordered materials. These different explanations remain to be checked, but at this stage we have to be careful about the values of γ crudely extracted by means of formula (1) from resistive measurements.

*See Ref. 17. A recent work on Mo–Ru–B[21] describes such a discrepancy, which progressively develops on successive thermal treatments.

4. NORMAL STATE RESISTIVITY

4.1. Results

The resistivity measured at room temperature is $153 \pm 3\ \mu\Omega$-cm for Zr–Cu and $168 \pm 3\ \mu\Omega$-cm for Zr–Ni in their "as-prepared" state. Both values are in excellent agreement with literature data for corresponding melt-spun alloys (for example, within a few percent to data of Ref. 6). Annealing induces an irreversible decrease of $\rho(300\ \mathrm{K})$ by about 1% for both systems. This variation is smaller than the uncertainty in the absolute value of this parameter, which is mainly due to the form factor of the sample. The thermal variation of the reduced resistivity $\rho(T)/\rho(273\ \mathrm{K})$ measured down to T_c for the three Zr–Ni samples is shown in Fig. 10. The value of ρ increases when T decreases from 300 K. A maximum appears at $T_{max} \simeq 10$ K and the resistivity decreases very rapidly when the superconducting transition is approached. The magnitude of the variation of ρ between T_{max} and room temperature is of the order of 5% and decreases upon annealing. The sample deposited at 300 K again shows an intermediate behavior. Similar effects of annealing have been obtained by Guimpel and de La Cruz[15] for amorphous Cu–Zr alloys prepared by rapid quenching.

4.2. Discussion

Different theories are used to describe the resistivity of amorphous metals.[26] The most appropriate one to account for the behavior of nonmagnetic metals is the Faber–Ziman diffraction model, originally introduced for liquid metals. However, we will discuss an alternative approach, the Kondo-like model,[27] where the resistivity results from the scattering of the conduction electrons by the two-level systems (TLS) characteristic of the amorphous state. By analogy to the real Kondo effect, the following expression was suggested[28] for the thermal variation of the resistivity:

$$\frac{\rho(T)}{\rho(273\ \mathrm{K})} = A - B \log\left(T^2 + \frac{\Delta^2}{k_B^2}\right) \tag{2}$$

where B is proportional to the number of efficient TLS and Δ is a characteristic tunneling splitting energy of the TLS. Such an expression with three free parameters accounts accurately for the smooth thermal variation of ρ for $T > T_{max}$, as shown in Fig. 9 in the case of the as-prepared sample. The parameters calculated by a least square fit for the three samples are listed in Table II. The value of B decreases by 20% on annealing and Δ remains practically constant. Reliable information about the TLS density of states over an energy of a few kelvins is obtained by specific heat and thermal conductivity measurements carried out on the same samples.[2] The specific

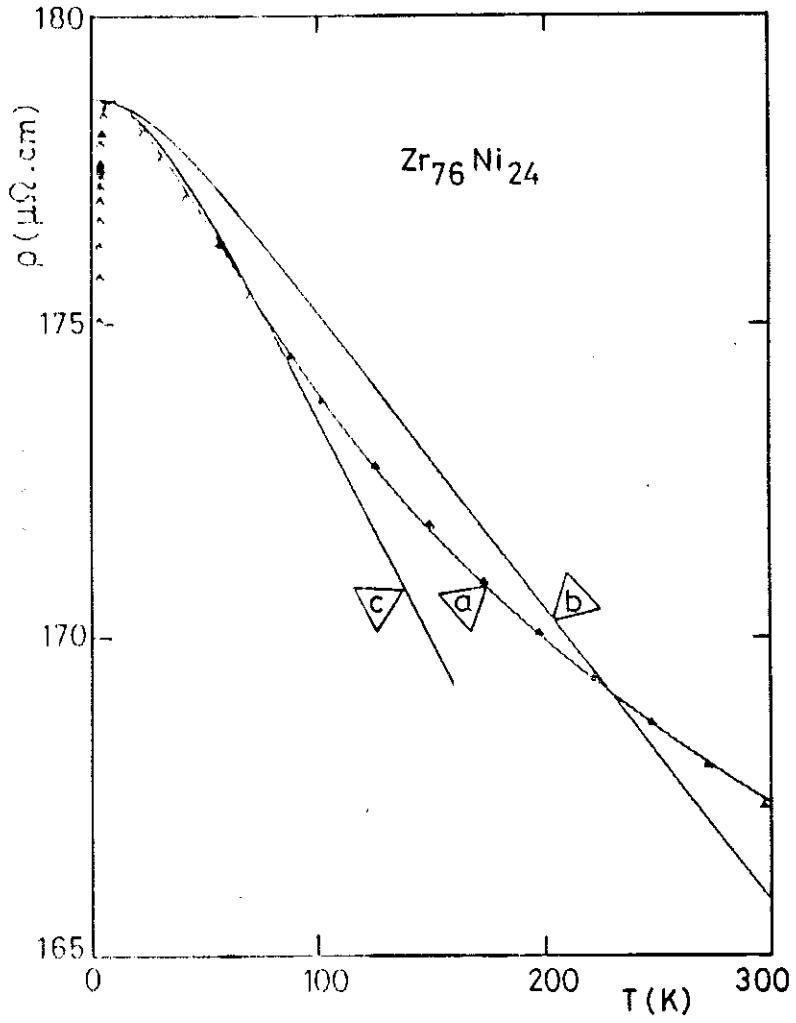

Fig. 9. Resistivity versus temperature for "as-prepared" $Zr_{76}Ni_{24}$ amorphous alloy. (a)–(c) calculated from expressions (2), (3), and (5), respectively (see text).

TABLE II
Parameters Used to Fit the Resistivity Following Formula (2)

	A	$B \times 100$	Δ/k_B, K
$Zr_{76}Ni_{24}$			
As-prepared	1.224	1.989	58
Annealed	1.182	1.613	57
$Zr_{76}Ni_{24}$			
Deposited at 300 K	1.215	1.904	59

heat shows unambiguously that the number of TLS decreases by a larger value, at least by 70%, and moreover that the energy distribution is strongly affected by annealing, which should induce a larger variation of Δ. This model in its simple form can also be ruled out on theoretical arguments.[29] A more sophisticated treatment of the interaction between the TLS and the conduction electrons[30] shows that under specific conditions a highly correlated state can occur at low temperature, which is reflected in the resistivity. However, the temperatures involved are smaller by at least one order of magnitude than the determined values of Δ. Finally, this model, which allows a good fit of the experimental data, gives neither physically acceptable values of the parameters nor the right amplitude of the variation on annealing.

In the diffraction model, following the Nagel's[31] simple formulation, the resistivity is expressed by

$$\rho(T) = \rho_0 S_T(2k_F)$$
$$= \rho_0\{1 + [S_0(2k_F) - 1] \exp(-2[W(T) - W(0)])\} \tag{3}$$

ρ_0 is a constant that accounts for the microscopic mechanism of the scattering of the conduction electrons by the potential of the ions. The temperature dependence of ρ is entirely determined by that of the structure factor. The Debye–Waller factor $W(T)$ is, in the Debye approximation,

$$W(T) - W(0) = \frac{3\hbar^2 k^2 T^2}{2Mk_B\theta_D^3} \int_0^{\theta_D/T} \frac{1}{e^z - 1} z\, dz \tag{4}$$

the thermal variation of ρ is given by expressions (3) and (4) as long as we know the following parameters: $S_0(2k_F)$, the value of the structure factor at $2k_F$ (as usual, $2k_F$ is assumed to be close to q_p, the position of the first diffraction peak); M, the atomic mass; and θ_D, the Debye temperature.

Using $S_0(q_p) = 3$ from the diffraction measurements on the Zr–Ni system,[32–34] $q_p = 2.53$ Å^{-1} measured on the studied samples, and θ_D deduced from the calorimetric measurements,[2] we obtain the variations of $\rho(T)$ quoted in Figs. 9 and 10.

Considering that there is no free parameter in this analysis, the agreement with experimental data is very good. Indeed, expressions (3) and (4) account for both the magnitude of the thermal variation of ρ and the evolution upon annealing that results from the only variation of θ_D. We note that q_p is constant for the three samples. The value $S_0(q_p)$ reported in the literature does not correspond exactly to the concentration studied here, but this value is not a sensitive parameter in formula (3) and does not vary significantly with concentration,[35] or with the constituent of the amorphous Zr-based alloys,[32] or with annealing.[36] However, deviations occur; in par-

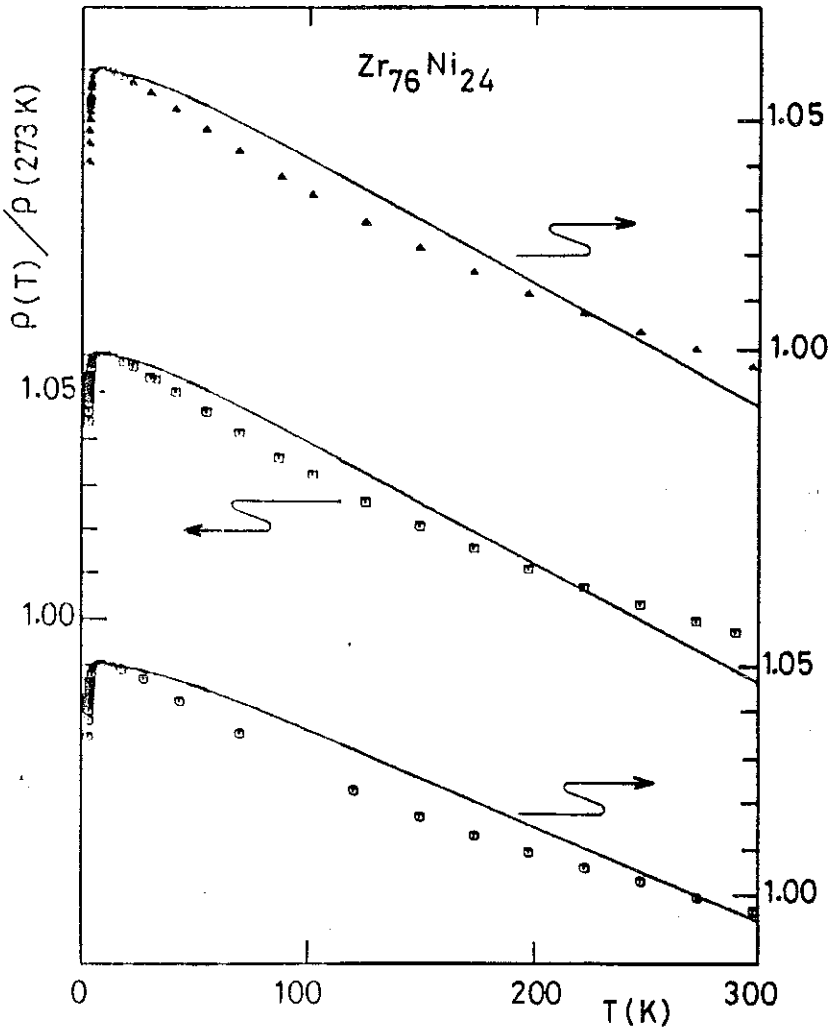

Fig. 10. Plots of $\rho(T)/\rho(273\,\mathrm{K})$ versus T for (△) "as-prepared", (□) deposited at 300 K. and (○) annealed amorphous $Zr_{76}Ni_{24}$. Curves are calculated from formula (3) with θ_D respectively of 161, 163, and 183 K (see text).

ticular, the upward curvature of $\rho(T)$ is not reproduced by the expressions (3) and (4); the same discrepancy is also observed with this simplified approach in other alloys.[31,37,38] Refinements of the model can be achieved by introducing the partial structure form factors.[38] However, this correction is only important when two constituents of the system are very different, for instance of their atomic number.*

The questionable hypothesis of the model seems to be the over-simplified thermal variation used for $S(k)$. Indeed, at high temperature

*In Ref. 38, the relevant ratio is $M_{Zr}/M_{Be}=10$, whereas M_{Zr}/M_{Ni} is only 1.5.

($T > \theta_D$), for which scattering of the electrons by phonons is quasielastic,[39] formulas (3) and (4) are rough approximations. At $T \simeq \theta_D$, collisions are inelastic, and at very low temperature ($T \ll \theta_D$), elastic collisions dominate because electrons do not have a sufficiently large energy ($\sim k_B T$) in order to create phonons. In this regime, a more reliable expression for $\rho(T)$ is available:[40]

$$\rho(T) = \rho_0 S_0(2k_F) \exp(-2[W(T) - W(0)]) \tag{5}$$

which is, however, only valid asymptotically for $T \to 0$, due to the existence of phonons of very low energy. As the temperature increases from $T = 0$, the one-phonon and n-phonon terms become important in the Debye–Waller factor,[40] but the exact expression is not easy to calculate. Figure 9 gives $\rho(T)$ from formula (5) for the as-prepared sample; it indeed becomes in excellent agreement with experimental data at low temperature. The extra contribution to $\rho(T)$ that appears at higher temperature could be interpreted as the inelastic contribution. We note that this term becomes negligible at low T, when ρ decreases as T^2, in contradiction with some theoretical predictions.[40]

5. CONCLUSION

The study of the effect of structural relaxation induced by annealing on the critical fields of $Zr_{76}Cu_{24}$ and $Zr_{76}Ni_{24}$ amorphous alloys indicates an identical behavior for both systems, which suggests that Ni does not present any magnetic character at this concentration. The measurements of $H_c(T)$ down to 100 mK unambiguously indicate that these alloys are weak coupling superconductors. Indeed, the absolute values and the thermal variation of $H_c(T)$, which are in excellent agreement with the BCS model, confirm more clearly previous investigations of the specific heat jump and of the ratio Δ_0/T_C.[2,3,11] However, a discrepancy occurs for the relation between the upper critical field slope at T_c, the resistivity in the normal state, and the γ coefficient, in contradiction with a hypothesis often found in the literature. Finally, the resistivity results of $Zr_{76}Ni_{24}$ are well interpreted within the framework of the Ziman diffraction model. In particular, it accounts, without a free parameter, for the amplitude of the thermal variation of ρ upon annealing. Nevertheless, an exact description of the experimental data needs a more detailed theoretical analysis.

REFERENCES

1. Les Amorphes Métalliques–Aussois Jan. 1983–A. Chamberod ed. (Les Editions de Physique–Paris–1984).
2. A. Ravex, J. C. Lasjaunias, and O. Béthoux, *Physica B* **107**, 395–397 (1981); *Solid State Commun.* **40**, 853 (1981).

3. A. Ravex, J. C. Lasjaunias, and O. Béthoux, *J. Phys. F: Metal Phys.* **14**, 329 (1984).
4. P. Garoche, Y. Calvayrac, W. Cheng, and J. J. Veyssié, *J. Phys. F: Met. Phys.* **12**, 2783 (1982).
5. S. Grondey, H. v. Löhneysen, and H. J. Schink, *Z. Phys. B* **51**, 287 (1983).
6. Z. Altounian and J. O. Strom-Olsen, *Phys. Rev. B* **27**, 4149 (1983).
7. K. H. J. Buschow, I. Vincze, and F. Van der Woude, *J. Non-Crystal. Solids* **54**, 101 (1983).
8. Z. Althounian, Tu Guo-Hua, and J. O. Stom-Olsen, *J. Appl. Phys.* **53**(7), 4755 (1982).
9. A. J. Drehman and W. L. Johnson, *Phys. Stat. Sol.* (*a*) **52**, 499 (1979).
10. S. J. Poon, *Phys. Rev. B* **27**, 5519 (1983).
11. K. Samwer and H. v. Löhneysen, *Phys. Rev. B* **26**, 107 (1982).
12. P. Garoche and J. Bigot, *Phys. Rev. B* **28**, 6886 (1983).
13. S. J. Poon and P. L. Dunn, *J. Low Temp. Phys.* **54**, 81 (1984).
14. B. Mühlschlegel, *Z. Phys.* **155**, 313 (1959).
15. B. Meservey and B. B. Schwartz, in: *Superconductivity*, Vol. 1, M. D. Parks, ed. (Marcel Dekker, New York, 1969), p. 117.
16. D. Saint-James and G. Sarma, *Type II Superconductivity* (Pergamon Press, Oxford, 1969), Chapter 5.
17. M. G. Karkut and R. R. Hake, *Phys. Rev. B* **28**, 1396 (1983).
18. W. L. McMillan, *Phys. Rev.* **167**, 331 (1968).
19. D. Rainer and G. Bergmann, *J. Low Temp. Phys.* **14**, 501 (1974).
20. S. T. Hopkins and W. L. Johnson, *Solid State Commun.* **43**, 537 (1982).
21. C. C. Koch, D. M. Kroeger, J. S. Lin, J. O. Scarborough, W. L. Johnson, and A. C. Anderson, *Phys. Rev. B* **27**, 1586 (1983).
22. M. Tenhover, W. L. Johnson, and C. C. Tsuei, *Solid State Commun.* **38**, 53 (1981).
23. C. O. Kim and W. L. Johnson, *Phys. Rev. B* **23**, 143 (1981).
24. E. Domb and W. L. Johnson, *J. Low Temp. Phys.* **33**, 29 (1978).
25. J. Guimpel and F. de La Cruz, *Solid State Commun.* **44**, 1045 (1982).
26. P. J. Cote and L. V. Meisel, in: *Glassy Metals I*, H. J. Güntherodt and H. Beck, eds. (Springer-Verlag, Berlin, 1981), p. 141.
27. R. W. Cochrane, R. Harris, J. O. Strom-Olsen, and M. J. Zuckermann, *Phys. Rev. Lett.* **35**, 676 (1975).
28. C. C. Tsuei, *Solid State Commun.* **27**, 691 (1978).
29. J. L. Black, B. L. Gyorffy, and J. Jäckle, *Phil. Mag. B* **40**, 331 (1979).
30. K. Vladár and A. Zawadowski, *Phys. Rev. B* **28**, 1596 (1983).
31. S. R. Nagel, *Phys. Rev. B* **16**, 1694 (1977).
32. Y. Waseda and H. S. Chen, *Rapidly Quenched Metals III*, Vol. 2 (Metal Society, London, 1978), p. 415.
33. H. S. Chen, K. T. Aust, and Y. Waseda, *J. Non-Crystal. Solids* **46**, 307 (1981).
34. C. N. J. Wagner and D. Lee, *J. Phys. C* **8**, 242 (1980).
35. H. S. Chen and Y. Waseda, *Phys. Stat. Sol.* (*a*) **51**, 593 (1979).
36. K. Samwer and J. C. Lasjaunias, *Solid State Commun.*, in press (1984).
37. S. Basack, R. Clarke, and S. R. Nagel, *Phys. Rev. B* **20**, 4278 (1979).
38. R. Clarke, S. R. Nagel, P. L. Hitterman, and M. H. Mueller, *Solid State Commun.* **36**, 751 (1980).
39. K. Frohöse and J. Jäckle, *J. Phys. F: Metal Phys.* **7**, 2331 (1977).
40. L. V. Meisel and P. J. Cote, *Phys. Rev. B* **17**, 4652 (1978).
41. S. J. Poon and K. M. Wong, *J. Low Temp. Phys.* **54**, 15 (1984).

- CIVALE L., DE LA CRUZ F., LUZURIAGA J., Solid State Comm. 48, 389 (1983).
- ESQUINAZI P., DE LA CRUZ M.E., RIDNER A., DE LA CRUZ F., Solid State Comm. 44, 941 (1982).
- GAROCHE P., CALVAYRAC Y., CHENG W., VEYSSIE J.J., J. Phys. F : Met. Phys. 12, 2783 (1982).
- GRONDEY S., von LÖHNEYSEN H., SCHINK H.J., SAMWER K., Z. Phys. B51, 287 (1983).
- KARKUT M.G. and HAKE R.R., Phys. Rev. B 28, 1396 (1983).
- LASJAUNIAS J.C., PENN G., RAVEX A., VANDORPE M., Journal Physique-Lettres 41, L-131 (1980).

C H A P I T R E V

ETUDE DE PROPRIETES STRUCTURALES

Afin de mieux caractériser les effets structuraux des recuits et de les relier aux variations observées des propriétés thermiques, nous avons soumis nos échantillons à diverses techniques expérimentales sensibles aux réarrangements de structure : analyse thermique différentielle, diffraction de rayons X, diffusion des rayons X aux petits angles, "EXAFS", résistivité. Ces mesures ont été effectuées en collaboration avec d'autres laboratoires. Les principaux résultats obtenus sont rapportés et analysés ci-après.

I - ANALYSE THERMIQUE DIFFERENTIELLE - APPARITION DE LA PHASE ω DU ZIRCONIUM

Les mesures de routine d'analyse thermique différentielle et de rayons X effectuées au laboratoire dans le cadre de la caractérisation des échantillons ont mis en évidence l'apparition comme première phase de cristallisation des alliages ZrCu, la phase ω du Zirconium. Cela a d'ailleurs été observé également par Buschow et al. (1983) dans des échantillons obtenus par trempe du liquide pour les fortes concentrations de Zirconium. Cet état de fait nous a amené à proposer une origine éventuelle pour les TLS et leur sensibilité aux recuits (Ravex et al., 1984) par analogie avec les observations effectuées par Lou (1976) dans des alliages cristallins ZrNb trempés où la coexistence des phases BCCβ-Zr et hexagonale ω-Zr entraîne un comportement de type "amorphe" des propriétés thermiques. On suppose que dans l'état brut de pulvérisation des groupes isolés d'atomes de Zirconium possèdent un ordre local du type ω-Zr et peuvent fluctuer par effet tunnel vers d'autres configurations métastables d'énergie voisine. Le traitement thermique entraînant une séparation de phase chimique entraînerait une croissance rapide de ces groupes, diminuant par là-même la fréquence des fluctuations et par conséquent la densité de TLS. Ce schéma rejoint l'hypothèse de Mon et Ashcroft (1978) qui associent, de façon générale, la présence de TLS au polymorphisme. Dans les alliages obtenus par trempe du liquide, la séparation de phase chimique peut s'effectuer durant la trempe

entraînant ainsi une densité plus faible de TLS et une relative insensibilité aux recuits ultérieurs comme observé expérimentalement (Grondey et al., 1983).

Des mesures d'analyse thermique différentielle très sensibles ont été effectuées sur nos échantillons ($Zr_{76}Cu_{24}$ et $Zr_{80}Cu_{20}$) et sur des échantillons trempés du liquide au Centre d'Etudes de Chimie Métallurgique du CNRS à Vitry-sur-Seine (M. Harmelin, 1984). Ces mesures ont porté sur plusieurs objectifs : recherche d'une transition vitreuse ; effet des recuits sur la relaxation structurale et sur la cinétique de précipitation de la phase ω-Zr ; comparaison du comportement des alliages trempés du liquide et pulvérisés.

a. Transition vitreuse :

L'existence d'un Tg (tempérautre de transition vitreuse) est souvent présentée comme un "critère de qualité" dans les échantillons pulvérisés. Une étude de Harmelin M. and al. (1984) a montré par étude comparative d'échantillons pulvérisés et trempés du liquide ($Zr_{60}Cu_{40}$ et $Zr_{50}Cu_{50}$) la présence (très nette dans le cas des échantillons trempés et plus floue surtout à l'état brut dans le cas des échantillons pulvérisés) d'un début de transition vitreuse caractérisée par un pic endothermique.

Dans notre échantillon $Zr_{80}Cu_{20}$ recuit 1 heure à 200°C, la mise en évidence d'un effet endothermique entre 150 et 260°C suggère l'existence d'une transition vitreuse. Sur les échantillons bruts de pulvérisation aucune transition vitreuse n'a été observée avant la formation de ω-Zr.

b. Relaxation structurale :

La relaxation structurale se traduit par un effet exothermique observable à partir d'une certaine température jusqu'au début de la cristallisation (phase ω-Zr). Le tableau ci-dessous récapitule les résultats expérimentaux.

Echantillon état		Relaxation structurale : effet exothermique			
		début °C	fin °C	intensité $Jmole^{-1}$	% relax.
$Zr_{76}Cu_{24}$	brut	110	300	1066	-
	recuit 1 minute 200°C	225	300	651	39 %
	1 heure	255	300	262	75 %
$Zr_{80}Cu_{20}$	brut (vieilli 7 mois ambiante)	134	275	1380	-
	recuit 1 minute 200°C	220	273	270	80 %
	1 heure			~ 0	100 %

Cette relaxation est irréversible et typique de l'état brut. Elle se produit dans les premiers instants du traitement. Les recuits diminuent son amplitude jusqu'à même l'éliminer ($Zr_{80}Cu_{20}$, recuit 1 h à 200°C). Elle a aussi été observée dans des échantillons trempés du liquide mais avec une intensité bien moindre que dans les échantillons pulvérisés de même composition (Harmelin M., 1984). Elle a été attribuée par les auteurs au relâchement de contraintes et de configurations anisotropes introduites lors de la trempe.

c. Formation de ω-Zr :

L'effet des recuits sur la formation de la phase ω-Zr au premier stade de la recristallisation peut être évalué en suivant la température du pic de cristallisation et l'énergie sous ce pic.

Ces paramètres sont résumés dans le tableau ci-après.

Echantillon	état	Cristallisation de la phase ω-Zr		
		température (°C)		ΔH(Jmole-1)
		début	pic	
$Zr_{76}Cu_{24}$	brut	316,6	326,2	1667
	recuit 1 minute 200°C	313,2	323,3	1734
	1 heure	312,6	322,4	1768
$Zr_{80}Cu_{20}$	brut	∿ 275	297,7	2340
	recuit 1 minute 200°C	∿ 273	297,7	2410
	1 heure	∿ 263	299,3	2550

On observe un effet des recuits dans un sens favorable à l'apparition de la phase ω-Zr : diminution de la température de début de cristallisation et augmentation de l'enthalpie sous le pic.

II - DIFFRACTION DES RAYONS X ET DIFFUSION AUX PETITS ANGLES

a. Rayons X "standards" :

Une étude sur la structure de l'échantillon $Zr_{76}Cu_{24}$ appelé "B" dans le travail rapporté au chapitre précédent (Ravex et al., 1984) a été effectuée par Samwer et Lasjaunias (1984) au California Institute of Technology. Le spectre de diffraction X obtenu est presque inchangé sous l'effet de recuits à 200°C de 1 heure et 13 heures. Les positions des deux premiers pics des fonctions d'interférence réduite ($i(K) = K\,[I(K) - 1]$) et de distributions radiales réduites ($G(r)$) sont rapportées dans le tableau ci-après ainsi que les densités et le nombre de coordination (C.N.) pour les différents états de l'échantillon.

Echantillon	état	densité (gcm^{-3})	i(K)		G(r)		C.N.
			K_1 ($Å^{-1}$)	K_2	R_1 (Å)	R_2	
$Zr_{76}Cu_{24}$	brut	6,805	2,548	4,412	3,109	5,459	12,38
Pulvérisé à 77 K	recuit 200°C 1 h	6,822	2,550	4,408	3,123	5,428	12,53
	recuit 200°C 13 h	6,820	2,549	4,405	3,118	5,421	12,48

Pour la composition étudiée, la position du premier pic de la fonction de distribution radiale est proche du rayon de Goldschmidt de la paire Zr-Zr(3,20 Å) : en effet la principale contribution à la fonction densité atomique observée en RX est celle des paires Zr-Zr vu leur concentration et leur nombre atomique. Les paires Zr-Cu apportent une légère correction alors que la contribution de paires Cu-Cu est négligeable. Les résultats obtenus sont en bon accord avec les modèles de sphères dures qui négligent les effets d'ordre chimique (pour ce point voir les mesures d'EXAFS). L'effet des recuits se traduit par

une légère augmentation du nombre de coordination et de la densité. On attribue ces effets à la relaxation structurale ; ils sont compatibles avec un récent modèle microscopique basé sur la description de défauts dans la matrice amorphe (Srolovitz et al., 1981). Par contre l'absence de différences significatives entre échantillons pulvérisés et trempés du liquide ne permet pas d'expliquer les différences observées dans les propriétés thermiques.

b. Diffusion aux petits angles :

Des mesures de diffusion aux petits angles des rayons X ont été entreprises en collaboration avec le laboratoire de Métallurgie Physique de Poitiers sur un échantillon de $Zr_{80}Cu_{20}$. Elles sont exposées dans la publication ci-après. Le résultat essentiel est l'observation de larges défauts (environ 100 Å et plus) dans l'échantillon pulvérisé que l'on ne retrouve pas dans des échantillons trempés du liquide. D'autre part l'intensité de Laue indique systématiquement une moins bonne homogénéité à courte et moyenne distance des échantillons pulvérisés par rapport aux trempés. Le recuit de l'échantillon induit un réarrangement des gros défauts et une homogénéisation à courte distance. De plus on voit croître le pic principal de la phase ω-Zr. Ces observations, mises en parallèle avec les effets mesurés sur la conduction thermique, sont compatibles avec le lien suggéré précédemment entre les TLS et la phase ω-Zr.

R.Q.5 - Würzburg 1984

RAPIDLY QUENCHED METALS
S. Steeb, H. Warlimont (eds.)

STRUCTURAL RELAXATION IN SPUTTERED Zr-Cu ALLOYS STUDIED BY LOW-TEMPERATURE THERMAL CONDUCTIVITY AND X-RAY SCATTERING

Philippe GOUDEAU*, Jean-Claude LASJAUNIAS+, André NAUDON*, Alain RAVEX+ and Olivier BETHOUX+

* Laboratoire de Métallurgie Physique, 40 av. du Recteur Pineau, 86022 Poitiers, France
+ Centre de Recherches sur les Très Basses Températures, CNRS, BP166 X, 38042 Grenoble-Cédex, France

1. INTRODUCTION

The structural relaxation of metallic glasses obtained by annealing induces a decrease of their free-energy, and consequently significant changes for some of their properties. We report here its effect on the low-temperature thermal conductivity, which is determined by intrinsic excitations of the disordered state (T.L.S.), together with very sensitive X-ray scattering experiments which give direct informations about the structural evolution.

2. EXPERIMENTAL

Samples of $Zr_{76}Cu_{24}$ and $Zr_{80}Cu_{20}$ are prepared in the form of large foils, about 100 µm thick, by a high-rate (10 µm/hr) DC magnetron sputtering technique. Characterization of the samples is described elsewhere[1]. For X-ray measurements, they are thinned down to around 15 µm for a good transmission with Cu-K_α radiation.

X-ray measurements are carried out with a specific small-angle scattering (S.A.S.) camera described in details elsewhere[2] which is well adapted for the study of amorphous materials. It allows measurements over a large angular scale from the small-angle region to the first diffraction halo. Furthermore, heating of the sample can be carried out in-situ inside the vacuum chamber ; consequently tiny variations of the scattered intensities upon annealing can be revealed by this highly sensitive device[3,4].

Thermal conductivity $\kappa(T)$ measurements are performed in the T-range from 70 mK to 5 K, which includes the critical temperature $T_c \simeq 3.5$ K of these superconducting materials. We use the permanent heat-flow technique with one heater and two thermometers[1] on a strip of 1 cm × 4 cm. The lower temperature is limited by the parasitic heat input in the dilution cryostat, about 10^{-10} W. In case of $Zr_{80}Cu_{20}$ sample where variations of κ are very small, thermal treatments were ensured without modification of the geometrical arrangement.

3. RESULTS

3.1. X-ray scattering

Fig. 1 shows the whole scattering curve obtained using three positions of the detector for $Zr_{80}Cu_{20}$ alloy (a) aged at room temperature for 6.5 months, and (b) after annealing 1 h at 200°C, well below the crystallization temperature determined to be about 290°C by differential scanning calorimetry (Fig. 3).

For the (a) state, there is a strong intensity near the primary beam indicating large defects of one hundred Å or more in size. We have always observed such an effect in sputtered alloys in opposition to liquid-quenched ones[3,4]. This scattered intensity varies as q^{-3}, a variation already observed in amorphous alloys by neutron S.A.S. at very low q values[5,6]. Then, a flat scattering curve till the first diffraction peak means that the flat Laue intensity is relevant to an homogeneous amorphous state for the short and medium range order. When comparison can be made[4,7] the Laue intensity is systematically higher in sputtered alloys than in liquid-quenched ones.

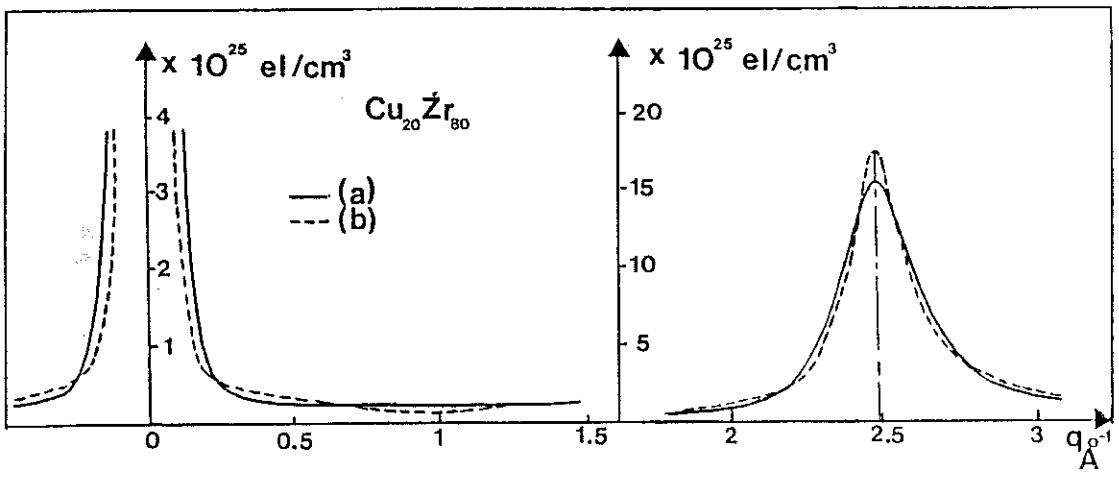

FIGURE 1
Scattering pattern of $Zr_{80}Cu_{20}$ alloy aged for 6.5 months at room temperature (a), and annealed for 1 h at 200°C (b). $[q = 4\pi(\sin\theta/\lambda)]$.

For the (b) state, there appears small but significant differences : (i) the intensity near the primary beam is more concentrated, indicating a rearrangement of the large defects ; (ii) an increase in the S.A.S. region corresponding to fluctuations in the medium-range order around q = 0.5 $Å^{-1}$; (iii) for higher q values a decrease of the monotonic Laue intensity, by about 7 % between 1 and 1.5 $Å^{-1}$, which indicates a better short-range order and is also in agreement with the increase of the intensity in the former q domain. This is a confirmation of the presence of fluctuations in composition, based on the fact that the total scattered intensity must remain constant[8] ; (iv) a narrowing by 12.5 % of the width of the diffraction peak (q = 2.493 $Å^{-1}$) together with a very small shift towards the angular origin.

This same alloy annealed now 7 h at 200°C does not show any more change in the small angle pattern, but a difference occurs in the diffraction region [Fig. 2] : the main streak (110) of the ω-Zr phase rises at q = 2.486 $Å^{-1}$, which is exactly the right value[9], superimposed on the amorphous halo. Thereafter, on increasing the annealing temperature, there is no noticeable evolution of the whole pattern till 250°C, except the sharpening of the ω-Zr main streak. At 300°C a mixture of ω-Zr and Zr_2Cu is observed, and at 400°C ω-Zr evolves into α-Zr.

Similar investigation on a $Zr_{76}Cu_{24}$ sample leads to the same evolution, but significant modification occurs only at 250°C, temperature at which the ω-Zr phase appears after 8 hours. This is in agreement with the crystallization data from D.S.C. (Fig. 3) : the first broad peak corresponding to the formation of ω-Zr decreases markedly from 316°C for $Zr_{76}Cu_{24}$ to 288°C for $Zr_{80}Cu_{20}$, that signifies an easier transformation into ω phase at higher Zr concentration.

3.2. Thermal conductivity

It is widely accepted that the $T^{1.9-2.0}$ regime of the phonon thermal conductivity below 1 K in amorphous materials originates in excitations characteristic of the disordered structure : atoms or groups of atoms can tunnel between two configurational positions which differ in energy by $\Delta E \lesssim 1$ K (or 10^{-4} eV) ; these entities are so-called Two Level Systems (TLS) or Tunneling States[10]. The T^2 regime of κ corres-

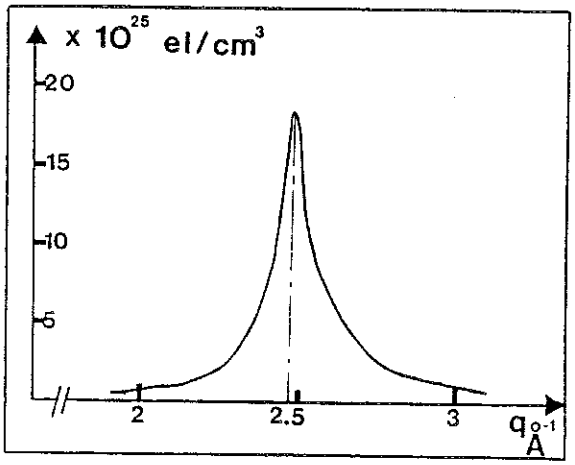

FIGURE 2
$Zr_{80}Cu_{20}$ alloy annealed 7 h at 200° C.

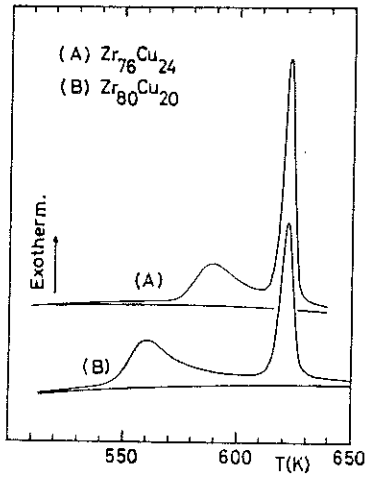

FIGURE 3
D.S.C. thermogram at 20 K/min (as-prepared state).

ponds to a distribution of TLS independent of energy (n(E) reduces to $\bar{n}$) and very strongly coupled to phonons (a coupling constant M of about 1 eV) : $\kappa(T) \propto \frac{\rho v_D}{\bar{n}M^2} T^2$, with v_D is a mean sound velocity, extracted here from specific heat[1], and ρ the density.

In Fig. 4 are shown the variations of $\frac{\kappa}{T^2}$ below 1 K for three different samples at different steps of the thermal history. We may conclude : (i) the $T^{1.9}$ or T^2 regime is rather well obeyed below about 0.7 K for samples "as-prepared" or aged at room temperature ; (ii) ageing or annealing results in an increase of κ , and is also to reduce progressively the domain of pure T^2 regime, what means a decrease of $\bar{n}M^2$ [11], much probably of $\bar{n}$, together with a modification of the distribution n(E). The decrease of n(E) between the "as-prepared" and annealed states is confirmed by simultaneous specific heat measurements[12]. Note that for $Zr_{76}Cu_{24}$ alloys large variations of κ occur on annealing at 200°C, whereas they are only tiny for the small-angle X-ray pattern, except near the primary beam.

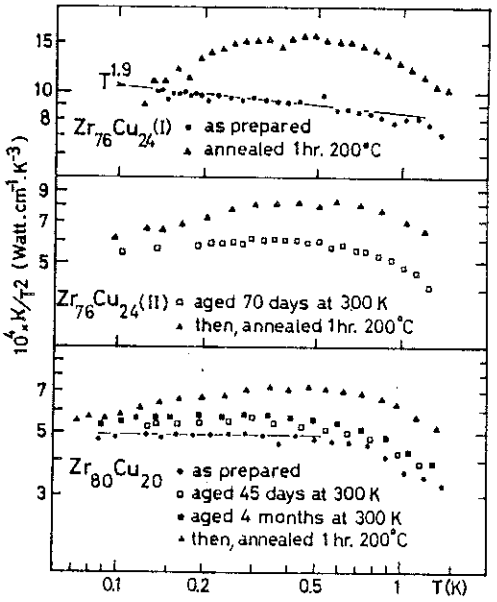

FIGURE 4
Thermal conductivity data

4. DISCUSSION

Both kinds of measurements indicate that the structural relaxation leads the initial alloy into a less disordered amorphous state. The diminution of $\bar{n}M^2$ or n(E) from the low temperature thermal properties is related to a decrease of the tunneling entities on a scale of a few atoms.

Although no straightforward hypothesis about their microscopic origin can be inferred from thermal measurements, authors of ref. 1 (1984) suggested a correlation between the decrease of n(E), that is in the possibility of rapid tunneling fluctuations, and the growth of small aggregates of nearly pure Zr phase.

For the X-ray measurements, the different q regions are modified : near the origin, indicating modifications of the larger defects ; in the small-angle range, indicating fluctuations in composition that correspond to the decrease of the Laue scattering ; the first diffraction peak sharpens towards lower q values, indicating *larger* distances between first neighbors. This last is unusual, we do observe the contrary[2,3,4]; but it is in accordance with recent X-ray diffraction data on the $Zr_{76}Cu_{24}$ alloy which show an *increase* of r_1 by 0.5 % on annealing at 200°C[13]. This result is more significant here with the very sensitive in-situ observation.

An explanation can be proposed, on the fact that the main streak of the ω-Zr phase appears a little bit shifted on the left side of the amorphous peak (a variation of 0.1° in 2θ). We conclude to a rearrangement on the atomic scale, because the variation of the S.A.S. pattern is too small to be significant. There is an increase in the distances of the Zr-Zr pairs, which have the highest weighting factor for the X-ray structure factor. So the structural relaxation leads to the early stage of formation of ω-Zr ; we suppose this process to be continuous and irreversible till the direct observation of crystallization. Therefore, the structural relaxation is emphasized when the formation of the ω-Zr phase becomes easier : that is the case when the Zr concentration increases.

REFERENCES

1. A. Ravex, J.C. Lasjaunias and O. Béthoux, Solid State Commun. 40 (1981) 853 ; J. Phys. F (Met. Phys.) 14 (1984) 329.
2. A.M. Flank, M. Harmelin, M. Jaulin and A. Naudon, Rev. Phys. Appl. 15 (1980) 1427.
3. A.M. Flank and A. Naudon, J. Physique C8, 41 (1980) 123.
4. A.M. Flank, M. Laridjani and A. Naudon, C.R. Acad. Sc. Paris t. 292 (1981) 995.
5. E. Nold, S. Steeb, P. Lamparter and G. Rainer-Harbach, J. Physique 41 (1980) C8, 186.
6. B. Boucher, J. Physique 41 (1980) C8, 135.
7. A. Naudon and A.M. Flank, Proc. of "Rapidly Quenched Metals-4" (Sendai, 1982), 425.
8. A. Guinier, in "Théorie et Technique de la Radiocristallographie", ed. Dunod, Paris (1964).
9. B. Olinger and J.C. Jamieson, High Temp.-High Press. 5 (1973) 123.
10. "Amorphous Solids-Low Temperature Properties" ed. by W.A. Phillips (Springer, Berlin, 1981).
11. We have verified by specific heat measurement of the same samples that the variations of v_D are negligible in view of those of κ.
12. J.C. Lasjaunias, A. Ravex and O. Béthoux in "Phonon Scattering in Condensed Matter", Springer Series in Solid-State Sciences-51 (1984) 410.
13. K. Samwer and J.C. Lasjaunias, Solid State Commun. (1984) in press.

III - EXAFS

Un échantillon de $Zr_{76}Cu_{24}$ a été étudié par EXAFS au LURE - laboratoire de Physique des Solides d'Orsay (A. Sadoç et J.C. Lasjaunias, 1985) afin de préciser l'ordre local au niveau des premiers voisins exclusivement et les effets de recuit sur cet ordre. Les mesures ont été effectuées à la fois sur le seuil du Cu et du Zr.Les informations sur la composition et le rayon des couches atomiques entourant chaque atome de Cu et de Zr tirées de ces mesures et de celles de rayons X "standards" sont reproduits sur le tableau ci-après :

Central atom	X as-prepared σ = .15 Å			EXAFS as prepared				EXAFS annealed			
	N		R	N		R	σ(Å)	N		R	σ(Å)
Cu	3	Cu	2,55 Å	3,3	Cu	2,50 Å	.116	3,5	Cu	2,52 Å	.116
	1,5	Cu	3,10 Å	1,5	Cu	3,10 Å		1,5-2	Cu	3,10 Å	
	4,5	Zr	2,80 Å	5	Zr	2,74 Å	.122	6±1	Zr	2,76 Å	.120
Zr	1,4	Cu	2,80 Å	1,5-2	Cu	2,70 Å	.122	2	Cu	2,69 Å	.127
	5	Zr	3,10 Å	5	Zr	3,12 Å	.137	5,5	Zr	3,13 Å	.132
	2,75	Zr	3,43 Å	1,5-2	Zr	3,45 Å		2	Zr	3,45 Å	

Table 1 - Structural parameters for amorphous $Cu_{24}Zr_{76}$

(Atomic diameter in Å : Cu-Cu = 2.56 Å, Cu-Zr = 2.88 Å, Zr-Zr = 3.20 Å)

On constate que les résultats obtenus par les deux méthodes sont en très bon accord : les écarts observés sont dans l'incertitude habituelle des mesures d'EXAFS pour des matériaux désordonnés (nombres de coordination : $\Delta N = 0,75$; rayons de couches : $\Delta R = 0,06$ Å). Les principales conclusions de cette étude sont les suivantes :

- l'entourage des atomes de Cu est identique à celui observé dans une série d'échantillons trempés du liquide de compositions différentes (Zr_xCu_{1-x} ; $67 \leqslant x \leqslant 40$, Sadoc et al., 1984);

- le paramètre de désordre structural (σ - voir tableau) est plus élevé pour notre échantillon pulvérisé que pour les échantillons trempés du liquide précédemment étudiés ;

- il n'apparaît aucune évidence d'ordre chimique dans l'échantillon étudié (pas de préférence pour les paires ZrCu par rapport à la statistique) ;

- le recuit se traduit par un réarrangement des paires Zr-Zr (le nombre de paires Zr-Zr augmente de 0,5, la distance Zr-Zr augmente et le paramètre de désordre σ diminue de 0,005 Å), que l'on peut interpréter comme une tendance à la formation d'amas de Zr (clustering). Cette tendance à l'augmentation de la distance Zr-Zr est accentuée sur les diagrammes EXAFS mesurés très récemment sur un échantillon partiellement cristallisé en phase ω (ceci confirme que dans nos échantillons, la cristallisation est un processus <u>continu</u> avec la relaxation structurale).

Ce dernier résultat est en bon accord avec les observations précédentes (rayons X, diffusion des RX aux petits angles, A.T.D.) montrant une tendance au regroupement des atomes de Zr sous l'effet du recuit qui pourrait être le premier stade de la formation des germes de ω-Zr.

IV - RESISTIVITE ELECTRIQUE ET MODULE DE CISAILLEMENT : EFFETS REVERSIBLES ET IRREVERSIBLES

Hillairet et al.(1984) au Centre d'Etudes Nucléaires de Grenoble (DRF) ont mis en évidence par des mesures de résistivité électrique et de module de cisaillement deux types de comportement distincts (l'un réversible et l'autre irréversible) associés à la relaxation structurale des verres métalliques. Ils interprètent les résultats expérimentaux en distinguant deux processus dans la relaxation structurale :

une réorganisation d'ordre topologique qui donne lieu aux effets irréversibles observés au cours du recuit à laquelle se superposent des variations relativement plus faibles et réversibles qui traduisent des modifications d'ordre local à caractère essentiellement chimique.

Ils ont effectué ces mesures sur l'un de nos échantillons pulvérisés ($Zr_{76}Ni_{24}$) et sur un échantillon de même composition préparé par trempe du liquide. Il ressort de cette étude comparative que les deux effets (réversibles et irréversibles) sont observables dans les deux échantillons. Le comportement réversible (associé à l'ordre chimique local) est absolument identique pour les deux types de préparation si l'on prend soin de faire subir des traitements de prestabilisation identiques aux deux échantillons.

Par contre les effets irréversibles (décroissance de la résistivité et augmentation du module de cisaillement de quelques pourcents) sont très importants dans les échantillons pulvérisés comparés aux trempés du liquide, tendant à prouver que le désordre topologique est plus important dans l'échantillon pulvérisé. Ce résultat est en parfait accord avec nos mesures thermiques.

De plus, O. Béthoux (communication privée) a vérifié sur la résistivité électrique que la relaxation irréversible commençait dès que la température du traitement dépassait celle de la fabrication de l'échantillon (autour de 100 K). Ainsi un échantillon séjournant à 300 K doit-il avoir déjà fortement relaxé par rapport à son état brut de préparation.

- BUSCHOW K.H.J., VINCZE I., van der WANDE F., J. Non Cryst. Solids 54, 101 (1983).
- GRAEBNER J.E., GOLDING B., SCHUTZ R.J., HSU F.S.L., CHEN H.S., Phys. Rev. Lett. 39, 1480 (1977).
- GRONDEY S., von LÖHNEYSEN H., SCHINK H.J. and SAMWER K., Z. Phys. B51, 287 (1983).
- HARMELIN M. (communication privée, 1984), à paraître.
- HARMELIN M., NAUDON A., FRIGERIO J.M., RIVORY J., "Rapidly Quenched Metals", 5e Conf. (1984), p. 659.
- HILLAIRET J., BALANZAT E., DERRADJI N.E., CHAMBEROD A., J. Non Cryst. Solids 61 et 62, 781 (1984).
- LOU L.F., Solid State Commun. 19, 335 (1976).
- MON K.K. and ASHCROFT N.W., Solid State Commun. 27, 609 (1978).
- RAVEX A., LASJAUNIAS J.C., BETHOUX O., J. Phys. F : Met. Phys. 14 (1984).
- SADOC A., CALVAYRAC Y., HARMELIN M., QUIRY A., FLANK A.M., J. Non Cryst. Solids 65, 109 (1984).
- SADOC A., LASJAUNIAS J.C., J. Phys. F 15, 1021 (1985)
- SAMWER K., LASJAUNIAS J.C., Solid State Commun. 51, 93 (1984).
- SROLOVITZ D., HAEDA K., VITEK V., EGAMI T., Phil. Mag. A44, 847 (1981).

CHAPITRE VI

CONCLUSION

Les mesures de chaleur spécifique et conduction thermique présentées dans ce mémoire mettent indubitablement en évidence l'existence d'excitations de basse énergie (SDN ou TLS) dans les alliages métalliques amorphes supraconducteurs étudiés.

Ces résultats confirment la première observation des TLS dans le système ZrPd par Graebner et al. (1977) en accord avec d'autres mesures tant thermiques qu'acoustiques. Ils présentent en outre les spécificités suivantes :

i) l'extension des mesures de chaleur spécifique au-dessous de 100 mK a été rendue possible par le développement de techniques de mesures très performantes notamment au niveau de la thermométrie (sensibilité, reproductibilité et faible capacité calorifique) et procure ainsi des possibilités expérimentales privilégiées.
Elles ont rendu possible l'observation d'un terme quadrupolaire nucléaire et permis de mettre en évidence un couplage entre TLS et noyaux de Zirconium qui restaure la relaxation nucléaire. D'autre part les lois de variations en température de la contribution des TLS à la chaleur spécifique ont pu être définies avec précision.

ii) la mesure de la chaleur spécifique dans une grande gamme de température, à la fois à l'état normal et supraconducteur a ouvert des possibilités d'analyse supplémentaires. En particulier cela a posé le problème encore mal éclairci d'une contribution en T^3, très probablement d'origine extra-phononique, qui est présente à l'état normal.

iii) l'élaboration des échantillons par pulvérisation a permis d'étendre les mesures à des compositions riches en Zirconium inaccessibles par trempe du liquide. On constate quand la comparaison est possible que les échantillons bruts de pulvérisation présentent une densité de TLS plus élevée que les échantillons obtenus par trempe du liquide (chaleur spécifique plus forte, conduction thermique plus faible). Si l'on admet que les TLS sont liés à des mouvements de groupes d'atomes cette différence traduit certainement des différences au niveau de

structure locale. De façon générale on peut parler d'un degré de désordre plus élevé pour les alliages pulvérisés en terme de défauts de structure à l'origine des systèmes à 2 niveaux.
Il en est de même pour la densité d'état électronique $N_o(E_F)$ beaucoup plus élevée (30 à 40 %) dans les alliages pulvérisés. Or cette densité est essentiellement déterminée par les orbitales d des atomes de Zirconium. Cela implique du fait du caractère très local de ces orbitales une structure au niveau des atomes premiers voisins de Zr différente.

iv) des effets de recuits importants ont été observés sur nos échantillons qui se traduisent par des variations cohérentes des propriétés thermiques associées aux TLS : diminution de la chaleur spécifique accompagnée d'une augmentation corrélée de la conduction thermique traduisant une diminution de la densité de TLS. Ces effets sont certainement associés à une réorganisation de la structure locale des échantillons lors des recuits.

Cette réorganisation entraîne également de fortes variations de la densité d'état électronique au niveau de Fermi.

Il est remarquable de noter que toutes les mesures d'ordre local effectuées sur nos échantillons mettent en évidence les mêmes tendances systématiques :

- degré de désordre plus élevé dans les échantillons pulvérisés à l'état brut que dans les échantillons trempés ;

- tendance au réarrangement sous l'effet de recuit favorisant l'apparition de la phase ω-Zr comme premier stade de cristallisation.

Mais en valeur absolue les variations expérimentales observées sont très faibles, souvent à la limite de résolution des techniques employées. Or les conséquences de ces très faibles modifications de l'ordre local se traduisent par des effets spectaculaires sur les propriétés thermiques macroscopiques attribuées aux TLS faisant de la chaleur spécifique et de la conduction thermique des outils expérimentaux privilégiés.

On peut raisonnablement affirmer que dans la série d'alliages étudiée il existe très probablement un lien entre la nature microscopique des TLS et la tendance à la séparation de la phase ω-Zr. Il reste cependant encore un sérieux travail expérimental et théorique à effectuer pour en préciser les mécanismes. Il en est de même pour la forte densité d'état électronique au niveau de Fermi qui est déterminée par l'ordre local des atomes de Zr. En l'absence de théorie suffisamment précise qui permette de relier le degré de désordre structural à la structure de bande, le problème est donc ouvert. Il s'agit en particulier de savoir si la sensibilité de $N(E_F)$ aux traitements thermiques est une propriété intrinsèque de ces alliages à forte concentration de Zirconium ou plus généralement si cela est dû au caractère particulièrement désordonné de ces matériaux.

A N N E X E A

CHALEUR SPECIFIQUE DE L'ALLIAGE PdCuSi AMORPHE ET CRISTALLISE

Les mesures de chaleur spécifique effectuées sur PdCuSi et analysées dans la publication ci-jointe n'ont pas permis de conclure avec certitude sur la contribution d'excitations de basse énergie (TLS) caractéristiques de l'état amorphe. En effet bien que le terme linéaire en température mis en évidence dans l'échantillon amorphe soit supérieur à ceux observés après recristallisation, la grande sensibilité de l'amplitude de ce terme aux conditions du recuit (400°C ou 550°C) ne permet pas de trancher entre une éventuelle contribution de TLS ou un simple effet de structure de bande sur la contribution électronique.

Toutefois l'apparition de deux constantes de temps distinctes dans le retour à la température d'équilibre de l'échantillon après le pulse de chaleur permet de mettre en évidence une contribution hyperfine des noyaux de Palladium. L'insensibilité de l'amplitude de cette contribution aux recuits montre que l'ordre local autour des atomes de Palladium est identique dans les états désordonné et ordonné.

Cette étude avortée quant à son objectif initial nous incitera à rechercher des systèmes supraconducteurs afin de s'affranchir de la contribution des électrons de conduction dans la quête des systèmes à deux niveaux !

J. Phys. F: Metal Phys., Vol. 9, No. 5, 1979. Printed in Great Britain

Low-temperature specific heat of glassy and crystallised $Pd_{0.775}Cu_{0.06}Si_{0.165}$ alloys

J C Lasjaunias, A Ravex and D Thoulouze
Centre de Recherches sur les Très Basses Températures, CNRS, BP 166 X, 38042 Grenoble Cédex, France

Received 7 February 1978, in final form 15 December 1978

Abstract. The specific heat of $Pd_{0.775}Cu_{0.06}Si_{0.165}$ alloys has been measured between 30 mK and 1 or 2 K successively in glassy and polycrystalline phases obtained by annealing at 400 and 550 °C. Well defined T terms appear between 0·15 and 1 K in each case, not very dependent upon the structure, but systematically higher in the glassy state. Below 80 mK, the specific heat is dominated by a hyperfine T^{-2} term, almost independent of the structure. This second point leads to the conclusion that the short-range order remains almost unchanged from the crystalline to the glassy states.

1. Introduction

In all amorphous insulators investigated up to now an important contribution to the specific heat below 1 K has been pointed out in recent years. This contribution, due to two-level systems characteristic of the vitreous state, leads to a term roughly proportional to T. In glassy metals such as the $Pd_{0.775}Cu_{0.06}Si_{0.165}$ alloy, an excess specific heat in the amorphous phase besides the crystalline ones had already been observed above 2 K (Chen and Haemmerle 1972, Golding *et al* 1972). The purpose of the present work was to extend to lower temperatures these specific heat measurements, seeking a term characteristic of the glassy state in a metallic alloy. In particular, it was necessary to compare this glassy state specific heat to a direct experimental value of the linear T term due to conduction electrons in the case of the crystalline samples, as the previous analyses led to large differences in their evaluation.

The Pd–Cu–Si system presents many advantages. It is easily obtained in bulk form, in the glassy state at room temperature, and it can be prepared with very low content of magnetic impurities so that it is possible to study the intrinsic properties related to the glassy state, which is not the case for most of the amorphous metals which present a strong magnetic character.

Recently two typical features already observed in insulating glasses have been pointed out in this system; the thermal conductivity measurements (Matey and Anderson 1977) show a phonon thermal conductivity very similar in magnitude and temperature dependence, and sound velocity measurements (Bellessa and Béthoux 1977) show a logarithmic variation with temperature below 1 K. However, in the latter case the magnitude of the effect is reduced by an order of magnitude as compared to insulators.

0305-4608/79/050803 + 12 $01.00

2. Experimental

2.1. Samples preparation and thermal treatments

The alloys were prepared from high-purity Pd (5N), Cu (5N) and Si in an induction furnace. Activation analysis on a final sample indicates a concentration of 30 PPM iron. The glassy specimens were prepared in the following way: the alloy is heated at 1200 °C under vacuum in a fused silica capillary for about ten minutes, and is then rapidly quenched either into water at room temperature in a capillary 2·2 mm ID and 1 mm wall thickness (alloy 1), or into a freezing bath at −22 °C in a capillary 1·85 mm ID and a wall thickness of 0·5 mm (alloy 2), so that the quenching rate was enhanced for this second sample. The length of the specimens was about 15 cm. At first, both specimens were studied in their 'as quenched' glassy phase; thereafter, alloy 2 has been annealed in an argon atmosphere successively at 395–400 °C for 22 h and at 550 °C for 24 h.

2.2. Characterisation of the samples

2.2.1. Optical micrography. On both glassy alloys 1 and 2, optical micrography with 10^3 magnification does not reveal any structure. Annealing at 395 °C of alloy 1 clearly shows the presence of a spherulitic crystallisation with a radius of the spherulites of about 10 to 15 μm; the same annealing on alloy 2 indicates crystallite grain boundaries of the order of 10 μm. No investigation has yet been made after annealing at 550 °C.

2.2.2. Thermal properties. Differential scanning calorimetry, with a Perkin–Elmer DSC 2, at a heating rate of 20 °C min^{-1}, yields a glass transition temperature of about 362–372 °C, depending upon the definition of T_g, and an initial crystallisation temperature (temperature at which the onset of the exothermic crystallisation peak is observed) of 412–415 °C. These values are close to those obtained by Chen and Turnbull (1969) and by Chen and Park (1973) with the same heating rate. Density values, measured by the Archimedes method in water, are reported in table 1.

2.2.3. X ray diffraction. The different phases of the alloys (quenched and annealed) have been studied by x ray diffraction, with the Debye–Scherrer technique on powder, using CuKα radiation. Typical diffractometer recordings are reported in figure 1. For the as-quenched specimens, the general shape of the pattern is typical of an amorphous structure, with a first diffraction ring maximum localised here at about $2\theta = 40$–$41°$; this first ring is much narrower than in the case of insulating vitreous systems as B_2O_3, GeO_2 for example; the width at half maximum is here about 4 to 5°; in good agreement with amorphous $Pd_{0.8}Si_{0.2}$ (Masumoto and Maddin 1975, Ino *et al* 1978). X ray patterns of amorphous $Pd_{100-x-y}Si_xFe_y$ alloys, with $y = 0·3$ and $15 \leqslant x \leqslant 20$, exhibit the two first diffraction rings respectively at $2\theta \simeq 40·5°$ and $\simeq 72°$ (Ino *et al* 1978). Our results are very similar, despite the presence of 6 at% copper in our case. Similar also are the patterns of our two as-quenched alloys, although the quenching conditions are slightly different.

After annealing at 395–400 °C for about 24 h, diffraction peaks appear at about the same positions as the diffuse maxima of the amorphous state, the first three

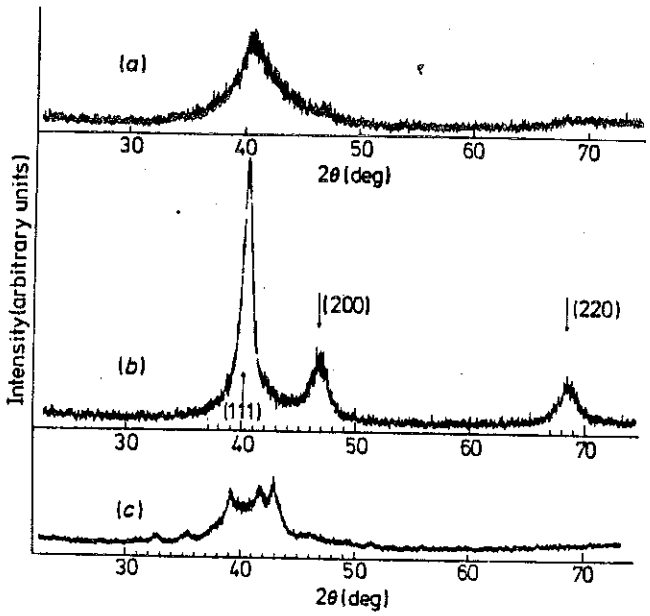

Figure 1. X ray diffraction patterns (CuKα radiation $\lambda = 1{\cdot}540$ Å) for the three phases of the alloys studied in specific heat measurements: (*a*), as-quenched; (*b*), after annealing at 395 400 C for about 24 h. The arrows indicate the position of pure Pd peaks, for comparison. (*c*), after a further annealing at 550 °C for 24 h.

ones being for values of 2θ of 40·3, 46·7–46·8 and 68·6; these positions are very close to the pure palladium peaks (FCC structure), respectively at $2\theta = 40{\cdot}1$ for the (111) reflection, 46·7 for the (200) and 68·1 for the (220). These small shifts correspond to a variation of the lattice parameter from 3·890 Å for pure Pd to 3·87–3·88 Å in this case. We shall call this first phase of crystallization phase A. Different durations of annealing of 2 h, and then 24 h more, give very similar intensity spectra, the first peak increasing slightly in the last case. Further annealing at 550 °C leads to a much more complex structure, not clearly identified and named here phase B, characterised by a band of peaks not well resolved between $2\theta \sim 32$ and 45° and by the disappearance of the peak at 68°.

Our observations for the vitreous phase and the crystalline phase A are in agreement with the results of Duwez (1967) and Masumoto and Maddin (1971, 1975) on $Pd_{0.8}Si_{0.2}$, who state that the structure of the amorphous phase and the first stage of crystallisation (metastable phase I for Masumoto and Maddin) are closely related to the FCC structure of pure Pd. Chen and Turnbull (1969) also observed that the $Pd_{0.78}Au_{0.06}Si_{0.16}$ alloy heated between 300 and 400 °C for durations always less than 6 h crystallises into a metastable FCC solid solution with a lattice parameter very close to that of Pd. Finally, Chen and Park (1973) report that for Pd–Cu–Si alloys of the same composition as here, the first stage of crystallisation of the glass, obtained by annealing at 400 °C for 24 h, is a metastable FCC solid solution.

On the other hand, Ino *et al* (1978) observed that amorphous $Pd_{0.79}Si_{0.20}Fe_{0.01}$ or $Pd_{0.80}Si_{0.20}$ alloys aged between 250 and 350 °C crystallise into a predominant Pd_3Si structure, which differs from the results of Masumoto and Maddin on $Pd_{0.8}Si_{0.2}$. The authors ascribe this discrepancy to differences in the methods of preparation, like the quenching conditions of the melt.

For the later stages of crystallisation, the appearance of a stable phase at an aging temperature of about 550 °C is reported for $Pd_{0.8}Si_{0.2}$ (Masumoto and Maddin 1971), this phase is identified as a mixture of Pd_3Si and Pd, of orthorhombic structure; for Pd–Cu–Si systems, Chen and Park (1973) indicate the decomposition of the metastable FCC phase into metastable silicides and the precipitation of the equilibrium

phases: Pd and Pd_3Si. However, concerning these later stages of crystallisation, we have never detected in the x ray patterns of our B phase the presence of any peaks of the Pd_3Si structure, even for the more characteristic, at $2\theta = 39{\cdot}4$–$39{\cdot}5°$ (220–112 reflections) or 48·1° (230–040).

We have made further x ray analysis of samples annealed in the temperature range 400–1000 °C for different durations. At this stage of our study it is difficult to assert if either A or B phases are metastable or not. Alternative heat treatments at 400 and 500 °C have not allowed us to decide at present. On the other hand, annealing at 400 °C for durations varying between 2 h and 8 days lead to the same A structure and the B phase is always obtained in the temperature range between about 500 and 700 °C. This phase can appear very rapidly in the amorphous phase; in a few minutes at 480°. The x ray patterns show minor modifications upon annealing at different temperatures inside this range.

Annealing amorphous samples at 800 or 1000 °C for durations between 2 h and a few days leads to x ray patterns intermediate between the amorphous state and the A phase. We interpret these results by supposing that the melting point of the crystalline B phase lies in the range 700–800 °C. Hence, when heated above this melting point, the samples can remelt. Depending upon the cooling rate, one obtains an almost amorphous state or a partial crystallisation in the A phase. We do not obtain the B phase because the cooling rate may be sufficiently rapid to prevent the crystallisation of the supercooled melt above about 500 °C, whereas at about 400 °C the onset of crystallisation in the A phase is then possible.

2.2.4. Electrical resistivity. Values of the electrical resistivity at room temperature for both samples are reported in table 1. These values depend strongly on the phase of the alloys (parts of alloy 1 have been annealed at 400 and 550 °C at the same time as alloy 2; both resistivity values are in agreement within 1 or 2 $\mu\Omega$ cm). For the amorphous phase the resistivity decreases with temperature, showing a relative variation of about 4% between 300 and 3 K, which is very similar to the variation observed by Duwez *et al* (1962) on a $Pd_{0{\cdot}83}Si_{0{\cdot}17}$ alloy.

Preliminary measurements between 0·1 and 4 K show a logarithmic dependence of ρ with temperature ($\Delta\rho/\rho = 2 \times 10^{-4}$ per decade). But this variation may probably be ascribed to the 30 PPM iron impurities of the sample. This is in agreement with the results of Hasegawa and Tsuei (1970), who observed a flat residual resistivity in an amorphous $Pd_{80}Si_{20}$ alloy when it was pure enough, and a resistivity minimum in a less pure sample.

2.3. Specific heat technique

We used a transient heat pulse technique described elsewhere (Lasjaunias *et al* 1977) in an adiabatic demagnetisation cryostat. The specific heat values are calculated from the ratio of the applied heat input to the temperature increment $(\Delta T)_{t=0}$. Samples of about 4 g have been measured between 30 mK and 2 K. Due to the small diameter of the rods, the arrangement has been modified; the initial rods have been cut into several pieces about 2 cm long, held together in a copper cylinder which also supports the heater (Pt–W wire), the thermometers (two phosphorus-doped silicon slabs (Frossati *et al* 1975) and the thermal link to the cold sink. Measurements are taken alternatively with one and the other Si thermometers. Within the experimental scatter no discrepancy appears in the results.

Table 1. Specifications of the samples and specific heat data.

Samples and heat treatments		Room-temperature electrical resistivity ($\mu\Omega$ cm)	Density (g cm^{-3})	Specific heat linear coefficient A (mJ mol^{-1} K^{-2}) (1 mol = 90·9 g)	Specific heat hyperfine term B (erg mol^{-1} K)
Alloy 1	as quenched (I)	70·5	10·64 ± 0·05	1·29 ± 0·030	3·85 ± 0·55
Alloy 2	as quenched (II)	Not measured	10·54 ± 0·05	1·31 ± 0·025	2·95 ± 0·65
	after annealing at 395–400 °C for 22 h (III)	35	10·75 ± 0·10	1·11 ± 0·035	3·60 ± 0·65
	after a further annealing at 550 °C for 24 h (IV)	33	10·61 ± 0·05	1·28 ± 0·020	2·85 ± 0·35

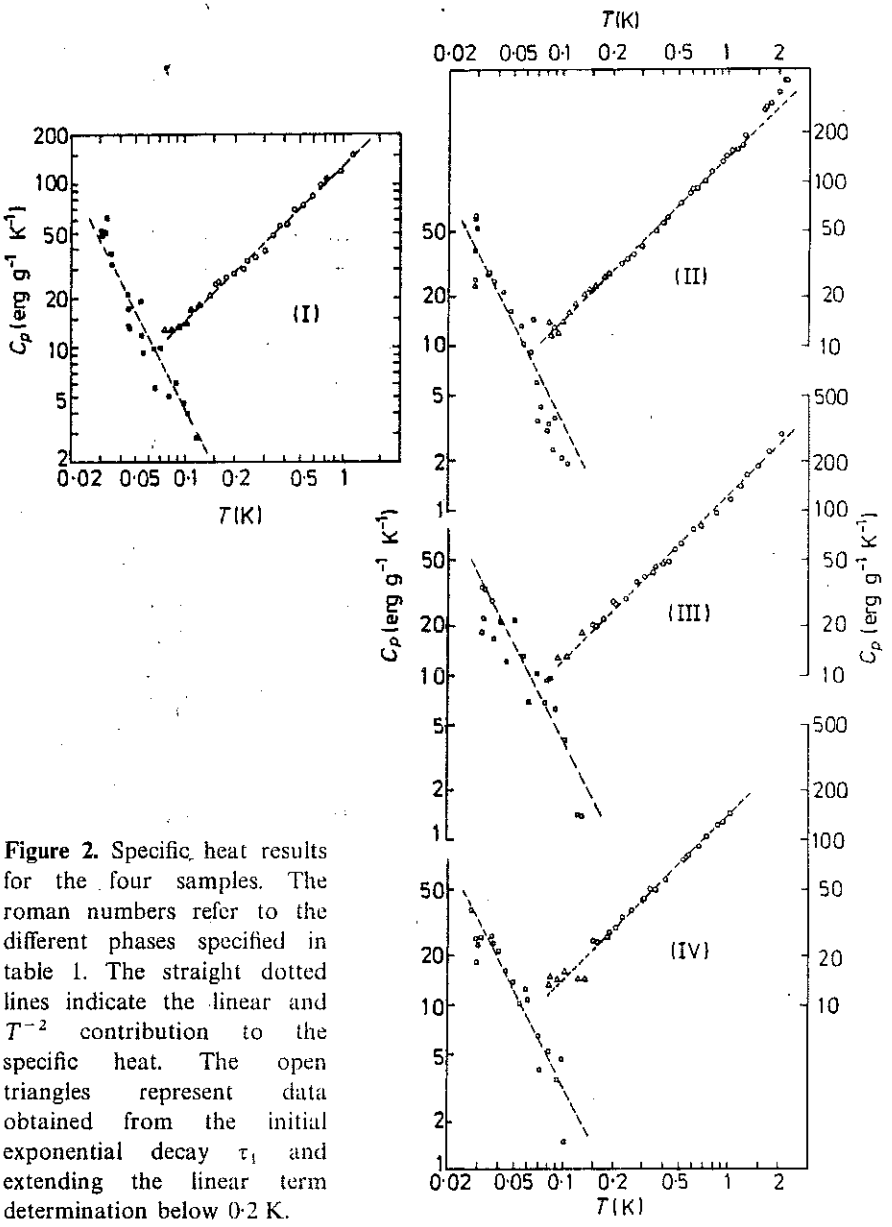

Figure 2. Specific heat results for the four samples. The roman numbers refer to the different phases specified in table 1. The straight dotted lines indicate the linear and T^{-2} contribution to the specific heat. The open triangles represent data obtained from the initial exponential decay τ_1 and extending the linear term determination below 0·2 K.

The thermal equilibrium between the sample (several rods) and the addenda can be checked by the time constant of the temperature increment following the heat pulse (labelled τ_{II}; Lasjaunias *et al* 1977); in the whole temperature range it lies between one and two seconds, that of the thermometer itself amounting to some milliseconds. The relaxation to the sink, once thermal equilibrium is reached between the different parts, takes about 100 s. The ratio of both time constants, which is an indication of the accuracy of the technique, is less than 1% below 0·1 K and increases to about 2 or 3% at 1–2 K.

The heat capacity of the sample holder, equivalent to about 4 g of copper, has been measured in separate experiments; at the lowest temperatures it shows a very slight excess above a T law, reaching 7 erg K^{-1} at 40 mK, compared to a total value of 23 erg K^{-1}.

3. Results and discussion

3.1. Experimental results

The specific heat results of the four different amorphous and annealed samples are shown in figure 2.

Above about 0·2 K, the temperature profile response to the heat pulse is very well described by an exponential decay corresponding to the relaxation of the whole system (sample + addenda) to the sink through the heat link of thermal resistance R_1. The results correspond to *a well defined linear variation for the specific heat* between 0·2 and 1 K (open circles on figure 2).

Below 0·2 K the heat pulse response can be described by the superposition of two exponential decays, as shown in figure 3, with two different time constants τ_1 and τ_2:

$$\Delta T(t) = \Delta T_1 \exp(-t/\tau_1) + \Delta T_2 \exp(-t/\tau_2).$$

The value of τ_1 remains fairly constant down to 30 mK, of the order of 20 to 40 s depending upon the samples, whereas τ_2 decreases from about 500 s at 30 mK to about 50 s at 0·2 K.

Our thermal circuit can be analysed as reported in figure 3, where C_E and C_N represent respectively the heat capacity of the electrons or excitations described by the linear T term and that of the nuclei. Above 0·2 K, C_N is negligible compared to C_E, which is thus directly obtained. Below 0·2 K these two heat capacities become comparable; as on the other hand the thermal resistances R_{en} and R_1 are also of the same order of magnitude, it is now necessary to solve exactly the equations of the thermal response of the system (Azevedo *et al* 1979).

From this calculation it appears that by extrapolating at zero time the measured temperature T_E, which is that of the electrons or excitations, using the time constant τ_1, we have direct access to the heat capacity C_E by

$$C_E = W/((\Delta T_1)_{t=0} + (\Delta T_2)_{t=0}).$$

We can calculate the heat capacity C_N of the nuclei using the relation (Azevedo *et al* 1979)

$$C_N = \frac{\tau_2}{R_1}\left(1 - \frac{\tau_1}{R_1 C_E}\right)\left(1 - \frac{R_1 C_E}{\tau_2}\right).$$

The link thermal resistance R_1 is obtained by extrapolating below 0·2 K the values measured between 0·2 K and 2 K, as the ratio of the time constant of the temperature exponential decay to the total heat capacity. The other parameters are extracted from the analysis of the recorded results. We have shown in figure 3 the calculated variation of the temperature of the nuclei. At short times the electrons are overheated by the heat pulse and thereafter the heat relaxes either to the nuclei through the resistance R_{en} or to the cold sink through R_1. For long times this temperature is delayed behind that of the electrons (or excitations).

The values of C_E obtained in this two-time-constants range using the extrapolation with τ_1 (points Δ) extend very well the linear variation defined at higher temperature where one only time constant is present. However, below about 80 mK it becomes impossible to extract C_E from the τ_1 regime as the overheating of the electrons

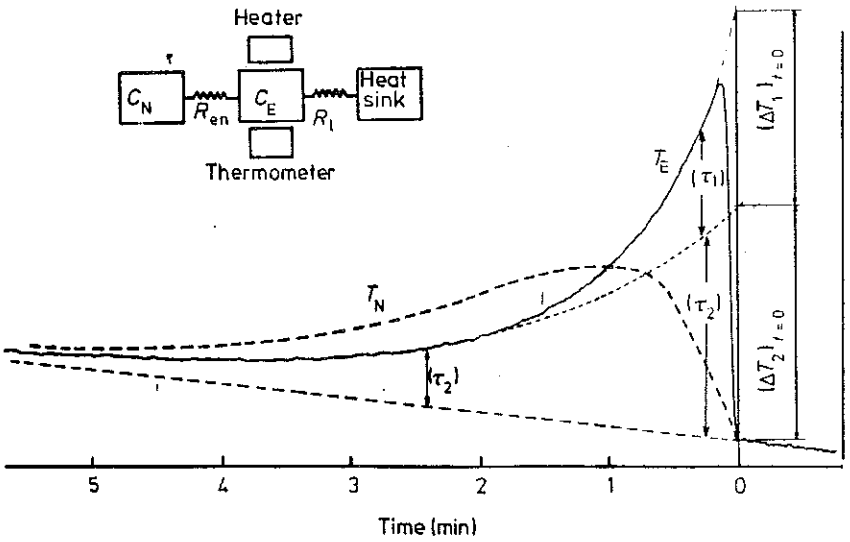

Figure 3. A typical temperature profile recording (T_E) showing the superposition of the two exponential decays of time constants τ_1 and τ_2 and the calculated variation of the temperature T_N of the nuclei. In this case, $\tau_1 = 31$ s, $\tau_2 = 100$ s, and the mean temperature is 90 mK. In the insert is drawn the thermal circuit where C_E represents the heat capacity of the electrons and excitations, and C_N that of the nuclei.

increases so much that the relaxation phenomenon can no longer be described by a well-defined time constant.

3.1.1. Linear specific heat. The numerical value of the linear term coefficient ($C_E = AT$) for the different samples is reported in table 1. It has been calculated by a least-squares method using the experimental results between 0·2 and 1 or 2 K, the temperature range corresponding to the only-one-time-constant regime. For the two amorphous samples the values are very close, although the quenching conditions are somewhat different. For the sample annealed near 400 °C, a decrease of the linear term of about 20% is observed, whereas further aging at 550 °C enhances this term to a value rather close to the amorphous value.

3.1.2. Hyperfine specific heat. The variation of the calculated specific heat C_N has been fitted by a T^{-2} law characteristic of the hyperfine contribution of the nuclei. The value of the coefficient B ($C_N = BT^{-2}$) is reported in table 1. Within the experimental dispersion of the data, it is impossible to evidence a noticeable variation of the T^{-2} term for all different phases of the alloys:

$$B = 3{\cdot}3 \pm 1 \text{ erg mol}^{-1} \text{ K}.$$

3.2. Comparison to previous results and analysis

The specific heat of alloys of the same composition has been measured above 2 K by two groups: the glassy phase and crystalline phases obtained by annealing at 400 °C, respectively for 16 min (Golding *et al* 1972) and 24 h (Chen and Haemmerle 1972). Their data were nearly the same, within a few per cent.

Comparison with our numerical values can only be made at 1·8–2 K, which is the low-temperature limit of the previous experiments: our values are 5–10% lower for the amorphous phase (sample II) and 25% lower for the 400 °C annealed sample.

From very similar experimental data, the two groups used very different analysis. On one hand, Chen and Haemmerle (1972) fit the data between 2 and 7 K by the expression

$$C = \gamma T + \beta T^3 + \alpha T^{-n}.$$

Their values of the coefficients γ and α are drastically different from ours; they deduced a γ value four times higher in the crystalline state than in the glass, with numerical values an order of magnitude lower than ours in the glass. The T^{-n} contribution is several orders of magnitude higher than in our results.

The analysis of Golding *et al* (1972) is in much better agreement with ours. They fit the data between 1·8 and 3·6 K by the law

$$C = aT + bT^3 + dT^5$$

with values of coefficient a respectively 1·21 mJ mol^{-1} K^{-2} for the glass and 1·27 mJ mol^{-1} K^{-2} for the crystal, which are not very far from our linear coefficient A but larger for the crystal than for the glass. It is difficult to compare the T^3 coefficient, since we observe only a slight deviation from the T law between 1 and 2 K which is difficult to analyse in such a limited temperature range.

3.3. Discussion

A first point concerns the *linear T term*. In the amorphous phase, in addition to the usual free electron specific heat, we expected a contribution of the excitations characteristic of this state leading to a term varying more or less as T, as observed in vitreous insulators. A contribution of this type has been evidenced in the heat conductivity of the same alloy by Matey and Anderson (1977) after subtracting the electronic contribution. Indeed in our case, the linear term is always larger in the vitreous state than in the crystalline one and one may attribute this difference to the amorphous structure. However, this difference is not very large, mainly that between the vitreous phase and the B phase of alloy 2 (sample IV), which reduces only to a few per cent. But this is not in disagreement with the magnitude of the effect already measured in insulators; in the case of SiO_2 for example, the contribution characteristic of the vitreous state may be, to a rough first approximation, described by a linear term of about 0·05 mJ mol^{-1} K^{-2} (Lasjaunias *et al* 1975) and this value is the typical magnitude for many systems (Stephens 1976). The difference observed here is of the same order of magnitude. A more precise estimation of such a contribution in the amorphous phase is not yet possible because the electronic density of states depends too much on the bandstructure, as proved by the variation of the A coefficient between the two crystalline phases, and must be evaluated by other experimental investigations.

The low relative amplitude of the effect is supported by recent sound velocity measurements performed on the same samples (Bellessa and Béthoux 1977). The value of the product $n_0 P^2$ (the two-level system density of states times the square of their coupling constant to the phonons) deduced from these experiments is an order of magnitude smaller than that in amorphous insulators. This is also the case of NiP, another non-magnetic amorphous metal (Bellessa *et al* 1977).

Susceptibility measurements had been planned on the same samples, but they would have lead to the same impossibility of separating a small Pauli susceptibility variation from the diamagnetic one (Bagley and Di Salvo 1973).

3.3.1. Nuclear specific heat. The low-temperature T^{-2} term may be attributed to the quadrupolar coupling between the Pd quadrupolar moment and the electric field gradients either created by the local noncubic symmetry or induced by the silicon and copper atoms, due to their charge difference with the palladium matrix. The proper contribution of silicon and copper is negligible since silicon, having a spin $\frac{1}{2}$, has no quadrupolar coupling and copper has a low concentration and a small quadrupolar moment compared to that of palladium.

This nuclear term is given by

$$\frac{C_N T^2}{R} = \frac{1}{80} \frac{e^4 q^2 Q^2}{k^2} \frac{(I+1)(2I+3)}{I(2I-1)}$$

where Q is the quadrupolar moment of Pd, estimated to about 4 barn (Narath *et al* 1966), $I = \frac{5}{2}$ its nuclear spin. The mean value of the electric field gradient deduced from this formula, $q \simeq 4 \times 10^{23}\,\mathrm{cm}^{-3}$, corresponds to a splitting $\Delta_0 = 3e^2qQ/[2I(2I-1)]$ of 0·4 mK. It is smaller than that induced on Au by surrounding non-magnetic 3d impurities (Thoulouze 1968). But comparatively, it is one order of magnitude larger than the nuclear hyperfine term induced on Pd by magnetic impurities of iron, of a concentration of 30 PPM.

We can make the comparison with the values obtained by recent Mössbauer experiments on amorphous $Pd_{99.7-x}Si_xFe_{0.3}$ (Ino *et al* 1978). In this case, the electric field gradient is that one experienced by the ^{57}Fe nuclei. For the Si concentration $x = 17{\cdot}5$ at%, which is the closest to our samples, the quadrupolar splitting ϵ is about $0{\cdot}45\,\mathrm{mm\,s}^{-1}$ at 77 K. For ^{57}Fe nuclei, this corresponds to $\Delta_0 = 0{\cdot}25$ mK. With a quadrupolar moment of about 0·20 barn and $I = \frac{3}{2}$ in the excited state, using the same above formula for Δ_0, this gives an electric field gradient at the Fe site of $1{\cdot}5 \times 10^{24}\,\mathrm{cm}^{-3}$.

The electric field gradient is mainly due to the first- and second-nearest neighbours so that the quadrupolar term is sensitive to the local structure. Owing to the very large dispersion of the experimental values, it is impossible to deduce any systematic variation. However, there appears to be no large local difference between the A structure, the almost FCC structure of Pd, and the B structure which we have not identified. But it means also that there is no important change in the local arrangement of atoms within a short distance around the Pd atoms between the amorphous and crystalline phases. This behaviour is analogous to that of glassy insulators in which the long-range order disappears when going from the crystalline to the amorphous state, while the short-range order stays almost unchanged.

This conclusion is also supported by the Mössbauer experiments of Ino *et al* (1978). For silicon concentration varying between 15 and 20 at% (amorphous alloys) and for 25 at% (crystalline Pd_3Si), the quadrupole splitting varies almost linearly from the amorphous alloys to Pd_3Si; the local field gradient is not sensitive to the phase, amorphous or crystalline, but depends mainly on the silicon concentration. However, the difference to our results is that their reference crystalline phase is Pd_3Si, whereas we have never obtained this structure in our crystalline samples.

4. Conclusion

Our present specific heat measurements have evidenced between 0·2 and 1 K linear T terms in both vitreous and crystalline phases. This term is larger in the vitreous state than when recrystallised but its large variations among the crystalline phases themselves prevent any precise evaluation of a contribution specific to the amorphous phase. However, its maximum value would be some per cent of the electronic term, of the same order of magnitude as that already observed in insulating glasses.

The hyperfine quadrupolar specific heat, almost invariable for the different phases, leads us to the conclusion that the local order remains also almost unchanged.

Preliminary electrical resistivity measurements have not shown any logarithmic temperature dependence which might be attributed to the vitreous state.

Anyway, the effect of the amorphous state on the very low-temperature specific heat is relatively small, especially when compared to the previous results above 2 K.

Acknowledgments

The authors would like to thank Dr O Bethoux for the sample preparation and stimulating discussions about the structure, B Picot for his expert technical assistance, Drs O Laborde and P Haen for the preliminary measurements of electrical resistivity, Professor H Ino of the University of Tokyo for communicating his results before publication and Professor F Gautier for fruitful discussions. We are also grateful to a referee who pointed out the analysis of the results for a precise determination of the nuclear term in these experiments.

Note added in proof. Recent measurements of Graebner *et al* (1977) show a linear contribution to the specific heat at about 0·1 K in the superconducting amorphous metal $Zr_{0.7}$–$Pd_{0.3}$. This term (about 0·10 mJ mol^{-1} K^{-2}) is of the same order of magnitude as in insulating glasses, leading the authors to the conclusion that the densities of disorder-induced excitations are rather similar in very different kinds of amorphous solids.

References

Azevedo L J, Clark W G, McLean E O and Hulin D 1979 to be published
Bagley B G and Disalvo F J 1973 *Amorphous Magnetism* ed H O Hooper and A M de Graaf (New York: Plenum)
Bellessa G and Béthoux O 1977 *Phys. Lett.* **62A** 125
Bellessa G, Doussineau P and Levelut A 1977 *J. Physique Lett.* **38** L65
Chen H S and Haemmerle W H 1972 *J. Non-Cryst. Solids* **11** 161
Chen H S and Park B K 1973 *Acta Metall.* **21** 395
Chen H S and Turnbull D 1969 *Acta Metall.* **17** 1021
Duwez P 1967 *Trans. Am. Soc. Metals.* **60** 625
——1976 *Ann. Rev. Mater. Sci.* **6** 97–104
Duwez P, Willens R H and Crewdson R C 1962 *J. Appl. Phys.* **36** 2267
Frossati G, Imbert D, Peccoud L, Thoulouze D and Waksmann B 1975 *Proc. Conf. LT 14, Helsinki*
Golding B, Bagley B G and Hsu F S L 1972 *Phys. Rev. Lett.* **29** 68
Graebner J E, Golding B, Schutz R J, Hsu F S L and Chen H S 1977 *Phys. Rev. Lett.* **39** 1480
Hasegawa R and Tsuei C C 1970 *Phys. Rev.* **B2** 1631

Ino H, Nanao S and Muto T 1978 to be published
Lasjaunias J C, Picot V, Ravex A, Thoulouze D and Vandorpe M 1977 *Cryogenics* **17** 111
Lasjaunias J C, Ravex A, Vandorpe M and Hunklinger S 1975 *Solid St. Commun.* **17** 1045
Masumoto T and Maddin R 1971 *Acta Metall.* **19** 725
——1975 *Mater. Sci. Engng* **19** 1
Matey J R and Anderson A C 1977 *J. Non-Cryst. Solids* **23** 129
Narath A, Fromhold A T and Jones E D 1966 *Phys. Rev.* **144** 428
Stephens R B 1976 *Phys. Rev.* **B13** 852
Thoulouze D 1968 *Thesis* University of Grenoble

A N N E X E B

CHALEUR SPECIFIQUE DE L'ALLIAGE LaZn AMORPHE ET CRISTALLISE - PROPRIETES SUPRACONDUCTRICES - RELAXATION D'ENERGIE

Alors qu'il s'avérait impossible de montrer clairement par mesure de chaleur spécifique l'existence d'états tunnels liés au désordre structural dans le verre métallique PdCuSi (Annexe A), de nombreux comportements typiques de l'état désordonné étaient par ailleurs observés dans le même système : variation logarithmique de la vitesse du son (Bellessa and Béthoux, 1977) et saturation de l'absorption ultrasonore (Doussineau et al., 1978). Quasi simultanément un excès de chaleur spécifique aussitôt attribué à l'existence de TLS est mis en évidence dans le supraconducteur amorphe ZrPd (Graebner et al., 1977), sans que d'autres origines, telles que contribution nucléaire (mise en évidence sur PdCuSi) ou précipitation d'une phase cristalline normale (Pd en l'occurrence), ne soient envisagées.

Aussi avons-nous entrepris l'étude d'un alliage à base de deux éléments supraconducteurs (La et Zn) dont les phases cristallines stables sont supraconductrices, et en étendant la gamme des mesures au-dessous de 0,1 K pour vérifier l'existence éventuelle de contributions nucléaires.

La préparation de l'échantillon (pulvérisation cathodique), sa caractérisation (rayons X, analyse thermique différentielle, densité) et la technique de mesure sont identique à celles exposées en détail dans ce mémoire (chapitre I) pour les alliages de Zirconium. Mentionnons simplement que deux échantillons ont été préparés correspondant respectivement à des puretés de Lanthane 3N (échantillon 1) et 4N (échantillon 2). La composition $La_{.78}Zn_{.22}$ contrôlée par analyse chimique, correspondant à un eutectique, a été choisie car stable à température ambiante, de T_c élevé ($\sim$ 4,2 K) de sorte que la contribution électronique supraconductrice à la chaleur spécifique devient rapidement négligeable au-dessous de 1 K.

Les résultats expérimentaux obtenus entre 60 mK et 6 K sont rapportés en figures 1 (échantillon 1 à l'état amorphe) et 2 (échantillon 2 à l'état amorphe puis recristallisé). Les courbes font apparaître pour les deux échantillons et dans les deux états ordonné ou désordonné une transition supraconductrice. Les propriétés électroniques et

supraconductrices, leur évolution au cours de la cristallisation, ainsi que la caractérisation structurale de la phase cristallisée sont analysées dans une publication jointe en fin de cette annexe (Béthoux et al., 1980).

Chaleur spécifique à basse température :

Au-dessous d'environ 0,5 K, les contributions des phonons (C_{ph}) et des électrons supraconducteurs (C_{es}) deviennent négligeables et l'on s'attend donc à observer les TLS. En fait au-dessous de 0,2 K on observe une importante chaleur spécifique résiduelle qui dépend peu et de la pureté du Lanthane et de la phase de l'alliage (plutôt plus forte même dans l'état cristallin). Par contre une différence très nette apparaît au niveau de la cinétique du retour à la température d'équilibre après le pulse de chaleur. Alors que dans la phase cristallisée le régime de décroissance est assez bien défini par une seule exponentielle, dans la phase amorphe existent deux régimes successifs caractérisés par deux constantes de temps très différentes. La plus courte (10-40 secondes) fournit la valeur de chaleur spécifique la plus faible alors que la plus longue (30-200 secondes) donne lieu à une contribution variant grossièrement en T^{-2}. Cette dernière, peu sensible à la pureté du Lanthane, peut donc être attribuée à un couplage quadrupolaire hyperfin des spins nucléaires de la matrice de Lanthane, plutôt qu'à des effets magnétiques. L'apparition d'une telle contribution exclusivement dans la phase amorphe a été observée par la suite systématiquement dans les alliages à base de Zirconium et interprétée comme la manifestation d'une interaction TLS - spins nucléaires (Lasjaunias and Ravex, 1983).

Pour l'échantillon 1 (fig. 1), attribuer le régime à constante de temps rapide qui apparaît dans une large gamme de température (entre 0,1 K et 0,7 K) à l'existence d'excitations du type TLS conduit à un bon accord entre les valeurs numériques tirées du premier régime transitoire (points noirs sur la figure 1) ou bien obtenues par différence entre la chaleur spécifique totale, correspondant à la constante de temps longue, et les différentes autres contributions (réseau, nucléaire et électronique supra) (cercles sur la figure 1). Une telle analyse conduit à une contribution des TLS : $C_{TLS} \simeq 40\ T^{0,5}$ erg/gK.

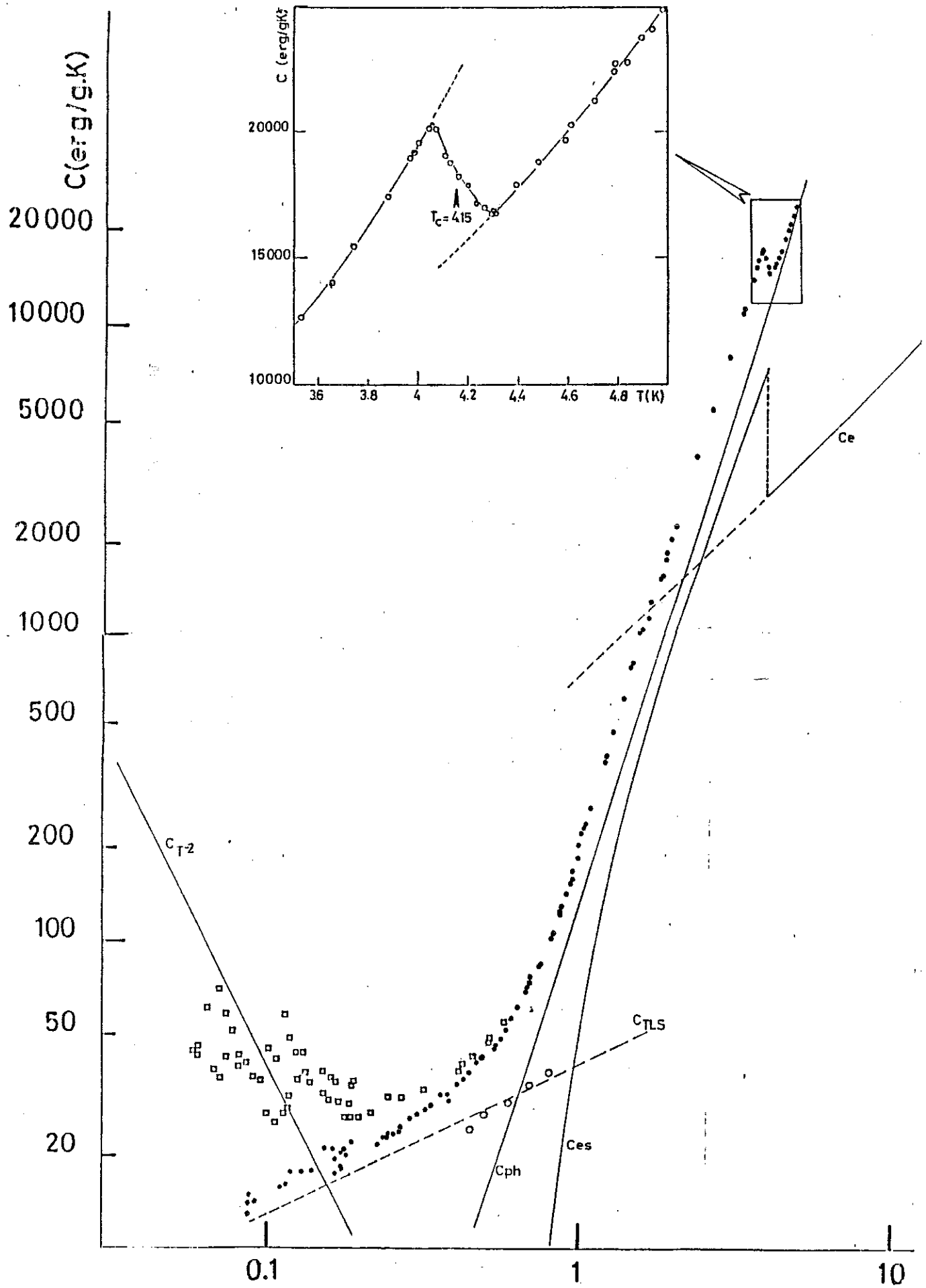

Fig.1 La Zn echantillon n°1

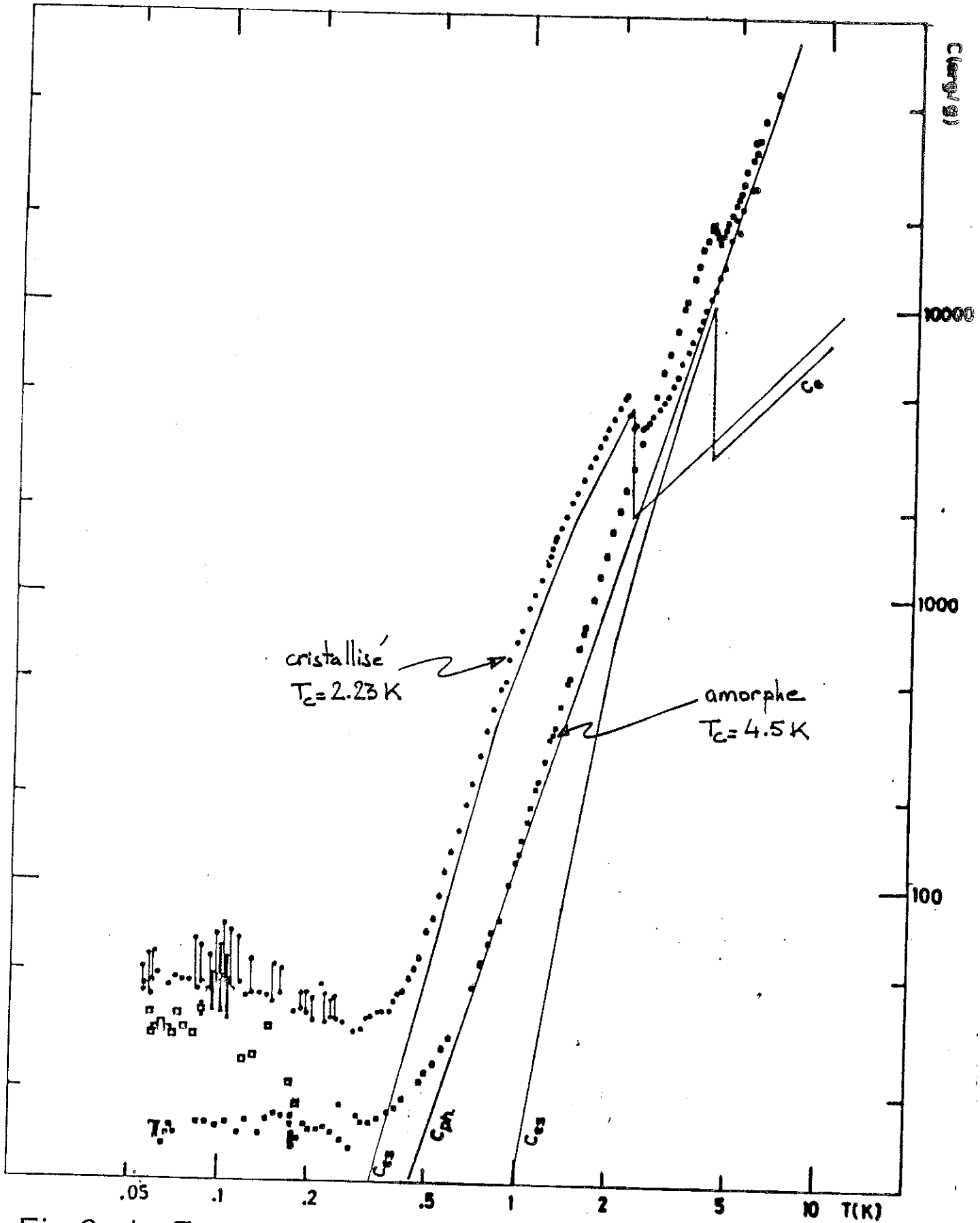

Fig.2 LaZn echantillon n° 2

Pour l'échantillon 2, il est difficile d'identifier un tel terme linéaire, ou presque, caractéristique des TLS. En effet la chaleur spécifique associée à la constante de temps courte dans l'état amorphe, quasiment indépendante de la température, apparaît très semblable à celle observée dans l'état recristallisé. Plusieurs origines magnétiques peuvent être invoquées : apparition d'ordre magnétique des spins des impuretés de terres rares, effet Kondo,...

Dans ces conditions, il est difficile d'affirmer en l'absence de référence à l'état cristallisé que l'excès de chaleur spécifique observé dans le cas de l'échantillon 1 est en toute certitude une manifestation des TLS. Cet ensemble de mesures montre toutefois combien il peut être hasardeux d'extraire une contribution intrinsèque des TLS sans référence à un état cristallisé et sur une gamme de température restreinte qui peut n'être qu'une transition entre un régime haute (supraconductivité, phonons) et basse (spins nucléaires) température.

Propriétés électroniques et supraconductrices :

Si les résultats expérimentaux obtenus au-dessous de 0,5 K n'ont pas permis de conclure avec certitude quant à la présence des TLS, l'analyse des données haute température permet d'établir les propriétés électroniques et supraconductrices de l'alliage et d'étudier leur évolution au cours de la cristallisation. Cette analyse, étayée par des mesures de résistivité électrique et de champ critique (H_{c_2}) est présentée dans la publication suivante.

En complément des résultats énoncés dans la publication, nous rapportons en figure 3 l'écart à une loi parabolique de la variation avec la température du champ critique thermodynamique. Le champ critique thermodynamique

$$H_c(T) = \left[\frac{8\pi}{V_M} \int_T^{T'} dT' \int_{T'}^{T_c} \frac{C_{es}(T'') - \gamma T''}{T''} dT''\right]^{1/2}$$

est calculé à partir de la courbe $C_p(T)$ expérimentale puis normalisé à sa valeur $H_c(0)$ (voir table I de la publication précédente). L'écart à la loi parabolique pour l'échantillon cristallisé est comparable aux écarts observés pour le Lanthane pur cristallisé dans ses phases hcp et fcc (Johnson and Finnemore, 1967) ainsi qu'à celui du modèle BCS, confirmant un couplage faible. Par contre l'écart à la loi parabolique dans le cas de l'échantillon amorphe est de signe opposé, caractéristique des matériaux supraconducteurs à couplage fort (Pb par exemple).

JOURNAL DE PHYSIQUE

Colloque C8, supplément au n°8, Tome 41, août 1980, page C8-754

SUPERCONDUCTIVITY OF A La-Zn 22 AT % AMORPHOUS ALLOY

O. Bethoux, O. Laborde, J.C. Lasjaunias and A. Ravex

Centre de Recherches sur les Très Basses Températures, C.N.R.S., B.P. 166 X, 38042 Grenoble Cédex, France.

ABSTRACT - We report here the main results of superconductivity measurements on a La-Zn 22 at % alloy, in amorphous and crystalline (hexagonal metastable phase) forms. The experimental details and a complete discussion of these results will be published elsewhere. The superconducting and relevant electronic properties have been extracted from specific heat, upper critical field and electrical resistivity measurements. The difference in the superconducting behaviour between the amorphous and crystalline states is compared to theoretical predictions. In conjunction with other results those presented here throw light on the problem of the electron-phonon coupling strength in amorphous transition metals alloys.

I. PREPARATION OF THE SAMPLES. The amorphous samples are obtained in the form of thick films (thickness about 100 µm) by high rate sputtering of a bulk pre-alloyed target at the eutectic composition (23 at % Zn). Condensation occurs on a substrate held at liquid nitrogen temperature. The sample weight is about 4 g and the chemical composition is 21.8 at % Zn. The X-ray diffraction spectrum is shown in fig. 1a. The single broad peak is located at $2\theta_m = 30.9°$. The nearest-neighbour distance (nnd) calculated by the Debye formula /1/ is 3.56 Å. The crystallisation of the amorphous alloy has been studied as a function of temperature and time. For the superconductivity studies, the sample was subjected to a thermal treatment of 2 minutes at 90°C followed by 2 minutes at 180°C. This treatment lead to a single hexagonal metastable phase with a = 6.48 Å and c/a = 0.593. The corresponding X-ray diffraction spectrum is shown in fig. 1b. A consideration of the number of atoms in a unit cell of this phase and the atomic volumes of La and Zn, indicates that there is no long-range order for the Zn atoms. The chemical disorder therefore must be of the same type in the amorphous and crystallised samples. Subsequently we shall designate this crystalline sample by hex-LaZn.

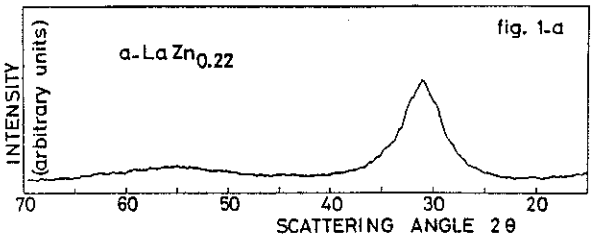

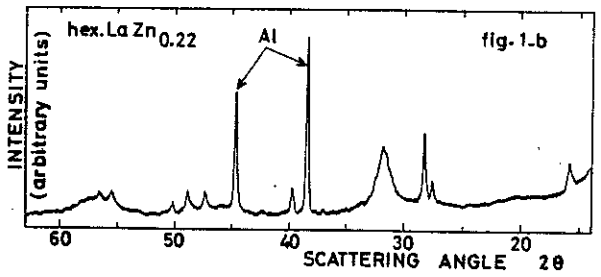

II. RESULTS OF THE LOW TEMPERATURE MEASUREMENTS. The specific heat has been measured from 0.06 K to 6.5 K for a-La-Zn and hex-La-Zn. Experimental details, the Cp(T) curves and a discussion of the very low temperature part of the Cp(T) curves are given in a separate paper /2/. The superconducting parameters and relevant quantities extracted from the Cp(T) data are summarized in table I. The symbols used here have the conventionnal meaning and the values have been obtained by the usual methods /3/. The superconducting electronic specific heat C_{es}, obtained

Table I

Alloy	T_c K	θ_D K	γ mJ / mole K^2	$H'_c(T_c)$* kOe K^{-1}	$H_c(0)$ kOe	$\Delta C/\gamma T_c$ $(T=T_c)$	$\Delta_o/k_B T_c$
a-$LaZn_{0.22}$	4,15	96	7,9	0.36	0.63	2.60	2.10
hex-$LaZn_{0.22}$	2,23	110	10,2	0.30	0.38	1.40	1.54
BCS theory						1.43	1.76

(*) $H'_c(T_c) = |dH_c/dT|_{T=T_c}$.

by subtracting the "lattice" T^3-term from the total specific heat Cps(T) below T_c, is plotted in fig. 2.

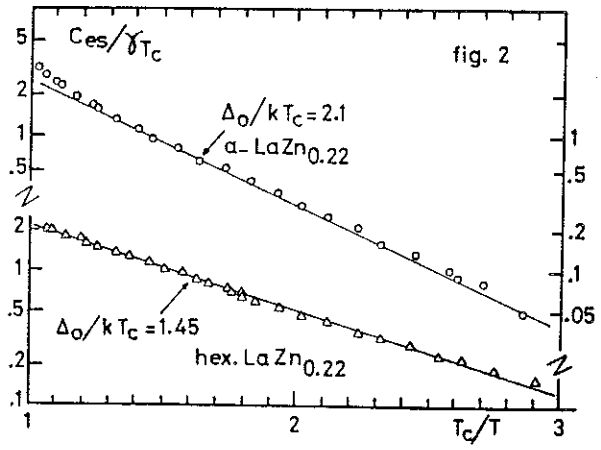

The electrical resistivity has been measured between T_c and 300 K by a 4-probes ac technique. The upper critical field H_{c_2} measurements have been carried out by the same method as the resistivity with a transverse magnetic field supplied by a superconducting magnet. For a-LaZn and hex-La Zn the measurements have been performed in liquid helium between 1.7 K and T_c. For a-LaZn, a second sample (with a slightly different T_c) has been measured down to 0.135 K in an adiabatic demagnetization apparatus. The experimental results are shown in fig. 3 and the reduced thermal variations of H_{c_2} for the two a-LaZn samples are plotted on fig. 4. Table II summarizes the low temperature electronic transport and electromagnetic properties. In this table we have also reported the theoretical value of $H'_{c_2}(T_c)$ calculated from the BCS-Gorkov theory /4/.

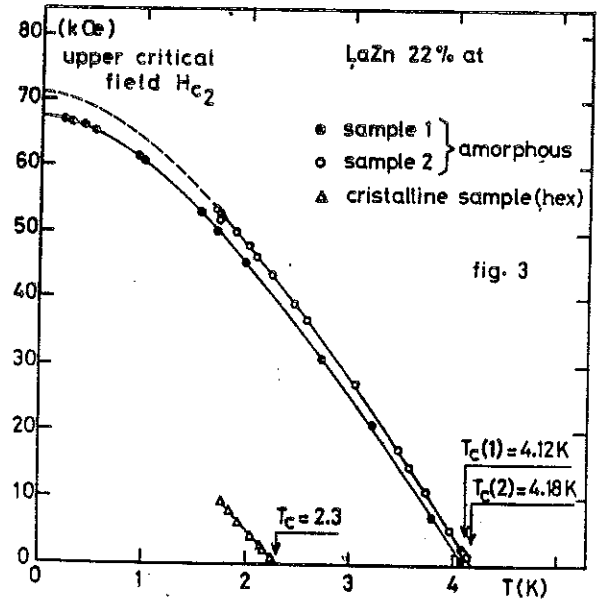

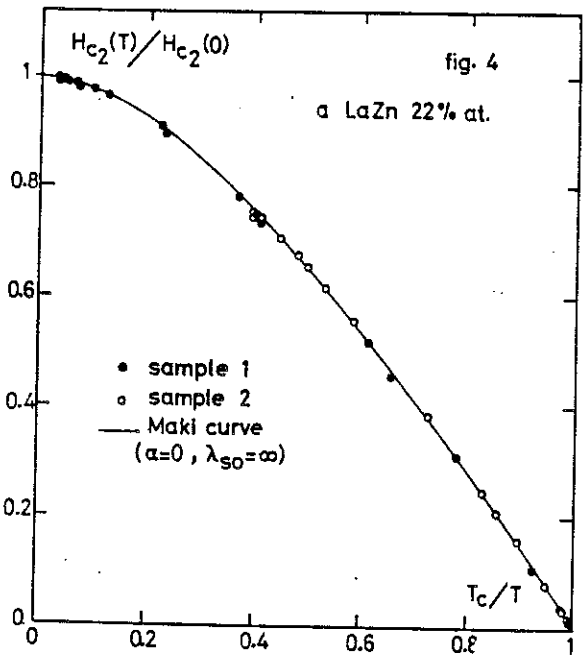

Table II

Alloy	$\rho(T_c)$ μΩ-cm	$H'_{c_2}(T_c)$ kOe K^{-1}	$H_{c_2}(0)$ kOe	$H'_{c_2}(T_c)_{BCS}$ kOe K^{-1}
a-$LaZn_{0.22}$	150	26.0	71.0	26.1
hex-$LaZn_{0.22}$	135	16.5	—	29.9

(*) $H'_{c_2}(T_c) = |dH_{c_2}/dT|_{T=T_c}$.

III. DISCUSSION. Electron-phonon coupling and T_c

From the values of $\Delta C/\gamma T_c$ and $\Delta_o/k_B T_c$ (table I) compared to the BCS values, its appears that a-LaZn is a strong coupling superconductor and hex-LaZn, a weak one. If we assume (see § I) that the chemical order is about the same for the amorphous and crystalline phases, the main difference between the two phases lies in the topological order. We can therefore conclude that topological disorder alone increases the electron-phonon coupling. This experimental fact is in agreement with the theoretical predictions of Bergmann /5/ that the lack of translational invariance in amorphous metals provides an additional phase space for electron-phonon coupling. We can see also from the table I that θ_D and N(O) (or γ) increase from the amorphous to the crystalline phases ; we can therefore associate the observed decrease of T_c with the decrease of the coupling. Such a decrease of T_c during the early stages of crystallisation, has already been observed in Zr-Rh /6/ and Zr-Pd/7/ alloys.

Upper critical field H_{c2}. It can be seen from table II that the experimental value of $H'_{c2}(T_c)$ for a-LaZn, agrees remarkably well with the theoretical value $H'_{c2}(T_c)_{BCS}$ calculated from the BCS-Gorkov theory of weak-coupling superconductors. Such a result has already been obtained 1°) by Rainer and Bergmann /8/ for amorphous s-p metals who explained it by the characteristic shape of the Eliashberg function $\alpha^2F(\omega)$ at low frequencies, peculiar to strong-coupling amorphous metals 2°) by Shull et al /9/ for amorphous alloys $LaGa_{0.20}$ and $LaGa_{0.22}$, which are intermediate coupled superconductors with d-electrons. On the contrary, $H'_{c2}(T_c)$ for hex-LaZn is different from the BCS value in spite of its weak coupling character. It is possible, for this badly crystallized sample with very small crystallites, that the measured $\rho(T_c)$ does not represent the "intra-crystal" resistivity which can be much smaller. Finally, fig. 4 shows, for a-LaZn, that $H_{c2}(T)$ follows the theoretical thermal variation predicted by Maki(4) with $\alpha = 0$ and $\lambda_{so} = \infty$. This agreement is perhaps fortuitous because in this alloy α is different from zero and λ_{so} is unknown. This thermal behaviour is different from that found for others amorphous alloys /8.10.11.12/ where $H_{c2}(T)$ decreases faster than the Maki law.

Comparison with other amorphous alloys of transition metals. In table III we show some published results on amorphous alloys where Cp(T), $\rho_o = \rho(T_c)$ and $H_{c2}(T)$ have been simultaneously measured. It can be seen from this table that the electron-phonon coupling (expressed by $\Delta C/\gamma T_c$) increases from one alloy to an other when $\rho(T_c)$ decreases. This behaviour is in qualitative agreement with a theory recently established by Meisel and Cote /13/ to calculate the decrease of T_c with increasing ρ_o, as observed in highly resistive crystalline alloys (Nb and A15). When the electronic mean free path, ℓ, is small enough, the electron-phonon coupling decreases with ℓ. This results from the Zimann-Pippard condition for the electron-phonon diffusion ($2\pi/q_{ph} < \ell$) which introduces a ℓ^{-1} low-frequency cut-off in the Eliashberg function $\alpha^2F(\omega)$ and causes a decrease of the coupling strength. If we assume that the variations of $\rho(T_c)$ reflect the variations of ℓ for the alloys of table III (N(O) varies only a little) and that $\alpha^2F(\omega)$ is about the same, then the

Table III

Alloy	T_c K	θ_D K	N(O) states / erg cm^3 spin	$\Delta C/\gamma T_c$ ($T=T_c$)	$\rho(T_c)$ μΩ-cm	$H'_{c2}(T_c)$ kOe K^{-1}	Ref.
a-$LaZn_{0.22}$	4.15	96	$3.1\ 10^{34}$	2.60	150	26.0	—
a-$LaGa_{0.22}$	3.64	109	$2.2\ 10^{34}$	1.96	200	22.5	(9)
a-$LaAu_{0.24}$	3.28	99	$(3.1\ 10^{34})$*	1.7	227	24.0	(10-15)
a-$ZrPd_{0.31}$	2.53	180	$3.0\ 10^{34}$	1.61	246	26.5	(7-15)

(*) Calculated with an estimated density.

electron-phonon coupling will decrease with increasing $\rho(T_c)$. More generally this model could qualitatively explain why some other amorphous alloys of transition metals have been found to be weak-coupling superconductors /14/. Likewise, such an inverse relation between the coupling strength and $\rho(T_c)$, associated with small variations of N(0), could explain the relative constancy of $H'_{c2}(T_c)$ observed in table III and for some fifteen other amorphous transition alloys /12.15/.

IV. CONCLUSION. A-$LaZn_{0.22}$ is a strong-coupling superconductor. After crystallisation into a metastable hexagonal phase the alloy becomes a weak coupled superconductor with a reduction of T_c by a factor of about 2 (amorphous T_c = 4.15 K, crystallised T_c = 2.23 K). The increase of coupling with topological disorder, theoretically predicted by Bergmann, is verified for this d-alloy. The experimental $|dH_{c2}/dT|_{T=T_c}$ value is in agreement with the value calculated by the BCS-Gorkov theory of weak coupled superconductors, such as found by Bergmann for strong coupled amorphous s-p superconductors. The present results on a-LaZn, together with those obtained with other amorphous La-based alloys and a-PdZr alloy, indicate an inverse relation between the residual resistivity and the coupling strength. Such a relation, theoretically introduced by Meisel and Cote using the Zimann-Pippard condition for electron-phonon diffusion, could qualitatively explain the spread of results concerning the coupling strength in d-amorphous alloys and the relative constancy of $|dH_{c2}/dT|_{T=Tc}$ observed in numerous d-amorphous alloys. Other experimental results on different d-amorphous alloys and more precise theoretical calculations will be necessary to confirm this trend.

REFERENCES

/1/ A. GUINIER "X-ray diffraction", Freeman and Co, (1963).

/2/ J.C. LASJAUNIAS and A. RAVEX, Proceedings of LAM4, Grenoble (1980).

/3/ R.D. PARKS "Superconductivity" Dekker, New York (1969)

/4/ D. St JAMES, S. SARMA and E.J. THOMAS "Type II superconductivity" Pergamon (1969).

/5/ G. BERGMANN, Phys. Rep. 27 C, 4, (1976), 159-185.

/6/ A.J. DREHMAN and W.L. JOHNSON, Phys. Stat. Sol. (a), 52, 499 (1979)

/7/ J.E. GRAEBNER, B. GOLDING, R.J. SCHUTZ, F.S. HSU and H.S. CHEN, Phys. Rev. Lett. 39, 1480 (1977)

/8/ D. RAINER and G. BERGMANN, J. of Low Temp. Phys. 14, 501 (1974).

/9/ W.H. SHULL, D.G. NAUGLE, S.J. POON and W.L. JOHNSON, Phys. Rev. B, 18, 3263 (1978).

/10/ W.L. JOHNSON, S.J. POON and P. DUVEZ, Phys. Rev. B, 11, 150 (1975).

/11/ W.L. JOHNSON, S.J. POON, J. DURAND and P. DUVEZ, Phys. Rev. B, 18, 206 (1978).

/12/ K. AGYEMAN, R. MULLER and C.C. TSUEI, Phys. Rev. B 19, 193 (1979).

/13/ L.V. MEISEL and P.J. COTE, Phys. Rev. B, 19, 4514 (1979).

/14/ C.C. TSUEI, W.L. JOHNSON, R.B. LAIBOWITZ and J.M. VIGGIANO, Sol. St. Com. 24, 615 (1977).

/15/ P. DUWEZ and W.L. JOHNSON, J. of less com. met. 62, 215 (1978).

/16/ W.H. SHULL and D.G. NAUGLE, Phys. Rev. Lett., 39, 1580 (1977).

Fig.3 La Zn - ecart a la loi parabolique du champ critique thermodynamique

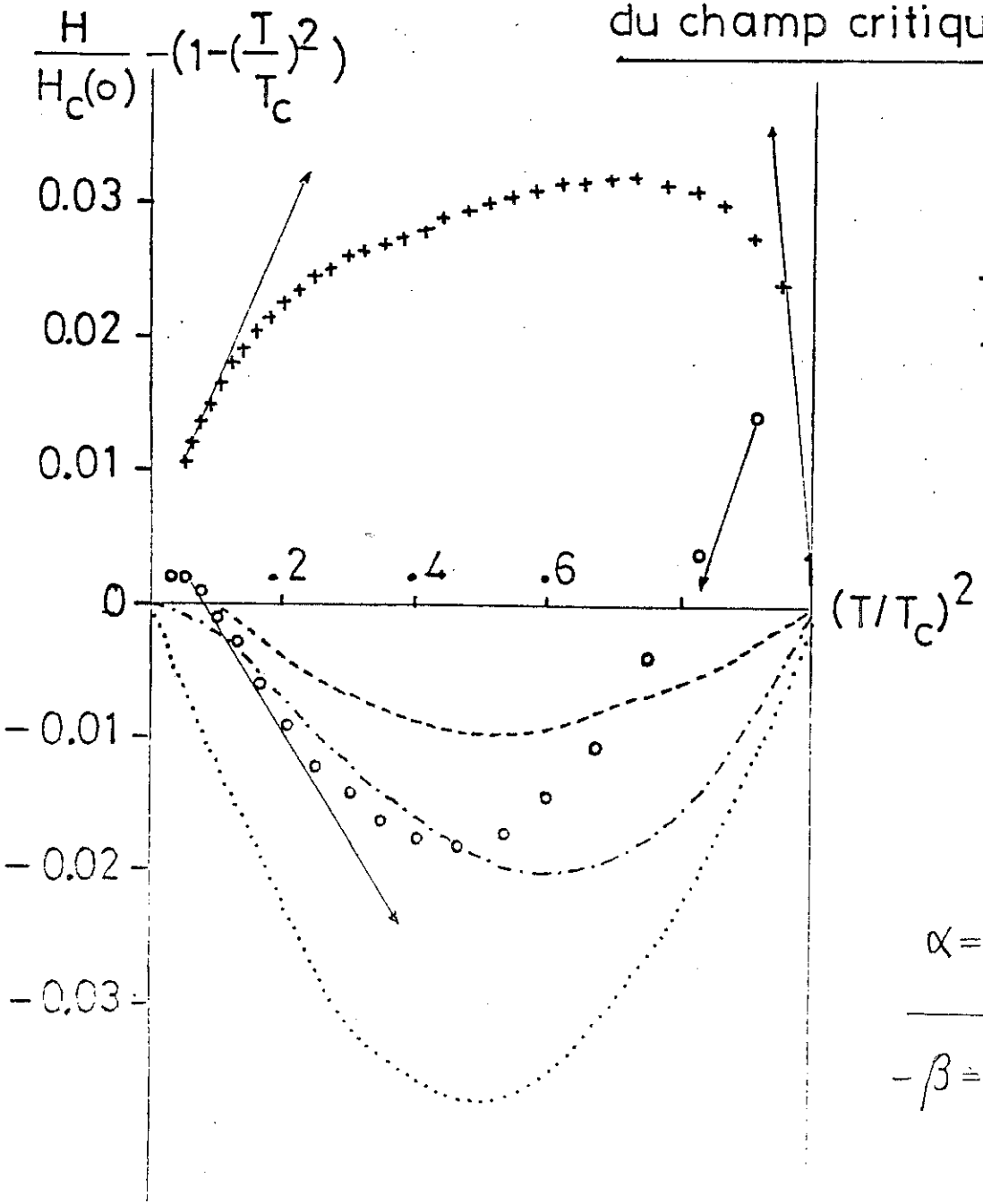

+ a: La Zn
∘ cr. La Zn
---- La hcp
-·-·- La fcc
····· BCS

	La Zn	
	a.m.	recr.
$\alpha = 1 - \frac{\gamma_M}{V_M} 2\pi \frac{T_c^2}{H_o^2}$	0.12	-0.47
$-\beta = 1 - \left(\frac{\Delta C_M}{V_M} \pi \frac{T_c}{H_o^2}\right)^{1/2}$	-0.08	0.19

Relaxation d'énergie :

Au cours des expériences de chaleur spécifique sur les échantillons 1 et 2 à l'état amorphe est apparu un comportement inhabituel : un ralentissement brutal du refroidissement de l'échantillon aux alentours de 250 mK dû à une dissipation d'énergie au sein même de l'échantillon. Ce phénomène analysé dans la publication ci-jointe est attribué à la transformation ortho-para d'hydrogène moléculaire piégé dans l'échantillon amorphe.

Depuis l'observation et l'analyse de cette relaxation d'énergie, la mise en évidence par d'autres auteurs (Löhneysen et al., 1983 ; Graebner et al., 1983) d'un phénomène analogue dans le silicium amorphe aSi:H vient confirmer nos hypothèses. Les quantités d'hydrogène moléculaire mises en jeu (quelques dizièmes de pourcent atomique) sont d'ailleurs comparables dans les deux cas.

Journal of Low Temperature Physics, Vol. 48, Nos. 1/2, 1982

Heat Relaxation Phenomena at Low Temperature in Amorphous LaZn

A. Ravex and J. C. Lasjaunias

Centre de Recherches sur les Très Basses Températures, CNRS, Grenoble, France

(Received November 10, 1981)

An anomalous heat relaxation with a very long time constant (about 60 h) has been observed in amorphous $La_{0.78}Zn_{0.22}$. The total heat release is about 1.5 mJ per gram of sample. This phenomenon can be attributed to the ortho–para transformation of hydrogen trapped in the sample. This behavior disappears after crystallization.

In specific heat measurements on an amorphous superconducting $La_{0.78}Zn_{0.22}$ alloy[1] we have encountered difficulties in cooling which are due to a heat release from the sample. The amorphous samples are prepared by a sputtering technique[2] in the form of foils (100 μm in thickness), with about 2.7 g used for the specific heat experiment. The measurements are performed by a transient heat-pulse technique.[3] The sample and the addenda (thermometer and heater) are connected to the heat sink (the paramagnetic salt of an adiabatic demagnetization cryostat or the mixing chamber of a dilution refrigerator) through a heat link consisting of a copper wire 35 μm in diameter. Different lengths were used (10 or 20 cm). With the experimental value of the thermal resistance R of these links,[3] we can calculate the heat flow ($\dot{Q} = \Delta T/R$) by measuring the temperatures of the sample and the heat sink. With such an experimental arrangement in the demagnetization apparatus the samples generally reach a temperature of about 50 mK with the heat sink kept at about 15 mK, indicating parasitic heat leaks $\dot{Q}_0$ of the order of $(0.5\text{–}1) \times 10^{-9}$ W.

In a usual first experimental run, the cooling of an amorphous LaZn sample stopped at an anomalously high temperature (170 mK). The sample was then kept for one week at liquid helium temperature and a second demagnetization was performed: then the sample reached a temperature of 60 mK.

To avoid any artefact due to the sample, we repeated a series of cooling runs on a second sample as shown in Fig. 1. We first stored the sample for

0022-2291/82/0700-0159$03.00/0

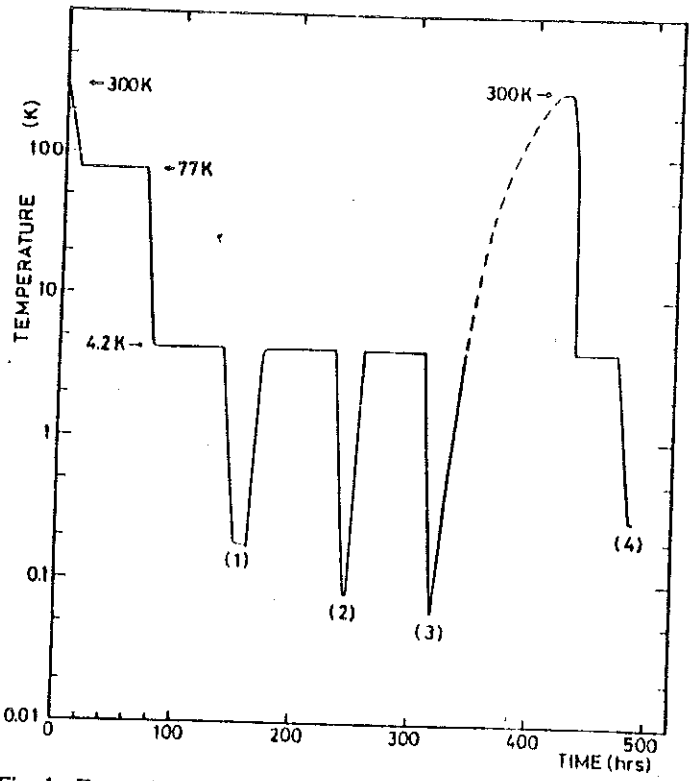

Fig. 1. Example of a thermal history for sample 2. The numbers correspond to the successive demagnetization cooling runs performed in the adiabatic demagnetization cryostat.

two days at nitrogen temperature, then performed three successive demagnetizations separated by storages of about 60 h each at liquid helium temperature. The limiting minimum temperature reached by the sample becomes lower after each run (180, 86, and 60 mK). After the third run, we warmed the sample to room temperature and then cooled it rapidly to 4.2 K using exchange gas without any intermediate storage at 77 K. In this procedure the sample reached a temperature of 280 mK.

To avoid any artefact due to the demagnetization apparatus, we repeated the measurements with the first sample in a dilution refrigerator. In a usual experimental run with a storage of a few hours at 77 and 4.2 K, the sample reaches a limiting temperature of 300 mK with the mixing chamber at 34 mK. Fifteen days later the sample reaches its equilibrium temperature (about 100 mK) compatible with a higher parasitic heat input in this apparatus ($\sim 3 \times 10^{-9}$ W).

In Fig. 2 we have plotted the heat flow $\dot{Q}_{\rm rel}$ released by the samples during these different experiments as a function of time. In the case of the demagnetization apparatus, $\dot{Q}_{\rm rel}$ is obtained from the temperature gradient

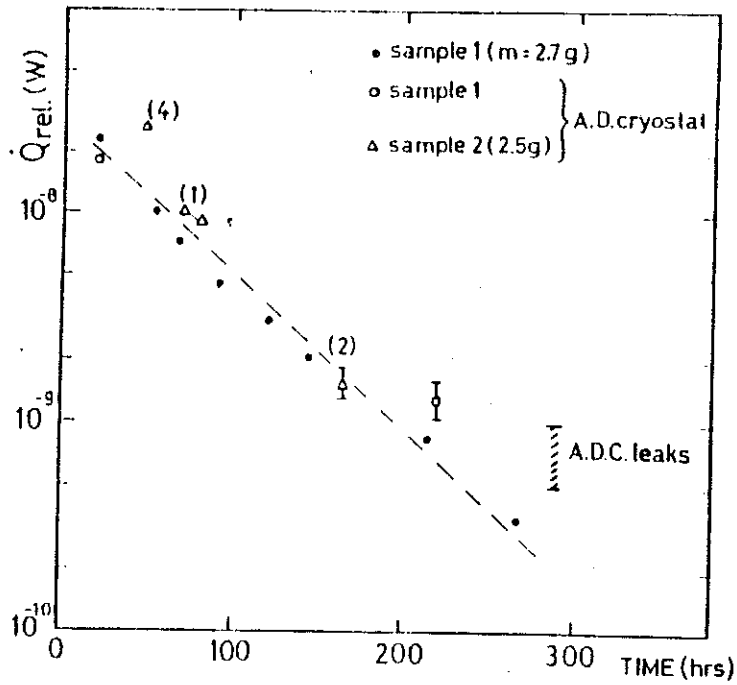

Fig. 2. Released power $\dot{Q}_{rel}$ as a function of time for different experiments on two different samples. The origin of time is taken as the time at which the sample reaches 4.2 K when it is cooled from higher temperatures. (●) Experiment with sample 1 in the dilution refrigerator. Other data correspond to experiments in the adiabatic demagnetization cryostat (ADC). (Δ) The power released at the end of the demagnetization cooling cycles 1, 2, and 4 as shown in Fig. 1. No estimate of $\dot{Q}_{rel}$ has been attempted for cycle 3 since $\dot{Q}_{rel}$ is less than the natural parasitic leaks ($0.5 \cdot \dot{Q}_0 \leq 1$ nW) as indicated by the dashed area. Error bars are due to this uncertainty in $\dot{Q}_0$.

$T_1 - T_0$ along the thermal link and from the parasitic heat input $\dot{Q}_0$:

$$\dot{Q}_{rel} + \dot{Q}_0 = \int_{T_0}^{T_1} \frac{dT}{R} \tag{1}$$

In the case of the dilution apparatus, we periodically warmed the sample to 250 mK with a measured heating power $\dot{Q}_h$ in order to get a constant temperature gradient along the thermal link. This method does not imply knowledge of the parasitic heat input $\dot{Q}_0$. Indeed at each time t the relation of thermal equilibrium is

$$\int_{T_0}^{T_1} \frac{dT}{R} = C^{ste} = \dot{Q}_0 + \dot{Q}_{rel}(t) + \dot{Q}_h(t)$$

Using this relation at the end of the relaxation process when $\dot{Q}_{rel}(\infty) \to 0$,

one obtains

$$\dot{Q}_{rel}(t) = \dot{Q}_h(\infty) - \dot{Q}_h(t) \tag{2}$$

From Fig. 2 we note that the released heat flow roughly obeys an exponential decay (dashed line) with a time constant $\tau_{rel} \approx 55$ h. Data from all different runs are in rather good agreement, except the higher value of point 4, which corresponds to the rapid cooling from room temperature without the usual storage for a minimum of 10 h at 77 K. Furthermore, this phenomenon is almost insensitive to the temperature at which we allow the relaxation to occur, either mainly 4.2 K in the demagnetization cryostat or mainly 200 mK in the dilution cryostat: this rules out any thermally activated process.

It is worth noting that the long time constant is comparable to those usually observed in the ortho to para transformation of molecular hydrogen.[4] This hypothesis can be checked by the dependence of the amount of energy released during the relaxation process with the initial concentration of ortho-hydrogen, since below 20 K the only stable phase is para-hydrogen, while equilibrium concentrations of ortho- and para-hydrogen are, respectively, 75–25 at 300 K and 50–50 at 77 K.[5]

In the experiment described in Fig. 1 the sample was either stored for 55 h at 77 K or rapidly cooled from room temperature: thus we have to verify that for these two runs the energies released are in the ratio of the ortho-hydrogen concentrations at nitrogen and room temperature, $75/50 = 1.5$. The energy released is $W = \int_0^\infty \dot{Q}_{rel}(t)\,dt$, with $\dot{Q}_{rel} = \dot{Q}_{rel}(0) \exp(-t/\tau_{rel})$. At the beginning of the relaxation process the sample temperature T_1 is much larger than the heat sink temperature T_0, and the parasitic heat input $\dot{Q}_0$ is negligible in comparison to $\dot{Q}_{rel}(0)$. Then from formula (1), with $R(T) \sim T^{-1}$, the ratio between the energies released during the two runs is equal to the ratio of the square of the temperatures achieved by the sample at the same time. Taking as the origin the time at which the sample reaches 4.2 K, from our experiments we obtain for this ratio a value of 1.65, which is rather close to the theoretically calculated value of 1.5.

In conclusion we think that this relaxational phenomenon can be explained by the ortho to para transformation of hydrogen.* Using the heat of transformation (330 J/mole of ortho-hydrogen) measured at 20 K,[6] and the estimated total heat released from our experiments (about 170 mJ/mole of sample), we get a rough estimate of the hydrogen content in our samples: about 0.1 at %. Others have mentioned[7] a Schottky anomaly near 1–2 K in the specific heat of copper containing hydrogen which

*The observation of this transformation is experimental evidence of the presence of molecular hydrogen trapped in the samples.

disappears by storage of the sample at about 20 K. In our case we do not observe any singularity of the specific heat in this range of temperature. Furthermore, the specific heat values at lowest temperature are unaffected by the heat relaxation within the experimental accuracy.

Moreover, we have observed that the relaxational phenomenon disappears after crystallizing the samples by thermal treatment (either 24 h at 250°C under vacuum or 2 h at 180°C). We think that hydrogen is either eliminated during the annealing or chemically bound to lanthanum in the form of hydrides.

In a recent study of amorphous zirconium alloys also obtained by the sputtering technique we did not observe any similar release of heat. This behavior is perhaps particular to this LaZn alloy due to the affinity of lanthanum for hydrogen.

ACKNOWLEDGMENTS

We are grateful to O. Béthoux, A. Lacaze, and D. Thoulouze for useful discussions.

REFERENCES

1. A. Ravex, J. C. Lasjaunias, and D. Thoulouze, *J. Phys.* (*Paris*) **41**, C8-749 (1980).
2. O. Béthoux, O. Laborde, J. C. Lasjaunias, and A. Ravex, *J. Phys.* (*Paris*) **41**, C8-754 (1980).
3. J. C. Lasjaunias, B. Picot, A. Ravex, D. Thoulouze, and M. Vandorpe, *Cryogenics* **17**, 111 (1977).
4. E. Crewer, *Z. Phys. Chem.* **28**, 199 (1935).
5. H. W. Woolley, R. B. Scott, and F. G. Brickwedde, *J. Res. NBS* **41** (1948).
6. F. Simon and G. V. Ebbe, *Z. Phys. Chem.* **6**, 79 (1929).
7. N. Waterhouse, *Can. J. Phys.* **47**, 1485 (1969).

- BELLESSA G. and BETHOUX O., Phys. Lett. 62A, 125 (1977).
- BETHOUX O., LABORDE O., LASJAUNIAS J.C., RAVEX A., Journal de Physique 41, C8-754 (1980).
- DOUSSINEAU P., LEGROS P., LEVELUT A., ROBIN A., J. Physique Lett. 39, L265 (1978).
- GRAEBNER J.E., GOLDING B., SCHUTZ R.J., HSU F.S.L., CHEN H.S., Phys. Rev. Lett. 39,1480 (1977).
- GRAEBNER J.E., GOLDING B., ALLEN L.C., BIEGELSEN D.K., STUTZMAN M., Phys. Rev. Lett. 52, 553 (1983).
- JOHNSON D.L. and FINNEMORE D.K., Phys. Rev. 158, 376 (1967).
- LASJAUNIAS J.C. and RAVEX A., J. Phys. F : Met. Phys. 13, L101 (1983).
- LÖHNEYSEN H., SCHINK H.J., BEYER W., Phys. Rev. Lett. 52, 549 (1983).

A N N E X E C

RESULTATS EXPERIMENTAUX DE LA SERIE ZrM - ANALYSE DES RESULTATS

echantillon: Zr.76 Ni .24 masse: 3.12 g

etat: brut (77K)

	T (mK)	ΔT/T(%)	mc(erg/K)	Cp(erg/gK)
1	+5.530E+01	+1.36E+01	+8.283E+00	+2.140E+00
2	+5.387E+01	+1.03E+01	+9.144E+00	+2.404E+00
3	+5.413E+01	+1.06E+01	+9.150E+00	+2.408E+00
4	+5.418E+01	+1.13E+01	+8.716E+00	+2.270E+00
5	+5.415E+01	+1.21E+01	+9.285E+00	+2.452E+00
6	+5.430E+01	+1.13E+01	+9.258E+00	+2.444E+00
7	+5.664E+01	+1.11E+01	+8.966E+00	+2.369E+00
8	+5.857E+01	+1.15E+01	+8.681E+00	+2.286E+00
9	+6.045E+01	+1.17E+01	+9.054E+00	+2.413E+00
10	+6.243E+01	+1.02E+01	+9.424E+00	+2.538E+00
11	+6.814E+01	+1.36E+01	+9.061E+00	+2.428E+00
12	+7.058E+01	+9.77E+00	+9.766E+00	+2.653E+00
13	+7.383E+01	+9.56E+00	+1.038E+01	+2.848E+00
14	+7.747E+01	+1.08E+01	+1.041E+01	+2.850E+00
15	+8.123E+01	+1.10E+01	+1.068E+01	+2.930E+00
16	+8.615E+01	+1.14E+01	+1.043E+01	+2.837E+00
17	+9.086E+01	+1.26E+01	+1.084E+01	+2.954E+00
18	+9.635E+01	+1.39E+01	+1.125E+01	+3.066E+00
19	+1.011E+02	+1.42E+01	+1.165E+01	+3.176E+00
20	+1.059E+02	+1.47E+01	+1.191E+01	+3.243E+00
21	+1.122E+02	+1.78E+01	+1.199E+01	+3.244E+00
22	+1.172E+02	+1.65E+01	+1.191E+01	+3.197E+00
23	+1.229E+02	+1.43E+01	+1.294E+01	+3.503E+00
24	+1.287E+02	+1.60E+01	+1.319E+01	+3.557E+00
25	+1.296E+02	+7.47E+00	+1.437E+01	+3.931E+00
26	+1.386E+02	+1.15E+01	+1.455E+01	+3.949E+00
27	+1.433E+02	+1.14E+01	+1.509E+01	+4.101E+00
28	+1.532E+02	+1.50E+01	+1.520E+01	+4.092E+00
29	+1.563E+02	+9.21E+00	+1.551E+01	+4.175E+00
30	+1.694E+02	+1.44E+01	+1.650E+01	+4.435E+00
31	+1.802E+02	+1.59E+01	+1.657E+01	+4.404E+00
32	+1.945E+02	+1.62E+01	+1.778E+01	+4.728E+00
33	+2.236E+02	+1.58E+01	+2.002E+01	+5.308E+00
34	+2.307E+02	+1.16E+01	+2.087E+01	+5.545E+00
35	+2.473E+02	+1.18E+01	+2.191E+01	+5.798E+00
36	+2.654E+02	+1.17E+01	+2.336E+01	+6.172E+00
37	+2.816E+02	+1.01E+01	+2.561E+01	+6.809E+00
38	+2.994E+02	+1.08E+01	+2.696E+01	+7.148E+00
39	+3.073E+02	+1.02E+01	+2.787E+01	+7.396E+00
40	+3.243E+02	+9.73E+00	+2.962E+01	+7.862E+00
41	+3.419E+02	+1.06E+01	+3.149E+01	+8.362E+00
42	+3.586E+02	+9.50E+00	+3.410E+01	+9.099E+00
43	+3.752E+02	+8.62E+00	+3.796E+01	+1.023E+01
44	+3.919E+02	+8.52E+00	+3.978E+01	+1.072E+01
45	+4.154E+02	+8.70E+00	+4.314E+01	+1.164E+01
46	+4.359E+02	+1.11E+01	+4.293E+01	+1.143E+01
47	+4.523E+02	+8.24E+00	+4.989E+01	+1.354E+01
48	+4.767E+02	+9.20E+00	+5.629E+01	+1.540E+01
49	+4.961E+02	+5.65E+00	+6.138E+01	+1.688E+01
50	+5.124E+02	+5.84E+00	+7.030E+01	+1.961E+01
51	+5.324E+02	+4.80E+00	+7.744E+01	+2.173E+01
52	+5.488E+02	+4.71E+00	+8.353E+01	+2.353E+01
53	+5.707E+02	+5.16E+00	+9.551E+01	+2.717E+01
54	+5.915E+02	+3.91E+00	+1.091E+02	+3.132E+01
55	+6.033E+02	+4.94E+00	+1.142E+02	+3.285E+01
56	+6.359E+02	+4.62E+00	+1.558E+02	+4.583E+01
57	+6.610E+02	+4.06E+00	+1.856E+02	+5.510E+01
58	+6.657E+02	+4.55E+00	+1.913E+02	+5.685E+01
59	+7.036E+02	+4.49E+00	+2.375E+02	+7.122E+01
60	+7.294E+02	+3.41E+00	+3.064E+02	+9.295E+01
61	+7.440E+02	+5.75E+00	+3.030E+02	+9.166E+01

62	+7.850E+02	+5.60E+00	+4.030E+02	+1.231E+02
63	+8.203E+02	+5.22E+00	+4.899E+02	+1.504E+02
64	+8.467E+02	+3.68E+00	+5.632E+02	+1.735E+02
65	+8.817E+02	+4.60E+00	+6.733E+02	+2.082E+02
66	+8.893E+02	+3.59E+00	+6.987E+02	+2.162E+02
67	+9.245E+02	+4.11E+00	+8.475E+02	+2.632E+02
68	+9.598E+02	+4.57E+00	+9.412E+02	+2.925E+02
69	+9.998E+02	+3.68E+00	+1.121E+03	+3.493E+02
70	+1.046E+03	+3.89E+00	+1.304E+03	+4.067E+02
71	+1.091E+03	+3.43E+00	+1.573E+03	+4.919E+02
72	+1.142E+03	+4.28E+00	+1.819E+03	+5.694E+02
73	+1.201E+03	+3.67E+00	+2.313E+03	+7.259E+02
74	+1.258E+03	+3.38E+00	+2.700E+03	+8.482E+02
75	+1.316E+03	+4.13E+00	+3.004E+03	+9.436E+02
76	+1.382E+03	+4.02E+00	+3.619E+03	+1.138E+03
77	+1.448E+03	+3.46E+00	+4.146E+03	+1.304E+03
78	+1.520E+03	+3.83E+00	+4.777E+03	+1.503E+03
79	+1.609E+03	+3.47E+00	+5.682E+03	+1.788E+03
80	+1.698E+03	+3.67E+00	+6.533E+03	+2.056E+03
81	+1.782E+03	+4.35E+00	+7.575E+03	+2.384E+03
82	+1.877E+03	+3.96E+00	+8.786E+03	+2.765E+03
83	+1.962E+03	+3.56E+00	+9.712E+03	+3.055E+03
84	+2.081E+03	+3.44E+00	+1.084E+04	+3.405E+03
85	+2.165E+03	+1.34E+00	+1.211E+04	+3.805E+03
86	+2.252E+03	+3.47E+00	+1.311E+04	+4.116E+03
87	+2.342E+03	+2.89E+00	+1.500E+04	+4.710E+03
88	+2.454E+03	+3.14E+00	+1.680E+04	+5.273E+03
89	+2.573E+03	+3.45E+00	+1.894E+04	+5.943E+03
90	+2.683E+03	+2.97E+00	+2.080E+04	+6.521E+03
91	+2.803E+03	+2.60E+00	+2.355E+04	+7.381E+03
92	+2.903E+03	+1.62E+00	+2.497E+04	+7.817E+03
93	+2.939E+03	+2.57E+00	+2.514E+04	+7.863E+03
94	+2.990E+03	+1.68E+00	+2.508E+04	+7.835E+03
95	+3.027E+03	+1.54E+00	+2.596E+04	+8.108E+03
96	+3.093E+03	+3.26E+00	+2.493E+04	+7.765E+03
97	+3.159E+03	+1.38E+00	+2.515E+04	+7.821E+03
98	+3.231E+03	+3.33E+00	+2.215E+04	+6.840E+03
99	+3.288E+03	+1.68E+00	+2.167E+04	+6.671E+03
100	+3.366E+03	+3.51E+00	+1.918E+04	+5.855E+03
101	+3.404E+03	+1.85E+00	+1.919E+04	+5.846E+03
102	+3.474E+03	+2.91E+00	+1.939E+04	+5.893E+03
103	+3.508E+03	+1.94E+00	+1.886E+04	+5.712E+03
104	+3.543E+03	+1.89E+00	+1.971E+04	+5.974E+03
105	+3.618E+03	+3.42E+00	+1.991E+04	+6.013E+03
106	+3.737E+03	+2.95E+00	+2.163E+04	+6.528E+03
107	+3.879E+03	+2.97E+00	+2.383E+04	+7.183E+03
108	+4.038E+03	+3.02E+00	+2.534E+04	+7.605E+03
109	+4.187E+03	+3.07E+00	+2.808E+04	+8.424E+03
110	+4.366E+03	+3.43E+00	+3.095E+04	+9.265E+03
111	+4.559E+03	+4.04E+00	+3.333E+04	+9.933E+03
112	+4.716E+03	+3.76E+00	+3.587E+04	+1.066E+04
113	+4.901E+03	+3.68E+00	+3.776E+04	+1.117E+04
114	+5.050E+03	+3.88E+00	+4.150E+04	+1.228E+04

echantillon: Zr.76 Ni.24 masse: 2.55g

etat: recuit 24h 250°c

	T (mK)	ΔT/T(%)	mc(erg/K)	Cp(erg/gK)
1	+3.795E+01	+8.94E+00	+6.082E+00	+1.103E+00
2	+3.799E+01	+1.04E+01	+5.856E+00	+1.019E+00
3	+3.728E+01	+9.01E+00	+6.233E+00	+1.083E+00
4	+3.791E+01	+1.11E+01	+6.034E+00	+1.080E+00
5	+3.887E+01	+1.36E+01	+5.948E+00	+1.144E+00
6	+3.964E+01	+1.05E+01	+5.705E+00	+1.116E+00
7	+4.162E+01	+9.04E+00	+5.636E+00	+1.227E+00
8	+4.378E+01	+8.15E+00	+6.109E+00	+1.521E+00
9	+4.524E+01	+8.09E+00	+6.610E+00	+1.774E+00
10	+5.075E+01	+9.49E+00	+5.968E+00	+1.655E+00
11	+5.345E+01	+8.87E+00	+5.776E+00	+1.616E+00
12	+5.542E+01	+8.85E+00	+5.894E+00	+1.682E+00
13	+5.727E+01	+8.38E+00	+5.832E+00	+1.672E+00
14	+5.943E+01	+9.05E+00	+5.630E+00	+1.606E+00
15	+6.046E+01	+6.94E+00	+5.829E+00	+1.688E+00
16	+6.319E+01	+9.61E+00	+5.517E+00	+1.574E+00
17	+6.536E+01	+8.68E+00	+5.761E+00	+1.674E+00
18	+6.745E+01	+8.03E+00	+6.064E+00	+1.795E+00
19	+7.201E+01	+1.16E+01	+5.376E+00	+1.524E+00
20	+7.375E+01	+1.04E+01	+5.596E+00	+1.607E+00
21	+7.637E+01	+1.06E+01	+5.561E+00	+1.589E+00
22	+7.882E+01	+1.01E+01	+5.535E+00	+1.573E+00
23	+8.132E+01	+9.86E+00	+5.683E+00	+1.625E+00
24	+8.476E+01	+1.14E+01	+5.359E+00	+1.487E+00
25	+8.821E+01	+8.89E+00	+5.686E+00	+1.603E+00
26	+9.347E+01	+1.07E+01	+5.566E+00	+1.535E+00
27	+9.665E+01	+8.00E+00	+5.806E+00	+1.616E+00
28	+1.000E+02	+8.46E+00	+6.144E+00	+1.734E+00
29	+1.031E+02	+9.10E+00	+6.142E+00	+1.718E+00
30	+1.073E+02	+1.12E+01	+6.231E+00	+1.733E+00
31	+1.125E+02	+1.38E+01	+6.370E+00	+1.762E+00
32	+1.161E+02	+7.84E+00	+6.943E+00	+1.968E+00
33	+1.230E+02	+1.01E+01	+6.959E+00	+1.939E+00
34	+1.287E+02	+9.86E+00	+6.976E+00	+1.915E+00
35	+1.339E+02	+9.76E+00	+7.406E+00	+2.056E+00
36	+1.381E+02	+8.59E+00	+7.537E+00	+2.084E+00
37	+1.434E+02	+8.73E+00	+7.777E+00	+2.149E+00
38	+1.494E+02	+4.95E+00	+8.156E+00	+2.265E+00
39	+1.554E+02	+5.28E+00	+8.559E+00	+2.389E+00
40	+1.622E+02	+5.87E+00	+8.403E+00	+2.290E+00
41	+1.632E+02	+6.82E+00	+8.589E+00	+2.357E+00
42	+1.649E+02	+5.78E+00	+8.483E+00	+2.306E+00
43	+1.639E+02	+5.12E+00	+9.178E+00	+2.584E+00
44	+1.679E+02	+5.77E+00	+8.671E+00	+2.363E+00
45	+1.703E+02	+5.24E+00	+8.999E+00	+2.477E+00
46	+1.724E+02	+5.58E+00	+8.720E+00	+2.356E+00
47	+1.769E+02	+5.73E+00	+8.639E+00	+2.299E+00
48	+1.829E+02	+6.62E+00	+9.552E+00	+2.623E+00
49	+1.914E+02	+7.60E+00	+9.845E+00	+2.689E+00
50	+1.970E+02	+6.28E+00	+1.020E+01	+2.796E+00
51	+2.060E+02	+6.91E+00	+1.077E+01	+2.970E+00
52	+2.195E+02	+7.81E+00	+1.113E+01	+3.029E+00
53	+2.330E+02	+1.04E+01	+1.213E+01	+3.341E+00
54	+2.384E+02	+7.72E+00	+1.222E+01	+3.347E+00
55	+2.526E+02	+6.13E+00	+1.419E+01	+4.033E+00
56	+2.654E+02	+4.78E+00	+1.432E+01	+4.005E+00
57	+2.847E+02	+5.39E+00	+1.577E+01	+4.450E+00
58	+2.982E+02	+6.55E+00	+1.693E+01	+4.818E+00
59	+3.126E+02	+6.46E+00	+1.782E+01	+5.072E+00
60	+3.258E+02	+6.11E+00	+1.881E+01	+5.370E+00
61	+3.420E+02	+6.46E+00	+2.111E+01	+6.161E+00

62	+3.584E+02	+7.06E+00	+2.294E+01	+6.761E+00
63	+3.744E+02	+7.00E+00	+2.479E+01	+7.365E+00
64	+3.888E+02	+6.36E+00	+2.711E+01	+8.165E+00
65	+4.136E+02	+8.23E+00	+2.862E+01	+8.557E+00
66	+4.345E+02	+8.86E+00	+3.220E+01	+9.786E+00
67	+4.506E+02	+3.76E+00	+3.787E+01	+1.187E+01
68	+4.751E+02	+4.61E+00	+3.911E+01	+1.213E+01
69	+5.011E+02	+4.87E+00	+4.759E+01	+1.520E+01
70	+5.196E+02	+3.85E+00	+5.556E+01	+1.814E+01
71	+5.471E+02	+2.80E+00	+6.580E+01	+2.186E+01
72	+5.742E+02	+3.14E+00	+7.951E+01	+2.692E+01
73	+5.988E+02	+3.47E+00	+9.295E+01	+3.190E+01
74	+6.274E+02	+3.58E+00	+1.137E+02	+3.968E+01
75	+6.576E+02	+4.50E+00	+1.425E+02	+5.054E+01
76	+6.908E+02	+4.38E+00	+1.797E+02	+6.465E+01
77	+7.248E+02	+4.36E+00	+2.141E+02	+7.762E+01
78	+7.598E+02	+4.27E+00	+2.787E+02	+1.023E+02
79	+7.937E+02	+4.08E+00	+3.212E+02	+1.184E+02
80	+8.239E+02	+3.88E+00	+4.059E+02	+1.510E+02
81	+8.720E+02	+4.52E+00	+5.050E+02	+1.889E+02
82	+9.258E+02	+5.45E+00	+6.338E+02	+2.382E+02
83	+9.903E+02	+3.69E+00	+8.161E+02	+3.080E+02
84	+1.074E+03	+7.51E+00	+1.127E+03	+4.277E+02
85	+1.114E+03	+4.86E+00	+1.219E+03	+4.624E+02
86	+1.165E+03	+4.67E+00	+1.466E+03	+5.573E+02
87	+1.225E+03	+4.25E+00	+1.754E+03	+6.681E+02
88	+1.297E+03	+5.71E+00	+2.079E+03	+7.924E+02
89	+1.410E+03	+7.36E+00	+2.622E+03	+1.000E+03
90	+1.482E+03	+7.59E+00	+3.040E+03	+1.160E+03
91	+1.562E+03	+9.02E+00	+3.739E+03	+1.428E+03
92	+1.648E+03	+9.40E+00	+3.977E+03	+1.517E+03
93	+1.678E+03	+4.57E+00	+4.363E+03	+1.666E+03
94	+1.765E+03	+4.02E+00	+4.921E+03	+1.878E+03
95	+1.876E+03	+4.14E+00	+5.759E+03	+2.197E+03
96	+1.969E+03	+4.65E+00	+6.596E+03	+2.516E+03
97	+2.081E+03	+5.06E+00	+7.762E+03	+2.960E+03
98	+2.174E+03	+4.40E+00	+7.856E+03	+2.986E+03
99	+2.276E+03	+4.64E+00	+9.694E+03	+3.692E+03
100	+2.355E+03	+2.93E+00	+1.041E+04	+3.960E+03
101	+2.376E+03	+4.60E+00	+1.051E+04	+3.998E+03
102	+2.461E+03	+3.93E+00	+1.114E+04	+4.230E+03
103	+2.557E+03	+3.47E+00	+1.242E+04	+4.717E+03
104	+2.678E+03	+3.42E+00	+1.377E+04	+5.222E+03
105	+2.797E+03	+3.26E+00	+1.416E+04	+5.348E+03
106	+2.841E+03	+1.64E+00	+1.405E+04	+5.297E+03
107	+2.922E+03	+1.69E+00	+1.381E+04	+5.182E+03
108	+2.990E+03	+1.72E+00	+1.314E+04	+4.903E+03
109	+3.062E+03	+1.76E+00	+1.185E+04	+4.379E+03
110	+3.143E+03	+1.87E+00	+1.110E+04	+4.064E+03
111	+3.255E+03	+1.54E+00	+1.053E+04	+3.806E+03
112	+3.354E+03	+1.55E+00	+1.086E+04	+3.905E+03
113	+3.445E+03	+1.99E+00	+1.121E+04	+4.011E+03
114	+3.543E+03	+2.91E+00	+1.207E+04	+4.313E+03
115	+3.676E+03	+3.20E+00	+1.294E+04	+4.604E+03
116	+3.845E+03	+4.12E+00	+1.437E+04	+5.093E+03
117	+3.944E+03	+2.94E+00	+1.512E+04	+5.344E+03
118	+4.113E+03	+3.28E+00	+1.683E+04	+5.934E+03
119	+4.251E+03	+3.69E+00	+1.793E+04	+6.293E+03
120	+4.382E+03	+3.85E+00	+1.894E+04	+6.617E+03
121	+4.531E+03	+3.86E+00	+2.029E+04	+7.056E+03
122	+4.690E+03	+3.77E+00	+2.182E+04	+7.557E+03
123	+4.861E+03	+3.70E+00	+2.363E+04	+8.152E+03
124	+5.027E+03	+3.67E+00	+2.547E+04	+8.752E+03

échantillon: Zr.76 Ni.24 masse: 2.475 g

etat: brut (300K)

	T (mK)	ΔT/T(‰)	mc(erg/K)	Cp(erg/gK)
10	+3.31E+01	+7.51E-02	+1.20E+01	+2.55E+00
11	+3.62E+01	+8.16E-02	+1.17E+01	+3.16E+00
12	+3.88E+01	+8.01E-02	+1.11E+01	+3.27E+00
13	+4.13E+01	+6.21E-02	+1.09E+01	+3.39E+00
14	+4.36E+01	+6.03E-02	+1.19E+01	+3.89E+00
15	+4.56E+01	+5.78E-02	+1.17E+01	+3.91E+00
16	+4.77E+01	+1.08E-01	+9.91E+00	+3.24E+00
17	+5.19E+01	+1.02E-01	+1.00E+01	+3.37E+00
18	+5.35E+01	+1.10E-01	+9.54E+00	+3.19E+00
19	+5.65E+01	+1.09E-01	+9.52E+00	+3.21E+00
20	+5.71E+01	+9.12E-02	+8.97E+00	+2.99E+00
21	+5.99E+01	+1.01E-01	+9.39E+00	+3.18E+00
22	+6.05E+01	+7.62E-02	+9.50E+00	+3.22E+00
23	+6.59E+01	+7.60E-02	+9.30E+00	+3.16E+00
24	+7.20E+01	+9.82E-02	+8.35E+00	+2.77E+00
25	+7.86E+01	+8.80E-02	+8.32E+00	+2.75E+00
26	+8.42E+01	+1.03E-01	+8.27E+00	+2.71E+00
27	+8.99E+01	+1.28E-01	+7.74E+00	+2.48E+00
28	+9.26E+01	+1.09E-01	+7.89E+00	+2.52E+00
29	+9.95E+01	+1.15E-01	+7.72E+00	+2.43E+00
30	+1.08E+02	+1.28E-01	+8.36E+00	+2.64E+00
31	+1.16E+02	+1.85E-01	+6.41E+00	+1.81E+00
32	+1.13E+02	+9.02E-02	+8.47E+00	+2.66E+00
33	+1.20E+02	+1.13E-01	+8.36E+00	+2.58E+00
34	+1.26E+02	+8.41E-02	+8.96E+00	+2.79E+00
35	+1.34E+02	+8.02E-02	+8.42E+00	+2.53E+00
36	+1.41E+02	+6.81E-02	+9.51E+00	+2.93E+00
37	+1.45E+02	+9.57E-02	+9.38E+00	+2.86E+00
38	+1.51E+02	+8.81E-02	+9.97E+00	+3.06E+00
39	+1.61E+02	+8.33E-02	+1.02E+01	+3.08E+00
40	+1.75E+02	+1.05E-01	+1.01E+01	+2.98E+00
41	+1.88E+02	+1.02E-01	+1.14E+01	+3.41E+00
42	+1.94E+02	+1.12E-01	+1.19E+01	+3.57E+00
43	+2.09E+02	+8.04E-02	+1.25E+01	+3.75E+00
44	+2.25E+02	+9.59E-02	+1.28E+01	+3.77E+00
45	+2.38E+02	+8.11E-02	+1.37E+01	+4.05E+00
46	+2.56E+02	+8.13E-02	+1.50E+01	+4.46E+00
47	+2.76E+02	+1.18E-01	+1.51E+01	+4.37E+00
48	+3.00E+02	+6.92E-02	+1.80E+01	+5.39E+00
49	+3.20E+02	+7.84E-02	+1.83E+01	+5.38E+00
50	+3.41E+02	+7.52E-02	+1.98E+01	+5.83E+00
51	+3.79E+02	+6.37E-02	+2.33E+01	+6.94E+00
52	+4.01E+02	+6.41E-02	+2.58E+01	+7.80E+00
53	+4.47E+02	+9.87E-02	+3.00E+01	+9.09E+00
54	+4.68E+02	+7.14E-02	+3.37E+01	+1.04E+01
55	+5.15E+02	+8.49E-02	+4.01E+01	+1.25E+01
56	+5.39E+02	+4.09E-02	+4.86E+01	+1.57E+01
57	+5.71E+02	+5.49E-02	+5.84E+01	+1.92E+01
58	+5.97E+02	+3.84E-02	+6.91E+01	+2.32E+01
59	+6.31E+02	+5.22E-02	+8.17E+01	+2.79E+01
60	+6.57E+02	+4.21E-02	+1.03E+02	+3.62E+01

60	+6.57E+02	+4.21E-02	+1.03E+02	+3.62E+01
61	+6.86E+02	+4.10E-02	+1.21E+02	+4.30E+01
62	+7.18E+02	+3.88E-02	+1.46E+02	+5.24E+01
63	+7.57E+02	+4.97E-02	+1.96E+02	+7.22E+01
64	+7.96E+02	+4.95E-02	+2.43E+02	+9.03E+01
65	+8.31E+02	+4.84E-02	+2.96E+02	+1.11E+02
66	+8.87E+02	+4.78E-02	+3.88E+02	+1.47E+02
67	+9.27E+02	+4.57E-02	+4.72E+02	+1.80E+02
68	+9.78E+02	+4.89E-02	+6.05E+02	+2.33E+02
69	+1.03E+03	+4.68E-02	+7.59E+02	+2.93E+02
70	+1.11E+03	+4.35E-02	+1.02E+03	+3.97E+02
71	+1.18E+03	+4.50E-02	+1.34E+03	+5.22E+02
72	+1.24E+03	+3.66E-02	+1.52E+03	+5.93E+02
73	+1.30E+03	+4.77E-02	+1.85E+03	+7.26E+02
74	+1.36E+03	+4.73E-02	+2.14E+03	+8.40E+02
75	+1.42E+03	+3.83E-02	+2.43E+03	+9.50E+02
76	+1.50E+03	+3.42E-02	+2.89E+03	+1.13E+03
77	+1.56E+03	+2.84E-02	+3.35E+03	+1.31E+03
78	+1.63E+03	+2.83E-02	+3.88E+03	+1.53E+03
79	+1.72E+03	+3.34E-02	+4.51E+03	+1.77E+03
80	+1.81E+03	+2.75E-02	+5.30E+03	+2.08E+03
81	+1.88E+03	+3.17E-02	+5.72E+03	+2.24E+03
82	+2.01E+03	+3.31E-02	+6.83E+03	+2.68E+03
83	+2.20E+03	+3.60E-02	+8.52E+03	+3.34E+03
84	+2.30E+03	+2.88E-02	+9.62E+03	+3.77E+03
85	+2.45E+03	+4.69E-02	+1.12E+04	+4.38E+03
86	+2.54E+03	+4.81E-02	+1.22E+04	+4.77E+03
87	+2.70E+03	+4.58E-02	+1.47E+04	+5.74E+03
88	+2.83E+03	+3.93E-02	+1.64E+04	+6.41E+03
89	+2.93E+03	+2.02E-02	+1.76E+04	+6.86E+03
90	+3.02E+03	+1.05E-02	+1.79E+04	+6.98E+03
91	+3.10E+03	+1.48E-02	+1.87E+04	+7.29E+03
92	+3.17E+03	+1.49E-02	+1.85E+04	+7.19E+03
93	+3.25E+03	+1.20E-02	+1.90E+04	+7.34E+03
94	+3.33E+03	+1.48E-02	+1.87E+04	+7.19E+03
95	+3.42E+03	+1.39E-02	+1.83E+04	+7.00E+03
96	+3.51E+03	+1.64E-02	+1.75E+04	+6.65E+03
97	+3.60E+03	+1.65E-02	+1.63E+04	+6.15E+03
98	+3.70E+03	+1.78E-02	+1.59E+04	+5.92E+03
99	+3.79E+03	+1.55E-02	+1.65E+04	+6.15E+03
100	+3.88E+03	+1.46E-02	+1.75E+04	+6.49E+03
101	+3.99E+03	+1.41E-02	+1.93E+04	+7.16E+03
102	+4.09E+03	+1.68E-02	+2.00E+04	+7.40E+03
103	+4.21E+03	+1.87E-02	+2.08E+04	+7.65E+03
104	+4.33E+03	+2.17E-02	+2.26E+04	+8.31E+03
105	+4.27E+03	+3.06E-02	+2.15E+04	+7.91E+03
106	+4.29E+03	+3.79E-02	+2.19E+04	+8.05E+03
107	+4.45E+03	+2.45E-02	+2.38E+04	+8.74E+03
108	+4.58E+03	+2.24E-02	+2.54E+04	+9.30E+03
109	+4.72E+03	+2.19E-02	+2.71E+04	+9.89E+03
110	+4.85E+03	+2.14E-02	+2.92E+04	+1.07E+04
111	+5.00E+03	+1.84E-02	+3.11E+04	+1.13E+04
112	+5.14E+03	+2.15E-02	+3.28E+04	+1.19E+04
113	+5.34E+03	+1.90E-02	+3.53E+04	+1.27E+04
114	+5.48E+03	+1.83E-02	+3.90E+04	+1.41E+04
115	+5.64E+03	+1.94E-02	+4.09E+04	+1.47E+04
116	+5.84E+03	+2.27E-02	+4.51E+04	+1.62E+04
117	+5.99E+03	+2.32E-02	+4.85E+04	+1.74E+04

échantillon: Zr.76 Cu.24 masse: 2.916 g

etat: brut (77 K)

	T (mK)	ΔT/T(%)	mc(erg/K)	Cp(erg/gK)
6	+4.314E+01	+1.10E+01	+6.158E+00	+1.322E+00
7	+4.377E+01	+1.13E+01	+6.041E+00	+1.306E+00
8	+4.440E+01	+8.90E+00	+6.122E+00	+1.357E+00
9	+4.742E+01	+1.30E+01	+5.312E+00	+1.162E+00
10	+4.730E+01	+1.13E+01	+5.793E+00	+1.324E+00
11	+4.891E+01	+1.10E+01	+5.033E+00	+1.096E+00
12	+4.954E+01	+1.13E+01	+5.536E+00	+1.280E+00
13	+5.084E+01	+8.09E+00	+5.661E+00	+1.343E+00
14	+5.212E+01	+1.05E+01	+5.517E+00	+1.310E+00
15	+5.464E+01	+1.23E+01	+5.355E+00	+1.280E+00
16	+5.701E+01	+1.11E+01	+5.557E+00	+1.367E+00
17	+5.962E+01	+9.53E+00	+5.425E+00	+1.335E+00
18	+6.151E+01	+9.54E+00	+5.741E+00	+1.449E+00
19	+6.430E+01	+1.01E+01	+5.442E+00	+1.353E+00
20	+6.812E+01	+1.24E+01	+5.022E+00	+1.212E+00
21	+7.074E+01	+1.16E+01	+5.180E+00	+1.266E+00
22	+7.523E+01	+1.32E+01	+4.973E+00	+1.190E+00
23	+7.826E+01	+1.08E+01	+5.182E+00	+1.256E+00
24	+8.202E+01	+1.21E+01	+5.101E+00	+1.219E+00
25	+8.574E+01	+1.30E+01	+5.076E+00	+1.200E+00
26	+8.840E+01	+1.26E+01	+5.093E+00	+1.198E+00
27	+9.247E+01	+6.33E+00	+5.656E+00	+1.377E+00
28	+9.774E+01	+7.99E+00	+5.646E+00	+1.354E+00
29	+1.016E+02	+7.97E+00	+5.593E+00	+1.321E+00
30	+1.073E+02	+9.19E+00	+5.664E+00	+1.321E+00
31	+1.144E+02	+1.52E+01	+5.732E+00	+1.314E+00
32	+1.175E+02	+1.27E+01	+5.574E+00	+1.245E+00
33	+1.262E+02	+1.14E+01	+6.391E+00	+1.486E+00
34	+1.272E+02	+7.33E+00	+5.977E+00	+1.339E+00
35	+1.339E+02	+8.82E+00	+6.514E+00	+1.492E+00
36	+1.403E+02	+9.88E+00	+6.606E+00	+1.493E+00
37	+1.473E+02	+9.46E+00	+6.739E+00	+1.504E+00
38	+1.592E+02	+8.15E+00	+7.198E+00	+1.604E+00
39	+1.666E+02	+9.84E+00	+7.455E+00	+1.656E+00
40	+1.766E+02	+1.07E+01	+8.089E+00	+1.823E+00
41	+1.904E+02	+1.38E+01	+9.078E+00	+2.094E+00
42	+2.002E+02	+1.08E+01	+9.108E+00	+2.055E+00
43	+2.092E+02	+9.19E+00	+9.247E+00	+2.057E+00
44	+2.216E+02	+8.87E+00	+1.024E+01	+2.333E+00
45	+2.352E+02	+8.82E+00	+1.069E+01	+2.418E+00
46	+2.474E+02	+7.04E+00	+1.166E+01	+2.688E+00
47	+2.632E+02	+9.65E+00	+1.196E+01	+2.704E+00
48	+2.776E+02	+1.08E+01	+1.285E+01	+2.930E+00
49	+3.018E+02	+1.05E+01	+1.438E+01	+3.318E+00
50	+3.218E+02	+1.23E+01	+1.529E+01	+3.513E+00
51	+3.492E+02	+8.10E+00	+1.824E+01	+4.357E+00
52	+3.639E+02	+7.82E+00	+1.960E+01	+4.731E+00
53	+3.925E+02	+1.01E+01	+2.273E+01	+5.611E+00
54	+3.964E+02	+6.86E+00	+2.251E+01	+5.510E+00
55	+4.198E+02	+7.97E+00	+2.440E+01	+5.992E+00
56	+4.389E+02	+8.80E+00	+2.704E+01	+6.754E+00
57	+4.355E+02	+6.24E+00	+2.651E+01	+6.597E+00
58	+4.562E+02	+6.87E+00	+2.892E+01	+7.263E+00
59	+4.809E+02	+8.20E+00	+3.193E+01	+8.095E+00
60	+5.034E+02	+8.72E+00	+3.473E+01	+8.864E+00
61	+5.263E+02	+7.18E+00	+4.006E+01	+1.048E+01

62	+5.500E+02	+6.68E+00	+4.764E+01	+1.286E+01
63	+5.676E+02	+1.09E+01	+4.902E+01	+1.316E+01
64	+5.773E+02	+8.55E+00	+5.169E+01	+1.397E+01
65	+5.892E+02	+5.36E+00	+5.715E+01	+1.572E+01
66	+6.121E+02	+5.18E+00	+6.575E+01	+1.842E+01
67	+6.447E+02	+5.99E+00	+8.010E+01	+2.296E+01
68	+6.699E+02	+4.67E+00	+9.626E+01	+2.819E+01
69	+7.033E+02	+4.17E+00	+1.172E+02	+3.494E+01
70	+7.444E+02	+5.50E+00	+1.514E+02	+4.607E+01
71	+7.916E+02	+6.09E+00	+1.980E+02	+6.134E+01
72	+8.324E+02	+5.41E+00	+2.518E+02	+7.910E+01
73	+8.743E+02	+4.62E+00	+3.398E+02	+1.085E+02
74	+9.156E+02	+4.81E+00	+4.010E+02	+1.287E+02
75	+9.588E+02	+4.82E+00	+4.867E+02	+1.572E+02
76	+1.000E+03	+4.22E+00	+6.194E+02	+2.017E+02
77	+1.069E+03	+2.31E+00	+8.141E+02	+2.667E+02
78	+1.106E+03	+3.53E+00	+9.209E+02	+3.023E+02
79	+1.161E+03	+4.01E+00	+1.177E+03	+3.884E+02
80	+1.222E+03	+3.54E+00	+1.364E+03	+4.507E+02
81	+1.274E+03	+3.34E+00	+1.608E+03	+5.326E+02
82	+1.339E+03	+3.42E+00	+1.941E+03	+6.440E+02
83	+1.396E+03	+2.52E+00	+2.214E+03	+7.351E+02
84	+1.461E+03	+2.04E+00	+2.596E+03	+8.632E+02
85	+1.561E+03	+2.11E+00	+3.271E+03	+1.089E+03
86	+1.659E+03	+2.66E+00	+3.898E+03	+1.299E+03
87	+1.767E+03	+3.41E+00	+4.829E+03	+1.610E+03
88	+1.867E+03	+3.09E+00	+5.667E+03	+1.890E+03
89	+1.950E+03	+2.53E+00	+6.544E+03	+2.184E+03
90	+2.055E+03	+3.54E+00	+7.672E+03	+2.561E+03
91	+2.292E+03	+3.33E+00	+1.006E+04	+3.353E+03
92	+2.401E+03	+3.27E+00	+1.155E+04	+3.848E+03
93	+2.504E+03	+3.09E+00	+1.286E+04	+4.285E+03
94	+2.613E+03	+3.10E+00	+1.422E+04	+4.732E+03
95	+2.742E+03	+3.13E+00	+1.674E+04	+5.573E+03
96	+2.886E+03	+3.25E+00	+1.887E+04	+6.276E+03
97	+3.015E+03	+3.79E+00	+2.078E+04	+6.902E+03
98	+3.152E+03	+3.78E+00	+2.296E+04	+7.619E+03
99	+3.283E+03	+3.96E+00	+2.626E+04	+8.713E+03
100	+3.283E+03	+3.96E+00	+2.626E+04	+8.713E+03
101	+3.283E+03	+3.96E+00	+2.626E+04	+8.713E+03
102	+3.424E+03	+5.17E+00	+2.359E+04	+7.758E+03
103	+3.452E+03	+1.90E+00	+2.286E+04	+7.502E+03
104	+3.526E+03	+2.60E+00	+2.033E+04	+6.609E+03
105	+3.580E+03	+1.50E+00	+1.845E+04	+5.948E+03
106	+3.662E+03	+2.14E+00	+1.761E+04	+5.633E+03
107	+3.750E+03	+2.14E+00	+1.891E+04	+6.046E+03
108	+3.881E+03	+3.08E+00	+1.949E+04	+6.198E+03
109	+3.982E+03	+3.13E+00	+2.163E+04	+6.890E+03
110	+4.083E+03	+2.58E+00	+2.393E+04	+7.636E+03
111	+4.201E+03	+2.52E+00	+2.454E+04	+7.792E+03
112	+4.288E+03	+1.80E+00	+2.583E+04	+8.195E+03
113	+4.441E+03	+1.28E+00	+2.766E+04	+8.745E+03
114	+4.577E+03	+1.42E+00	+2.990E+04	+9.442E+03
115	+4.701E+03	+1.25E+00	+3.151E+04	+9.927E+03
116	+4.820E+03	+1.38E+00	+3.495E+04	+1.103E+04
117	+4.994E+03	+1.39E+00	+3.707E+04	+1.165E+04
118	+5.128E+03	+1.56E+00	+3.844E+04	+1.203E+04
119	+5.293E+03	+1.53E+00	+4.103E+04	+1.280E+04
120	+5.460E+03	+1.38E+00	+4.527E+04	+1.413E+04
121	+5.623E+03	+1.45E+00	+4.907E+04	+1.530E+04
122	+5.798E+03	+1.50E+00	+5.229E+04	+1.626E+04
123	+5.992E+03	+1.51E+00	+5.768E+04	+1.793E+04
124	+6.148E+03	+1.60E+00	+6.080E+04	+1.885E+04
125	+6.483E+03	+1.49E+00	+7.101E+04	+2.200E+04
126	+6.611E+03	+1.54E+00	+7.509E+04	+2.325E+04

échantillon: Zr.76 Cu.24 masse: 2.310g

état: recuit 1h 200°c

	T (mK)	ΔT/T(%)	mc(erg/K)	Cp(erg/gK)
1	+4.754E+01	+8.19E+00	+3.188E+00	+5.510E-01
2	+4.870E+01	+1.20E+01	+2.973E+00	+4.875E-01
3	+4.876E+01	+1.28E+01	+2.783E+00	+4.068E-01
4	+5.063E+01	+1.17E+01	+2.943E+00	+5.149E-01
5	+5.133E+01	+1.37E+01	+2.828E+00	+4.770E-01
6	+5.288E+01	+1.08E+01	+3.041E+00	+5.925E-01
7	+5.536E+01	+1.04E+01	+3.010E+00	+6.078E-01
8	+5.796E+01	+1.15E+01	+2.976E+00	+6.147E-01
9	+6.161E+01	+9.85E+00	+2.862E+00	+5.838E-01
10	+6.439E+01	+9.09E+00	+2.968E+00	+6.374E-01
11	+6.913E+01	+1.02E+01	+2.822E+00	+5.779E-01
12	+7.366E+01	+1.43E+01	+2.760E+00	+5.472E-01
13	+7.663E+01	+1.29E+01	+2.943E+00	+6.204E-01
14	+7.962E+01	+1.20E+01	+3.052E+00	+6.596E-01
15	+8.345E+01	+1.12E+01	+3.121E+00	+6.772E-01
16	+8.766E+01	+1.10E+01	+3.036E+00	+6.247E-01
17	+9.354E+01	+1.36E+01	+3.123E+00	+6.371E-01
18	+9.848E+01	+1.58E+01	+3.188E+00	+6.416E-01
19	+1.044E+02	+1.43E+01	+3.321E+00	+6.689E-01
20	+1.096E+02	+1.29E+01	+3.498E+00	+7.179E-01
21	+1.151E+02	+1.20E+01	+3.591E+00	+7.275E-01
22	+1.192E+02	+1.12E+01	+3.714E+00	+7.573E-01
23	+1.246E+02	+1.20E+01	+3.966E+00	+8.350E-01
24	+1.297E+02	+1.13E+01	+4.072E+00	+8.508E-01
25	+1.373E+02	+1.32E+01	+4.303E+00	+9.057E-01
26	+1.434E+02	+1.18E+01	+4.610E+00	+1.001E+00
27	+1.506E+02	+1.09E+01	+4.756E+00	+1.021E+00
28	+1.595E+02	+9.52E+00	+5.121E+00	+1.124E+00
29	+1.681E+02	+1.11E+01	+5.216E+00	+1.111E+00
30	+1.758E+02	+9.73E+00	+5.683E+00	+1.266E+00
31	+1.868E+02	+1.05E+01	+5.966E+00	+1.319E+00
32	+1.951E+02	+1.14E+01	+6.141E+00	+1.342E+00
33	+2.038E+02	+1.16E+01	+6.574E+00	+1.474E+00
34	+2.152E+02	+1.36E+01	+6.788E+00	+1.493E+00
35	+2.237E+02	+1.23E+01	+7.203E+00	+1.618E+00
36	+2.445E+02	+1.02E+01	+7.943E+00	+1.801E+00
37	+2.592E+02	+9.27E+00	+8.259E+00	+1.839E+00
38	+2.701E+02	+7.77E+00	+9.457E+00	+2.283E+00
39	+2.836E+02	+7.58E+00	+9.226E+00	+2.089E+00
40	+3.000E+02	+9.82E+00	+1.053E+01	+2.534E+00
41	+3.127E+02	+8.81E+00	+1.125E+01	+2.755E+00
42	+3.281E+02	+9.97E+00	+1.137E+01	+2.692E+00
43	+3.486E+02	+1.04E+01	+1.225E+01	+2.914E+00
44	+3.693E+02	+1.11E+01	+1.305E+01	+3.090E+00
45	+3.903E+02	+1.10E+01	+1.460E+01	+3.583E+00
46	+4.114E+02	+1.13E+01	+1.541E+01	+3.748E+00
47	+4.280E+02	+1.05E+01	+1.780E+01	+4.628E+00
48	+4.445E+02	+9.21E+00	+1.938E+01	+5.156E+00
49	+4.701E+02	+1.25E+01	+2.116E+01	+5.670E+00
50	+5.216E+02	+1.35E+01	+2.464E+01	+6.614E+00
51	+5.532E+02	+1.07E+01	+2.930E+01	+8.253E+00
52	+5.812E+02	+9.91E+00	+3.446E+01	+1.013E+01
53	+6.029E+02	+8.25E+00	+3.990E+01	+1.219E+01
54	+6.292E+02	+7.35E+00	+4.827E+01	+1.544E+01
55	+6.600E+02	+7.22E+00	+5.859E+01	+1.944E+01
56	+6.957E+02	+9.04E+00	+7.887E+01	+2.764E+01
57	+7.260E+02	+8.58E+00	+9.552E+01	+3.432E+01
58	+7.520E+02	+7.86E+00	+1.175E+02	+4.337E+01
59	+8.053E+02	+5.34E+00	+1.617E+02	+6.143E+01
60	+8.359E+02	+4.54E+00	+2.090E+02	+8.124E+01
61	+8.778E+02	+4.06E+00	+2.504E+02	+9.817E+01

62	+9.087E+02	+3.59E+00	+3.937E+02	+1.205E+02
63	+9.726E+02	+4.85E+00	+4.121E+02	+1.657E+02
64	+1.006E+03	+4.39E+00	+4.406E+02	+1.770E+02
65	+1.063E+03	+6.80E+00	+5.388E+02	+2.177E+02
66	+1.123E+03	+4.79E+00	+7.238E+02	+2.957E+02
67	+1.170E+03	+6.07E+00	+8.218E+02	+3.363E+02
68	+1.223E+03	+4.82E+00	+9.911E+02	+4.073E+02
69	+1.296E+03	+5.61E+00	+1.228E+03	+5.067E+02
70	+1.368E+03	+8.90E+00	+1.468E+03	+6.068E+02
71	+1.422E+03	+7.56E+00	+1.663E+03	+6.880E+02
72	+1.482E+03	+6.25E+00	+1.930E+03	+8.000E+02
73	+1.560E+03	+4.98E+00	+2.300E+03	+9.547E+02
74	+1.621E+03	+4.87E+00	+2.547E+03	+1.057E+03
75	+1.726E+03	+7.45E+00	+3.131E+03	+1.301E+03
76	+1.804E+03	+6.43E+00	+3.467E+03	+1.440E+03
77	+1.891E+03	+7.68E+00	+4.158E+03	+1.730E+03
78	+1.996E+03	+6.18E+00	+4.895E+03	+2.037E+03
79	+2.115E+03	+6.99E+00	+5.444E+03	+2.260E+03
80	+2.213E+03	+4.50E+00	+6.394E+03	+2.658E+03
81	+2.291E+03	+4.01E+00	+6.924E+03	+2.875E+03
82	+2.390E+03	+3.40E+00	+7.830E+03	+3.251E+03
83	+2.484E+03	+2.96E+00	+8.651E+03	+3.589E+03
84	+2.595E+03	+2.55E+00	+9.607E+03	+3.981E+03
85	+2.741E+03	+4.19E+00	+1.108E+04	+4.585E+03
86	+2.863E+03	+3.59E+00	+1.240E+04	+5.126E+03
87	+2.993E+03	+2.95E+00	+1.442E+04	+5.967E+03
88	+3.170E+03	+2.55E+00	+1.577E+04	+6.495E+03
90	+3.310E+03	+1.45E+00	+1.327E+04	+5.367E+03
91	+3.402E+03	+1.64E+00	+1.141E+04	+4.531E+03
92	+3.497E+03	+1.74E+00	+1.045E+04	+4.076E+03
93	+3.581E+03	+1.63E+00	+1.095E+04	+4.261E+03
94	+3.667E+03	+1.51E+00	+1.154E+04	+4.481E+03
95	+3.781E+03	+2.71E+00	+1.245E+04	+4.822E+03
96	+3.880E+03	+2.50E+00	+1.315E+04	+5.078E+03
97	+3.983E+03	+2.33E+00	+1.375E+04	+5.284E+03
98	+4.087E+03	+2.08E+00	+1.500E+04	+5.771E+03
99	+4.198E+03	+1.97E+00	+1.546E+04	+5.907E+03
100	+4.311E+03	+1.76E+00	+1.677E+04	+6.408E+03
101	+4.429E+03	+1.64E+00	+1.753E+04	+6.662E+03
102	+4.556E+03	+2.96E+00	+1.893E+04	+7.185E+03
103	+4.686E+03	+2.67E+00	+2.041E+04	+7.735E+03
104	+4.817E+03	+2.45E+00	+2.166E+04	+8.178E+03
105	+4.971E+03	+2.24E+00	+2.292E+04	+8.604E+03
106	+5.124E+03	+1.99E+00	+2.510E+04	+9.416E+03
107	+5.287E+03	+1.83E+00	+2.644E+04	+9.853E+03
108	+5.457E+03	+1.74E+00	+2.698E+04	+9.924E+03
109	+5.631E+03	+2.91E+00	+3.118E+04	+1.156E+04
110	+5.790E+03	+2.56E+00	+3.454E+04	+1.285E+04
111	+5.980E+03	+2.35E+00	+3.644E+04	+1.345E+04
112	+6.178E+03	+2.07E+00	+4.000E+04	+1.475E+04
113	+6.411E+03	+2.69E+00	+4.445E+04	+1.637E+04
114	+6.613E+03	+2.37E+00	+4.900E+04	+1.805E+04
115	+6.838E+03	+2.14E+00	+5.243E+04	+1.920E+04
116	+7.109E+03	+2.51E+00	+5.742E+04	+2.092E+04
117	+7.315E+03	+2.26E+00	+6.189E+04	+2.249E+04
118	+7.539E+03	+2.03E+00	+6.708E+04	+2.432E+04
119	+7.738E+03	+1.86E+00	+7.122E+04	+2.571E+04

échantillon: Zr.76 Pt.24 masse: 3.487g

etat: brut (77 K)

	T (mK)	ΔT/T(%)	mc(erg/K)	Cp(erg/gK)
5	+3.19E+01	+1.24E-01	+8.58E+00	+5.47E-01
6	+3.27E+01	+1.53E-01	+8.03E+00	+6.03E-01
7	+3.34E+01	+1.18E-01	+7.98E+00	+7.54E-01
8	+3.51E+01	+1.37E-01	+7.45E+00	+8.86E-01
9	+3.54E+01	+8.45E-02	+7.98E+00	+1.09E+00
10	+3.72E+01	+8.97E-02	+7.67E+00	+1.20E+00
11	+3.85E+01	+1.01E-01	+6.82E+00	+1.06E+00
12	+4.02E+01	+8.45E-02	+7.83E+00	+1.46E+00
13	+4.10E+01	+7.82E-02	+7.79E+00	+1.49E+00
14	+4.31E+01	+9.09E-02	+7.94E+00	+1.62E+00
15	+4.49E+01	+8.60E-02	+7.90E+00	+1.66E+00
16	+4.69E+01	+7.79E-02	+7.66E+00	+1.63E+00
17	+4.89E+01	+6.18E-02	+8.69E+00	+1.96E+00
18	+5.11E+01	+5.98E-02	+8.02E+00	+1.80E+00
19	+5.40E+01	+5.79E-02	+8.27E+00	+1.90E+00
20	+5.71E+01	+4.47E-02	+7.90E+00	+1.82E+00
21	+6.24E+01	+3.51E-02	+8.74E+00	+2.07E+00
22	+6.68E+01	+4.87E-02	+8.33E+00	+1.96E+00
23	+7.09E+01	+6.23E-02	+7.72E+00	+1.79E+00
24	+7.63E+01	+5.32E-02	+8.70E+00	+2.06E+00
25	+8.27E+01	+5.34E-02	+8.20E+00	+1.91E+00
26	+9.12E+01	+6.07E-02	+7.89E+00	+1.80E+00
27	+9.69E+01	+5.50E-02	+8.22E+00	+1.87E+00
28	+1.04E+02	+7.29E-02	+8.10E+00	+1.81E+00
29	+1.09E+02	+7.67E-02	+8.42E+00	+1.89E+00
30	+1.16E+02	+9.94E-02	+8.36E+00	+1.85E+00
31	+1.21E+02	+7.09E-02	+9.13E+00	+2.05E+00
32	+1.28E+02	+6.05E-02	+9.31E+00	+2.07E+00
33	+1.37E+02	+9.73E-02	+9.29E+00	+2.03E+00
34	+1.44E+02	+1.02E-01	+9.53E+00	+2.07E+00
35	+1.54E+02	+9.97E-02	+9.95E+00	+2.15E+00
36	+1.64E+02	+1.23E-01	+1.01E+01	+2.14E+00
37	+1.61E+02	+7.26E-02	+1.02E+01	+2.19E+00
38	+1.67E+02	+5.63E-02	+1.13E+01	+2.49E+00
39	+1.80E+02	+5.95E-02	+1.15E+01	+2.50E+00
40	+1.93E+02	+7.92E-02	+1.11E+01	+2.32E+00
41	+2.09E+02	+7.10E-02	+1.30E+01	+2.79E+00
42	+2.22E+02	+7.94E-02	+1.27E+01	+2.67E+00
43	+2.33E+02	+6.63E-02	+1.38E+01	+2.94E+00
44	+2.63E+02	+5.72E-02	+1.62E+01	+3.47E+00
45	+2.81E+02	+6.37E-02	+1.73E+01	+3.72E+00
46	+2.94E+02	+7.67E-02	+1.76E+01	+3.75E+00
47	+3.03E+02	+6.24E-02	+1.92E+01	+4.15E+00
48	+3.26E+02	+6.55E-02	+2.01E+01	+4.31E+00
49	+3.43E+02	+5.16E-02	+2.19E+01	+4.72E+00
50	+3.64E+02	+6.17E-02	+2.40E+01	+5.21E+00
51	+3.82E+02	+7.12E-02	+2.52E+01	+5.46E+00
52	+4.06E+02	+6.37E-02	+2.85E+01	+6.27E+00
53	+4.36E+02	+7.62E-02	+3.29E+01	+7.36E+00
54	+4.59E+02	+6.72E-02	+3.92E+01	+9.01E+00
55	+4.84E+02	+8.09E-02	+4.28E+01	+9.86E+00
56	+5.12E+02	+5.14E-02	+5.34E+01	+1.27E+01
57	+5.37E+02	+5.98E-02	+6.39E+01	+1.55E+01
58	+5.62E+02	+5.47E-02	+7.34E+01	+1.80E+01
59	+5.94E+02	+6.11E-02	+9.48E+01	+2.39E+01
60	+6.24E+02	+6.14E-02	+1.21E+02	+3.11E+01
61	+6.60E+02	+4.23E-02	+1.58E+02	+4.13E+01

62	+6.87E+02	+4.48E-02	+1.88E+02	+4.98E+01
63	+7.29E+02	+4.52E-02	+2.46E+02	+6.57E+01
64	+7.67E+02	+5.13E-02	+3.04E+02	+8.21E+01
65	+8.23E+02	+8.28E-02	+4.00E+02	+1.09E+02
66	+8.51E+02	+4.93E-02	+4.79E+02	+1.31E+02
67	+8.95E+02	+5.26E-02	+5.91E+02	+1.62E+02
68	+9.38E+02	+5.68E-02	+7.24E+02	+2.00E+02
69	+1.00E+03	+5.21E-02	+9.03E+02	+2.50E+02
70	+1.16E+03	+4.02E-02	+1.55E+03	+4.32E+02
71	+1.22E+03	+3.55E-02	+1.86E+03	+5.20E+02
72	+1.28E+03	+3.67E-02	+2.19E+03	+6.13E+02
73	+1.35E+03	+3.83E-02	+2.58E+03	+7.22E+02
74	+1.43E+03	+3.65E-02	+2.95E+03	+8.26E+02
75	+1.50E+03	+3.76E-02	+3.54E+03	+9.92E+02
76	+1.58E+03	+2.99E-02	+4.12E+03	+1.15E+03
77	+1.67E+03	+3.00E-02	+4.87E+03	+1.36E+03
78	+1.79E+03	+5.10E-02	+5.63E+03	+1.58E+03
79	+1.87E+03	+3.79E-02	+6.50E+03	+1.82E+03
80	+1.96E+03	+3.48E-02	+7.28E+03	+2.04E+03
81	+2.07E+03	+3.41E-02	+8.38E+03	+2.34E+03
82	+2.18E+03	+3.12E-02	+9.23E+03	+2.58E+03
83	+2.32E+03	+3.87E-02	+1.10E+04	+3.07E+03
84	+2.43E+03	+3.68E-02	+1.23E+04	+3.43E+03
85	+2.53E+03	+3.72E-02	+1.35E+04	+3.77E+03
86	+2.61E+03	+2.92E-02	+1.48E+04	+4.13E+03
87	+2.67E+03	+2.09E-02	+1.60E+04	+4.45E+03
88	+2.74E+03	+3.08E-02	+1.65E+04	+4.60E+03
89	+2.76E+03	+1.95E-02	+1.65E+04	+4.59E+03
90	+2.81E+03	+1.88E-02	+1.65E+04	+4.58E+03
91	+2.86E+03	+3.72E-02	+1.58E+04	+4.37E+03
92	+2.91E+03	+2.31E-02	+1.49E+04	+4.10E+03
93	+3.01E+03	+1.79E-02	+1.29E+04	+3.52E+03
94	+3.07E+03	+1.91E-02	+1.22E+04	+3.29E+03
95	+3.16E+03	+2.36E-02	+1.23E+04	+3.31E+03
96	+3.25E+03	+2.53E-02	+1.27E+04	+3.42E+03
97	+3.40E+03	+4.86E-02	+1.42E+04	+3.81E+03
98	+3.55E+03	+5.18E-02	+1.54E+04	+4.10E+03
99	+3.73E+03	+4.37E-02	+1.73E+04	+4.61E+03
100	+3.90E+03	+3.70E-02	+1.98E+04	+5.27E+03
101	+4.09E+03	+4.73E-02	+2.22E+04	+5.89E+03
102	+4.26E+03	+4.65E-02	+2.48E+04	+6.56E+03
103	+4.34E+03	+4.20E-02	+2.61E+04	+6.93E+03
104	+4.43E+03	+4.05E-02	+2.73E+04	+7.22E+03
105	+4.62E+03	+4.26E-02	+2.99E+04	+7.87E+03
106	+4.82E+03	+3.53E-02	+3.31E+04	+8.70E+03
107	+5.01E+03	+3.65E-02	+3.68E+04	+9.64E+03
108	+5.23E+03	+3.72E-02	+3.96E+04	+1.03E+04
109	+5.45E+03	+3.57E-02	+4.60E+04	+1.20E+04
110	+5.76E+03	+3.70E-02	+4.74E+04	+1.22E+04
111	+5.86E+03	+4.26E-02	+5.32E+04	+1.38E+04
112	+6.03E+03	+4.68E-02	+5.96E+04	+1.55E+04
113	+6.22E+03	+4.26E-02	+6.47E+04	+1.68E+04
114	+6.43E+03	+4.04E-02	+7.19E+04	+1.87E+04
115	+6.62E+03	+3.66E-02	+7.76E+04	+2.02E+04

échantillon: Zr.65 Ag.35 masse: 3.168 g

état: brut (300K)

	T (mK)	ΔT/T(%)	mc(erg/K)	Cp(erg/gK)
1	+6.26E+01	+1.42E-01	+3.84E+00	+7.36E-01
2	+6.22E+01	+1.14E-01	+3.65E+00	+6.77E-01
3	+6.33E+01	+1.45E-01	+3.79E+00	+7.24E-01
4	+6.25E+01	+1.07E-01	+3.92E+00	+7.62E-01
5	+6.47E+01	+1.47E-01	+3.90E+00	+7.58E-01
6	+6.62E+01	+1.45E-01	+3.73E+00	+7.06E-01
7	+7.05E+01	+7.73E-02	+3.68E+00	+6.91E-01
8	+7.35E+01	+6.78E-02	+3.98E+00	+7.85E-01
9	+7.64E+01	+7.99E-02	+3.82E+00	+7.29E-01
10	+7.96E+01	+7.67E-02	+3.71E+00	+6.88E-01
11	+8.36E+01	+8.91E-02	+3.83E+00	+7.18E-01
12	+8.87E+01	+7.86E-02	+3.91E+00	+7.27E-01
13	+9.26E+01	+8.89E-02	+4.01E+00	+7.49E-01
14	+9.71E+01	+8.48E-02	+4.18E+00	+7.86E-01
15	+1.02E+02	+7.68E-02	+4.25E+00	+7.92E-01
16	+1.06E+02	+7.59E-02	+4.46E+00	+8.41E-01
17	+1.11E+02	+9.24E-02	+4.50E+00	+8.34E-01
18	+1.17E+02	+9.85E-02	+4.76E+00	+8.91E-01
19	+1.23E+02	+9.89E-02	+5.02E+00	+9.48E-01
20	+1.28E+02	+1.03E-01	+5.21E+00	+9.85E-01
21	+1.34E+02	+7.64E-02	+5.65E+00	+1.10E+00
22	+1.40E+02	+8.73E-02	+5.68E+00	+1.08E+00
23	+1.46E+02	+8.29E-02	+6.01E+00	+1.16E+00
24	+1.52E+02	+8.74E-02	+6.02E+00	+1.14E+00
25	+1.61E+02	+1.02E-01	+6.63E+00	+1.29E+00
26	+1.69E+02	+1.17E-01	+6.91E+00	+1.34E+00
27	+1.76E+02	+8.12E-02	+7.46E+00	+1.48E+00
28	+1.84E+02	+6.81E-02	+7.55E+00	+1.47E+00
29	+1.93E+02	+7.46E-02	+7.91E+00	+1.55E+00
30	+2.04E+02	+7.11E-02	+8.47E+00	+1.67E+00
31	+2.13E+02	+7.08E-02	+9.11E+00	+1.83E+00
32	+2.24E+02	+7.25E-02	+9.80E+00	+2.00E+00
33	+2.34E+02	+6.74E-02	+1.08E+01	+2.28E+00
34	+2.40E+02	+9.91E-02	+1.13E+01	+2.41E+00
35	+2.49E+02	+5.33E-02	+1.26E+01	+2.75E+00
36	+2.63E+02	+5.87E-02	+1.41E+01	+3.16E+00
37	+2.75E+02	+5.88E-02	+1.56E+01	+3.59E+00
38	+2.86E+02	+1.09E-01	+3.13E+01	+8.49E+00
39	+2.88E+02	+1.09E-01	+1.86E+01	+4.47E+00
40	+2.87E+02	+5.22E-02	+1.77E+01	+4.17E+00
41	+2.96E+02	+5.14E-02	+2.02E+01	+4.93E+00
42	+3.03E+02	+1.06E-01	+2.11E+01	+5.17E+00
43	+3.13E+02	+7.32E-02	+2.60E+01	+6.68E+00
44	+3.28E+02	+8.90E-02	+2.83E+01	+7.32E+00
45	+3.37E+02	+5.99E-02	+3.52E+01	+9.42E+00
46	+3.57E+02	+5.39E-02	+4.67E+01	+1.30E+01
47	+3.68E+02	+5.90E-02	+5.52E+01	+1.56E+01
48	+3.86E+02	+6.30E-02	+6.88E+01	+1.97E+01
49	+4.03E+02	+6.78E-02	+8.25E+01	+2.40E+01
50	+4.30E+02	+7.07E-02	+1.12E+02	+3.31E+01
51	+4.47E+02	+4.70E-02	+1.39E+02	+4.14E+01
52	+4.70E+02	+4.72E-02	+1.78E+02	+5.35E+01
53	+4.95E+02	+3.57E-02	+2.24E+02	+6.78E+01
54	+5.17E+02	+4.05E-02	+2.74E+02	+8.36E+01
55	+5.46E+02	+4.56E-02	+3.39E+02	+1.04E+02
56	+5.77E+02	+5.25E-02	+4.30E+02	+1.32E+02
57	+5.98E+02	+3.89E-02	+4.93E+02	+1.52E+02
58	+6.32E+02	+5.24E-02	+6.21E+02	+1.92E+02
59	+6.74E+02	+5.21E-02	+7.80E+02	+2.42E+02

60	+6.97E+02	+4.62E-02	+8.78E+02	+2.72E+02
61	+7.27E+02	+4.56E-02	+9.92E+02	+3.08E+02
62	+7.55E+02	+2.78E-02	+1.16E+03	+3.61E+02
63	+7.99E+02	+3.36E-02	+1.35E+03	+4.21E+02
64	+8.48E+02	+3.57E-02	+1.63E+03	+5.07E+02
65	+8.95E+02	+3.61E-02	+1.89E+03	+5.88E+02
66	+9.50E+02	+3.65E-02	+2.25E+03	+7.02E+02
67	+1.01E+03	+3.25E-02	+2.62E+03	+8.17E+02
68	+1.05E+03	+3.35E-02	+2.87E+03	+8.96E+02
69	+1.11E+03	+3.61E-02	+3.34E+03	+1.04E+03
70	+1.19E+03	+4.27E-02	+4.03E+03	+1.26E+03
71	+1.30E+03	+5.50E-02	+4.87E+03	+1.52E+03
72	+1.41E+03	+4.79E-02	+5.63E+03	+1.76E+03
73	+1.50E+03	+4.90E-02	+6.37E+03	+1.98E+03
74	+1.58E+03	+7.41E-02	+6.06E+03	+1.88E+03
75	+1.70E+03	+5.81E-02	+6.85E+03	+2.12E+03
76	+1.75E+03	+3.40E-02	+6.08E+03	+1.88E+03
77	+1.80E+03	+4.65E-02	+6.27E+03	+1.93E+03
78	+1.86E+03	+4.25E-02	+5.75E+03	+1.77E+03
79	+1.91E+03	+5.35E-02	+6.07E+03	+1.86E+03
80	+1.96E+03	+3.29E-02	+5.59E+03	+1.71E+03
81	+2.02E+03	+3.97E-02	+5.72E+03	+1.75E+03
82	+2.09E+03	+5.01E-02	+5.04E+03	+1.52E+03
83	+2.14E+03	+5.61E-02	+5.44E+03	+1.64E+03
84	+2.18E+03	+3.26E-02	+5.38E+03	+1.62E+03
85	+2.25E+03	+4.53E-02	+5.94E+03	+1.79E+03
86	+2.36E+03	+3.19E-02	+6.37E+03	+1.91E+03
87	+2.48E+03	+2.99E-02	+7.18E+03	+2.15E+03
88	+2.60E+03	+3.19E-02	+7.81E+03	+2.33E+03
89	+2.74E+03	+3.06E-02	+8.48E+03	+2.52E+03
90	+2.87E+03	+2.89E-02	+9.30E+03	+2.76E+03
91	+3.01E+03	+2.87E-02	+1.01E+04	+2.97E+03
92	+3.15E+03	+3.53E-02	+1.10E+04	+3.24E+03
93	+3.31E+03	+3.85E-02	+1.20E+04	+3.52E+03
94	+3.47E+03	+3.83E-02	+1.37E+04	+3.99E+03
95	+3.65E+03	+3.79E-02	+1.49E+04	+4.34E+03
96	+3.83E+03	+4.41E-02	+1.73E+04	+5.03E+03
97	+4.02E+03	+3.71E-02	+1.93E+04	+5.58E+03
98	+4.23E+03	+3.42E-02	+2.24E+04	+6.48E+03
99	+4.43E+03	+3.27E-02	+2.58E+04	+7.47E+03
100	+4.62E+03	+3.32E-02	+2.72E+04	+7.81E+03

echantillon: Zr.76 Cu.24

masse: 1.996 g

etat: brut(77K)

	T (mK)	ΔT/T(%)	mc(erg/K)	Cp(erg/gK)
1	+4.795E+01	+6.90E+00	+5.997E+00	+2.058E+00
2	+4.737E+01	+4.40E+00	+5.942E+00	+2.012E+00
3	+4.920E+01	+6.76E+00	+5.965E+00	+2.076E+00
4	+4.868E+01	+5.07E+00	+6.024E+00	+2.092E+00
5	+4.893E+01	+6.78E+00	+5.976E+00	+2.075E+00
6	+5.119E+01	+6.78E+00	+5.717E+00	+1.997E+00
7	+5.332E+01	+6.51E+00	+5.710E+00	+2.030E+00
8	+5.487E+01	+7.72E+00	+5.851E+00	+2.121E+00
9	+5.762E+01	+7.49E+00	+5.747E+00	+2.097E+00
10	+6.047E+01	+7.28E+00	+5.630E+00	+2.057E+00
11	+6.329E+01	+7.16E+00	+5.472E+00	+1.989E+00
12	+6.481E+01	+5.68E+00	+5.383E+00	+1.948E+00
13	+6.717E+01	+5.58E+00	+5.296E+00	+1.908E+00
14	+7.077E+01	+6.14E+00	+5.136E+00	+1.828E+00
15	+7.410E+01	+6.60E+00	+5.070E+00	+1.789E+00
16	+7.691E+01	+6.67E+00	+4.834E+00	+1.664E+00
17	+7.930E+01	+6.21E+00	+5.034E+00	+1.758E+00
18	+8.271E+01	+5.72E+00	+5.238E+00	+1.847E+00
19	+8.709E+01	+9.29E+00	+4.805E+00	+1.612E+00
20	+9.110E+01	+5.26E+00	+5.075E+00	+1.728E+00
21	+9.590E+01	+5.05E+00	+5.013E+00	+1.671E+00
22	+9.926E+01	+5.70E+00	+5.149E+00	+1.721E+00
23	+1.035E+02	+6.15E+00	+5.343E+00	+1.793E+00
24	+1.083E+02	+6.60E+00	+5.435E+00	+1.809E+00
25	+1.136E+02	+6.98E+00	+5.519E+00	+1.817E+00
26	+1.181E+02	+7.39E+00	+5.571E+00	+1.814E+00
27	+1.231E+02	+7.07E+00	+5.584E+00	+1.787E+00
28	+1.296E+02	+7.56E+00	+6.072E+00	+1.988E+00
29	+1.352E+02	+7.24E+00	+6.081E+00	+1.953E+00
30	+1.418E+02	+8.43E+00	+6.637E+00	+2.186E+00
31	+1.482E+02	+9.18E+00	+6.562E+00	+2.103E+00
32	+1.555E+02	+9.54E+00	+6.686E+00	+2.113E+00
33	+1.610E+02	+5.09E+00	+7.266E+00	+2.364E+00
34	+1.701E+02	+5.87E+00	+6.951E+00	+2.141E+00
35	+1.776E+02	+6.19E+00	+7.215E+00	+2.219E+00
36	+1.859E+02	+5.30E+00	+8.045E+00	+2.574E+00
37	+1.943E+02	+6.28E+00	+8.123E+00	+2.552E+00
38	+2.029E+02	+5.63E+00	+8.690E+00	+2.772E+00
39	+2.137E+02	+7.01E+00	+9.090E+00	+2.892E+00
40	+2.246E+02	+7.55E+00	+9.171E+00	+2.851E+00
41	+2.362E+02	+7.60E+00	+9.739E+00	+3.048E+00
42	+2.476E+02	+7.56E+00	+1.060E+01	+3.391E+00
43	+2.612E+02	+8.30E+00	+1.098E+01	+3.474E+00
44	+2.717E+02	+9.17E+00	+1.114E+01	+3.474E+00
45	+2.862E+02	+1.09E+01	+1.150E+01	+3.534E+00
46	+2.986E+02	+9.35E+00	+1.280E+01	+4.082E+00
47	+3.137E+02	+1.03E+01	+1.384E+01	+4.478E+00
48	+3.289E+02	+1.12E+01	+1.449E+01	+4.669E+00
49	+3.444E+02	+1.24E+01	+1.490E+01	+4.735E+00
50	+3.579E+02	+1.12E+01	+1.580E+01	+5.065E+00
51	+3.753E+02	+1.00E+01	+1.687E+01	+5.433E+00
52	+3.948E+02	+1.06E+01	+1.893E+01	+6.274E+00
53	+4.133E+02	+1.02E+01	+1.874E+01	+5.987E+00
54	+4.331E+02	+1.07E+01	+2.047E+01	+6.639E+00
55	+4.518E+02	+9.98E+00	+2.464E+01	+8.516E+00
56	+4.776E+02	+1.15E+01	+2.607E+01	+8.930E+00
57	+4.989E+02	+1.08E+01	+2.653E+01	+8.897E+00
58	+5.247E+02	+1.16E+01	+2.931E+01	+9.949E+00
59	+5.492E+02	+1.16E+01	+3.368E+01	+1.180E+01
60	+5.747E+02	+1.11E+01	+3.902E+01	+1.411E+01
61	+5.980E+02	+5.00E+00	+4.774E+01	+1.811E+01

62	+6.268E+02	+5.25E+00	+5.428E+01	+2.092E+01
63	+6.591E+02	+5.59E+00	+6.786E+01	+2.716E+01
64	+6.896E+02	+5.88E+00	+7.831E+01	+3.183E+01
65	+7.254E+02	+6.33E+00	+9.681E+01	+4.037E+01
66	+7.637E+02	+7.44E+00	+1.258E+02	+5.408E+01
67	+8.035E+02	+8.39E+00	+1.483E+02	+6.443E+01
68	+8.398E+02	+7.64E+00	+1.981E+02	+8.846E+01
69	+8.835E+02	+8.23E+00	+2.446E+02	+1.106E+02
70	+9.266E+02	+8.40E+00	+2.940E+02	+1.340E+02
71	+9.749E+02	+9.23E+00	+3.812E+02	+1.762E+02
72	+1.027E+03	+1.02E+01	+4.350E+02	+2.013E+02
73	+1.060E+03	+6.96E+00	+5.509E+02	+2.581E+02
74	+1.112E+03	+6.72E+00	+6.803E+02	+3.209E+02
75	+1.163E+03	+6.64E+00	+7.896E+02	+3.733E+02
76	+1.221E+03	+6.87E+00	+9.702E+02	+4.610E+02
77	+1.286E+03	+7.75E+00	+1.148E+03	+5.467E+02
78	+1.347E+03	+7.67E+00	+1.329E+03	+6.338E+02
79	+1.411E+03	+7.25E+00	+1.565E+03	+7.479E+02
80	+1.490E+03	+6.59E+00	+1.865E+03	+8.929E+02
81	+1.553E+03	+3.35E+00	+2.200E+03	+1.056E+03
82	+1.638E+03	+3.25E+00	+2.582E+03	+1.239E+03
83	+1.728E+03	+3.48E+00	+3.047E+03	+1.464E+03
84	+1.809E+03	+3.10E+00	+3.628E+03	+1.746E+03
85	+1.897E+03	+2.58E+00	+4.165E+03	+2.005E+03
86	+2.003E+03	+3.40E+00	+4.789E+03	+2.304E+03
87	+2.105E+03	+4.67E+00	+5.059E+03	+2.424E+03
88	+2.225E+03	+4.33E+00	+6.194E+03	+2.973E+03
89	+2.356E+03	+4.69E+00	+7.194E+03	+3.450E+03
90	+2.462E+03	+1.95E+00	+8.276E+03	+3.970E+03
91	+2.611E+03	+2.38E+00	+9.601E+03	+4.600E+03
92	+2.766E+03	+2.24E+00	+1.123E+04	+5.376E+03
93	+2.932E+03	+2.11E+00	+1.289E+04	+6.157E+03
94	+3.110E+03	+1.96E+00	+1.472E+04	+7.018E+03
95	+3.310E+03	+2.39E+00	+1.233E+04	+5.744E+03
96	+3.229E+03	+2.18E+00	+1.384E+04	+6.529E+03
97	+3.400E+03	+2.87E+00	+1.000E+04	+4.539E+03
98	+3.479E+03	+2.73E+00	+1.026E+04	+4.633E+03
99	+3.563E+03	+2.51E+00	+1.091E+04	+4.921E+03
100	+3.787E+03	+2.54E+00	+1.218E+04	+5.444E+03
101	+3.978E+03	+2.47E+00	+1.392E+04	+6.207E+03
102	+4.179E+03	+2.42E+00	+1.547E+04	+6.855E+03
103	+4.389E+03	+2.28E+00	+1.755E+04	+7.754E+03
104	+4.675E+03	+2.17E+00	+1.962E+04	+8.567E+03
105	+4.933E+03	+2.48E+00	+2.281E+04	+9.937E+03
106	+5.287E+03	+3.18E+00	+2.670E+04	+1.153E+04
107	+5.607E+03	+3.60E+00	+3.112E+04	+1.338E+04
108	+5.979E+03	+3.23E+00	+3.726E+04	+1.598E+04
109	+6.332E+03	+3.07E+00	+4.160E+04	+1.764E+04
110	+6.770E+03	+2.53E+00	+5.249E+04	+2.237E+04
111	+3.684E+03	+2.43E+00	+1.092E+04	+4.862E+03
112	+3.872E+03	+2.50E+00	+1.211E+04	+5.358E+03
113	+4.082E+03	+2.37E+00	+1.412E+04	+6.240E+03
114	+4.311E+03	+2.29E+00	+1.582E+04	+6.939E+03
115	+4.557E+03	+2.19E+00	+1.762E+04	+7.658E+03
116	+4.820E+03	+2.01E+00	+2.057E+04	+8.917E+03
117	+5.111E+03	+2.04E+00	+2.291E+04	+9.817E+03
118	+5.420E+03	+1.90E+00	+2.715E+04	+1.161E+04

echantillon: Zr .76 Cu.24 masse:

etat : vieilli 70 j 300 K + recuit 1h 200°c

	T (mK)	ΔT/T(%)	mc(erg/K)	Cp(erg/gK)
1	5.049E+01	2.169E+00	5.375E+01	2.068E+00
2	5.701E+01	1.960E+00	5.884E+01	2.025E+00
3	6.083E+01	1.931E+00	5.929E+01	1.740E+00
4	6.166E+01	1.835E+00	6.383E+01	1.871E+00
5	6.753E+01	1.914E+00	7.072E+01	1.862E+00
6	7.590E+01	1.959E+00	8.201E+01	1.881E+00
7	8.855E+01	1.900E+00	9.392E+01	1.915E+00
8	9.899E+01	2.019E+00	1.045E+02	1.771E+00
9	1.111E+02	2.205E+00	1.173E+02	2.042E+00
10	1.251E+02	2.062E+00	1.343E+02	2.258E+00
11	1.432E+02	2.157E+00	1.536E+02	2.184E+00
12	1.610E+02	2.551E+00	1.739E+02	2.405E+00
13	1.865E+02	2.743E+00	1.992E+02	2.747E+00
14	2.104E+02	3.068E+00	2.242E+02	2.779E+00
15	2.379E+02	3.252E+00	2.488E+02	2.839E+00
16	2.656E+02	2.901E+00	2.865E+02	2.899E+00
17	3.055E+02	3.240E+00	3.274E+02	3.873E+00
18	3.512E+02	4.621E+00	3.784E+02	4.927E+00
19	4.026E+02	5.374E+00	4.325E+02	5.930E+00
20	4.651E+02	5.892E+00	4.991E+02	7.357E+00
21	5.361E+02	1.010E+01	5.729E+02	1.398E+01
22	6.179E+02	1.917E+01	6.628E+02	2.609E+01
23	6.970E+02	3.525E+01	7.441E+02	5.350E+01
24	8.074E+02	7.503E+01	8.872E+02	1.183E+02
25	9.363E+02	1.554E+02	1.006E+03	2.097E+02
26	1.086E+03	2.881E+02	1.169E+03	3.817E+02
27	1.247E+03	4.899E+02	1.341E+03	6.365E+02
28	1.450E+03	8.455E+02	1.552E+03	1.044E+03
29	1.668E+03	1.320E+03	1.788E+03	1.621E+03
30	1.915E+03	1.945E+03	2.039E+03	2.326E+03
31	2.182E+03	2.685E+03	2.333E+03	3.135E+03
32	2.500E+03	3.758E+03	2.678E+03	4.433E+03
33	2.840E+03	5.283E+03	3.016E+03	5.830E+03
34	3.176E+03	5.271E+03	3.305E+03	3.891E+03
35	3.414E+03	3.910E+03	3.550E+03	4.068E+03
36	3.656E+03	4.374E+03	3.790E+03	4.726E+03
37	3.907E+03	5.227E+03	4.074E+03	5.655E+03
38	4.220E+03	5.982E+03	4.371E+03	6.569E+03
39	4.525E+03	6.805E+03	4.694E+03	7.298E+03
40	4.895E+03	8.292E+03	5.111E+03	8.931E+03
41	5.350E+03	9.869E+03	6.794E+07	2.211E+00
42	1.522E+02	8.547E-02	6.882E+00	2.251E+00
43	1.595E+02	4.841E-02	7.729E+00	2.630E+00
44	1.723E+02	5.300E-02	7.624E+00	2.497E+00
45	1.848E+02	5.753E-02	8.418E+00	2.814E+00
46	1.974E+02	6.820E-02	8.687E+00	2.865E+00
47	2.085E+02	5.893E-02	9.518E+00	3.206E+00
48	2.222E+02	6.731E-02	9.126E+00	2.915E+00
49	2.358E+02	6.576E-02	1.026E+01	3.389E+00
50	2.467E+02	8.380E-02	9.625E+00	2.990E+00
51	2.633E+02	9.036E-02	1.003E+01	3.071E+00
52	2.839E+02	9.456E-02	1.037E+01	3.079E+00
53	3.027E+02	8.098E-02	1.136E+01	3.421E+00
54	3.245E+02	8.462E-02	1.304E+01	4.078E+00
55	3.481E+02	6.917E-02	1.487E+01	4.781E+00
56	3.752E+02	7.429E-02	1.605E+01	5.115E+00
57	3.993E+02	6.425E-02	1.744E+01	5.566E+00

58	4.290E+02	6.525E-02	1.919E+01	6.113E+00
59	4.615E+02	7.817E-02	1.985E+01	6.060E+00
60	4.953E+02	8.156E-02	2.364E+01	7.521E+00
61	5.321E+02	7.943E-02	3.012E+01	1.025E+01
62	5.688E+02	8.075E-02	3.898E+01	1.412E+01
63	6.137E+02	6.890E-02	5.082E+01	1.928E+01
64	6.584E+02	6.570E-02	6.624E+01	2.616E+01
65	6.924E+02	4.268E-02	8.618E+01	3.545E+01
66	7.394E+02	4.155E-02	1.243E+02	5.349E+01
67	8.025E+02	4.193E-02	1.702E+02	7.488E+01
68	8.824E+02	4.367E-02	2.602E+02	1.175E+02
69	9.316E+02	4.047E-02	3.377E+02	1.547E+02
70	1.001E+03	4.535E-02	4.485E+02	2.076E+02
71	1.081E+03	5.190E-02	6.123E+02	2.862E+02
72	1.165E+03	4.880E-02	8.061E+02	3.792E+02
73	1.243E+03	4.013E-02	1.020E+03	4.822E+02
74	1.337E+03	3.986E-02	1.337E+03	6.348E+02
75	1.445E+03	4.459E-02	1.778E+03	8.478E+02
76	1.548E+03	4.744E-02	2.184E+03	1.042E+03
77	1.664E+03	3.582E-02	2.734E+03	1.306E+03
78	1.784E+03	3.386E-02	3.371E+03	1.612E+03
79	1.911E+03	2.624E-02	4.061E+03	1.942E+03
80	2.034E+03	2.465E-02	4.874E+03	2.331E+03
81	2.182E+03	2.299E-02	5.683E+03	2.712E+03

ADDENDA : $Cp = \sum_{i}^{6}{}_{0} a_i T^i$

a6	.005360794230	a3	.591190128721
a5	.003133557977	a1	2.235146826266
a4	-.071361858998	a0	3.442134506469
a3	-.042944567758		

T(mK)	C(exper.) erg/K	C (calcul) erg/K	ΔC/C
45.92244,	1.87067,	2.03058,	.07875,
47.37321,	1.89745,	1.92602,	.01483,
51.41024,	1.78832,	1.72272,	-.03808,
60.30962,	1.58163,	1.52571,	-.03665,
75.29276,	1.55271,	1.50322,	-.03293,
50.99100,	1.85120,	1.73915,	-.06443,
50.42200,	1.68720,	1.76295,	.04297,
57.06500,	1.73670,	1.57121,	-.10533,
65.30800,	1.54620,	1.49191,	-.03639,
70.43200,	1.44520,	1.48789,	.02869,
75.51300,	1.47640,	1.50425,	.01852,
80.72300,	1.46210,	1.53556,	.04784,
84.88500,	1.56450,	1.56827,	.00240,
92.39700,	1.51400,	1.63973,	.07668,
95.96500,	1.64990,	1.67788,	.01667,
99.56900,	1.61400,	1.71852,	.06082,
103.21000,	1.71840,	1.76138,	.02440,
109.75000,	1.85610,	1.84199,	-.00766,
114.02000,	1.87900,	1.89662,	.00929,
118.78000,	1.93790,	1.95896,	.01075,
126.44000,	2.09930,	2.06180,	-.01819,
138.98000,	2.36400,	2.23481,	-.05781,
174.39000,	2.81450,	2.73960,	-.02734,
196.68000,	3.24380,	3.06455,	-.05849,
219.96000,	3.54610,	3.40986,	-.03996,
235.24000,	3.71190,	3.64063,	-.01958,
255.91000,	4.00920,	3.95934,	-.01259,
291.95000,	4.43620,	4.53755,	.02234,
355.91000,	5.51100,	5.65702,	.02581,
462.52000,	7.23230,	7.88460,	.08273,
548.12000,	9.96920,	10.09426,	.01239,
710.59000,	15.97000,	15.61481,	-.02275,
812.44000,	19.67400,	20.15844,	.02403,
980.51000,	29.79900,	29.91532,	.00389,
1055.80000,	35.67300,	35.34779,	-.00920,
1179.10000,	47.63100,	45.88695,	-.03801,
1307.40000,	61.27200,	59.29528,	-.03334,
1447.60000,	79.43400,	77.19618,	-.02899,
1612.80000,	104.36000,	103.26116,	-.01064,
1803.40000,	140.90000,	140.99482,	.00067,
1896.30000,	164.09000,	162.71185,	-.00847,
2146.50000,	223.37000,	233.41168,	.04302,
2374.10000,	310.17000,	315.05651,	.01551,
2550.90000,	382.76000,	391.26708,	.02174,
2755.50000,	490.61000,	494.81168,	.00849,
2940.50000,	587.51000,	603.78734,	.02696,
3197.40000,	798.63000,	781.34769,	-.02212,
3491.10000,	1020.20000,	1024.93675,	.00462,
3590.10000,	1115.70000,	1117.47183,	.00159,
3878.40000,	1407.00000,	1418.84547,	.00835,
4176.50000,	1839.60000,	1783.41607,	-.03150,
4409.60000,	2176.40000,	2108.51728,	-.03219,
4685.00000,	2531.40000,	2540.66428,	.00365,
4965.40000,	3032.70000,	3037.18273,	.00148,
5253.10000,	3629.70000,	3609.40129,	-.00562,
5602.00000,	4280.10000,	4394.00579,	.02592,
5958.60000,	5325.90000,	5305.56293,	-.00383,

LOI D'ETALONNAGE DU THERMOMETRE SILICIUM

$$\text{Log}\,R = A(\text{Log}\,T)^2 + B\,\text{Log}\,T + C$$

N=4
A=-.0498876032 B=-1.20255704 C=13.1244669

T=+1.91E+01	DT/T=+4.72E-03
T=+2.68E+01	DT/T=-1.04E-02
T=+4.00E+01	DT/T=+2.01E-03
T=+4.38E+01	DT/T=+2.32E-03
T=+4.98E+01	DT/T=+1.90E-03
T=+5.41E+01	DT/T=+1.11E-02
T=+6.01E+01	DT/T=-1.15E-02

N=5
A=.0497350468 B=-1.9525021 C=14.5298044

T=+2.68E+01	DT/T=+3.73E-04
T=+4.00E+01	DT/T=-1.46E-03
T=+4.38E+01	DT/T=-1.49E-03
T=+4.98E+01	DT/T=-6.24E-04
T=+5.41E+01	DT/T=+1.09E-02
T=+6.01E+01	DT/T=-8.84E-03
T=+7.33E+01	DT/T=+1.23E-03

N=6
A=.167414554 B=-2.88224714 C=16.362564

T=+4.00E+01	DT/T=+1.27E-03
T=+4.38E+01	DT/T=-1.58E-03
T=+4.98E+01	DT/T=-2.79E-03
T=+5.41E+01	DT/T=+8.74E-03
T=+6.01E+01	DT/T=-9.79E-03
T=+7.33E+01	DT/T=+8.47E-03
T=+8.18E+01	DT/T=-4.15E-03

N=7
A=.327485865 B=-4.18431038 C=19.0046563

T=+4.38E+01	DT/T=+2.91E-03
T=+4.98E+01	DT/T=-3.70E-03
T=+5.41E+01	DT/T=+5.51E-03
T=+6.01E+01	DT/T=-1.35E-02
T=+7.33E+01	DT/T=+1.08E-02
T=+8.18E+01	DT/T=+5.09E-03
T=+9.29E+01	DT/T=-6.81E-03

N=8
A=.462215553 B=-5.32313596 C=21.4056487

T=+4.98E+01	DT/T=+1.27E-03
T=+5.41E+01	DT/T=+6.47E-03
T=+6.01E+01	DT/T=-1.52E-02
T=+7.33E+01	DT/T=+7.26E-03
T=+8.18E+01	DT/T=+4.27E-03
T=+9.29E+01	DT/T=-1.16E-03
T=+1.04E+02	DT/T=-2.66E-03

N=9
A=.448322134 B=-5.20995172 C=21.1766479

T=+5.41E+01	DT/T=+7.36E-03
T=+6.01E+01	DT/T=-1.43E-02
T=+7.33E+01	DT/T=+7.85E-03
T=+8.18E+01	DT/T=+4.23E-03
T=+9.29E+01	DT/T=-2.36E-03
T=+1.04E+02	DT/T=-5.53E-03
T=+1.16E+02	DT/T=+3.02E-03

N=10
A=.503959801 B=-5.73305708 C=22.4006702

T=+6.01E+01	DT/T=-4.55E-03
T=+7.33E+01	DT/T=+1.02E-02
T=+8.18E+01	DT/T=+3.63E-03
T=+9.29E+01	DT/T=-5.68E-03
T=+1.04E+02	DT/T=-1.05E-02
T=+1.16E+02	DT/T=-2.68E-03
T=+1.25E+02	DT/T=+1.03E-02

N=11
A=.200292721 B=-2.94651547 C=16.0174817

T=+7.33E+01	DT/T=-2.12E-03
T=+8.18E+01	DT/T=+3.19E-03
T=+9.29E+01	DT/T=+1.52E-03
T=+1.04E+02	DT/T=-2.66E-03
T=+1.16E+02	DT/T=-1.03E-03
T=+1.25E+02	DT/T=+1.24E-04
T=+1.40E+02	DT/T=+9.87E-04

N=12
A=.167112098 B=-2.62950683 C=15.2613911

T=+8.18E+01	DT/T=+2.07E-04
T=+9.29E+01	DT/T=+7.26E-04
T=+1.04E+02	DT/T=-2.19E-03
T=+1.16E+02	DT/T=-1.10E-05
T=+1.25E+02	DT/T=+1.10E-03
T=+1.40E+02	DT/T=+1.15E-03
T=+1.59E+02	DT/T=-9.77E-04

N=13
A=.21747013 B=-3.11001938 C=16.4063011

T=+9.29E+01	DT/T=+2.07E-03
T=+1.04E+02	DT/T=-2.69E-03
T=+1.16E+02	DT/T=-1.27E-03
T=+1.25E+02	DT/T=-4.50E-05
T=+1.40E+02	DT/T=+1.33E-03
T=+1.59E+02	DT/T=+2.43E-03
T=+1.87E+02	DT/T=-1.81E-03

N=14
A=.240138707 B=-3.33968924 C=16.986874

T=+1.04E+02	DT/T=-1.12E-04
T=+1.16E+02	DT/T=-2.08E-04
T=+1.25E+02	DT/T=+3.82E-05
T=+1.40E+02	DT/T=+4.71E-04
T=+1.59E+02	DT/T=+1.14E-03
T=+1.87E+02	DT/T=-2.45E-03
T=+2.21E+02	DT/T=+1.14E-03

N=15
A=.224059621 B=-3.1779654 C=16.5808553

T=+1.16E+02	DT/T=-8.01E-04
T=+1.25E+02	DT/T=+4.81E-05
T=+1.40E+02	DT/T=+1.01E-03
T=+1.59E+02	DT/T=+1.82E-03
T=+1.87E+02	DT/T=-2.48E-03
T=+2.21E+02	DT/T=-8.98E-04
T=+2.53E+02	DT/T=+1.32E-03

N=16
A=.189598703 B=-2.82248954 C=15.6657811

T=+1.25E+02	DT/T=-1.99E-03
T=+1.40E+02	DT/T=+1.08E-03
T=+1.59E+02	DT/T=+3.35E-03
T=+1.87E+02	DT/T=-7.44E-04
T=+2.21E+02	DT/T=-1.30E-03
T=+2.53E+02	DT/T=-3.17E-03
T=+2.95E+02	DT/T=+2.83E-03

N=17
A=.17051908 B=-2.61748783 C=15.1161203

T=+1.40E+02	DT/T=-1.59E-03
T=+1.59E+02	DT/T=+2.53E-03
T=+1.87E+02	DT/T=+1.21E-05
T=+2.21E+02	DT/T=-2.02E-05
T=+2.53E+02	DT/T=-2.45E-03
T=+2.95E+02	DT/T=+1.45E-03
T=+3.47E+02	DT/T=+8.74E-05

N=18
A=.147717543 B=-2.36793529 C=14.4345067

T=+1.59E+02	DT/T=-3.20E-04
T=+1.87E+02	DT/T=-1.19E-04
T=+2.21E+02	DT/T=+1.36E-03
T=+2.53E+02	DT/T=-9.34E-04
T=+2.95E+02	DT/T=+1.63E-03
T=+3.47E+02	DT/T=-3.09E-03
T=+4.17E+02	DT/T=+1.50E-03

N=19
A=.132010728 B=-2.19221526 C=13.9439488

T=+1.87E+02	DT/T=-1.52E-03
T=+2.21E+02	DT/T=+1.75E-03
T=+2.53E+02	DT/T=+2.28E-04
T=+2.95E+02	DT/T=+2.75E-03
T=+3.47E+02	DT/T=-3.23E-03
T=+4.17E+02	DT/T=-2.07E-03
T=+5.05E+02	DT/T=+2.13E-03

N=20
A=.109654671 B=-1.93244247 C=13.1907517

T=+2.21E+02	DT/T=-1.40E-03
T=+2.53E+02	DT/T=-1.57E-04
T=+2.95E+02	DT/T=+4.37E-03
T=+3.47E+02	DT/T=-1.08E-03
T=+4.17E+02	DT/T=-1.52E-03
T=+5.05E+02	DT/T=-2.19E-03
T=+6.21E+02	DT/T=+2.00E-03

N=21
A=.101988932 B=-1.83981435 C=12.9115189

T=+2.53E+02	DT/T=-2.12E-03
T=+2.95E+02	DT/T=+3.85E-03
T=+3.47E+02	DT/T=-6.21E-04
T=+4.17E+02	DT/T=-5.64E-04
T=+5.05E+02	DT/T=-1.61E-03
T=+6.21E+02	DT/T=+8.73E-04
T=+7.68E+02	DT/T=+2.17E-04

N=22
A=.0814881509 B=-1.58750032 C=12.1368413

T=+2.95E+02	DT/T=-2.75E-04
T=+3.47E+02	DT/T=-1.02E-03
T=+4.17E+02	DT/T=+1.69E-03
T=+5.05E+02	DT/T=+1.12E-03
T=+6.21E+02	DT/T=+1.00E-03
T=+7.68E+02	DT/T=-6.20E-03
T=+9.19E+02	DT/T=+3.73E-03

N=23
A=.0714172871 B=-1.46103291 C=11.7407257

T=+3.47E+02	DT/T=-2.53E-03
T=+4.17E+02	DT/T=+2.22E-03
T=+5.05E+02	DT/T=+2.69E-03
T=+6.21E+02	DT/T=+2.26E-03
T=+7.68E+02	DT/T=-6.91E-03
T=+9.19E+02	DT/T=-6.17E-04
T=+1.11E+03	DT/T=+2.96E-03

N=24
A=.064445184 B=-1.36796616 C=11.4309338

T=+4.17E+02	DT/T=-1.28E-03
T=+5.05E+02	DT/T=+1.60E-03
T=+6.21E+02	DT/T=+2.97E-03
T=+7.68E+02	DT/T=-5.42E-03
T=+9.19E+02	DT/T=+6.68E-04
T=+1.11E+03	DT/T=+2.85E-03
T=+1.24E+03	DT/T=-1.36E-03

N=25
A=.0554085111 B=-1.24693869 C=11.0263604

T=+5.05E+02	DT/T=-8.15E-04
T=+6.21E+02	DT/T=+3.04E-03
T=+7.68E+02	DT/T=-4.20E-03
T=+9.19E+02	DT/T=+1.70E-03
T=+1.11E+03	DT/T=+2.24E-03
T=+1.24E+03	DT/T=-3.55E-03
T=+1.32E+03	DT/T=+1.63E-03

N=26
A=.0465358733 B=-1.12559837 C=10.6120142

T=+6.21E+02	DT/T=+1.26E-03
T=+7.68E+02	DT/T=-3.89E-03
T=+9.19E+02	DT/T=+2.74E-03
T=+1.11E+03	DT/T=+2.70E-03
T=+1.24E+03	DT/T=-4.00E-03
T=+1.32E+03	DT/T=+4.02E-04
T=+1.39E+03	DT/T=+8.13E-04

N=27
A=.0542823004 B=-1.23575014 C=11.0031141

T=+7.68E+02	DT/T=-1.50E-03
T=+9.19E+02	DT/T=+3.03E-03
T=+1.11E+03	DT/T=+1.82E-03
T=+1.24E+03	DT/T=-5.04E-03
T=+1.32E+03	DT/T=-5.61E-04
T=+1.39E+03	DT/T=+3.53E-05
T=+1.50E+03	DT/T=+2.24E-03

N=28
A=.0187291356 B=-.731361684 C=9.21497141

T=+9.19E+02	DT/T=-6.52E-04
T=+1.11E+03	DT/T=+3.06E-03
T=+1.24E+03	DT/T=-3.42E-03
T=+1.32E+03	DT/T=+5.17E-04
T=+1.39E+03	DT/T=+9.02E-05
T=+1.50E+03	DT/T=+5.03E-05
T=+1.59E+03	DT/T=+3.61E-04

N=29
A=-6.11851723E-03B=-.37156426 C=7.91285278

T=+1.11E+03	DT/T=+1.21E-03
T=+1.24E+03	DT/T=-3.38E-03
T=+1.32E+03	DT/T=+1.13E-03
T=+1.39E+03	DT/T=+8.74E-04
T=+1.50E+03	DT/T=+5.28E-04
T=+1.59E+03	DT/T=+1.83E-04
T=+1.72E+03	DT/T=-5.40E-04

N=30
A=.0280765866 B=-.87260092 C=9.74775803

T=+1.24E+03	DT/T=-1.30E-03
T=+1.32E+03	DT/T=+1.68E-03
T=+1.39E+03	DT/T=+4.96E-04
T=+1.50E+03	DT/T=-3.92E-04
T=+1.59E+03	DT/T=-5.85E-04
T=+1.72E+03	DT/T=-3.05E-04
T=+1.87E+03	DT/T=+4.09E-04

N=31
A=7.91627472E-03B=-.574154246 C=8.64348391

T=+1.32E+03	DT/T=+1.70E-04
T=+1.39E+03	DT/T=-1.06E-04
T=+1.50E+03	DT/T=-1.75E-04
T=+1.59E+03	DT/T=-7.11E-05
T=+1.72E+03	DT/T=+1.40E-04
T=+1.87E+03	DT/T=+2.00E-04
T=+1.99E+03	DT/T=-1.58E-04

N=32
A=.0134311184 B=-.65597476 C=8.94690714

T=+1.39E+03	DT/T=+1.52E-04
T=+1.50E+03	DT/T=-1.72E-04
T=+1.59E+03	DT/T=-1.72E-04
T=+1.72E+03	DT/T=+2.74E-05
T=+1.87E+03	DT/T=+2.33E-04
T=+1.99E+03	DT/T=+9.53E-05
T=+2.16E+03	DT/T=-1.64E-04

N=33
A=.0197428463 B=-.750680791 C=9.30208462

T=+1.50E+03	DT/T=+1.28E-04
T=+1.59E+03	DT/T=-1.23E-04
T=+1.72E+03	DT/T=-1.19E-04
T=+1.87E+03	DT/T=+6.29E-05
T=+1.99E+03	DT/T=+3.12E-05
T=+2.16E+03	DT/T=+9.49E-05
T=+2.36E+03	DT/T=-7.47E-05

N=34
A=.0226095881 B=-.794149885 C=9.46683085

T=+1.59E+03	DT/T=+6.79E-05
T=+1.72E+03	DT/T=-9.41E-05
T=+1.87E+03	DT/T=-3.33E-06
T=+1.99E+03	DT/T=-4.95E-05
T=+2.16E+03	DT/T=+7.47E-05
T=+2.36E+03	DT/T=+6.59E-05
T=+2.59E+03	DT/T=-6.15E-05

N=35
A=.0237006037 B=-.811057477 C=9.53230046

T=+1.72E+03	DT/T=+3.92E-05
T=+1.87E+03	DT/T=+3.13E-05
T=+1.99E+03	DT/T=-7.01E-05
T=+2.16E+03	DT/T=+7.59E-06
T=+2.36E+03	DT/T=-1.24E-05
T=+2.59E+03	DT/T=-1.12E-04
T=+2.77E+03	DT/T=+1.16E-04

N=36
A=.0203253388 B=-.759115751 C=9.33252643

T=+1.87E+03 DT/T=-3.57E-05
T=+1.99E+03 DT/T=-1.59E-05
T=+2.16E+03 DT/T=+1.36E-04
T=+2.36E+03 DT/T=+7.74E-05
T=+2.59E+03 DT/T=-1.85E-04
T=+2.77E+03 DT/T=-1.71E-04
T=+2.98E+03 DT/T=+1.95E-04

N=37
A=.0141014671 B=-.662442075 C=8.95722453

T=+1.99E+03 DT/T=-2.02E-04
T=+2.16E+03 DT/T=+2.55E-04
T=+2.36E+03 DT/T=+3.02E-04
T=+2.59E+03 DT/T=-7.76E-05
T=+2.77E+03 DT/T=-3.12E-04
T=+2.98E+03 DT/T=-3.43E-04
T=+3.27E+03 DT/T=+3.79E-04

N=38
A=6.08701006E-03B=-.536032239 C=8.45889209

T=+2.16E+03 DT/T=-2.33E-04
T=+2.36E+03 DT/T=+3.29E-04
T=+2.59E+03 DT/T=+1.90E-04
T=+2.77E+03 DT/T=-5.94E-05
T=+2.98E+03 DT/T=-2.86E-04
T=+3.27E+03 DT/T=-1.26E-04
T=+3.61E+03 DT/T=+1.85E-04

N=39
A=4.20014876E-03B=-.505625887 C=8.33643093

T=+2.36E+03 DT/T=+5.37E-05
T=+2.59E+03 DT/T=+1.04E-04
T=+2.77E+03 DT/T=-4.83E-05
T=+2.98E+03 DT/T=-2.18E-04
T=+3.27E+03 DT/T=-4.73E-05
T=+3.61E+03 DT/T=+1.92E-04
T=+3.89E+03 DT/T=-3.58E-05

N=40
A=-.0100002955 B=-.277633558 C=7.42154686

T=+2.59E+03 DT/T=-2.90E-04
T=+2.77E+03 DT/T=+1.68E-04
T=+2.98E+03 DT/T=+2.95E-04
T=+3.27E+03 DT/T=+3.52E-04
T=+3.61E+03 DT/T=-1.33E-04
T=+3.89E+03 DT/T=-1.32E-03
T=+4.18E+03 DT/T=+9.30E-04

N=41
A=-.0233967995 B=-.059950001 C=6.53747145

T=+2.77E+03 DT/T=-5.15E-04
T=+2.98E+03 DT/T=+3.21E-04
T=+3.27E+03 DT/T=+8.36E-04
T=+3.61E+03 DT/T=+2.41E-04
T=+3.89E+03 DT/T=-1.41E-03
T=+4.18E+03 DT/T=+5.16E-05
T=+4.51E+03 DT/T=+4.72E-04

N=42
A=-.0171124737 B=-.161659954 C=6.94881172

T=+2.98E+03 DT/T=-1.97E-06
T=+3.27E+03 DT/T=+3.89E-04
T=+3.61E+03 DT/T=-6.32E-05
T=+3.89E+03 DT/T=-1.43E-03
T=+4.18E+03 DT/T=+4.68E-04
T=+4.51E+03 DT/T=+1.48E-03
T=+4.88E+03 DT/T=-8.46E-04

N=43
A=3.97425064E-03B=-.509973757 C=8.3868704

T=+3.27E+03 DT/T=+9.69E-04
T=+3.61E+03 DT/T=-5.56E-04
T=+3.89E+03 DT/T=-2.14E-03
T=+4.18E+03 DT/T=+5.95E-05
T=+4.51E+03 DT/T=+1.93E-03
T=+4.88E+03 DT/T=+1.02E-03
T=+5.30E+03 DT/T=-1.28E-03

N=43
A=3.97425064E-03B=-.509973757 C=8.3868704

T=+3.27E+03 DT/T=+9.69E-04
T=+3.61E+03 DT/T=-5.56E-04
T=+3.89E+03 DT/T=-2.14E-03
T=+4.18E+03 DT/T=+5.95E-05
T=+4.51E+03 DT/T=+1.93E-03
T=+4.88E+03 DT/T=+1.02E-03
T=+5.30E+03 DT/T=-1.28E-03

N=44
A=.0350656635 B=-1.03198709 C=10.5775374

T=+3.61E+03 DT/T=+1.33E-03
T=+3.89E+03 DT/T=-1.92E-03
T=+4.18E+03 DT/T=-6.97E-04
T=+4.51E+03 DT/T=+9.73E-04
T=+4.88E+03 DT/T=+7.16E-04
T=+5.30E+03 DT/T=+1.69E-05
T=+5.77E+03 DT/T=-4.09E-04

N=45
A=.0416293514 B=-1.14534204 C=11.066675

T=+3.89E+03 DT/T=-5.46E-04
T=+4.18E+03 DT/T=-1.99E-05
T=+4.51E+03 DT/T=+1.08E-03
T=+4.88E+03 DT/T=+3.94E-04
T=+5.30E+03 DT/T=-5.60E-04
T=+5.77E+03 DT/T=-1.04E-03
T=+6.29E+03 DT/T=+6.99E-04

N=46
A=.0183170123 B=-.747482989 C=9.36951004

T=+4.18E+03 DT/T=-1.23E-03
T=+4.51E+03 DT/T=+1.12E-03
T=+4.88E+03 DT/T=+1.10E-03
T=+5.30E+03 DT/T=+1.48E-04
T=+5.77E+03 DT/T=-1.09E-03
T=+6.29E+03 DT/T=-9.78E-04
T=+6.86E+03 DT/T=+9.32E-04

N=47
A=-7.33195119E-03B=-.3045315 C=7.45749404

T=+4.51E+03 DT/T=-8.48E-04
T=+4.88E+03 DT/T=+8.44E-04
T=+5.30E+03 DT/T=+8.66E-04
T=+5.77E+03 DT/T=-1.96E-04
T=+6.29E+03 DT/T=-7.71E-04
T=+6.86E+03 DT/T=-4.94E-04
T=+7.50E+03 DT/T=+6.01E-04

N=48
A=-.0214612737 B=-.0578361258 C=6.38092093

T=+4.88E+03 DT/T=-4.57E-04
T=+5.30E+03 DT/T=+6.42E-04
T=+5.77E+03 DT/T=+2.02E-04
T=+6.29E+03 DT/T=-2.23E-04
T=+6.86E+03 DT/T=-2.86E-04
T=+7.50E+03 DT/T=-4.37E-05
T=+8.21E+03 DT/T=+1.65E-04

N=49
A=-.0254745228 B=.0133613916 C=6.06524521

T=+5.30E+03 DT/T=+4.58E-05
T=+5.77E+03 DT/T=+1.20E-05
T=+6.29E+03 DT/T=-1.44E-04
T=+6.86E+03 DT/T=-7.80E-05
T=+7.50E+03 DT/T=+1.50E-04
T=+8.21E+03 DT/T=+1.98E-04
T=+8.87E+03 DT/T=-1.83E-04

A N N E X E D

CHALEUR SPECIFIQUE DU ZIRCONIUM CRISTALLIN À L'ETAT NORMAL ET SUPRACONDUCTEUR

Volume 88A, number 3 PHYSICS LETTERS 1 March 1982

VERY LOW TEMPERATURE SPECIFIC HEAT OF CRYSTALLINE ZIRCONIUM IN NORMAL AND SUPERCONDUCTING STATES

J.C. LASJAUNIAS and A. RAVEX
Centre de Recherches sur les Très Basses Températures, C.N.R.S., 38042 Grenoble Cedex, France

Received 29 October 1981

Specific heat measurements of zirconium between 0.03 and 1.2 K in both normal and superconducting states are reported. In the normal state a purely linear electronic contribution is observed down to 0.1 K; at lower temperatures there appears the onset of a nuclear hyperfine contribution which is unobservable in the superconducting state within our experimental time scale.

We have measured the very low temperature specific heat of crystalline zirconium in order to obtain information about the magnitude of the expected hyperfine quadrupole contribution due to the ^{91}Zr isotope with a nuclear spin $I = 5/2$. Up to now, no NMR or specific heat data have been reported which could permit a determination of the quadrupolar coupling.

The sample in the form of a rod 7 mm in diameter, about 5.8×10^{-2} mole, was obtained by melting high purity zirconium in an induction furnace and quenching in a water-cooled crucible. No subsequent thermal annealing was performed so that this sample was measured in its "as-quenched" state. Results of chemical analysis made on this sample give: Cr, Mn, Co, Ni, each <10 ppm; Fe, 35 ppm; Hf, 100 ppm. Specific heat measurements between 30 mK and 1.2 K were performed in a double stage adiabatic demagnetization cryostat with the heat pulse technique. The thermal link between sample and heat sink was ensured either by a superconducting tin thermal switch, but this technique limits the high temperature range to about 0.5 K, or by a permanent link which is a 35 μm diameter copper wire [1]. The second technique was used for the measurements in the superconducting state, between 30 mK and 0.5 K, and up to 1.2 K. The normal state was obtained by supplying a magnetic field of about 100 G (critical field of Zr: $H_c = 47$ G). Data of the two experiments, with and without external magnetic field, are reported in fig. 1. The sample undergoes a superconductive transition between 0.45 and 0.5 K, in rather good agreement with previously published data: 0.49–0.52 K [2–4].

In the normal state, the specific heat obeys a linear variation from 0.1 up to 1.2 K. A slight difference (about 3%) exists between the electronic γ coefficient in the presence or in absence of the magnetic field; it is probably due to a small magneto-resistance effect on the thermometer, a doped Si slice, that we have not tried to correct. The value of γ obtained in the normal state in absence of a magnetic field, 3.0 mJ mole^{-1} K^{-2}, is in good agreement with the value of 2.91 ± 0.12 previously reported by Gschneider [5], but slightly larger than 2.80 from Collings and Ho [6]; both correspond to measurements above 1.2 K. We obtain a purely linear specific heat up to 1.2 K, the lattice contribution remaining still negligible in this temperature range ($\approx$2% at 1 K).

Below 0.1 K there appears a deviation from the linear variation that we ascribe to the onset of the nuclear quadrupolar contribution due to the nuclear spin $I = 5/2$ of the ^{91}Zr isotope (11% natural abundance). Although a precise evaluation of its magnitude is difficult to establish since we do not actually observe a T^{-2} variation, we estimate the quadrupolar contribution C_Q to be $(1.7 \pm 0.4)T^{-2}$ erg mole^{-1} K^{-1} from the excess of the measured values over the γT law. From expression of the Schottky anomaly related to this nuclear contribution and limited to the

0 031-9163/82/0000–0000/$ 02.75

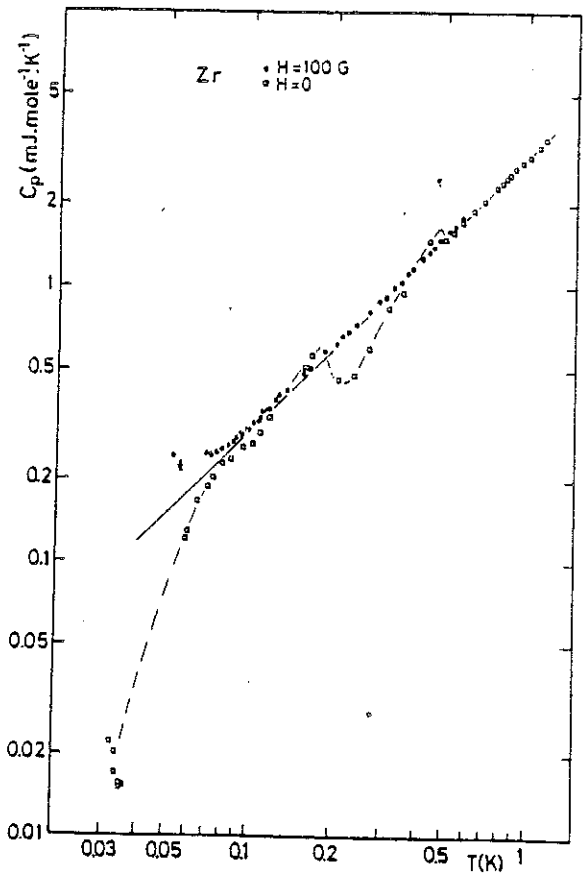

Fig. 1. Specific heat of zirconium in both normal and superconducting states in a log–log plot. Normal state below $T_c \approx 0.5$ K was obtained by applying a magnetic field of 100 G. The straight line corresponds to the electronic term γT, with $\gamma = 3.0$ mJ mole^{-1} K^{-2}.

first term,

$$\frac{C_Q}{R} = \frac{1}{80}\left(\frac{e^2qQ}{k_B}\right)^2 \frac{(I+1)(2I+3)}{I(2I-1)}\, T^{-2},$$

we evaluate the quadrupolar frequency $\nu_Q = e^2qQ/h = 50 \pm 5$ MHz.

Additionally we have to estimate the possible nuclear contribution of hafnium, in concentration of 100 ppm in our sample, which has two isotopes with nuclear spins different from 1/2: 18% ^{177}Hf ($I = 7/2$) and 14% ^{179}Hf ($I = 9/2$). Its nuclear specific heat has already been measured [7]: $C_Q = 850\, T^{-2}$ erg mole^{-1} K^{-1}. With the above concentration its contribution is only a few percent of the measured nuclear term.

In the superconducting state, below the first expected transition near 0.5 K we observe a second transition between 0.17 and 0.2 K which is not understood. Two successive transitions have been reported when 1 at% Sc is added to zirconium [3,4]. Can the presence of impurities (i.e. 100 ppm Hf) be the origin [‡1]? Another explanation could be the presence of different crystalline phases as our sample was measured in its "as-quenched" state without being subjected to further thermal treatment.

Anyway the specific heat decreases exponentially below 0.2 K and down to the lowest temperature reached: 30 mK. No contribution from the nuclear term detected in the normal state was present: the value of C at 30 mK is *ten times smaller* than the estimated expected value of C_Q in the normal state. Such an absence of quadrupolar term in the superconducting state in comparison to the normal state has already been pointed out in a few metals [8]: it is ascribed to the increasing spin–lattice relaxation time T_1 below T_c in consequence of the condensation of normal electrons [9]. From time constants of the transient regimes measured in our specific heat technique [1] corresponding to the recovery of thermal equilibrium after a heat pulse, typically 30–60 s at 35 mK, one can put a lower limit of about a few minutes on T_1.

In a next paper, we shall demonstrate that in amorphous superconducting alloys based on zirconium one can partly recover this quadrupolar contribution, as the T_1 relaxation time is considerably lowered by the presence of low-energy excitations related to configurational defects (TLS defects).

We are grateful to D. Thoulouze and O. Bethoux for useful discussions.

‡1 Furthermore a slight bump appears in the specific heat (fig. 1) at about 90 mK which is the superconducting transition temperature of Hf reported by Jensen [4].

[1] J.C. Lasjaunias, B. Picot, A. Ravex, D. Thoulouze and M. Vandorpe, Cryogenics 17 (1977) 111.
[2] E. Bucher, J. Muller, J.L. Olsen and C. Palmy, Phys. Lett. 15 (1965) 303.
[3] M.A. Jensen and J.P. Maita, Phys. Rev. 149 (1966) 409.
[4] M.A. Jensen, Ph.D. Thesis.
[5] K.A. Gschneider, Solid State Phys. 16 (1964) 351.
[6] E.W. Collings and J.C. Ho, Phys. Rev. B4 (1971) 349.
[7] D. Thoulouze, private communication.
[8] N.E. Phillips, Phys. Rev. 134 (1964) A385.
[9] Y. Masuda and A.G. Redfield, Phys. Rev. 125 (1962) 159.

A N N E X E E

ANALYSE "B.C.S." DES RESULTATS EXPERIMENTAUX AU-DESSOUS DE T_c

Comme mentionné lors de l'Analyse des Résultats, nos échantillons se comportent comme des supraconducteurs à couplage électron-phonon plutôt faible. La théorie B.C.S. décrit avec succès le comportement thermodynamique de tels matériaux, nous avons donc développé une forme d'analyse des résultats expérimentaux obtenus au-dessous de T_c différente de celle exposée précédemment et reposant principalement sur les prédictions du modèle B.C.S.

Dans la gamme de température que nous explorons expérimentalement la chute de chaleur spécifique électronique exponentielle qui suit la transition supraconductrice s'exprime dans le modèle BCS par la formule numérique suivante :

$$C_{es}(T) = C_{en}(T_c)\ a\ \exp(-b\ \frac{T_c}{T}) \quad \text{avec } a = 8{,}5 \text{ et } b = 1{,}44$$

Dans la gamme de température où cette formule est valide ($2{,}5 < \frac{T}{T_c} < 6$), la chaleur spécifique totale mesurée C comporte trois contributions :

- les phonons $C_{ph} = \beta_{ph} T^3$
- les T.L.S. $C_{T.L.S.} = aT^n$
- les électrons supraconducteurs $C_{es} = C_{en}(T_c)\ a\ \exp(-b\ \frac{T_c}{T})$

soit $C = \beta_{ph} T^3 + C_{TLS} + C_{en}(T_c) a\ \exp(-b\ \frac{T_c}{T})$

que l'on peut écrire

$$\frac{C - C_{TLS}}{T^3} = \beta_{ph} + \frac{C_{en}(T_c)}{T_c} \cdot \frac{1}{T^2} \frac{T_c}{T}\ a\ \exp(-b\ \frac{T_c}{T})$$

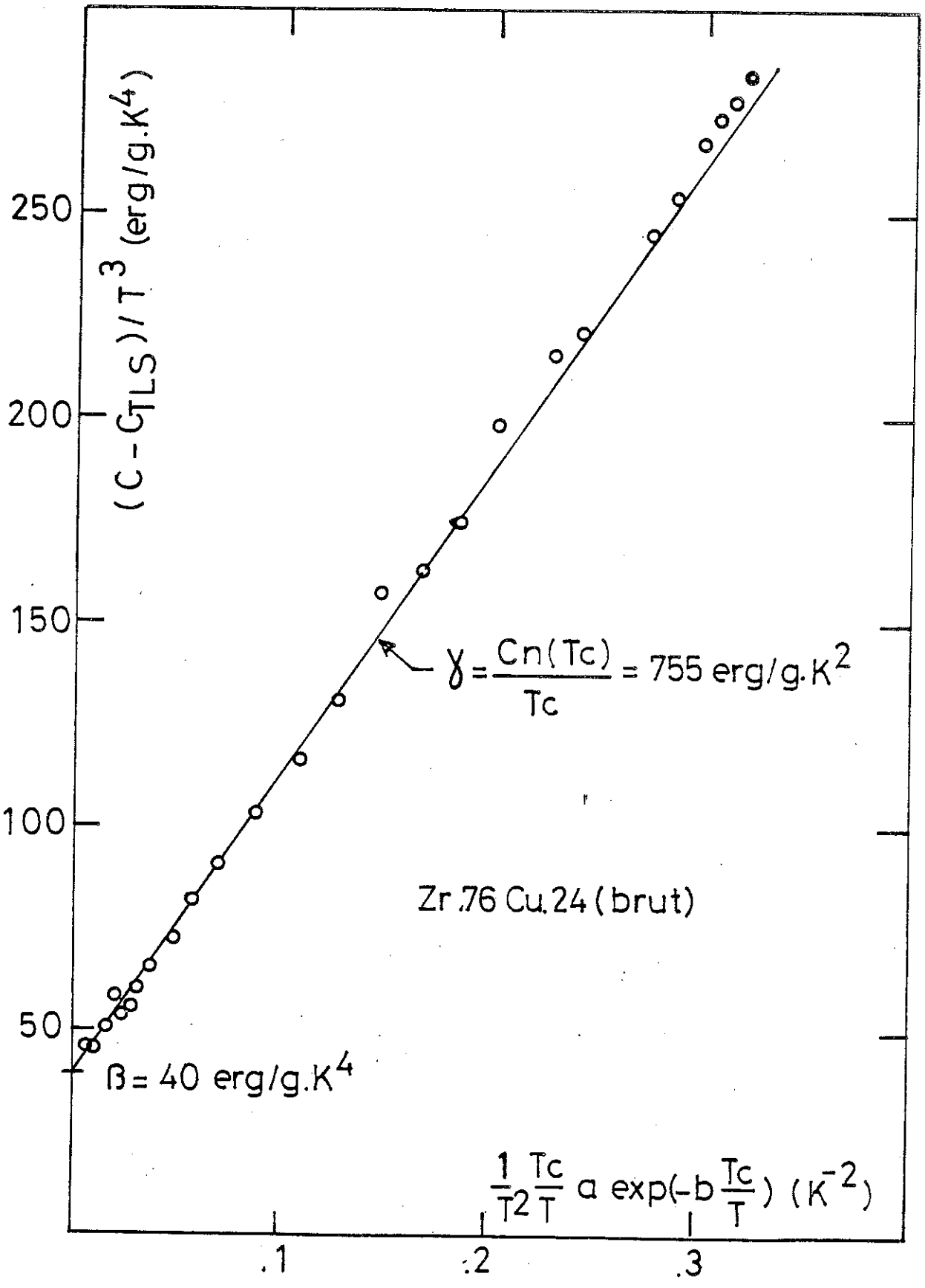
250
200
150
100
50
$(C-C_{TLS})/T^3$ (erg/g.K^4)
$\gamma = \frac{Cn(Tc)}{Tc}$ = 755 erg/g.K^2
Zr .76 Cu .24 (brut)
β = 40 erg/g.K^4
$\frac{1}{T^2}\frac{Tc}{T}$ a exp$(-b\frac{Tc}{T})$ (K^{-2})
.1
.2
.3

Dans un tracé $\frac{C-C_{TLS}}{T^3}$ en fonction de $\frac{1}{T^2}\left[\frac{T_c}{T} a \exp(-b \frac{T_c}{T})\right]$, on doit obtenir une droite d'ordonnée à l'origine β_{ph} et de pente $\frac{C_{en}(T_c)}{T_c}$ si l'échantillon étudié suit le modèle B.C.S.

La figure 1 montre un tel fit pour l'échantillon $Zr_{76}Cu_{24}$ brut de pulvérisation pour lequel nous avons rencontré (Ravex et al., 1984) le plus de problèmes liés à l'extrapolation vers les basses températures du terme phononique déterminé au-dessus de T_c.

On constate que l'on obtient une droite qui permet de tirer les valeurs suivantes :

$$\beta_{ph} = 40 \pm 2 \text{ erg/gK}^4 \quad (0,338 \quad \text{mJ/mole K}^4)$$

$$\frac{C_N(T_c)}{T_c} = 755 \pm 5 \text{ erg/gK}^2 (6,39 \quad \text{mJ/mole K}^2)$$

et de confirmer le bon accord avec BCS. La valeur obtenue pour β_{ph} est très différente de la valeur tirée de l'analyse en $C/T = f(T^2)$ au-dessus de T_c. Cette valeur beaucoup plus faible correspond à peu près à celle choisie empiriquement pour analyser les résultats dans la publication citée précédemment (Ravex et al., 1984). Si l'on considère que cette valeur obtenue au-dessous de T_c est la valeur correcte pour les phonons (il est à noter que cette nouvelle valeur correspond à une température de Debye plus forte - $\theta_D = 180$ K - en meilleur accord avec celle des échantillons trempés du liquide), on peut affecter le terme cubique supplémentaire observé au-dessus de T_c à une contribution électronique du type $\beta_e T^3$ ($\beta_e = \beta - \beta_{ph}$) dont l'origine reste à déterminer. Dans cette hypothèse on peut chercher à calculer le saut de chaleur spécifique à T_c. Il vaut :

$$\frac{C_{es}(T_c) - C_N(T_c)}{C_N(T_c)} = \frac{(C_{totale} - \beta_{ph} T_c^3) - (\beta_c T_c^3 + \gamma T_c)}{\beta_c T_c^3 + \gamma T_c} = 1,41$$

très proche de la valeur BCS alors que dans l'analyse précédente on obtenait 1,89. Ce résultat confirme à nouveau le bon accord avec BCS et la nature certainement électronique du terme d'excès.

Cette analyse donne des résultats semblables pour l'ensemble des échantillons étudiés.

dernière page de la thèse

AUTORISATION DE SOUTENANCE

VU les dispositions de l'article 5 de l'arrêté du 16 Avril 1974,

VU les rapports de M. J. DURAND

M. W.E. PHILLIPS

M. J.C. LASJAUNIAS

M. Alain RAVET est autorisé

à présenter une thèse en soutenance pour l'obtention du grade de

DOCTEUR D'ETAT ES SCIENCES.

Fait à GRENOBLE, le 26/12/86

Le Président de l'U.S.M.G.

Le Président

M. TANCHE

Le Président de l'I.N.P.G.

D. BLOCH
Président
de l'Institut National Polytechnique
de Grenoble

P.O. le Vice-Président,

RESUME

Ce mémoire présente un travail expérimental sur les propriétés thermiques (chaleur spécifique et conduction thermique) à très basses températures d'alliages métalliques amorphes supraconducteurs.

On précise les méthodes d'élaboration et de caractérisation des échantillons.

On décrit les techniques expérimentales développées pour la mesure de faibles capacités calorifiques et fortes conductions thermiques à très basse température ainsi que les méthodes d'analyse des résultats expérimentaux.

Les propriétés électroniques et supraconductrices ainsi que les propriétés caractéristiques de l'état amorphe (excitations de basse énergie) sont présentées et analysées pour les échantillons bruts de pulvérisation.

Les effets de recuits à l'état amorphe (relaxation structurale) sur ces propriétés sont ensuite étudiés.

Enfin on présente une série d'études sur les propriétés structurales des échantillons (ATD, EXAFS, Rayons X).

MOTS-CLEFS

Métal amorphe - supraconducteur - pulvérisation cathodique - excitations de basse énergie (T.L.S.) - relaxation structurale - chaleur spécifique - conduction thermique - couplage T.L.S. - noyaux.